UC Berkeley
UC Berkeley Electronic Theses and Dissertations

Title

Mechanism-Guided Discovery of Catalytic Processes and Organic Materials

Permalink

https://escholarship.org/uc/item/47c7h3bq

Author

Huang, Banruo

Publication Date

2022

Peer reviewed|Thesis/dissertation

eScholarship.org Powered by the California Digital Library
University of California

Mechanism-Guided Discovery of Catalytic Processes and Organic Materials

By

Banruo Huang

A dissertation submitted in partial satisfaction of the

requirements for the degree of

Doctor of Philosophy

in

Chemistry

in the

Graduate Division

of the

University of California, Berkeley

Committee in charge:

Professor F. Dean Toste, Chair

Professor Thomas Maimone

Professor Niren Murthy

Spring 2022

Abstract

Mechanism-Guided Discovery of Catalytic Processes and Organic Materials

by

Banruo Huang

Doctor of Philosophy in Chemistry

University of California, Berkeley

Professor F. Dean Toste, Chair

This thesis represents the efforts to develop new catalytic methods, and to discover new organic materials. These efforts were driven by mechanistic thinking in organic and organometallic chemistry.

Chapter 1 offers a historical overview of how mechanistic understandings drive reaction development and inspire the development in other related fields such as chemical biology and materials science.

Chapter 2 discusses a new strategy to activate transition metal complexes by hydrogen-bond donors (HBDs). Anion binding catalysis using HBDs, Au(I)/Au(III) redox chemistry, and the prevalence of anion abstraction in Au(I) catalysis are introduced as a foundational design principle of the new strategy. Attempts to achieve anion abstraction from Au(I) and Au(III) complexes using this strategy are then presented. This led to the development of an enantioselective intermolecular Au(I)-catalyzed hydro(hetero)arylation reaction of allenes. Experimental and computational studies showed an interplay of non-covalent interactions that led to the observed enantioselectivities. Computational studies on the origin of enantioselectivities were conducted in collaboration with Dr. Binh Khanh Mai from Prof. Peng Liu's lab at University of Pittsburgh.

Chapter 3 focuses on the design and synthesis of cyclic acylsilanes and their applications in ring-opening metathesis polymerization (ROMP). First, photochemical reactivities of acylsilanes and how these reactivities can be translated to macroscopic properties, such as degradability of materials, are discussed. The synthesis of eight-membered-ring acylsilane-based cyclic olefins as monomers for ROMP led to photodegradable polymers. Photochemical ring expansion reactions of the cyclic acylsilane were also discovered. The resulting product holds promise to yield degradable polymers with controlled release properties. This work was done in collaboration with Mufeng Wei, Emma Vargo, and Yiwen Qian from Prof. Ting Xu's lab at UC Berkeley.

Chapter 4 describes the discovery of a new linker for covalent organic frameworks (COFs), namely nitrone linkages. This was driven by the diverse reactivities of nitrone functionalities. The resulting COFs were found to undergo a photochemical isomerization reaction. This work was

done in collaboration with Dr. Daria Kurandina, and Dr. Wentao Xu from Prof. Omar Yaghi's lab at UC Berkeley.

ACKNOWLEDGEMENTS

I could not be luckier to spend the past five years as a graduate student, and one year before that as an undergraduate researcher, here at Berkeley. Looking back, it has not been easy, I cannot make it without so many people, their help and inspiration.

Over the course of my graduate career, the influence of my research advisor, F. Dean Toste, cannot be overstated. He is dedicated to supporting his students, not only in the form of research guidance, but also the career management. Seeing senior students secure their next step either in industry or academia is reassuring to me, from the beginning, that I can freely pursue my interest in fundamental research without worrying too much about the future. I'm also thankful to Dean for the freedom he grants to explore various ideas under broad range of research topics. Only with that I can find my passion in materials science and secure a postdoctoral position in that area. Talking to Dean has always been joyful: he offers deep research insights in the grand scheme and our exchange has touched many aspects outside the chemical research.

In addition, Dean has cultivated a unique intellectual environment in his research group by recruiting people from diverse backgrounds and conducting research in different areas. I really benefit from that by talking to these outstanding scientists, learning from their advice on my research, their way of thinking, and their research. Personal connections that stemmed from these interactions also support me through the years, especially in this rapidly changing world. Among the long list of people that I owe gratitude to, I would like to thank, in particular, Mark Levin, Spencer Scholz, Suhong Kim, Willie Wolf, Andrew Neel, Kacper Skakuj, Anna Wuttig, Alex Zhukhovitskiy, Alec Christian, Cindy Hong, Edward Miller, Mariko Morimoto, TJ O'Connor, Jacob Tracy, Lily hale, Christine Le, Junqi Li, Rene Rahimoff, Patrick Moon, John Lee, Jie Zhao, Wenhao Zhang, Mingyou Hu, Zeng Rong Wong, Kay Xia, Katie Chung, Annika Page for helpful discussions and feedbacks.

I am truly blessed with a lovely cohort in the Chemistry Department, particularly my peers in the Toste Group: Stephen Bierschenk and Megan Neubig. Stephen is the nicest person I have ever met. I enjoyed so many social events organized by him. His presence in the lab, and the support he offered are indispensable. I also cherish the friendship with Megan and feel happy for her industrial career.

My time at Berkeley is also characterized by active collaborations with other labs. I would like to thank Ting Xu for being an incredible collaborator, constantly challenging me on the intellectual front, as well as all her students who worked or discussed with me. I'm grateful to Daria Kurandina for being an efficient and helpful coworker, as well as Omar Yaghi for encouraging this collaboration to take place. I also want to thank Binh Khanh Mai and Peng Liu for conducting computational studies. Special thanks are also extended to Nick Settineri, Miao Zhang, Hasan Celik, Alicia Lund for maintaining the instruments and providing help that are necessary for my research.

To friends who shared the Ph.D. experience, Tieyi Lu, Xingpin Li, Ershuai Liu, Weijie Feng, Xiaokun Pei and many others, you all fight hard and thank you for the friendship and patience, I know I'm not the easiest person to get along with.

To my parents, Jun Gu and Wenxun Huang: thank you for providing me unconditional support to my decisions, constant care and love in your own ways. I can only speculate the unease of your only child moving abroad. I know the past few years hasn't been easy for you as well. I wish I can be there. I love you.

Finally, I would like to thank Alison, her mom, Gem, and my two cats, Dragon and Gold. Meeting Alison is, in all likelihood, the best thing that could ever happen to me. I could not be where I am without her love, friendship, support, and understandings. I cannot wait for our adventure at Santa Barbara and celebrating every milestone with her in the future. I also want to thank Gem for treating me as family. Dragon and Gold are the cutest cats on earth. Their company helped me go through some dark time. And it is always a joy to have them around, healthy and naughty.

To Alison,
On ne voit bien qu'avec le cœur. L'essentiel est invisible pour les yeux.

Mechanism-Guided Discovery of Catalytic Processes and Organic Materials

TABLE OF CONTENTS

Chapter 1. Mechanism-Guided Approach in the Research Fields of Organic Chemistry, Chemical Biology, and Organic Materials

1.1 Introduction 2
1.2 Development of Catalytic Processes Enabled by Mechanistic Understanding 2
1.3 Development of Bioconjugation Methods Guided by Mechanistic Understanding 3
1.4 Discoveries of Organic materials Guided by Mechanistic Understanding 4
1.5 Conclusions 6
1.6 References and Notes 6

Chapter 2. Anion-Binding Strategy in Homogeneous Gold-mediated Chemistry

2.1 Introduction 9
2.1.1 Overview of Homogeneous Gold Chemistry 9
2.1.2 Anion-Binding Catalysis 19
2.2 Results and Discussion 21
2.2.1 Computational Studies on Thermodynamics of Chloride Binding from Gold(I) 21
2.2.2 Studies on Activation of Gold(I) and Gold(III) Precatalysts in Lactonization, Conia-Ene and Enyne Isomerization Reactions 23
2.2.3 Development of Enantioselective Intermolecular Hydroarylation Reaction of Allene 30
2.2.4 Computational Studies of Enantioselective Intermolecular Hydroarylation Reaction of Allene 33
2.3 Conclusion 35
2.4 References and Notes 35
2.5 Supporting Information 39
2.5.1 General Information 39
2.5.2 Computational Studies on Thermodynamics of Chloride Binding from Gold(I) 40
2.5.3 Synthetic Procedures 42
2.5.4 General procedure for catalytic reactions (lactonization, conia-ene reaction, enyne isomerization and hydroarylation of allene with indole) 44
2.5.5 Procedure for NMR Studies of Interaction Between **53**, **54** and **55** 44
2.5.6 HPLC Trace for Hydroarylation Product **65** 44
2.5.7 Computational Details on the Origin of Enantioselectivities in Hydroarylation of Allene 45
2.5.8 NMR spectra 95
2.5.9 References 102

Chapter 3. Mechanism-Guided Discoveries of Backbone-Degradable Polymers Based on New Cyclic Acylsilane Compounds

3.1 Introduction 105

3.2 Results and Discussion 106
3.2.1 Synthetic Routes of Unsaturated Acylsilane Monomers for ROMP 106
3.2.2 Copolymerization of Acylsilane Monomers via ROMP 107
3.2.3 Photodegradation Studies in Solution 108
3.2.4 Mechanistic Studies of the Photodegradation Process in Solution 110
3.2.5 Photodegradation Studies in Solid 112
3.2.6 Initial Studies on Photochemical Ring Expansion Reactions of Cyclic Acylsilane Precursors to Access Unsaturated Cyclic Siloxyacetal Compounds 114
3.3 Conclusion 114
3.4 References and Notes 115
3.5 Supporting Information 116
3.5.1 General Information 116
3.5.2 Monomer Synthesis 117
3.5.3 Strain Energy Calculations in ROMP 122
3.5.4 Polymer Synthesis and Solution Photodegradation Protocols 123
3.5.5 Photodegradation Protocols in Solid State 129
3.5.5.1 Preparation of polymer film and its photodegradation studies 129
3.5.5.2 Preparation of 8a and dicyclopentadiene copolymer and its photodegradation studies 130
3.5.6 Mechanistic Studies 136
3.5.6.1 Measurements of initial rate constants 136
3.5.6.2 Isotope labeling studies 137
3.5.6.3 Additional Irradiation Studies of **11** 138
3.5.7 Protocol of Photochemical Ring Expansion Reactions 143
3.5.8 References 143
3.5.9 Crystallographic Data 143
3.5.10 NMR Spectra 158

Chapter 4. Discovery of Porous Crystalline Nitrone-Linked Covalent Organic Framework

4.1 Introduction 172
4.2 Results and Discussion 172
4.2.1 Preparation of Nitrone-Linked Covalent Organic Framework 172
4.2.2 Characterization of Nitrone-Linked Covalent Organic Framework 173
4.2.3 Studies of Photochemical Properties of Nitrone-Linked Covalent Organic Framework 175
4.3 Conclusion 175
4.4 References and Notes 175
4.5 Supporting Information 176
4.5.1 General Information 176
4.5.2 Synthetic Procedures 177
4.5.3 Gas Sorption Experiments 179
4.5.4 Scanning Electron Microscopy Image 180
4.5.5 Irradiation Studies 181
4.5.6 NMR Spectra 182

Chapter 1

Mechanism-Guided Approach in the Research Fields of Organic Chemistry, Chemical Biology, and Organic Materials

1.1 Introduction

This chapter serves to illustrate the overarching context associated with mechanism-driven research. Though not a comprehensive survey, selected reports are discussed to showcase the importance of this approach in discoveries made in the fields of organic chemistry, chemical biology, and organic materials. More detailed introductions that serves as direct context of the work in each chapter are presented at the beginnings of Chapters 2-4. To disambiguate, the word 'mechanism' in this dissertation specifically refers to 'reaction mechanism' or 'molecular mechanism' of various processes.

One of the fundamental goals in chemical research is to identify general principles of designing catalysts with superior activities and selectivities. Advances in physical organic chemistry in the past decades, including kinetic analysis, kinetic isotope effect experiments, free energy relationship studies, and computational studies, provide powerful tools for this goal.[1] The insights obtained through these methods have led to highly effective catalysts and efficient route to functional small molecules. The implications of this approach reach beyond catalysis: residue-specific bioconjugation methods and high-performance materials have been discovered, which are only possible with mechanistic knowledge or thinking.

1.2 Development of Catalytic Processes Enabled by Mechanistic Understanding

Mechanism-informed design has led to improved catalytic processes. In this section, two examples are discussed to show the prevalence of this strategy to achieve different goals.

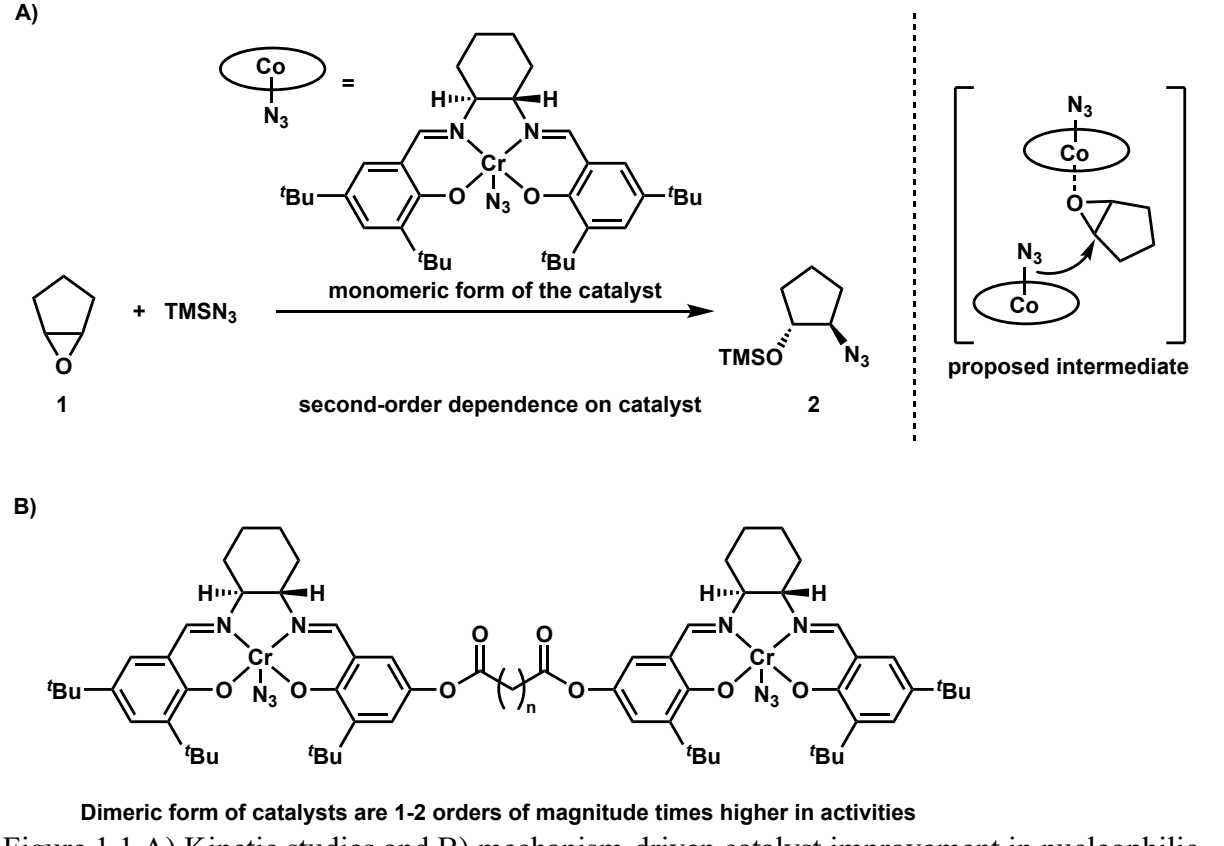


Figure 1.1 A) Kinetic studies and B) mechanism-driven catalyst improvement in nucleophilic ring-opening reactions of epoxides.

In 1996, Jacobsen and coworkers reported the kinetic studies of nucleophilic ring-opening reactions of epoxides catalyzed by chiral (Salen)Cr^{III} complexes (Figure 1.1A).[2] A second-order dependence of the rate on the monomeric Cr catalyst was observed. The kinetic data provided support for an intermediate, in the rate-determining step, that involves catalyst activation of epoxide substrate **1,** as well as the azide delivery from another catalyst molecule. The proposed mechanism led the authors to test covalently linked catalyst dimer (Figure 1.1B).[3] Dimeric (Salen)Cr^{III} complexes were found to be 1-2 orders of magnitude times higher in activities (measured by initial rates) in the same transformation. This example highlights the nonintuitive changes guided by mechanistic studies resulting in a drastically improved catalyst.

Beyond enantioselective catalysis, mechanistic understanding also illuminates new catalytic methods for the syntheses of radio-labeled compounds. In 2017, O'Neil, Toste, and coworkers discovered a C(alkyl)−CF_3 reductive elimination reaction which proceeded via a fluoride-rebound mechanism (Figure 1.2).[4] The trifluoromethylated product, trifluoroethane, was first obtained upon treatment of complex **3** with $B(C_6F_5)_3$. Mechanistic investigation pointed to a pathway in which fluoride abstraction from **3** formed a cationic difluorocarbene Au(III) complex **4**, which underwent carbon-carbon bond-forming migratory insertion of methyl group into difluorocarbene. Final recombination of fluoride to **5** furnished the final product. This understanding established the possibility of ^{18}F-incorporation into the product with external [^{18}F] fluoride addition. Indeed, a protocol was developed for synthesizing ^{18}F-radiolabeled aliphatic CF_3-containing compounds including a cannabinoid agonist **6**.

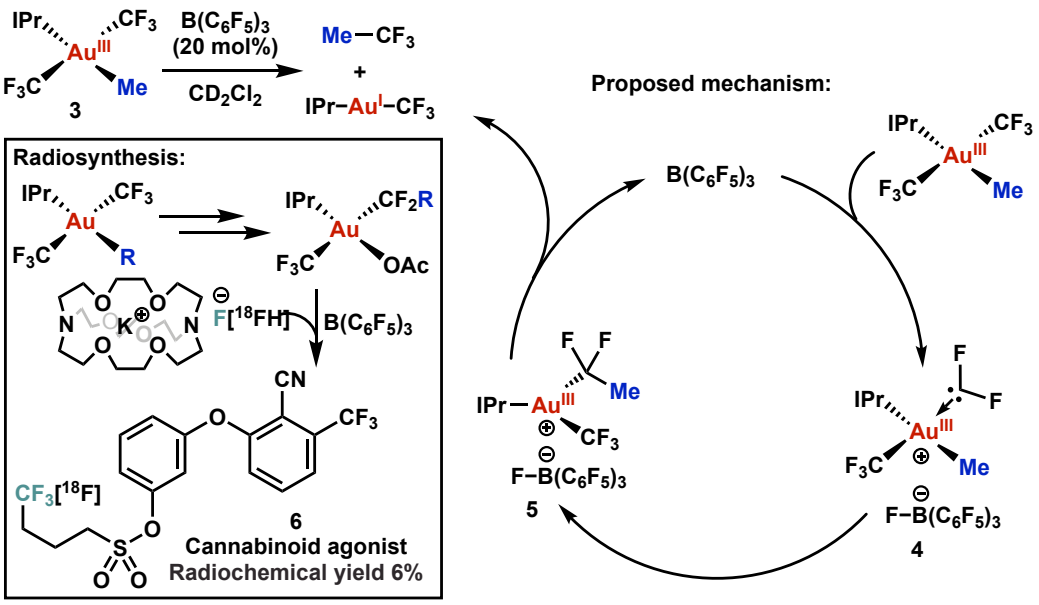


Figure 1.2 Mechanism-guided discovery of catalytic ^{18}F-incorporation.

1.3 Development of Bioconjugation Methods Guided by Mechanistic Understanding

Mechanistic understanding of reactivities has led to advances in selective bioconjugation methods, a prime example being the development of methionine conjugation method with oxaziridines. Amino acid-selective bioconjugation relies on the unique reactivity of the amino acid of interest. Like methionine, cysteine is one of the only two sulfur-containing proteinogenic amino acids. A broad range of cysteine bioconjugation methods using electrophile have been developed, exploiting the high nucleophilicity of the thiol/thiolate (Figure 1.3A).[5,6] In contrast, methionine

conjugation was considered challenging due to the relatively weak nucleophilicity, which precludes the selective electrophilic transformations in the presence of more nucleophilic amino acids such as cysteine. Mechanistically distinct to the nucleophilicity, Chang, Toste, and coworkers were inspired by the redox regulation functions of methionines in biological systems and designed an oxidative sulfur imidation reaction.[7] The redox process involving the oxaziridine was proven efficient and selective. Application of this method ranges from payload ligation to proteins, synthesis of antibody-drug conjugates, and proteomic identification of hyperreactive methionine residues.

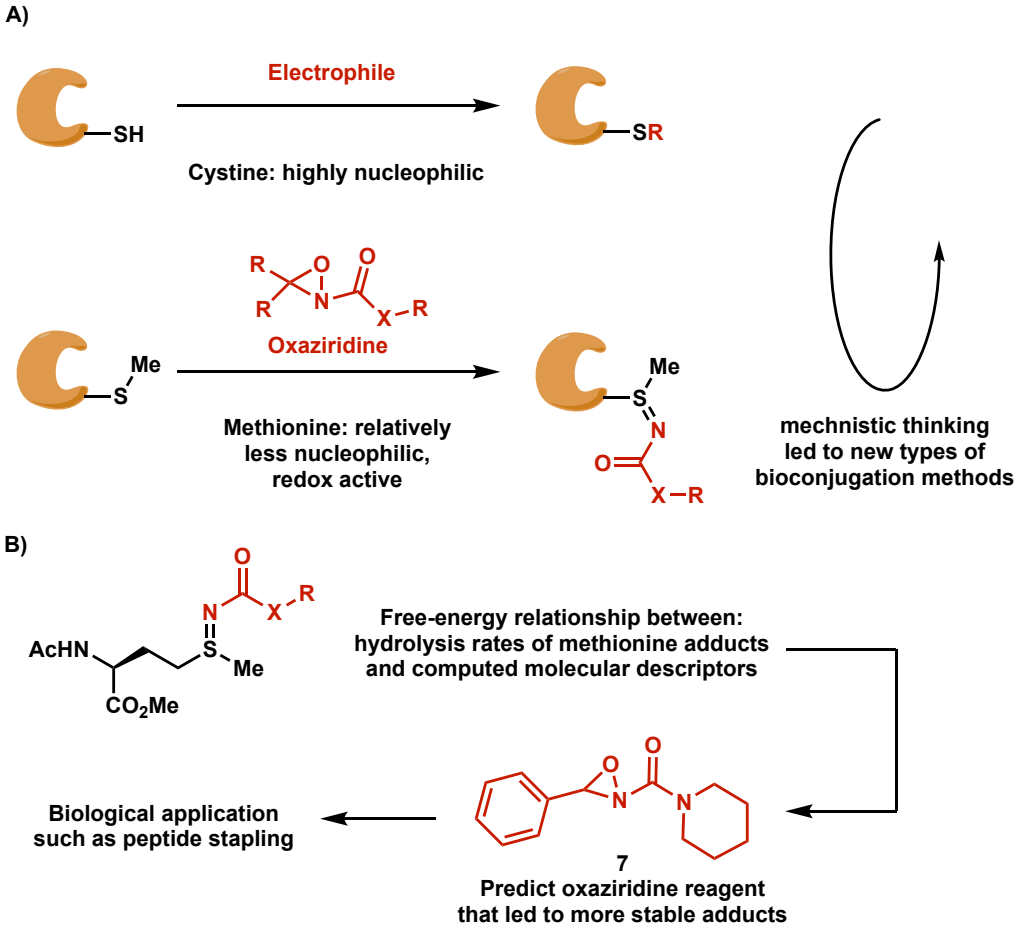


Figure 1.3 Mechanism-guided A) design and B) improvement of methionine conjugation method with oxaziridine.

In improving the methionine adduct stability towards hydrolysis, mechanistic understanding again played an important role: researchers from the same labs established free-energy relationships between hydrolysis rate of the adducts and various molecular descriptors.[8] The identified correlation was found predictive for new oxaziridine reagent **7** that led to improved adduct stability (Figure 1.3B). Peptide stapling was achieved with dimeric form of **7**, which was much more effective than previously reported reagents. The development of the methionine bioconjugation method with oxaziridines underscores how mechanistic thinking can enable new and improved protocol in chemical biology.

1.4 Discoveries of Organic materials Guided by Mechanistic Understanding

Discoveries of new materials are critical to technological advancement in all aspects of modern society. Among which, organic materials have seen broad applications including packaging, electronics, biomedicine, etc. Organic polymers, arguably the most prominent class of organic materials, have undergone rapid development in the past century, after Hermann Staudinger presented the molecular understanding of the high-molecular-weight compounds in 1920.[9,10] The understanding of molecular level reactivities, energetics, and non-covalent interactions has continued to drive the research for organic materials with desired properties.

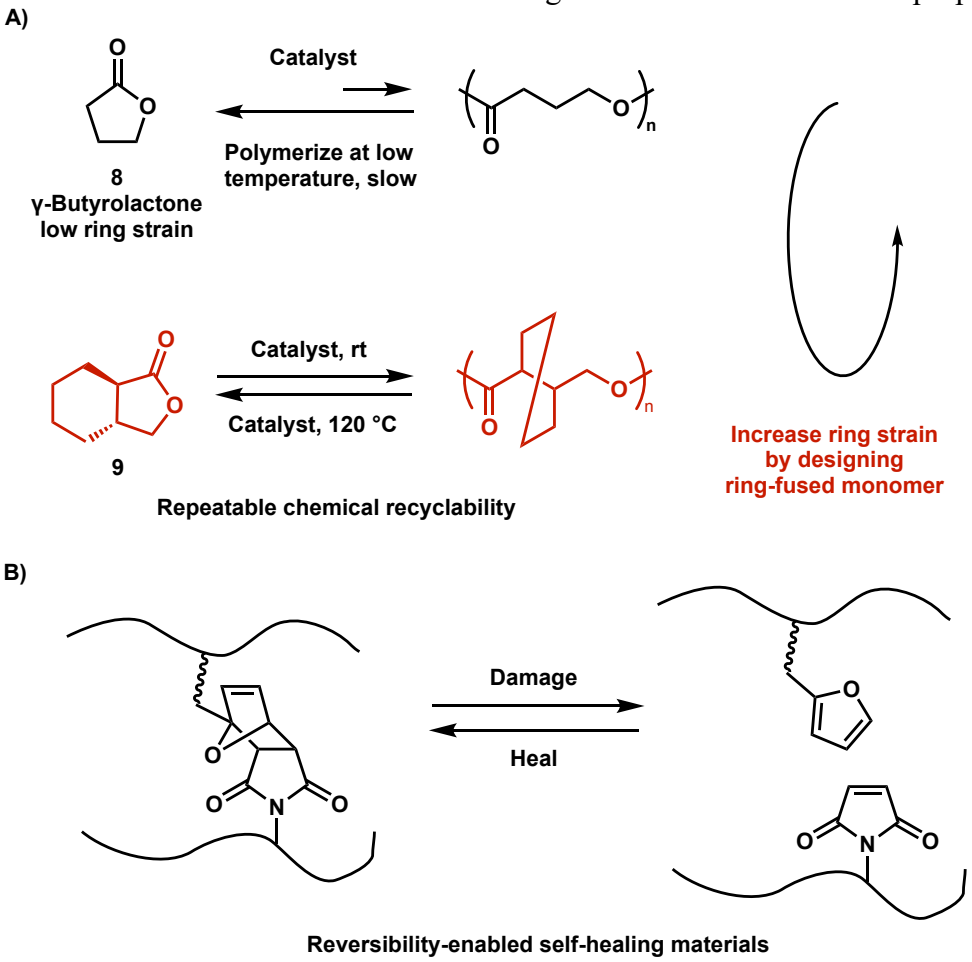


Figure 1.4 A) Design of monomer with proper ring strain for chemically recyclable polymers; B) Design of self-healing materials with reversibility of Diels-Alder reactions.

Closed-loop chemical recycling has been recognized as one of the potential solutions to the unsustainable production of synthetic polymers.[11,12] This requires the recovery of the precursor chemicals via depolymerization. The understanding of energetics, both in the thermodynamic and kinetic senses, is critical to the design of building blocks and processes in the realm of circular recycling. For example, polyethylene is the most widely used plastic in the world. But the extreme ceiling temperature of 610 °C renders poor depolymerization selectivity as alternative decomposition occurs at lower temperatures.[13] The high ceiling temperatures of many commodity polymers, originated from the exceedingly exothermic polymerization process, also leave the potential depolymerization processes energetically intensive. In contrast, poly(*γ*-butyrolactone), a polymer with a low ceiling temperature of −9 °C, can be readily depolymerized in the presence of

a catalyst under room temperature (Figure 1.4A).[14] The ease of depolymerization, however, leads to a slow polymerization process from γ-butyrolactone (**8**), usually carried out under −40 °C to achieve appreciable degree of polymerization. From the aforementioned examples, it is concluded that suitable exergonicities are required for the balance between polymerization and depolymerization.

Guided by the principle of altering exergonicity, Chen and coworkers reported a trans-fused γ-butyrolactone (**9**) monomer.[15] Unlike original γ-butyrolactone, higher ring strain of **9**, attributed to the trans-fused structure, enabled its bulk polymerization even at 40 °C. Chemical recycling with $ZnCl_2$ at 120 °C led to the recovery of monomer **9**. The circular monomer-polymer-monomer cycle was repeated three times at multigram scale. This report underscores the effectiveness of mechanistic thinking in creating sustainable plastics.

Apart from the chemical recyclability, mechanistic understanding also grants other desired properties to organic materials.[16,17] For example, thermal reversibility of Diels–Alder reaction of furan and maleimide moieties was exploited in crosslinked polymer networks to warrant the self-healing property (Figure 1.4B). [18]

1.5 Conclusions

Based on the discussion in this chapter, mechanistic insights and mechanism-driven thinking are shown to be invaluable to the design of new catalytic methodologies, bioconjugation reactions, and materials with sought-after properties. Efforts to implement this strategy in different context are presented in the following chapters.

1.6 References and Notes

[1]. Anslyn, E. V.; Dougherty, D. A. *Modern Physical Organic Chemistry*; University Science Books: Sausalito, CA, 2006.
[2]. Hansen, K. B.; Leighton, J. L.; Jacobsen, E. N. *J. Am. Chem. Soc.* **1996**, *118*(44), 10924–10925.
[3]. Konsler, R. G.; Karl, J.; Jacobsen, E. N. *J. Am. Chem. Soc.* **1998**, *120*(41), 10780–10781.
[4]. Levin, M. D.; Chen, T. Q.; Neubig, M. E.; Hong, C. M.; Theulier, C. A.; Kobylianskii, I. J.; Janabi, M.; O'Neil, J. P.; Toste, F. D. *Science* **2017**, *356*, 1272–1276.
[5]. O. Boutureira; G. J. L. Bernardes. *Chem. Rev.* **2015**, *115*(5), 2174–2195.
[6]. Zhang, C.; Welborn, M.; Zhu, T.; Yang, N. J.; Santos, M. S.; Van Voorhis, T.; Pentelute, B. L. *Nat. Chem.* **2016**, 8, 120–128.
[7]. Lin, S.; Yang, X.; Jia, S.; Weeks, A. M.; Hornsby, M.; Lee, P. S.; Nichiporuk, R. V.; Iavarone, A. T.; Wells, J. A.; Toste, F. D.; Chang, C. J. *Science* **2017**, *355*, 597–602.
[8]. Christian, A. H.; Jia, S.; Cao, W.; Zhang P.; Tena Meza, A.; Sigman, M. S.; Chang, C. J.; Toste, F. D. *J. Am. Chem. Soc.* **2019**, *141*(32), 12657–12662.
[9]. Rowan, S. J. *ACS Macro Lett.* **2021**, *10*(4), 466–468.
[10]. Staudinger, H. *Ber. Dtsch. Chem. Ges. B* **1920**, *53* (6), 1073–1085.
[11]. Shi, C.; Reilly, L. T.; Kumar, V. S. P.; Coile, M. W.; Nicholson, S. R.; Broadbelt, L. J.; Beckham, G. T.; Chen, E. Y. X. Chem **2021**, *7*(11), 2896–2912.
[12]. Coates, G. W.; Getzler, Y. D. *Nat. Rev. Mater.* **2020**, *5*(7), 501–516.
[13]. Diaz-Silvarrey, L. S.; Zhang, K.; Phan, A. N. *Green Chem.* **2018**, *20*, 1813–1823.
[14]. Hong, M.; Chen, E. Y. X. Nat. Chem. **2016**, *8*, 42–49.
[15]. Zhu, J. B.; Watson, E. M.; Tang, J.; Chen, E. Y. X. *Science* **2018,** *360*, 398–403.
[16]. Zheng, N.; Xu, Y.; Zhao, Q.; Xie, T. *Chem. Rev.* **2021**, *121*(3), 1716–1745.

[17]. Wang, S.; Urban, M. W. *Nat. Rev. Mater.* **2020**, *5*(8), 562–583.
[18]. Chen, X.; Dam, M.A.; Ono, K.; Mal, A.; Shen, H.; Nutt, S.R.; Sheran, K.; Wudl, F. *Science* **2002**, *295*, 1698–1702.

Chapter 2

Anion-Binding Strategy in Homogeneous Gold-mediated Chemistry

2.1 Introduction

2.1.1 Overview of Homogeneous Gold Chemistry

The chemistry of gold has attracted tremendous research efforts over the past two decades. Despite rapid development, the majority of reactions discovered with homogeneous gold complexes involve the electrophilic activation of carbon-carbon π-bonds and/or generation of electrophilic gold carbene intermediates (Figure 2.1A). [1–12] Within these activation manifolds, the formal oxidation state of gold remains unchanged throughout the stoichiometric reaction or catalytic cycle. In comparison, relatively few transformations have been proposed to access gold intermediates with different oxidation states (e.g., I/II/III).[13,14]

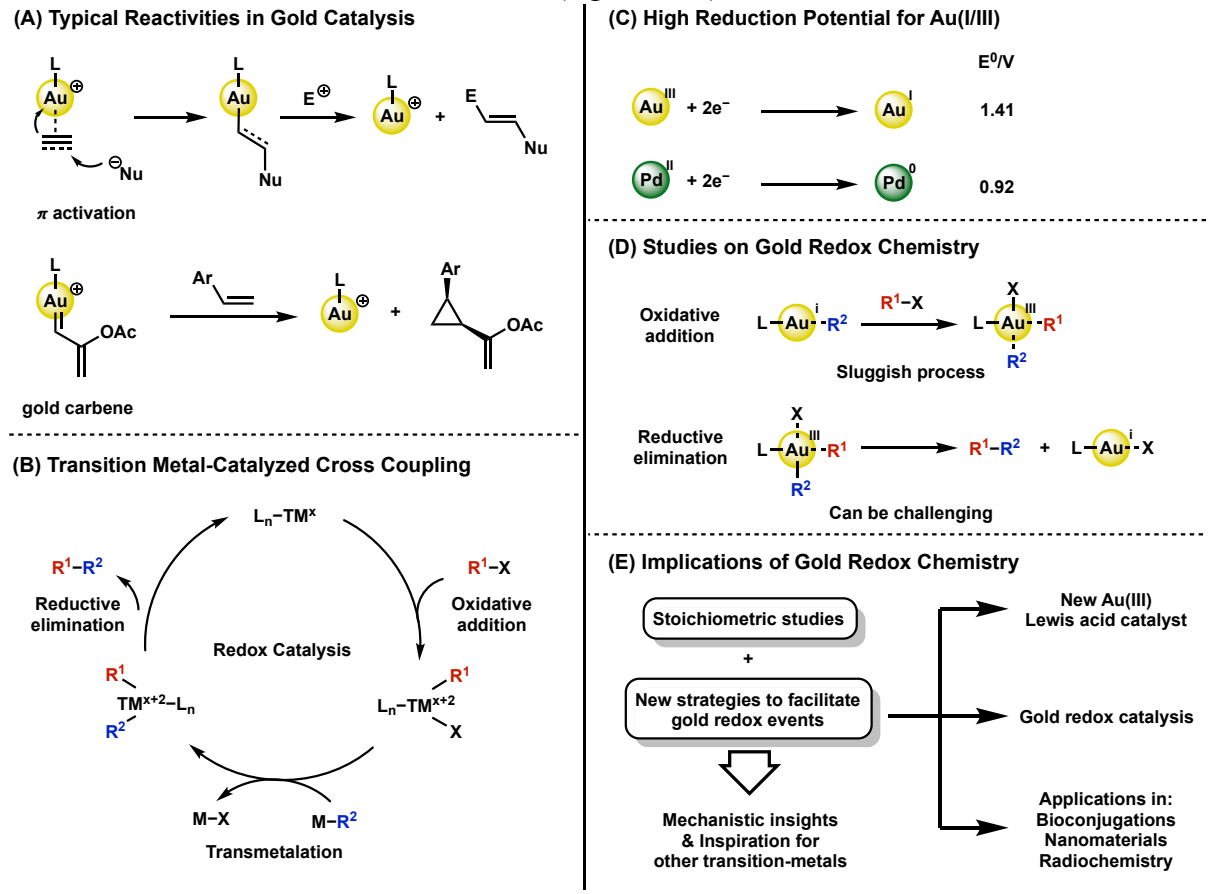


Figure 2.1 Introduction of Gold Redox Chemistry. (A) Typical reactivities in gold catalysis; (B) transition metal-catalyzed cross coupling; (C) high reduction potential for Au(I/III); (D) Studies on gold redox chemistry; and (E) implications of gold redox chemistry.

Transition metal-catalyzed cross-coupling reactions are among the most frequently used methods in synthetic chemistry.[15] These methodologies typically rely on the ability of transition metals (e.g., Pd, Ni, or Cu) to effectively cycle between oxidation states (Figure 2.1B). The elementary steps bridging oxidation states of metals are called oxidative addition and reductive elimination. Despite Au(I/III) and Pd(0/II) sharing the same d-electron counts, redox events are far less common for gold complexes, especially oxidative addition. Thermodynamically, this is manifested by a redox potential of $E^0(Pd^{II/0}) = 0.92$ V, whereas $E^0(Au^{III/I}) = 1.41$ V (Figure 2.1C).[16] Moreover, the symmetry and steric changes rising from oxidative addition to linear Au(I) complexes kinetically disfavor the process. The challenge of enabling redox processes with gold

has aroused significant interest in stoichiometric elementary oxidation-state conversions at gold and the mechanistic details of these transformations. Ultimately, these insights yield new catalytic transformations for chemical synthesis and/or applications in chemical biology, materials science, and radiochemistry (Figure 2.1D,E).

Although still in the early stage of discovery, notable advancement in homogeneous gold redox chemistry has been made in the past six years. The reactivities revealed during this time already show distinct features from other transition metals. The studies are organized by oxidative addition or reductive elimination processes, with a focus on the fundamental organometallic studies, and where possible, the potentially useful chemical transformations arising from these findings.

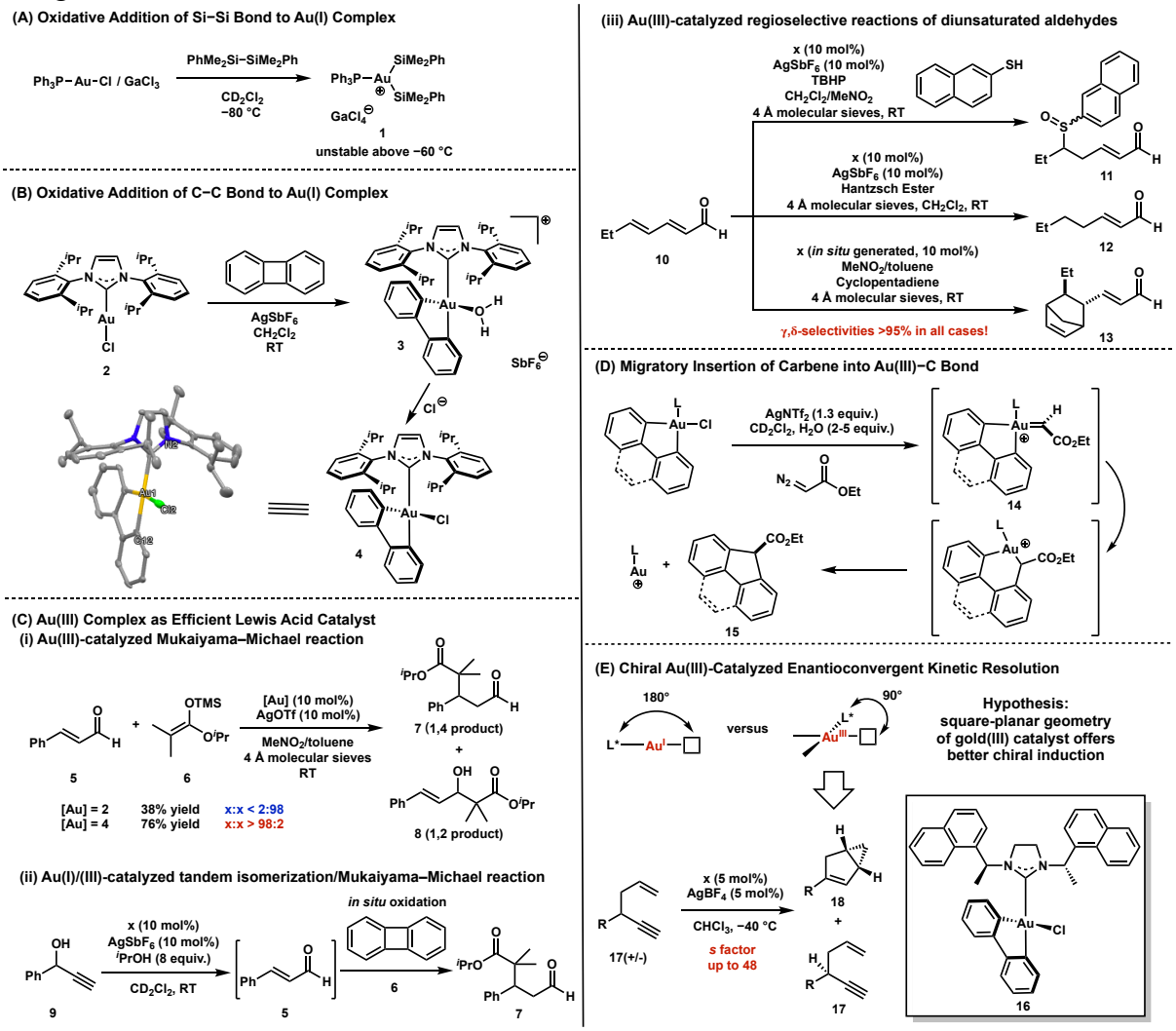


Figure 2.2 Oxidative Addition Reactions Leading to Stable Au(III) Catalysts. (A) Oxidative addition of a Si−Si bond to a Au(I) complex; (B) Oxidative addition of a C−C bond to a Au(I) complex; (C) Au(III) complexes as efficient Lewis acid catalysts, (i) a Au(III)-catalyzed Mukaiyama–Michael reaction, (ii) a Au(I)/(III)-catalyzed tandem isomerization/Mukaiyama–Michael reaction, and (iii) Au(III)-catalyzed regioselective reactions of unsaturated aldehydes; (D) migratory insertion of a carbene into a Au(III)−C bond; and (E) chiral Au(III)-catalyzed enantioconvergent kinetic resolution.

Strong external oxidants (such as I(III) compounds and $[X]^+$ reagents, X = halogen) are usually required to access Au(III) complexes or intermediates from Au(I) species.[17–21] Oxidative addition under milder conditions may lead to broader scope and utilities of the resulting Au(III) complexes. In 2013, Amgoune, Bourissou, and coworkers reported that cationic phosphine Au(I) complexes underwent oxidative additions of disilanes at −80 °C.[22] The ensuing Au(III) complex **1** was characterized by NMR spectroscopy; however, it was unstable even at low temperatures (−80 to −60 °C) (Figure 2.2A).

In 2015, Toste and coworkers reported oxidative addition of the strained C−C bond in biphenylene to a cationic NHC (N-heterocyclic carbene) Au(I) complex **2** at room temperature (Figure 2.2B).[23] The resulting cationic NHC biphenyl-Au(III) complex **3** was air- and moisture-stable. An X-ray structure of the corresponding Au(III) chloride complex **4** indicated a Cs-symmetric distorted square-planar geometry.

Upon chloride abstraction, **4** was also found to act as a Lewis acid catalyst. This feature is especially valuable since the number of stable and tunable of Au(III) catalysts was limited compared to their Au(I) counterparts. Up to this point, most Au(III)-catalyzed reactions employed Au(III) salts, or it's ligated forms, as a catalyst or precatalyst.[24–26] Moreover, many putative Au(III) precatalysts undergo facile reduction to Au(I) or Au(0) species in the presence of other electron-rich reagents.[27–29] Stable, well-defined and yet catalytically active Au(III) catalysts remain rare.

The cationic biphenylene-derived Au(III) complex catalyzed a Mukaiyama–Michael reaction of **5** and **6** with excellent 1,4-selectivity, in stark contrast to the high 1,2-selectivity rendered by corresponding cationic Au(I) catalyst (Figure 2.2C,i). The mild conditions of the oxidative addition of biphenylene allowed the in-situ oxidation of a Au(I) catalyst, leading to a tandem isomerization/Mukaiyama–Michael reaction (Figure 2.2C,ii). Excellent remote selectivities were observed for reactions with α,β,γ,δ-unsaturated aldehyde **10**: 1,6-addition/oxidation of naphthalene thiol, γ,δ-reduction by Hantzsch ester, and γ,δ-Diels-Alder addition with cyclopentadiene (Figure 2.2C,iii). The remote selectivities were attributed to the sterically hindered binding pocket of the complex. The potential reductive elimination of biphenyl ligand from this Au(III) catalyst was recently addressed by incorporation into metal-organic frameworks.[30] The activity and stability of this Au(III) catalyst across various reaction conditions (oxidative, reductive conditions) provides a promising platform to enable new catalytic reactions with new selectivities, and thus invites further investigation.

In 2017, Toste and coworkers demonstrated that cationic ligand-supported biphenyl- or 4,5-phenanthryl-Au(III) carbene complexes **14** underwent sequential migratory insertions/reductive eliminations at temperatures ≥ −40 °C (Figure 2.2D).[31] The effects of spectator ligands and counter anions on the migratory insertion yields were systematically studied. While catalytic processes involving bond-forming migratory insertion at gold remain rare, this work paves the way for Au(III)-catalyzed transformation involving the elementary step such as carbene polymerization reactions. Moreover, it highlights the challenge of circumventing migratory insertion as a side reaction when developing Au(III)-catalyzed reaction involving a carbene intermediate in the future.

Another inherent advantage of this type of Au(III) complex in asymmetric catalysis is that, compared to its Au(I) counterpart, the square-planar geometry can more effectively transmit the chiral information from the ancillary ligand on the reaction site.[32–37] It has long been postulated that the linear geometry of Au(I) complexes renders the chiral induction less favorable (Figure 2.2E). Indeed, this principle was validated by Toste and cowokers.[36] A series of chiral NHC-supported biphenyl-Au(III) complexes were synthesized and employed as catalysts for the

cycloisomerization reaction of racemic 1,5-enyne **17** resulting in an enantioconvergent kinetic resolution with *s*-factors up to 48 (Figure 2.2E). Using the corresponding chiral NHC Au(I) catalyst afforded the product with no ee (enantiomeric excess), which supported the aforementioned hypothesis that square-planar Au(III) catalysts can be superior in asymmetric catalysis. More recently, chiral NHC(biphenyl) Au(III)-catalyzed enantioselective *γ,δ*-Diels-Alder reaction of 2,4-dienals was also reported.[38]

Ligand design is an attractive approach to tune the reactivities of transition-metal complexes.[13,15] Several ligand designs have emerged over the years to facilitate the oxidative addition to Au(I) complexes, namely the use of bimetallic Au(I) complexes, the use of Au(I) complexes chelated by small bite angle bidentate ligands, and the use of P,N-hemilabile bidentate ligand-supported Au(I) complexes. Some of the strategies have resulted in cross-coupling reactivities with stoichiometric or catalytic amounts of gold complexes.

The two-electron oxidation of bimetallic complexes has a lower barrier relative to a two-electron oxidation at a single metal center through electronic cooperation. Fackler and coworkers reported the oxidation of bimetallic Au(I) complexes by oxidants that are not reactive towards mononuclear Au(I) complexes.[39] More recently, Goddard, Toste, and coworkers conducted electrochemical and computational studies that indicated a reduced oxidation potential of bimetallic Au(I) species compared to that of mononuclear Au(I) complexes.[40]

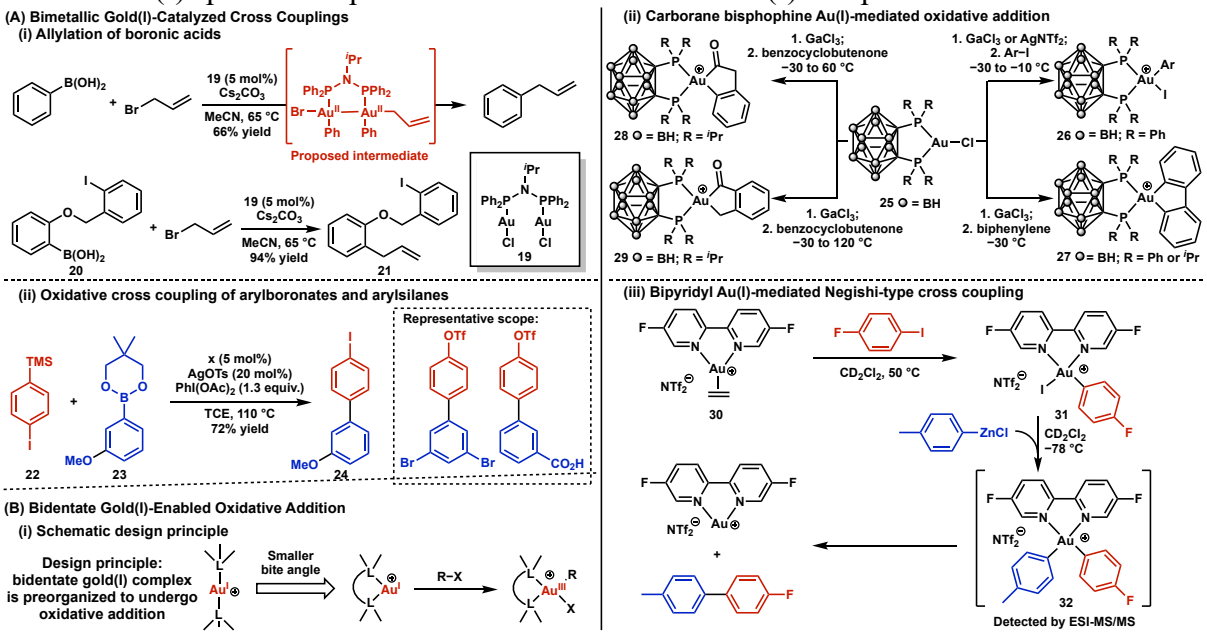


Figure 2.3 Ligand Designs to Facilitate Oxidative Addition to Au(I) Complexes Part 1. (A) Bimetallic Au(I)-catalyzed cross couplings, (i) allylation of boronic acids, (ii) oxidative cross coupling of arylboronates and arylsilanes; and (B) Bidentate Au(I)-enabled oxidative addition, (i) schematic design principle, (ii) carborane bisphophine Au(I)-mediated oxidative addition, and (iii) Bipyridyl Au(I)-mediated Negishi-type cross coupling.

Inspired by these previous reports, Toste and coworkers presented a Au(I)-catalyzed allylation of aryl boronic acids (Figure 2.3A,i).[41] A bis(diphenylphosphino)amine ligand supported Au(I) complex **19** was identified as the optimal catalyst whereas mononuclear Au(I) catalysts led to much lower yields. The accelerated oxidative addition to bimetallic gold complexes was suggested to account for the higher yields. The method is orthogonal to traditional palladium-

catalyzed cross-coupling reactions: substrate **20** containing boronic acid and aryl iodide was subjected to the allylation condition and **21** was obtained in 94% yield with no competitive cyclization. This work demonstrated how stoichiometric transformations and mechanistic insights can inspire the design of a new catalytic system with unique selectivity.

More recently, Xie and coworkers demonstrated that the same bimetallic Au(I) complex catalyzed a highly efficient oxidative cross-coupling reaction of arylboronate **22** and arylsilane **23** to furnish **24** (Figure 2.3A,ii).[42] In comparison, monomeric Au(I) catalysts showed extremely low activities despite their successes in other reported oxidative biaryl couplings.[43–49] Good-to-excellent yields were obtained for a wide range of substrates by employing this bimetallic Au(I) catalyst. Aryl halides and aryl triflates were untouched in the reaction, which again showed unusual selectivity and functional group tolerance of gold catalysis compared to traditional cross-coupling catalysts.

A strategy using bidentate ligands with small bite angles was also postulated to facilitate oxidative addition to Au(I). It was previously demonstrated that distorting the L-M-L (M = Pd or Pt) bond angle raises the HOMO energy of the transition-metal complex, preorganizing them towards the square-planar geometry of the oxidative addition products (Figure 2.3B,i).[50] Amgoune, Bourissou, and coworkers demonstrated that this design also promoted oxidative addition to Au(I) complexes. Carborane diphosphino-chelated Au(I) triflimidate (NTf_2^-) complexes (PAuP bite angles = 90–100°) were treated with various aryl iodides and oxidative addition products **26** was observed under mild conditions (Figure 2.3B,ii).[51] The same groups later reported oxidative addition of strained C−C bonds in benzocyclobutenone and biphenylene to a similar carborane diphosphino-chelated Au(I) complex.[52]

Applying a similar strategy, McGrady, Bower, Russell, and coworkers recently demonstrated that a 2,2′-bipyridine (bipy) chelated Au(I) ethylene complex **30** participated in sequential oxidative addition, transmetalation, and reductive elimination to furnish biaryl coupling products (Figure 2.3B,iii).[53] The cationic (κ^2-bipy) biaryl Au(III) intermediate **32** was detected by mass spectrometry. Furthermore, this study may provide insights into the mechanism of previous examples of gold-catalyzed redox processes that were assisted by bipy-type ligands and inspire future developments in this arena.[54–57] More recently, Bower, Russell, and coworkers showed similar redox cycles of alkenyl and alkynyl iodides.[58]

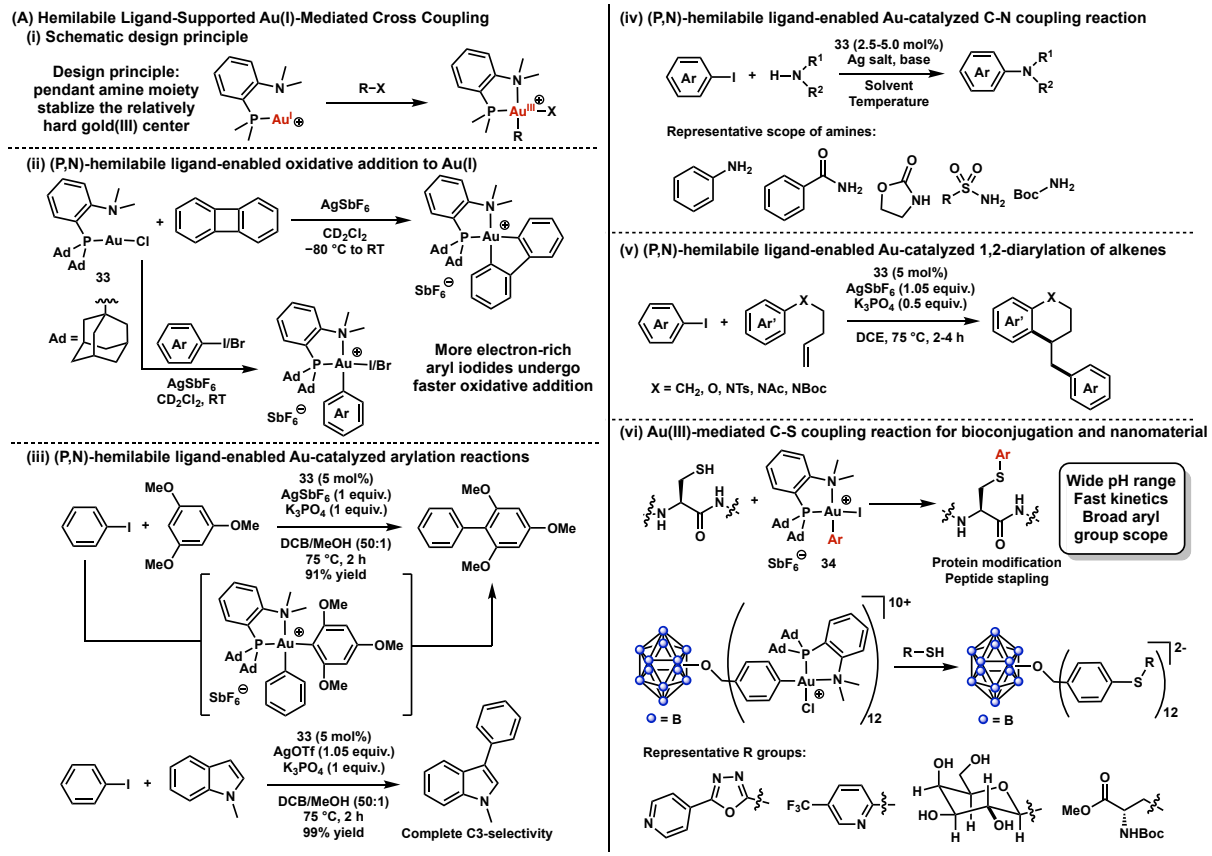


Figure 2.4 Ligand Designs to Facilitate Oxidative Addition to Au(I) Complexes Part 2. (A) Hemilabile ligand-supported Au(I)-mediated cross coupling, (i) schematic design principle, (ii) (P,N)-hemilabile ligand-enabled oxidative addition to Au(I), (iii) (P,N)-hemilabile ligand-enabled Au-catalyzed arylation reactions, (iv) (P,N)-hemilabile ligand-enabled Au-catalyzed C-N coupling reaction, (v) (P,N)-hemilabile ligand-enabled Au-catalyzed 1,2-diarylation of alkenes, and (vi) Au(III)-mediated C-S coupling reaction for bioconjugation and nanomaterials.

Despite the successes achieved by the chelation strategy, the strong preference of Au(I) to form bis(gold) complexes with most bidentate ligands limited its applicability.[2] To circumvent this limitation, in 2017, Amgoune, Bourissou, and coworkers proposed that hemilabile bidentate ligands could trigger oxidative addition by stabilizing the Au(III) product (Figure 2.4A,i-iii).[59] By employing a hemilabile (P,N) bidentate ligand (Me-Dalphos), the Au(I) complex **33** underwent chloride abstraction followed by oxidative addition of aryl iodides or biphenylene under mild conditions. In the cases of aryl iodides, subsequent iodide abstraction, C-H auration, and reductive elimination afforded biaryl coupling products. A catalytic system was also developed for the C-H arylation of trimethoxybenzene. Several aryl iodides and bromides were successfully coupled under catalytic conditions. Mechanistic studies were detailed in a later publication, along with the C3-arylation of protected indoles (Figure 2.4A, iii).[60] The complete C3-selectivity of this arylation, along with excellent functional group tolerance, rendered a highly useful synthetic method. This concept was further explored by the Bourissou group, as well as Patil and coworkers, to realize C-N coupling reactions of aryl iodides (Figure 2.4A,iv).[61,62] More recently, Patil and coworkers exploited the same Au(III) intermediate to achieve catalytic 1,2-diarylation of alkenes (Figure 2.4A,v).[63]

The Au(III)-mediated arylation reactivity has found applications beyond synthetic organic chemistry. Given the previous examples of Pd(II)-mediated cysteine S−arylation,[64] Maynard, Spokoyny, and coworkers explored similar transformations using Au(III) complexes **34** (Figure 2.4A,vi).[65] An efficient and chemoselective cysteine arylation procedure was developed employing [(Me-DalPhos)AuArCl][SbF_6]. The protocol was further applied to protein-labeling and peptide-stapling. This methodology offered much broader scope of aryl group than previous Au(III)-mediated S-arylation reactions.[66–69] Compared to Pd(II)-mediated cysteine S−arylations, the Au(III)-promoted version was effective in a wider pH range and displayed a faster reaction rate.[70] The mechanism of this methodology was studied later by Zhang and coworkers.[71] More recently, this C-S coupling reactivity was used to construct atomically precise hybrid nanomaterials (Figure 2.4A,vi).[72]

Photochemical conditions can allow access to high-energy intermediates (e.g., radicals) that are difficult to access under mild thermal conditions.[73] Naturally, these conditions been exploited to facilitate the otherwise sluggish oxidative addition to Au(I) complexes. This section covers examples of photoinitiated oxidative addition, photoredox-gold dual catalysis, and photosensitized oxidative addition.

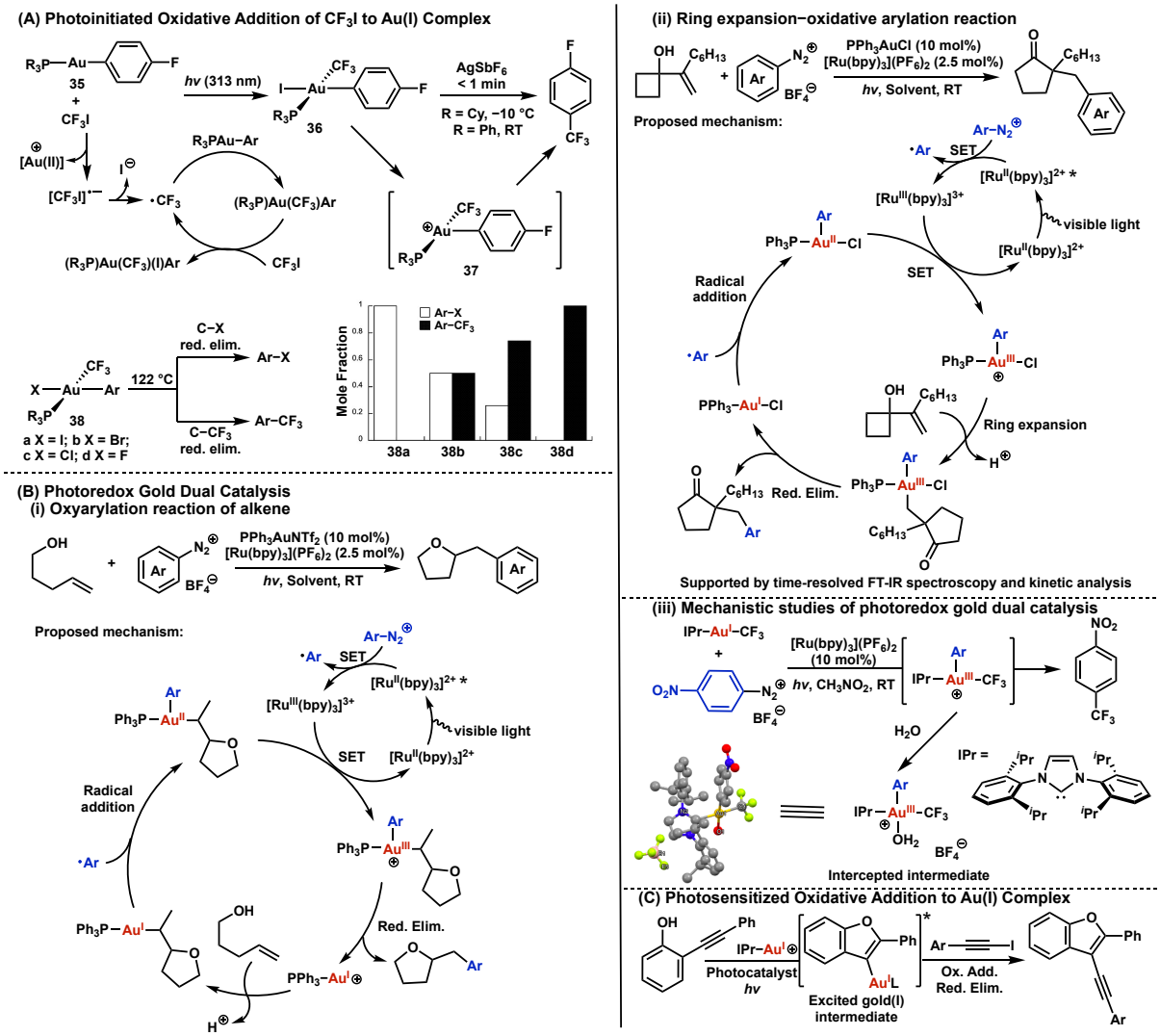


Figure 2.5 Photochemically-Triggered Oxidative Addition to Au(I) Complexes. (A) Photoinitiated oxidative addition of CF_3I to a Au(I) complex; (B) photoredox gold dual catalysis, (i) an oxyarylation reaction of alkene, (ii) ring expansion−oxidative arylation reaction, and (iii) mechanistic studies of photoredox gold dual catalysis; and (C) photosensitized oxidative addition to a Au(I) complex.

In 2014, Toste and coworkers reported photoinitiated oxidative addition of CF_3I to phosphine Au(I) aryl complex **35** (Figure 2.5A).[74] The reaction proceeded through radical chain process from light-promoted excitation of CF_3I. Iodide abstraction from the resulting Au(III) complex **37** led to fast C(aryl)−CF_3 reductive elimination from cationic tricoordinate Au(III) species. A closely related CF_2H-containing complex was later reported by other groups to undergo fast C(aryl)−CF_2H reductive elimination as well.[75] Derived from the iodide-containing complex, a series of Au(III) complexes **38** bearing other halides were synthesized and were found to undergo thermal reductive elimination.[76] Product distributions (C(aryl)−CF_3 versus C(aryl)−X formation, X = halides) were found to depend on the identity of the halide (Figure 2.5A).

Photoredox catalysis has also been combined with transition-metal catalysis to enable novel reactivities.[77] Inspired by the early examples of photoredox-enabled mild oxidative additions to Pd(II) and Cu(I),[78–80] Glorius and Toste independently reported a similar strategy for Au(I) catalysis. Glorius and coworkers demonstrated oxy- and aminoarylation reactions of alkenes (Figure 2.5B,i).[81] Frei, Toste, and coworkers reported a ring expansion−oxidative arylation reaction (Figure 2.5B,ii).[82] In these publications, two different mechanisms were proposed, differing only with regard to the timing of Au(I) intermediate undergoing oxidative addition. Glorius and coworkers proposed a Au(I)-mediated cyclization followed by photoredox-facilitated oxidative addition of the aryldiazonium salt (Figure 2.5B,i), whereas Frei, Toste, and coworkers suggested that photoredox-facilitated oxidative addition of the aryldiazonium salt occurred prior to the ring-expansion (Figure 2.5B,ii). The later mechanism was supported by time-resolved FT-IR spectroscopy and kinetic analysis.

Following these reports, many dual photoredox gold catalytic systems have been discovered. These reactions were reviewed elsewhere and are not elaborated here;[83,84] however, it is worth noting that examples of gold redox catalysis using aryl diazonium salts, without additional photocatalyst, have been reported under either photochemical or thermal conditions.[85–94]

Given the proposed involvement of light-generated radical species in these dual gold-photoredox processes, another general mechanistic question was whether the bond-forming events were reductive eliminations from Au(III) or intermediates. To gain insights into this question, Toste and coworkers recently reported the mechanistic studies of photoredox-initiated arylation of IPrAu(I)−CF_3 and IPrAu(I)−succinimide (Figure 2.5B,iii).[95] Photochemical and electrochemical data, along with crystallographic characterization of key Au(III) intermediates, supported a mechanism involving reductive elimination from Au(III) center as the bond-forming step. This study may also provide mechanistic insights into other metallaphotoredox catalysis.

Most recently, a Au(I)-catalyzed alkynylative cyclization reaction system using photocatalysts was disclosed (Figure 2.5C). Instead of the aforementioned electron transfer mechanism for aryl diazonium salts, the authors proposed an energy transfer mechanism based on experimental and theoretical evidence.[96] It is worth noting that another alkynylative cyclization was reported by Hashmi and coworkers around same time.[97] Direct oxidative addition of bromoalkynes to Au(I) intermediates was proposed without invoking photosensitization. Further studies will help elucidate the role and principle of photosensitization in these systems.

Many of the reductive elimination reactions presented above are subsequent steps to an oxidative addition. Other examples of reductive elimination reactions of Au(III) complexes made from more conventional oxidation-transmetalation routes are discussed as following.

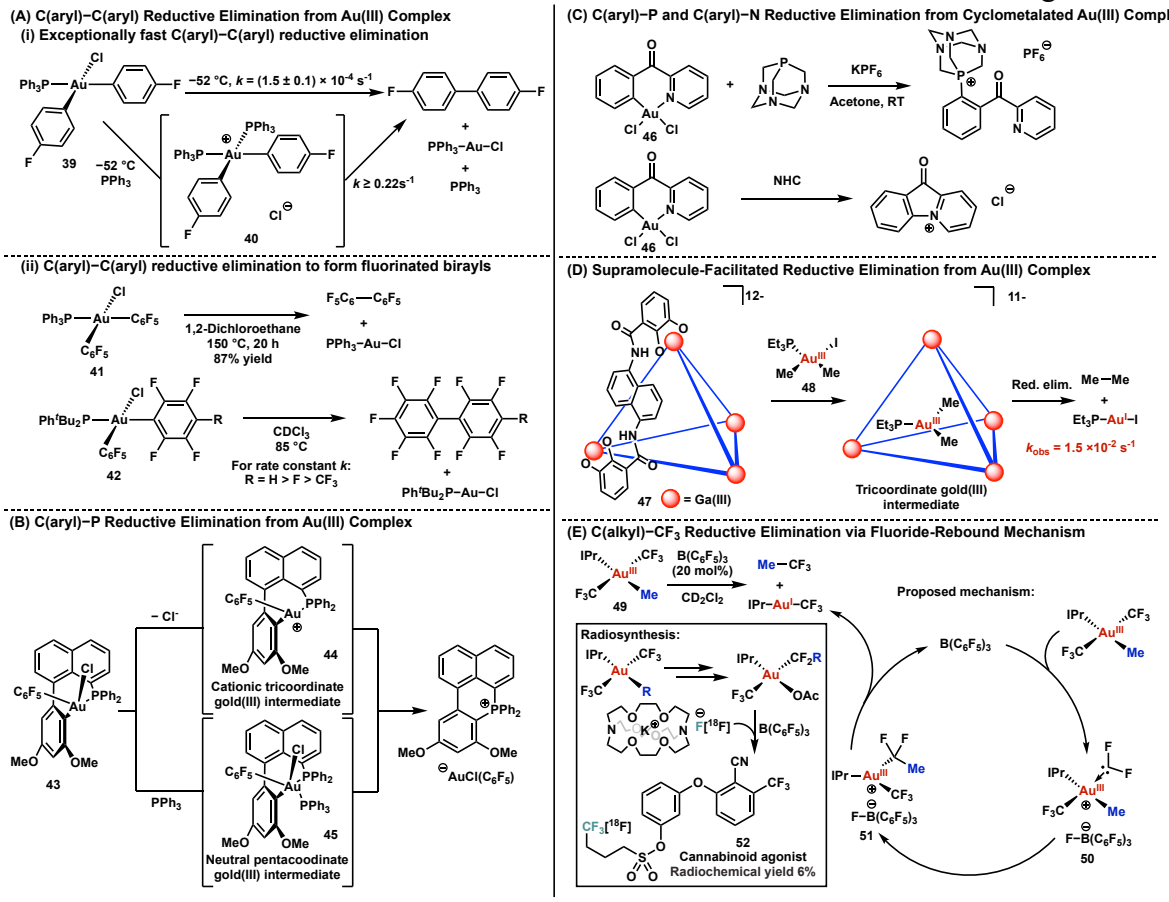


Figure 2.6 Other Reductive Elimination Reactions from Au(III) Centers. (A) C(aryl)−C(aryl) reductive elimination from a Au(III) complex, (i) Exceptionally fast C(aryl)−C(aryl) reductive elimination, and (ii) C(aryl)−C(aryl) reductive elimination to form fluorinated birayls; (B) C(aryl)−P reductive elimination from a Au(III) complex; (C) C(aryl)−P and C(aryl)−N reductive elimination from cyclometalated Au(III) complexes; (D) supramolecule-facilitated reductive elimination from a Au(III) complex; and (E) C(alkyl)−CF_3 reductive elimination via a fluoride-rebound mechanism.

In 2014, Toste and coworkers reported that very rapid C(aryl)−C(aryl) reductive elimination from **39** occurred even below −20°C (Figure 2.6A,i).[98] Kinetic studies indicated a unimolecular pathway with one of the fastest measured rates of transition metal-mediated C−C reductive elimination. Surprisingly, a significant rate enhancement was observed in the presence of excess triphenylphosphine, while adding NBu_4Cl had no impact on the rate. This implied a different mechanism from the "phosphine dissociation mechanism" proposed by Kochi for C(alkyl)−C(alkyl) reductive elimination.[99] A mechanism was proposed to account for the rate acceleration by extra phosphine: a transient cationic $(Ph_3P)_2$bis(aryl)Au(III) specie **40** was formed and rendered faster reductive elimination. More recently, Rocchigiani, Budzelaar, Bochmann, and coworkers also reported fast C(aryl)−C(aryl) reductive elimination of Au(III) complexes.[100]

Around the same time in 2014, the group of Nevado studied a related Au(III) complex **41** and reported an extremely slow $C_6F_5-C_6F_5$ reductive elimination even under elevated temperature (150°C, 20 h, 87% yield) (Figure 2.6A,ii).[101] More recently, Lan, Shen, and coworkers conducted systematic studies on a series of phosphine biarylAu(III) chloride complexes **42**.[102] While the electronic properties of ligands had a trivial effect on the reductive elimination rate, more electron-deficient arenes underwent slower reductive elimination (Figure 2.6A,ii). These reports were consistent with the computational studies by Datta and coworkers.[103]

In the course of studying cis-[(R_3P)(Aryl)$AuCl_2$], the precursor of **39** described above, Toste and coworkers reported that facile C(aryl)−P reductive elimination ensued from a related Au(III) complex **43** upon heating/addition of $AgSbF_6$ or addition of nucleophiles (Figure 2.6B).[104] A cationic tricoordinate Au(III) intermediate **44** and a neutral pentacoodinate Au(III) specie **45** were proposed, respectively, as intermediates in these reductive elimination reactions. This study disclosed a decomposition pathway for phosphine-supported Au(III) catalysts, which was valuable to future Au(III) catalyst development. A recent study from Barone, Casini, and coworkers also showed C(aryl)−P coupling from a cyclometalated Au(III) complex **46** (Figure 2.6C).[105] The same complex was reported to undergo C(aryl)−N reductive elimination upon treatment of NHCs (Figure 2.6C).[106]

As noted above, reductive eliminations can be triggered by halide abstraction from neutral Au(III) complexes. Motivated by the previous work that halide dissociation was promoted by a highly anionic self-assembled tetrahedral host **47**,[107] Bergman, Raymond, Toste, and coworkers envisioned the host catalyzing the reductive elimination from Au(III) center.[108,109] The strategy was applied to complex **48**. Upon addition of host **47**, C(alkyl)− C(alkyl) reductive elimination was observed with a 1.9×10^7-times faster rate compared to the uncatalyzed reaction (Figure 2.6D). Notably, subsequent computational studies from several research groups unveiled the critical role of electrostatic interaction between the supramolecular assembly and the cationic Au(III) complex in facilitating the reductive elimination.[110–112] Since the development of alkyl-alkyl cross-coupling processes is hampered, in part, by the slow C(alkyl)−C(alkyl) reductive elimination,[15] the successful implementation of the supramolecular assembly-catalyzed reductive elimination provided new strategy to resolving this challenging problem.

In 2017, O'Neil, Toste, and coworkers discovered a C(alkyl)−CF_3 reductive elimination reaction which proceeded via a fluoride-rebound mechanism (Figure 2.6E). Trifluoromethylated product, trifluoroethane, was first obtained upon treatment of complex **49** with $B(C_6F_5)_3$. Mechanistic investigation pointed to a pathway in which fluoride abstraction from **49** formed a cationic difluorocarbene Au(III) complex **50**, which underwent carbon-carbon bond-forming migratory insertion of methyl group into difluorocarbene. Final recombination of fluoride to **51** furnished the final product. This understanding established the possibility of ^{18}F-incorporation into the product with external [^{18}F] fluoride addition. Indeed, a protocol was developed for synthesizing ^{18}F-radiolabeled aliphatic CF_3-containing compounds including a cannabinoid agonist **52**.[113]

As described above, many exciting details about the gold redox events were unfurled in the last eight years. Retrospectively, detailed stoichiometric studies and mechanistic investigation were critical to developing catalytic transformations, as well as applications proceeded of gold-promoted transformations aimed at biology- or materials science. The importance of serendipity should also be marked as many of the discoveries came unexpectedly.

It is becoming increasingly apparent that this field of research has the potential to not just replicate that of palladium or nickel cross-coupling catalysis; but instead can offer milder reaction

conditions, complementary substrate scope, and unprecedented reactivities or selectivities. To reach this potential, many important questions and opportunities remain.

First, the utility of stable Au(III) complexes arising for the oxidative addition to Au(I) remains underexplored. Taking the biphenylene-supported Au(III) complex as an example, studies need to be carried out to understand the structural influence of both ancillary ligands (NHC ligand and substituted biphenylene) on the rate of oxidative addition. Moreover, the discovery of other thermodynamically favored oxidative additions to Au(I) that produce stable Au(III) complexes can lead to a library of Au(III) complexes, creating a larger chemical space for exploration. New catalysts in this area can reveal new opportunities in asymmetric catalysis, especially in cases where remote regioselectivities and high enantioselectivities are desired.

In addition to ligands that enable stable Au(III) catalysts, opportunities exist to discover new strategies that allow for facile entry into Au(I)/Au(III) catalytic cycles. In this context, the P,N hemilabile ligands provide inspire the search for additional hemilabile ligands that can be investigated to increase reactivity, and provide tunability, using this platform. Discoveries in this area will likely lead to coupling reactivities may be complimentary to existing transition metal-catalyzed processes or further provide opportunities in chemical synthesis, biology, and materials science.

Much remains to be learned about migratory insertion processes at gold centers. For example, studies aimed at further understanding of carbene migratory insertion at gold can inform how ligands can been chosen to either disfavor migratory insertion to avoid catalyst decomposition or support this step and lead to polymerization reactivity. As a specific example, ligand effects on Au(III)-mediated C(alkyl)−CF_3 bond formation, via migratory insertion, can result in improved radiochemical yield and specific activity for ^{18}F-incorporation. Along these lines, a bonding model for Au(III) carbene complexes, as a comparison to Au(I) version,[114–116] remains to be established.

Similarly, while photochemical gold catalysis also has enormous potential, much remains to be explored and developed. For example, photoredox gold-catalyzed aryl amination and trifluoromethylation have not been realized despite all the elementary steps demonstrated. Finding reaction conditions in which transmetalation, reductive elimination and other elementary processes at gold are compatible with photoredox catalysis, is likely to reveal many new opportunities for reaction development. Additionally, outside of combined photoredox/gold catalysis, additional examples of photosensitized oxidative addition must be discovered in order to establish this reaction manifold as design principle for gold-only catalytic reactivity. Lastly, metallaelectrochemistry has experienced a renaissance over the past several years.[117–119] Its application to facilitate gold redox chemistry has also started to emerge in the literature.[120] With more detailed mechanistic studies, the development of new electro/gold catalysis is on the horizon.

2.1.2 Anion-Binding Catalysis

As discussed in the previous section, cationic Au(I) and Au(III) complexes are often identified as active catalysts or intermediates in homogeneous gold chemistry. Silver(I) salts such as $AgSbF_6$, $AgNTf_2$, AgOTf, and $AgBF_4$ are commonly used to abstract halides from gold and generate corresponding cationic gold complexes. Alternative strategies to generate cationic gold complexes without using silver salts can be valuable as background/side reactions can be promoted by silver(I).[121-123]

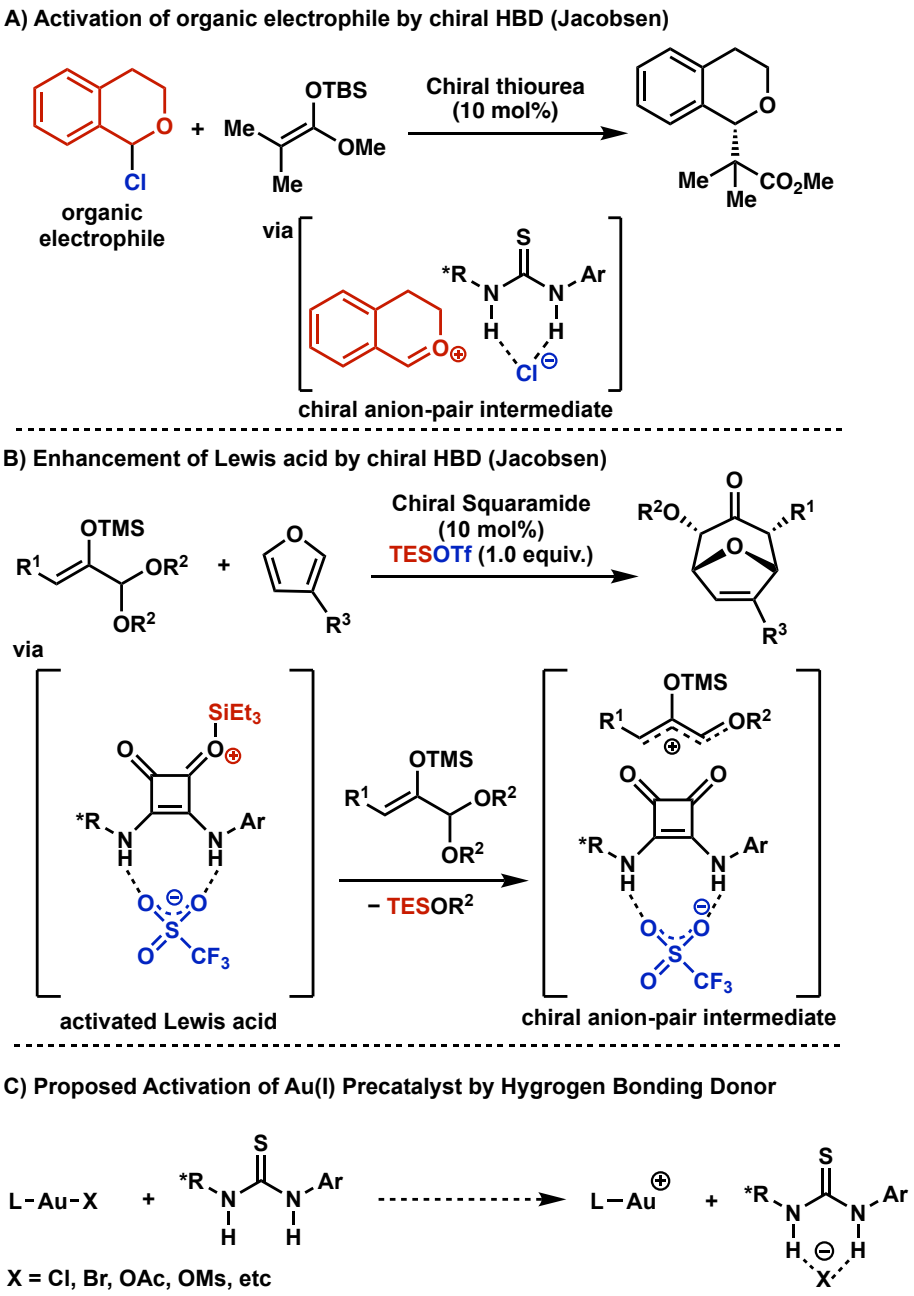


Figure 2.7 Strategies of asymmetric anion-binding catalysis. (A) Representative example of enhanced electrophilicity of organic substrates by chiral HBDs; (B) representative example of enhanced reactivity of silicon-based Lewis acids by chiral HBDs; (C) proposed activation of Au(I) precatalyst by hygrogen bonding donor.

In the field of organocatalysis, anion-binding catalysis has garnered interest in the past two decades as a method to generate and control the reactivities or selectivities of cationic organic intermediates.[124] The transformations are most commonly catalyzed by chiral dual hydrogen-bond donors (HBDs), such as ureas, thioureas, and squaramides. Mechanistically, HBDs assist the ionization of labile carbon-heteroatom single bonds to generate chiral ion-pair electrophilic intermediates followed by nucleophilic substitution under enantiocontrol (Figure 2.7A). More

recently, this principle has also been applied to enhance the reactivity of silicon-based Lewis acids or Brønsted acid (HBr) (Figure 2.7B).[125,126] Despite the significant progress made to activate organic substrates or stoichiometric reagents, the anion-binding strategy is still underexplored in the activation of catalysts, especially transition metal catalysts. It is hypothesized that chiral HBDs can bind the X-type ligand from neutral transition metal complexes and generate the chiral ion-paired cationic complexes (Figure 2.7C). This strategy is potentially powerful as a wide range of catalytically active transition metal complexes are in their cationic forms.

2.2 Results and Discussion

2.2.1 Computational Studies on Thermodynamics of Chloride Binding from Gold(I)

One possible caveat of this dual catalytic manifold is coordination of hydrogen bonding motifs, such as a thiourea, to the gold center, which can inhibit the catalytic activity. I began with computational studies to probe the enthalpy of: 1) the anion-binding event to gold(I) and 2) the coordination between the hydrogen bond donor and the cationic gold(I) species. Specifically, the four possible states of equilibrium are shown in Figure 2.8. Gaussian 16 was employed to optimize the geometry and carry out single-point electronic energy calculation. Three factors were examined combinatorically: ligand, hydrogen bond donor structure and solvent. Truncated ligands and hydrogen bond donors were used in the computation for the sake of time.

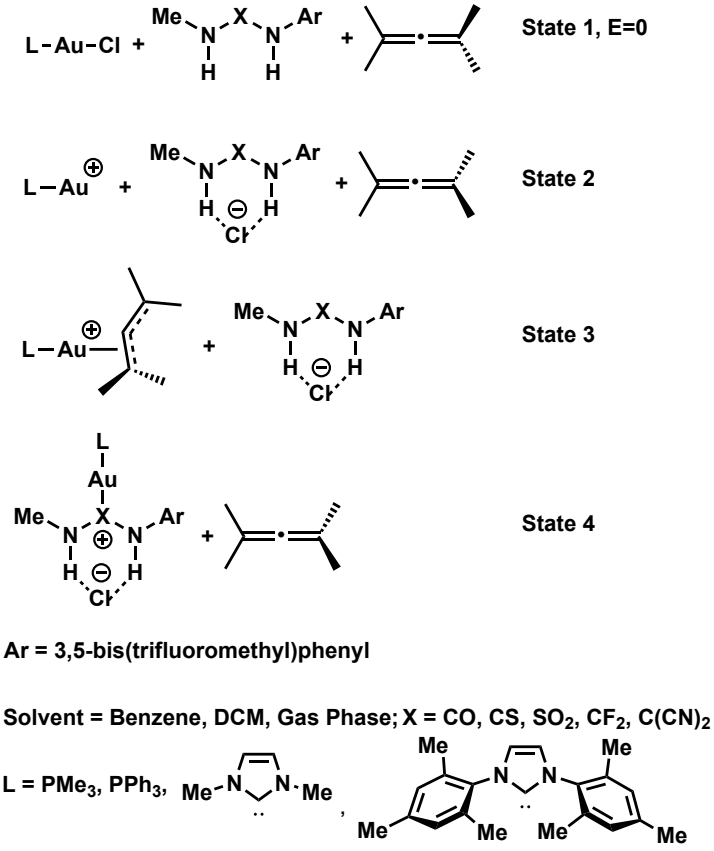


Figure 2.8 Possible states of equilibrium under computational study.

Because of the synthetic difficulty in accessing urea analogs for which X = CF_2, $C(CN)_2$, the corresponding results will not be presented here. Additionally, state 2 containing free cationic gold(I) is too high in energy (30-101 kcal/mol higher than state 1) and is thus omitted here. The

ligand effect is relatively small compared to the effects of solvent and hydrogen bond donor structure, so only the computational data of Ph_3PAuCl will be presented below (for omitted data, see the Supporting Information).

Table 2.1 Influence of H-bonding moiety structure and solvent on relative enthalpy of States 3 and 4 (L = PPh_3)[a]

X	Solvent	E(State 3) (kcal/mol)	E(State 4) (kcal/mol)
C=S	Benzene	15.0	−22.2
C=S	DCM	−1.2	−21.1
C=S	Gas Phase	46.5	−26.5
C=O	Benzene	17.1	−9.7
C=O	DCM	−0.3	−8.1
C=O	Gas Phase	50.2	−10.5
SO_2	Benzene	18.8	−5.9
SO_2	DCM	1.7	0.2
SO_2	Gas Phase	50.6	−2.5

[a]Geometry optimization: M06/6-31g(d,p),+SDD with SDD ECP; Single point energy: M06/6-311g++(d,p)+SDD with SDD ECP; Solvent correction: PCM.

The effects of hydrogen bond donor structure and solvent on relative enthalpy of state 3 and 4 are shown in Table 2.1 (enthalpy of state 1 is defined as 0). It can be concluded that:

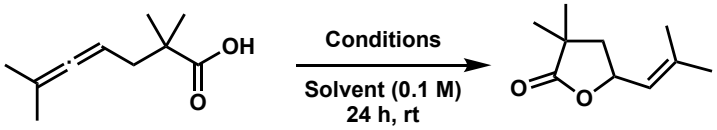
1) Solvent is the most decisive factor determining energies of state 3, which originates from the drastic difference of hydrogen bonding strength in different solvents. DCM is a better solvent than benzene for the anion binding event. In DCM, when X is C=S or C=O, state 3 is lower in energy than state 1. However, if the entropy is taken into account (with an estimation of -30 cal/(mol•K) for translational entropy loss of one molecule), ΔG becomes positive and abstraction of chloride from gold becomes unlikely.

2) The identity of the hydrogen bonding moiety has the most influence on the energies of state 4. With the thiourea, the much lower energies of state 4 compared to those of state 3 agree with the aforementioned speculation that the coordination of sulfur to gold might hamper the effectiveness of this anion-binding strategy. In contrast, the urea is not as coordinating. But the energies of state 4 are still lower than those of state 3. Furthermore, sulfonamides are even less coordinating.

Previous research (unpublished) in our group has shown that thioureas inhibit reactions catalyzed by cationic gold(I), which is consistent with computational studies shown here. Although the computational studies predict the chloride abstraction from gold(I) to be difficult, it was determined that it was still worth verifying them experimentally. Additionally, the sulfonamide is predicted to have comparable binding affinity to the chloride and much less coordinating than thiourea and urea. Given it has not been reported in anion binding catalysis, it would be interesting to explore its effect on a gold(I) precatalyst.

2.2.2 Studies on Activation of Gold(I) and Gold(III) Precatalysts in Lactonization, Conia-Ene and Enyne Isomerization Reactions

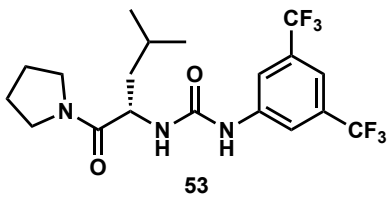
Table 2.2 Studies of LAu(I)-Cl activation by urea and squaramide in lactonization reaction



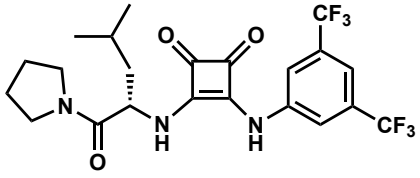
55 56

Entry	Solvent	Conditions	Yield (%)[a]
1	DCM-d_2	5 mol% IPrAuCl	9 (29)[b]
2	DCM-d_2	5 mol% IPrAuCl 3 equiv. NEt_4Cl	0
3	DCM-d_2	5 mol% IPrAuCl 5 mol% **53** or **54**	10 (31)[b]
4	DCM-d_2	5 mol% Ph_3PAuCl	0
5	DCM-d_2	5 mol% Ph_3PAuCl 5 mol% **53** or **54**	0
6	Toluene-d_8	5 mol% Ph_3PAuCl 5 mol% **53** or **54**	0
7	Toluene-d_8	5 mol% IPrAuCl 5 mol% **53** or **54**	0
8	MTBE	5 mol% Ph_3PAuCl 5 mol% **53** or **54**	0
9	MTBE	5 mol% IPrAuCl 5 mol% **53** or **54**	0
10	Cyclohexane	5 mol% Ph_3PAuCl 5 mol% **53** or **54**	0
11	Cyclohexane	5 mol% IPrAuCl 5 mol% **53** or **54**	0

[a]Derived by product to reactant ratio from ^{1}H-NMR. [b]Reaction time: 3 d.



53



54

With several hydrogen bond donors in hand, I set off to examine their capability of activating gold complexes by conducting reactivity-based studies. The first model reaction tested was a gold(I)-catalyzed lactonization reaction of **55**.[127] IPrAuCl was found to catalyze a background reaction, giving **56** in 9% yield in 24 h (Table 2.2, entry 1). But when a large excess of NEt_4Cl was added, the reaction was shut down (Table 2.2, entry 2), which suggests that the background reaction was catalyzed by small amounts of gold(I) cation generated by IPrAuCl ionization. This observation was encouraging because hydrogen bond donor should be able to shift

the equilibrium toward the ionized catalyst and accelerate the reaction. Unfortunately, only background reactivity was observed in the presence of **53** or **54** (Table 2.2, entry 3). The absence of acceleration upon adding hydrogen bond donors might originate from their interaction with the carboxylic acid group of the substrate. Since the substrate was the predominant species in solution, the resting state of the urea or squaramide would be the complex with substrate, which precluded the activation of gold(I) chloride. To validate this hypothesis, an NMR study was conducted: when **55** was mixed with **53** or **54**, the ^{1}H-NMR signal of allylic hydrogens shifted upfield and its splitting pattern also changed (Figure 2.9). The changes in splitting pattern were indicative of the protons becoming diastereotopic, which implied a hydrogen bonding interaction between **55** and **53** or **54**.

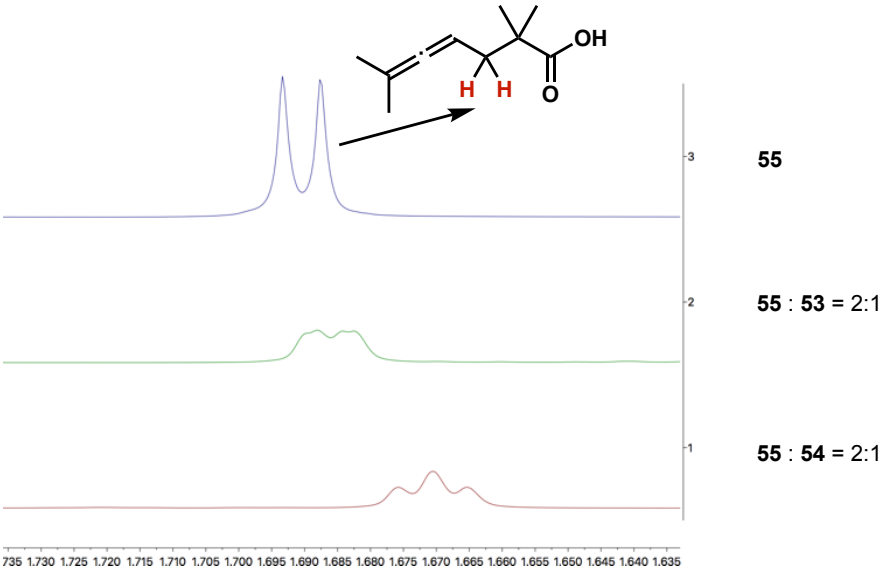
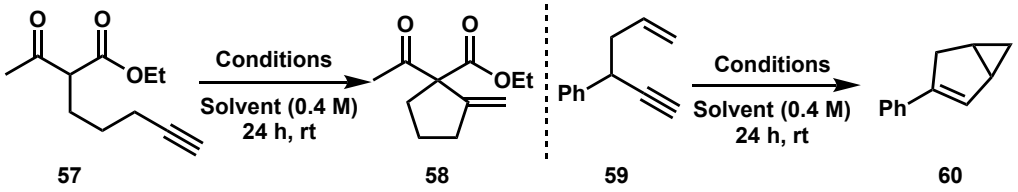


Figure 2.9 ^{1}H-NMR studies of interaction between **55** and **53**, **55** and **54**

Any other combinations of IPrAuCl/Ph_3PAuCl and **53**/**54** in DCM-d_2, toluene-d_8, MTBE and cyclohexane (the most commonly used solvents in either gold(I) catalysis or anion binding catalysis) led to no lactonization product (Table 2.2, entries 4-15). But given the interaction between **55** and **53** or **54**, these results were not sufficient to draw any conclusions.

Table 2.3 Studies of Au(I)-Cl activation by urea and squaramide in Conia-Ene Reaction and enyne isomerization reaction



57 58 59 60

Conditions (combinatorial):

5 mol% [Au(I)]		5 mol% H-Bonding Donor		Solvent
Ph_3PAuCl	+	**53**	+	$DCM\text{-}d_2$
IPrAuCl		**54**		$Toluene\text{-}d_8$
				MTBE
				$MeCN\text{-}d_3$
				Cyclohexane

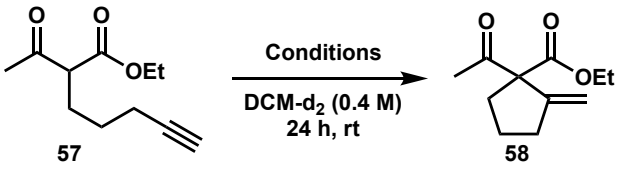
No product was observed by ^{1}H-NMR in any case.

To avoid substrates bearing carboxylic acid group, the Conia-ene reaction of **57**and enyne isomerization of **59** were studied as model reactions.[128,129] After combinatorial screening of gold(I) chloride precatalysts, hydrogen bond donors and solvents, no product was observed in any case (Table 2.3). This result suggested that urea and squaramide cannot abstract chloride from gold(I) precatalyst to enable catalytic reactivity.

At this point, gold(I) precatalysts containing other X-type ligands were subjected to both reaction conditions in $DCM\text{-}d_2$ with hydrogen bond donors. In both reactions, $Ph_3PAuOAc$ and $Ph_3PAuOBz$ were inactive with or without hydrogen bond donors (Table 2.4, entries 1-6; Table 2.5, entries 1-6). This result is consistent with the calculation reported by Xu *et al* that gold(I) affinity of carboxylates are even stronger than that of chloride.[17] Background reactivity was observed with $Ph_3PAuOMs$ and (Table 2.4, entries 7 and 10; Table 2.5, entries 7 and 10), but adding **53** or **54** gave higher yields than the background reactions (Table 2.4, entries 8, 9, 11, 12; Table 2.5, entries 8, 9, 11, 12).

The solvent effect of $Ph_3PAuOTs$ activation was then studied in the enyne isomerization of **59**. No reactivity was observed in MTBE and $Toluene\text{-}d_8$ (Table 2.6, entries 1-6). In both $MeCN\text{-}d_3$ and $MeNO_2\text{-}d_3$, higher yields were obtained upon adding **54** (Table 2.6, entries 7 and 9, 10 and 12). The reason why addition of **53** decreased yield in these two solvents remains unclear. One possible explanation was that in these solvents, the urea-tosylate complex was more coordinating than the tosylate itself.

Table 2.4 Studies of $Ph_3PAu(I)$ carboxylates and sulfonates activation by urea and squaramide in Conia-Ene Reaction

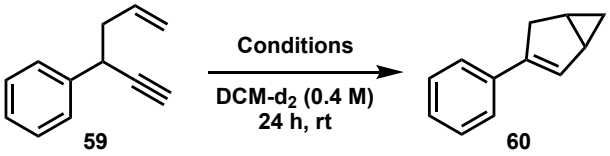


57 58

Entry	Conditions	Yield (%)[a]
1	5 mol% $Ph_3PAuOAc$	0
2	5 mol% $Ph_3PAuOAc$ 5 mol% **53**	0
3	5 mol% $Ph_3PAuOAc$ 5 mol% **54**	0
4	5 mol% $Ph_3PAuOBz$	0
5	5 mol% $Ph_3PAuOBz$ 5 mol% **53**	0
6	5 mol% $Ph_3PAuOBz$ 5 mol% **54**	0
7	5 mol% $Ph_3PAuOMs$	3
8	5 mol% $Ph_3PAuOMs$ 5 mol% **53**	9
9	5 mol% $Ph_3PAuOMs$ 5 mol% **54**	23
10	5 mol% $Ph_3PAuOTs$	10
11	5 mol% $Ph_3PAuOTs$ 5 mol% **53**	19
12	5 mol% $Ph_3PAuOTs$ 5 mol% **54**	30

[a]Derived by product to reactant ratio from ^{1}H-NMR.

Table 2.5 Studies of $Ph_3PAu(I)$ carboxylates and sulfonates activation by urea and squaramide in enyne isomerization reaction

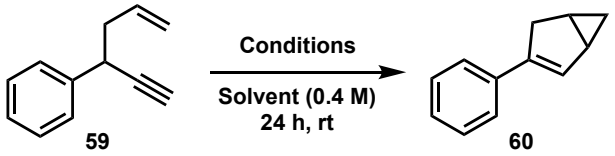


59 **60**

Entry	Conditions	Yield (%)[a]
1	5 mol% $Ph_3PAuOAc$	0
2	5 mol% $Ph_3PAuOAc$ 5 mol% **53**	0
3	5 mol% $Ph_3PAuOAc$ 5 mol% **54**	0
4	5 mol% $Ph_3PAuOBz$	0
5	5 mol% $Ph_3PAuOBz$ 5 mol% **53**	0
6	5 mol% $Ph_3PAuOBz$ 5 mol% **54**	0
7	5 mol% $Ph_3PAuOMs$	3
8	5 mol% $Ph_3PAuOMs$ 5 mol% **53**	3
9	5 mol% $Ph_3PAuOMs$ 5 mol% **54**	9
10	5 mol% $Ph_3PAuOTs$	5
11	5 mol% $Ph_3PAuOTs$ 5 mol% **53**	7
12	5 mol% $Ph_3PAuOTs$ 5 mol% **54**	15

[a]Derived by product to reactant ratio from ^{1}H-NMR.

Table 2.6 Studies solvent effect of $Ph_3PAuOTs$ activation by urea and squaramide in enyne isomerization reaction

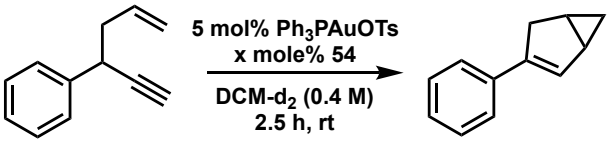


Entry	Solvent	Conditions	Yield (%)[a]
1	MTBE	5 mol% $Ph_3PAuOTs$	0
2	MTBE	5 mol% $Ph_3PAuOTs$ 5 mol% **53**	0
3	MTBE	5 mol% $Ph_3PAuOTs$ 5 mol% **54**	0
4	Toluene-d_8	5 mol% $Ph_3PAuOTs$	0
5	Toluene-d_8	5 mol% $Ph_3PAuOTs$ 5 mol% **53**	0
6	Toluene-d_8	5 mol% $Ph_3PAuOTs$ 5 mol% **54**	0
7	MeCN-d_3	5 mol% $Ph_3PAuOTs$	14
8	MeCN-d_3	5 mol% $Ph_3PAuOTs$ 5 mol% **53**	13
9	MeCN-d_3	5 mol% $Ph_3PAuOTs$ 5 mol% **54**	28
10	$MeNO_2$-d_3	5 mol% $Ph_3PAuOTs$	34
11	$MeNO_2$-d_3	5 mol% $Ph_3PAuOTs$ 5 mol% **53**	26
12	$MeNO_2$-d_3	5 mol% $Ph_3PAuOTs$ 5 mol% **54**	53

[a]Derived by product to reactant ratio from ^{1}H-NMR.

The influence of the hydrogen bond donor loading on yield was then examined. Saturation behavior was observed when the loading of **54** was increased (Table 2.7, entries 1-4). The reason for this saturation behavior is unclear. The proposed schematic mechanism and derived rate law for the initial rate, as shown in Scheme 2.1, may be responsible for this saturation behavior.

Table 2.7 Loading effect of **54** on enyne isomerization yield

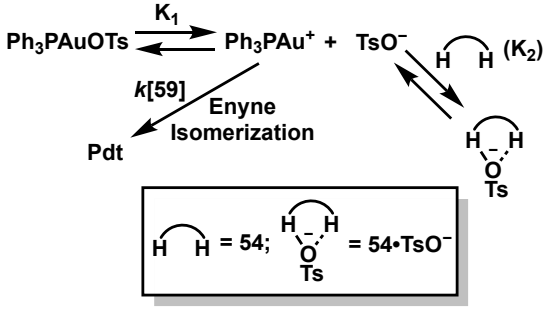


59 60

Entry	x	Yield (%)[a]
1	0	4
2	5	13
3	10	14
4	20	15

[a]Derived by product to reactant ratio from ^{1}H-NMR.

Scheme 2.1 Proposed schematic mechanism of enyne isomerization involving **54** and derived rate law for the initial rate



$$\text{Initial Rate} = k[S]_0[Ph_3PAu^+] = \frac{kK_1[59]_0[Ph_3PAuOTs]_0}{K_1 + [TsO^-]}$$

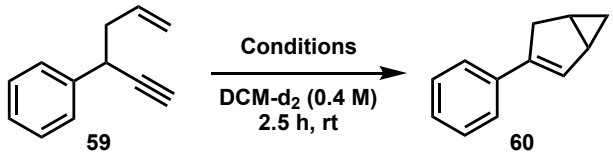
$$= \frac{kK_1K_2[59]_0[Ph_3PAuOTs]_0}{K_1K_2 - 1 + [54]_0/[54]}$$

When $[54]_0$ increases, the initial rate will increase. When [54] is large enough that $[54]_0/[54] = 1$, the initial rate will finally approach the upper limit of $k[59]_0[Ph_3PAuOTs]_0$.

Because enyne isomerization could also be catalyzed by a cationic biphenyl gold(III) complex, the compatibility of **53** or **54** with gold(III) complex was also evaluated.[131] Gold(III) fluoride (**61a**), chloride(**61b**) and tosylate (**61c**) were first subjected to enyne isomerization conditions with and without **53** or **54**. No product was observed (Table 2.8, entries 1-9), whereas the reaction catalyzed by gold(III) triflate (**61d**) went to completion within 2.5 h (Table 2.8, entry 10). In comparison, addition of **53** or **54** greatly decelerated the reaction (Table 2.8, entries 11 and 12). But under more dilute reaction conditions with extended reaction time (24 h), the reaction still went to completion. This means urea- or squaramide-triflate complexes are compatible chiral anions with cationic gold(III). Given the fact that chiral phosphate anions shut down the catalytic

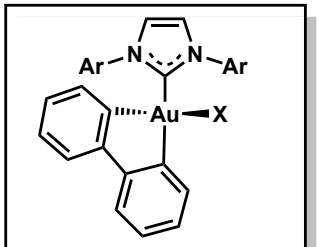
activity of cationic gold(III) complexes, the strategy presented here might offer new opportunities for asymmetric gold(III) catalysis.

Table 2.8 Study of compatibility of urea and squaramide with Au(III) complex in enyne isomerization reaction



59 **60**

Entry	Conditions	Yield (%)[a]
1	5 mol% **61a**	0
2	5 mol% **61a** 5 mol% **53**	0
3	5 mol% **61a** 5 mol% **54**	0
4	5 mol% **61b**	0
5	5 mol% **61b** 5 mol% **53**	0
6	5 mol% **61b** 5 mol% **54**	0
7	5 mol% **61c**	0
8	5 mol% **61c** 5 mol% **53**	0
9	5 mol% **61b** 5 mol% **54**	0
10	5 mol% **61d**	99
11	5 mol% **61d** 5 mol% **53**	5 (99)[b]
12	5 mol% **61b** 5 mol% **54**	8 (99)[b]



Ar = 2,6-Diisopropylphenyl

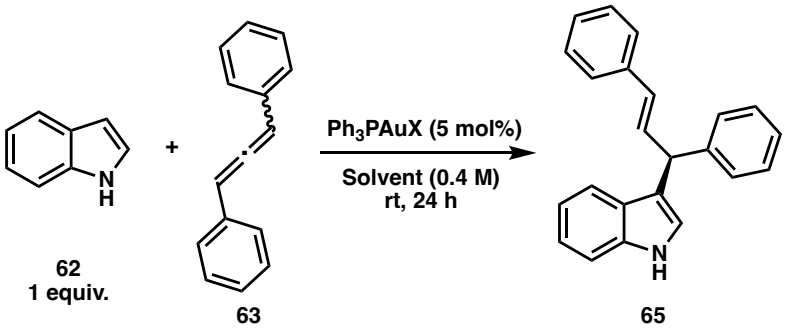
X = F **61a**
X = Cl **61b**
X = OTs **61c**
X = OTf **61d**

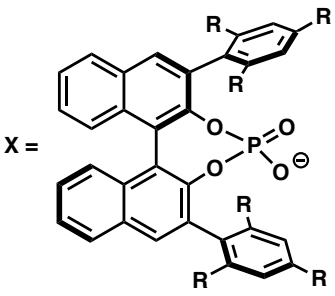
[a]Derived by product to reactant ratio from ^{1}H-NMR; [b]Condition change: **59** (0.1 M), 24 h.

2.2.3 Development of Enantioselective Intermolecular Hydroarylation Reaction of Allene

Significant progress has been made in the past two decades to develop enantioselective gold(I) catalysis.[34] However, challenges remain, especially for the intermolecular transformations. Indeed, one such reaction is the intermolecular hydroarylation of racemic allenes with indoles. To date, the reported conditions employed gold(I) catalysts with chiral phosphine ligands, leading to moderate enantiomeric excess (ee) (up to 63%).[132] Initial studies established that reaction between **62** and **63** with chiral phosphate resulted in low yields and low enantioselectivities (Table 2.9). This provided an opportunity for anion binding as a new approach to this challenge.

Table 2.9 Gold(I) chiral phosphate-catalyzed intermolecular hydroarylation of allene

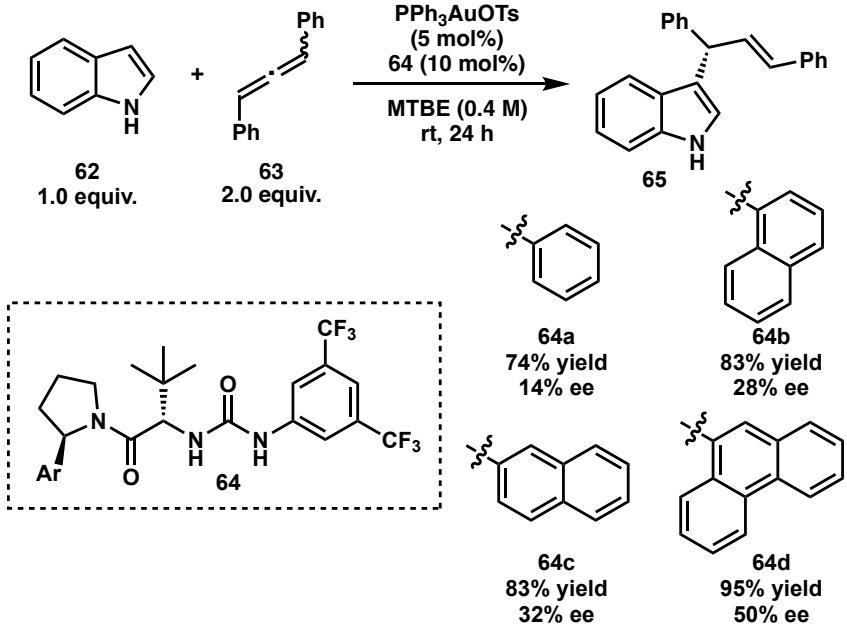




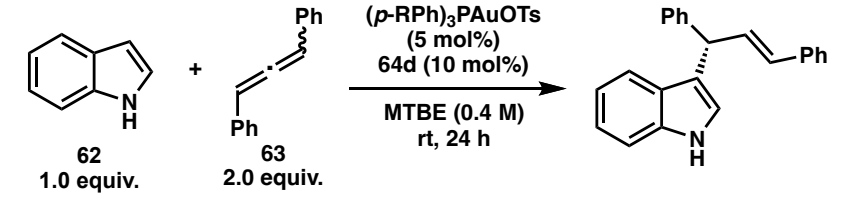
Entry	Solvent	NMR Yield (%)	ee (%)[b]
1	MTBE	0	-
2	Toluene	2	-
3	Cyclohexane	21	7

HBDs containing aryl-pyrrolidne-*tert*-leucine moiety have shown promises in various enantioselective organocatalytic reactions. Naturally, chiral ureas with similar structures were synthesized and used as co-catalysts in the gold(I)-catalyzed hydroarylation of **63** with **62**. Initial reaction investigations with $Ph_3PAuOTs$ showed that expanded aryl substituent on the chiral urea led to improved enantioselectivities, with 50% enantiomeric excess (ee) using catalyst **64d** (Figure 2.10A). This is similar to the trend observed in organocatalytic reaction, suggesting a π interaction of the aryl group with other reaction component in the enantiodetermining transition state. Next, the substituent effect of achiral phosphine ligand on gold catalyst was examined. A positive correlation between the σ_p of the substituents and $\Delta\Delta G^{\ddagger}$ (derived from ee values) was observed, with *para*-CF_3 substituted ligand affording product in 75% ee (Figure 2.10B). It was reasoned that the aryl group of the achiral ligand played an important role to achieve high enantioselectivity, potentially through attractive π interaction. The mechanism involving ligand dissociation was also deemed unlikely due to the observed ligand effect.

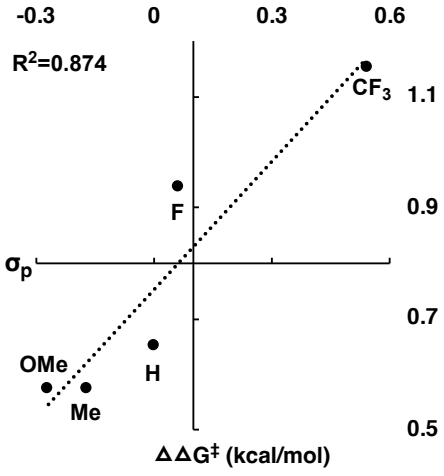
A)



B)



Entry	R	Yield (%)	ee (%)
1	OMe	87	45
2	Me	92	45
3	H	95	50
4	F	97	66
5	CF_3	97	75



C)

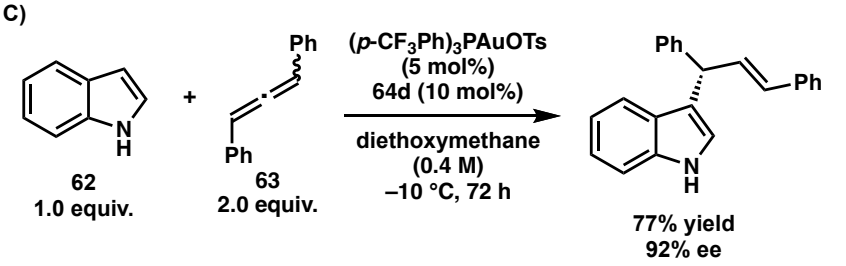


Figure 2.10 (A) Structural effects of chiral ureas on the enantioselectivities of the gold(I)-catalyzed hydroarylation of allene with indole; (B) electronic effects of achiral phosphine ligands on the enantioselectivities of the gold(I)-catalyzed hydroarylation of allene with indole; the inset coordinate showing the correlation between σ_p of the ligand substituents and $\Delta\Delta G^{\ddagger}$ derived from ee values; (C) optimized conditions for enantioselective hydroarylation of allene with indole.

Following the findings about the HBD and achiral ligand, changing the solvent to diethoxymethane and lowering the temperature to –10 °C resulted in 77% yield and 92% ee (Figure 2.10C). Using 1-methyl-indole as the substrate instead of 1-H-indole, led to much lower yield and ee of 31% and 5%, respectively. This suggested a hydrogen bonding interaction present in the transition state of the catalyzed pathway.

2.2.4 Computational Studies of Enantioselective Intermolecular Hydroarylation Reaction of Allene

To gain more detailed understandings about the origin of the enantioselectivities, density functional theory (DFT) calculations were carried out. For this multicomponent reaction with a flexible catalyst, a thorough conformation search is exceedingly important to identify the lowest energy conformation for every stationary point. To tackle this challenge, an extensive conformational sampling was carried out using metadynamics simulation with genetic z-matrix crossing (iMTD-GC) approach, which is implemented in xTB package (see SI for details).

The lowest-energy conformer of two transition states **TS-S** and **TS-R**, which form (*S*)- and (*R*)-products, respectively, are shown in Figure 2.11. The activation barriers of **TS-S** and **TS-R** are calculated to be 14.1 and 18.7 kcal/mol, respectively, relative to reactant complex **RC** (see SI for optimized structure of **RC**). DFT calculations are consistent with the experimental finding that (*S*)-product is the major one of the hydroheteroarylation of allenes (vide supra). To identify the key factor that controls the enantioselectivity of this reaction, non-covalent interactions were visualized by using NCIPLOT code and the π/CH-π interaction energies ($\Delta E_{\pi/\text{CH-}\pi}$) were calculated by using Grimme's DFT-D4 method. At both transition states **TS-S** and **TS-R**, π-π interactions between the indole and the phenanthrenyl group on the pyrrolidine and between the phenyl group of the phosphine ligand and the phenyl moiety on the urea are found. Futhermore, the indole is activated by a general base activation via catalyst amide – indole hydrogen bond. These findings are consistent with the ee's observed in the experiments (vide supra), as well as the proposed transition state for the indole addition to the episulfonium ion suggested by Lin and Jacobsen.[133]

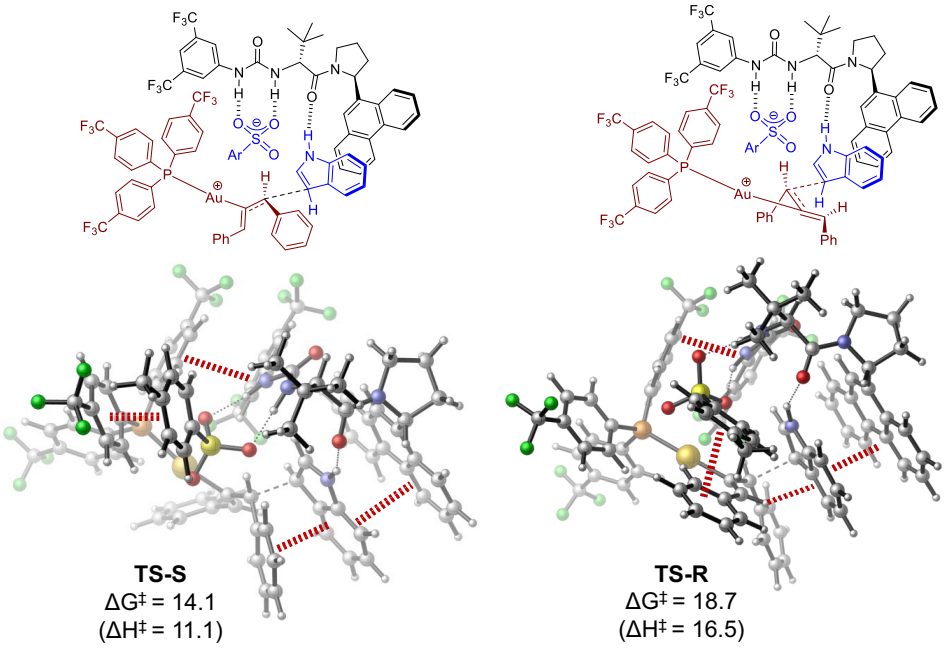


Figure 2.11 Optimized structures of transition states **TS-S** and **TS-R**. All energy (kcal/mol) are relative to reactant complex **RC**.

Interestingly, **TS-S** is further stabilized by π-stacking interactions between the phenyl group of phosphine ligand and the sulfonate anion and between phenyl moiety of allene and the indole with the calculated interaction energies $\Delta E_{\pi\text{-}\pi}$ are −12.8 and −12.4 kcal/mol, respectively. On the other hand, **TS-R** is stabilized by a π-π interaction between the sulfonate anion and phenyl moiety of the substrate and a CH-π interaction between the allene and indole with the $\Delta E_{\pi\text{-}\pi}$ and $\Delta E_{\text{CH-}\pi}$ are calculated to be −11.1 and −9.5 kcal/mol, respectively. These results suggested that the stronger stabilization of non-covalent interactions at **TS-S** over **TS-R** is the key factor that controls the enantioselectivity of the hydroheteroarylation.

Next, DFT calculations were performed to unravel the role of phosphine ligand on the enantioselectivity of this reaction. A good correlation between experimental and calculated energy difference of **TS-S** and **TS-R** for various phosphine ligands is found (Figure 2.12). DFT calculations are in agreement with experimental finding that more electron-deficient triaryl phosphine ligand can give higher ee (vide supra). As mentioned above, π-π interaction between the phenyl group of phosphine ligand and the sulfonate anion was only identified at **TS-S**, which benefit from the modification of phosphine ligand. A stronger ligand-sulfonate π-π interaction can thus render higher ee. Electron-withdrawing substituents, including CF_3 and F groups, decrease the π electron density on the phenyl group of phosphine ligands reducing electrostatic repulsion with the sulfonate anion and thus enhancing the π-staking interaction. Moreover, the ligand-sulfonate π-π interaction is also controlled by through-space interactions of the substituent groups on phosphine ligand with sulfonate anion. Electrostatic attraction between CF_3/F substituent group and the Me group of sulfonate cation can enhance the ligand-sulfonate π-π interaction; whereas, steric repulsion between Me/OMe group and the Me group of sulfonate weakens the ligand-sulfonate π-π interaction.

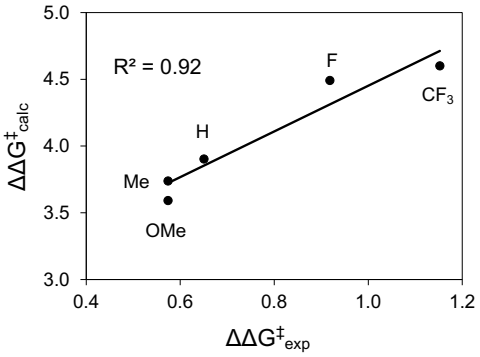


Figure 2.12 Correlation between experimental and calculated $\Delta\Delta G^{\ddagger}$ values for various phosphine ligands ($\Delta\Delta G^{\ddagger} = \Delta G^{\ddagger}$(TS-S) − $\Delta G^{\ddagger}$(TS-R)).

2.3 Conclusion

In conclusion, the activation of transition metal catalysts with chiral HBDs was studied in gold(I)-catalyzed transformations. An enantioselective hydroheteroarylation reaction of allenes was discovered. It was observed that the structures of chiral ureas and achiral phosphine ligands had a cooperative effect on the enantioselectivities. The cooperativity originated from π-stacking interactions in the stereodetermining transition state as revealed by computational studies. Other critical noncovalent interactions were also detailed with the energy decomposition method. The strategy, along with the mechanistic understandings, opens up opportunities for activating other transition-metal catalysts or intermediates for asymmetric catalysis.

2.4 References and Notes

[1]. Hashmi, A. S. K. *Chem. Rev.* **2007**, *107*, 3180–3211.
[2]. Gorin, D. J.; Toste, F. D. *Nature* **2007**, *446*, 395–403.
[3]. Fürstner, A.; Davies, P. W. *Angew. Chem. Int. Ed.* **2007**, *46*, 3410–3449.
[4]. Gorin, D. J.; Sherry, B.D.; Toste, F. D. *Chem. Rev.* **2008**, *108*, 3351–3378.
[5]. Li, Z.; Brouwer, C.; He, C. *Chem. Rev.* **2008**, *108*, 3239–3265.
[6]. Jiménez-Núñez, E.; Echavarren, A. M *Chem. Rev.* **2008**, *108*, 3326–3350.
[7]. Shapiro, N.D.; Toste, F. D. *Synlett* **2010**, *2010*, 675–691.
[8]. Zhang, L. *Acc. Chem. Res.* **2014**, *47*, 877–888.
[9]. Zheng, Z.; Wang, Z.; Wang, Y.; Zhang, L. *Chem. Soc. Rev.* **2016**, *45*, 4448–4458.
[10]. Dorel, R.; Echavarren, A. M. *Chem. Rev.* **2015**, *115*, 9028–9072.
[11]. Zhao, X.; Rudolph, M.; Hashmi, A. S. K. *Chem. Commun.* **2019**, *55*, 12127–12135.
[12]. Nugent, W. A. *Angew. Chem. Int. Ed.* **2012**, *51*, 8936–8949.
[13]. Joost, M.; Amgoune, A.; Bourissou, D. *Angew. Chem. Int. Ed.* **2015**, *54*, 15022–15045.
[14]. Mertens, R. T.; Awuah, S. G. *ACS Symposium Series* **2019**, *vol. 1317*, pp. 19–55.
[15]. Hartwig, J. F. *Organotransition Metal Chemistry: From Bonding to Catalysis*, University Science Books, 2006.
[16]. Bratsch, S. G. *J. Phys. Chem. Ref. Data* **1989**, *18*, 1–21.
[17]. Hopkinson, M. N.; Gee, A. D.; Gouverneur, V. *Chem. Eur. J.* **2011**, *17*, 8248–8262.
[18]. Garcia, P.; Malacria, M.; Aubert, C.; Gandon, V.; Fensterbank, L. *ChemCatChem* **2010**, *2*, 493–497.
[19]. Wegner, H. A.; Auzias, M. *Angew. Chem. Int. Ed.* **2011**, *50*, 8236–8247.
[20]. Boorman, T. C.; Larrosa, I. *Chem. Soc. Rev.* **2011**, *40*, 1910–1925.

[21]. Hashmi, A. S. K.; Ramamurthi, T. D.; Rominger, F. *J. Organomet. Chem.* **2009**, *694*, 592–597.
[22]. Joost, M.; Gualco, P.; Coppel, Y.; Miqueu, K.; Kefalidis, C. E.; Maron, L.; Amgoune, A.; Bourissou, D. *Angew. Chem. Int. Ed.* **2014**, *53*, 747–751.
[23]. Wu, C. Y.; Horibe, T.; Jacobsen, C. B.; Toste, F. D. *Nature* **2015**, *517*, 449–454.
[24]. Schmidbaur, H.; Schier, A. *Arab. J. Sci. Eng.* **2012**, *37*, 1187–1225.
[25]. Kumar, R.; Nevado, C. *Angew. Chem. Int. Ed.* **2017**, *56*, 1994–2015.
[26]. Hashmi, A. S. K.; Weyrauch, J. P.; Rudolph, M.; Kurpejović, E. *Angew. Chem. Int. Ed,* **2004**, *43*, 6545–6547.
[27]. Hashmi, A. S. K.; Blanco, M. C.; Fischer, D.; Bats, J. W. *European J. Org. Chem.* **2006**, 1387–1389.
[28]. Gaillard, S.; Slawin, A. M.; Bonura, A.T.; Stevens, E. D.; Nolan, S. P.; *Organometallics* **2010**, *29*, 394–402.
[29]. De Frémont, P.; Singh, R.; Stevens, E. D.; Petersen, J. L;Nolan, S. P. *Organometallics* **2007**, *26*, 1376–1385.
[30]. Lee, J. S.; Kapustin, E. A.; Pei, X.; Llopis, S.; Yaghi, O. M.; Toste, F. D. *Chem* **2020**, *6*, 142–152.
[31]. Zhukhovitskiy, A. V.; Kobylianskii, I. J.; Wu, C. Y.; Toste, F. D. *J. Am. Chem. Soc.* **2018**, *140*, 466–474.
[32]. López, F.;Mascareñas, J. L. *Beilstein J. Org. Chem.* **2013**, *9*, 2250–2264.
[33]. Wang, Y. M.; Lackner, A. D.; Toste, F. D. *Acc. Chem. Res.* **2014**, *47*, 889–901.
[34]. Zi, W.; Toste, F. D. *Chem. Soc. Rev.* **2016**, *45*, 4567–4589.
[35]. Li, Y.; Li, W.; Zhang, J. *Chem. Eur. J.* **2017**, *23*, 467–512.
[36]. Bohan, P.T.; Dean Toste, F. D. *J. Am. Chem. Soc.* **2017**, *139*, 11016–11019.
[37]. Rodriguez, J.; Bourissou, D. *Angew. Chem. Int. Ed.* **2018**, *57*, 386–388.
[38]. Reid, J. P.; Hu, M.; Ito, S.; Huang, B.; Hong, C.; Xiang, H.; Sigman, M. S.; Toste, F. D. *Chem. Sci.* **2020**, *11*, 6450-6456.
[39]. Abdou, H. E.; Mohamed, A. A.; Fackler, J. P. *Inorg. Chem.* **2007**, *46*, 9692–9699.
[40]. Tkatchouk, E.; Mankad, N. P.; Benitez, D.; Goddard III, W. A.; Toste, F. D. *J. Am. Chem. Soc.* **2011**, *133*, 14293–14300.
[41]. Levin, M. D.; Toste, F. D. *Angew. Chem. Int. Ed.* **2014**, *53*, 6211–6215.
[42]. Liu, K.; Li, N.; Ning, Y.; Zhu, C.; Xie, J. *Chem* **2019**, *5*, 2718–2730.
[43]. Ball, L. T.; Lloyd-Jones, G. C.; Russell, C. A. *Science* **2012**, *337*, 1644–1648.
[44]. Ball, L. T.; Lloyd-Jones, G. C.; Russell, C. A. *J. Am. Chem. Soc.* **2014**, *136*, 254–264.
[45]. Cambeiro, X. C.; Ahlsten, N.; Larrosa, I. *J. Am. Chem. Soc.* **2015**, *137*, 15636–15639.
[46]. Robinson, M. P.; Lloyd-Jones, G. C. *ACS Catal.* **2018**, *8*, 7484–7488.
[47]. Fricke, C.; Dahiya, A.; Reid, W. B.;Schoenebeck, F. *ACS Catal.* **2019**, *9*, 9231–9236.
[48]. Li, W.; Yuan, D.; Wang, G.; Zhao, Y.; Xie, J.; Li, S.; Zhu, C. *J. Am. Chem. Soc.* **2019**, *141*, 3187–3197.
[49]. Dahiya, A.; Fricke, C.; Schoenebeck, F. *J. Am. Chem. Soc.* **2020**, *142*, 7754–7759.
[50]. van Leeuwen, P. W.; Kamer, P. C.; Reek, J. N.; Dierkes, P. *Chem. Rev.* **2000**, *100*, 2741–2769.
[51]. Joost, M.; Zeineddine, A.; Estevez, L.; Mallet− Ladeira, S.; Miqueu, K.; Amgoune, A.; Bourissou, D. *J. Am. Chem. Soc.* **2014**, *136*, 14654–14657.
[52]. Joost, M.; Estévez, L.; Miqueu, K.; Amgoune, A.; Bourissou, D. *Angew. Chem. Int. Ed.* **2015**, *54*, 5236–5240.

[53]. Harper, M. J.; Arthur, C. J.; Crosby, J.; Emmett, E. J.; Falconer, R. L.; Fensham-Smith, A. J.; Gates, P. J.; Leman, T.; McGrady, J. E.; Bower, J. F.; Russell, C. A. *J. Am. Chem. Soc.* **2018**, *140*, 4440–4445.
[54]. Peng, H.; Xi, Y.; Ronaghi, N.; Dong, B.; Akhmedov, N. G.; Shi, X. *J. Am. Chem. Soc.* **2014**, *136*, 13174–13177.
[55]. Cai, R.; Lu, M.; Aguilera, E. Y.; Xi, Y.; Akhmedov, N.G.; Petersen, J.L.; Chen, H.; Shi, X. *Angew. Chem. Int. Ed.* **2015**, *54*, 8772–8776.
[56]. Ye, X.; Peng, H.; Wei, C.; Yuan, T.; Wojtas, L.; Shi, X. *Chem* **2018**, *4*, 1983–1993.
[57]. Yang, Y.; Antoni, P.; Zimmer, M.; Sekine, K.; Mulks, F. F.; Hu, L.; Zhang, L.; Rudolph, M.; Rominger, F.; Hashmi, A. S. K. *Angew. Chem. Int. Ed.* **2019**, *58*, 5129–5133.
[58]. Cadge, J. A.; Sparkes, H. A.; Bower, J. F.; Russell, C. A. *Angew. Chem. Int. Ed.* **2020**, *59*, 6617–6621.
[59]. Zeineddine, A.; Estévez, L.; Mallet-Ladeira, S.; Miqueu, K.; Amgoune, A.; Bourissou, D. *Nat. Commun.* **2017**, *8*, 1–8.
[60]. Rodriguez, J.; Adet, N.; Saffon-Merceron, N.; Bourissou, D. *Chem. Sci.* **2019**, *10*, 7183–7192.
[61]. Rodriguez, J.; Adet, N.; Saffon-Merceron, N.; Bourissou, D. *Chem. Commun.* **2020**, *56*, 94–97.
[62]. Akram, M.O.; Das, A.; Chakrabarty, I.; Patil, N. T., *Org. Lett.* **2019**, *21*, 8101–8105.
[63]. Chintawar, C. C.; Yadav, A. K.; Patil, N. T. *Angew. Chem. Int. Ed.* **2020**, *59*, 11808–11813.
[64]. Vinogradova, E. V.; Zhang, C.; Spokoyny, A.M.; Pentelute, B.L.; Buchwald, S. L. *Nature* **2015**, *526*, 687–691.
[65]. Messina, M. S.; Stauber, J. M.; Waddington, M. A.; Rheingold, A. L.; Maynard, H.D.; Spokoyny, A. M. *J. Am. Chem. Soc.* **2018**, *140*, 7065–7069.
[66]. Kung, K. K. Y.; Ko, H. M.; Cui, J. F.; Chong, H. C.; Leung, Y. C.; Wong, M. K. *Chem. Commun.* **2014**, *50*, 11899–11902.
[67]. de Paiva, R. E.; Du, Z.; Nakahata, D. H.; Lima, F. A.; Corbi, P. P.; Farrell, N. P. *Angew. Chem. Int. Ed.* **2018**, *57*, 9305–9309.
[68]. Wenzel, M. N.; Bonsignore, R.; Thomas, S. R.; Bourissou, D.; Barone, G.; Casini, A. *Chem. Eur. J.* **2019**, *25*, 7628–7634.
[69]. Currie, L.; Rocchigiani, L.; Hughes, D. L.; Bochmann, M. *Dalton Trans.* **2018**, *47*, 6333–6343.
[70]. Zhang, C.; Vinogradova, E. V.; Spokoyny, A. M.; Buchwald, S. L.; Pentelute, B. L. *Angew. Chem. Int. Ed.* **2019**, *58*, 4810–4839.
[71]. Zhang, S. L.; Dong, J. J. *Org. Biomol. Chem.* **2019**, *17*, 1245–1253.
[72]. Stauber, J. M.; Qian, E. A.; Han, Y.; Rheingold, A. L.; Král, P.; Fujita, D.; Spokoyny, A. M. *J. Am. Chem. Soc.* **2019**, *142*, 327–334.
[73]. Turro, N.J. *Modern Molecular Photochemistry*, University Science Books, 1991.
[74]. Winston, M. S.; Wolf, W. J.; Toste, F. D. *J. Am. Chem. Soc.* **2014**, *136*, 7777–7782.
[75]. Liu, S.; Kang, K.; Liu, S.; Wang, D.; Wei, P.; Lan, Y.; Shen, Q. *Organometallics* **2018**, *37*, 3901–3908.
[76]. Winston, M. S.; Wolf, W. J.; Toste, F. D. *J. Am. Chem. Soc.* **2015**, *137*, 7921–7928.
[77]. Levin, M. D.; Kim, S.; Toste, F. D. *ACS Cent. Sci.* **2016**, *2*, 293–301.
[78]. Kalyani, D.; McMurtrey, K. B.; Neufeldt, S. R.; Sanford, M. S. *J. Am. Chem. Soc.* **2011**, *133*, 18566–18569.
[79]. Neufeldt, S. R.; Sanford, M. S. *Adv. Synth. Catal.* **2012**, *354*, 3517–3522.

[80]. Ye, Y.; Sanford, M. S. *J. Am. Chem. Soc.* **2012**, *134*, 9034–9037.
[81]. Sahoo, B.; Hopkinson, M. N.; Glorius, F. *J. Am. Chem. Soc.* **2013**, *135*, 5505–5508.
[82]. Shu, X.Z. *et al.* (2014) Dual visible light photoredox and gold-catalyzed arylative ring expansion. *J. Am. Chem. Soc.* **2014**, *136*, 5844–5847.
[83]. Hopkinson, M. N.; Tlahuext-Aca, A.; Glorius, F. *Chem. Res.* **2016**, *49*, 2261–2272.
[84]. Zidan, M.; Rohe, S.; McCallum, T.; Barriault, L. *Catal. Sci. Technol.* **2018**, *8*, 6019–6028.
[85]. Huang, L.; Rudolph, M.; Rominger, F.; Hashmi, A. S. K. *Angew. Chem. Int. Ed.* **2016**, *55*, 4808–4813.
[86]. Deng, J. R.; Chan, W. C.; Lai, N. C. H.; Yang, B.; Tsang, C. S.; Ko, B. C. B.; Chan, S. L. F.; Wong, M. K. *Chem. Sci.* **2017**, *8*, 7537–7544.
[87]. Witzel, S.; Sekine, K.; Rudolph, M.; Hashmi, A. S. K. *Chem. Commun.* **2018**, *54*, 13802–13804.
[88]. Xie, J.; Sekine, K.; Witzel, S.; Krämer, P.; Rudolph, M.; Rominger, F.; Hashmi, A. S. K. *Angew. Chem. Int. Ed.* **2018**, *130*, 16890–16895.
[89]. Taschinski, S.; Döpp, R.; Ackermann, M.; Rominger, F.; de Vries, F.; Menger, M. F.; Rudolph, M.; Hashmi, A. S. K.; Klein, J. E. *Angew. Chem. Int. Ed.* **2019**, *58*, 16988–16993.
[90]. Peng, H.; Cai, R.; Xu, C.; Chen, H.; Shi, X. *Chem. Sci.* **2016**, *7*, 6190–6196.
[91]. Dong, B.; Peng, H.; Motika, S. E.; Shi, X. *Chem. Eur. J.* **2017**, *23*, 11093–11099.
[92]. Akram, M. O.; Shinde, P. S.; Chintawar, C. C.; Patil, N. T. *Org. Biomol. Chem.* **2018**, *16*, 2865–2869.
[93]. Jimoh, A. A.; Hosseyni, S.; Ye, X.; Wojtas, L.; Hu, Y.; Shi, X. *Chem. Commun.* **2019**, *55*, 8150–8153.
[94]. Witzel, S.; Xie, J.; Rudolph, M.; Hashmi, A. S. K. *Adv. Synth. Catal.* **2017**, *359*, 1522–1528.
[95]. Kim, S.; Toste, F. D. *J. Am. Chem. Soc.* **2019**, *141*, 4308–4315.
[96]. Xia, Z.; Corcé, V.; Zhao, F.; Przybylski, C.; Espagne, A.; Jullien, L.; Le Saux, T.; Gimbert, Y.; Dossmann, H.; Mouriès-Mansuy, V.; Ollivier, C. *Nat. Chem.* **2019**, *11*, 797–805.
[97]. Yang, Y.; Schießl, J.; Zallouz, S.; Göker, V.; Gross, J.; Rudolph, M.; Rominger, F.; Hashmi, A. S. K. *Chem. Eur. J.* **2019**, *25*, 9624–9628.
[98]. Wolf, W. J.; Winston, M.S.; Toste, F. D. *Nat. Chem.* **2014**, *6*, 159–164.
[99]. Komiya, S.; Kochi, J.K. *J. Am. Chem. Soc.* **1976**, *98*, 7599–7607.
[100]. Rocchigiani, L.; Fernandez-Cestau, J.; Budzelaar, P.H.; Bochmann, M.; *Chem. Eur. J.* **2018**, *24*, 8893–8903.
[101]. Hofer, M.; Gomez-Bengoa, E.; Nevado, C. *Organometallics* **2014**, *33*, 1328–1332.
[102]. Kang, K.; Liu, S.; Xu, T.; Wang, D.; Leng, X.; Bai, R.; Lan, Y.; Shen, Q. *Organometallics* **2017**, *36*, 4727–4740.
[103]. Nijamudheen, A.; Karmakar, S.; Datta, A. *Chem. Eur. J.* **2014**, *20*, 14650–14658.
[104]. Kawai, H.; Wolf, W. J.; DiPasquale, A. G.; Winston, M. S.; Toste, F. D. *J. Am. Chem. Soc.* **2016**, *138*, 587–593.
[105]. Bonsignore, R.; Thomas, S. R.; Klooster, W. T.; Coles, S. J.; Jenkins, R. L.; Bourissou, D.; Barone, G.; Casini, A. *Chem. Eur. J.* **2020**, *26*, 4226–4231.
[106]. Kim, J. H.; Mertens, R. T.; Agarwal, A.; Parkin, S.; Berger, G.; Awuah, S. G. *Dalt. Trans.* **2019**, *48*, 6273–6282.
[107]. Hong, C. M.; Bergman, R. G.; Raymond, K. N.; Toste, F. D. *Acc. Chem. Res.* **2018**, *51*, 2447–2455.

[108]. Kaphan, D. M.; Levin, M. D.; Bergman, R. G.; Raymond, K. N.; Toste, F. D. *Science* **2015**, *350*, 1235–1238.
[109]. Levin, M. D.; Kaphan, D. M.; Hong, C. M.; Bergman, R. G.; Raymond, K. N.; Toste, F. D. *J. Am. Chem. Soc.* **2016**, *138*, 9682–9693.
[110]. Vaissier Welborn, V.; Head-Gordon, T. *J. Phys. Chem. Lett.* **2018**, *9*, 3814–3818.
[111]. Norjmaa, G.; Marechal, J. D.; Ujaque, G. *J. Am. Chem. Soc.* **2019**, *141*, 13114–13123.
[112]. Welborn, V. V.; Li, W. L.; Head-Gordon, T. *Nat. Commun.* **2020**, *11*, 1–6.
[113]. Levin, M. D.; Chen, T. Q.; Neubig, M. E.; Hong, C. M.; Theulier, C. A.; Kobylianskii, I. J.; Janabi, M.; O'Neil, J. P.; Toste, F. D. *Science* **2017**, *356*, 1272–1275.
[114]. Benitez, D.; Shapiro, N. D.; Tkatchouk, E.; Wang, Y.; Goddard, W. A.; Toste, F. D. *Nat. Chem.* **2009**, *1*, 482–486.
[115]. Wang, Y.; Muratore, M. E.; Echavarren, A. M. *Chem. Eur. J.* **2015**, *21*, 7332–7339.
[116]. Harris, R. J.; Widenhoefer, R. A. *Chem. Soc. Rev.* **2016**, *45*, 4533–4551.
[117]. Meyer, T. H.; Finger, L. H.; Gandeepan, P.; Ackermann, L. *Trends Chem.* **2019**, *1*, 63–76.
[118]. Sauermann, N.; Meyer, T. H.; Qiu, Y.; Ackermann, L. *ACS Catal.* **2018**, *8*, 7086–7103.
[119]. Ma, C.; Fang, P.; Mei, T. S. *ACS Catal.* **2018**, *8*, 7179–7189.
[120]. Ye, X.; Zhao, P.; Zhang, S.; Zhang, Y.; Wang, Q.; Shan, C.; Wojtas, L.; Guo, H.; Chen, H.; Shi, X. *Angew. Chem. Int. Ed.* **2019**, *58*, 17226–17230.
[121]. Wang, D.; Cai, R.; Sharma, S.; Jirak, J.; Thummanapelli, S. K.; Akhmedov, N. G.; Zhang, H.; Liu, X.; Petersen, J. L.; Shi, X. *J. Am. Chem. Soc.* **2012**, *134,* 9012–9019.
[122]. Lu, Z.; Han, J.; Hammond, G. B.; Xu, B. *Org. Lett.* **2015**, 17, 4534–4537.
[123]. Weber, D.; Gagné, M. R. *Org. Lett.* **2009**, 11, 4962–4965.
[124]. Brak, K.; Jacobsen, E. N. *Angew. Chem., Int. Ed.* **2013**, *52*, 534–561.
[125]. Banik, S. M.; Levina, A.; Hyde, A. M.; Jacobsen, E. N. *Science* **2017**, *358*, 761–764.
[126]. Strassfeld, D. A.; Algera, R. F.; Wickens, Z. K.; Jacobsen, E. N. *J. Am. Chem. Soc.* **2021**, *143*, 9585–9594.
[127]. Shu, X.-Z.; Nguyen, S. C.; He, Y.; Oba, F.; Zhang, Q.; Canlas, C.; Somorjai, G. A.; Alivisatos, A. P.; Toste, F. D. *J. Am. Chem. Soc.* **2015**, *137,* 7083–7086.
[128]. Corkey, B. K.; Toste, F. D. *J. Am. Chem. Soc.* **2005**, *127*, 17168–17169.
[129]. Luzung, M. R.; Markham, J. P.; Toste, F. D. *J. Am. Chem. Soc.* **2004**, *126*, 10858–10859.
[130]. Lu, Z.; Han, J.; Okoromoba, O. E.; Shimizu, N.; Amii, H.; Tormena, C. F.; Hammond, G. B.; Xu, B. *Org. Lett.* **2017**, *19*, 5848–5851.
[131]. Bohan, P.T.; Toste, F.D. *J. Am. Chem. Soc.* **2017**, *139,* 11016–11019.
[132]. Wang, M. Z.; Zhou, C. Y.; Guo, Z.; Wong, E. L. M.; Wong, M. K.; Che, C. M. *Chem. Asian J.* **2011**, *6*, 812–824.
[133]. Lin, S.; Jacobsen, E. N. *Nature Chem.* **2012**, *4*, 817–824.

2.5 Supporting Information

2.5.1 General Information

Unless otherwise noted, reagents and solvents were obtained from commercial sources and used without further purification. Tetrahydrofuran (THF), diethyl ether (Et_2O), dichloromethane (CH_2Cl_2), *N,N*-dimethylformamide (DMF), and triethylamine (Et_3N) were dried by passing through commercially available pre-dried activated alumina columns under argon. Except otherwise indicated, all reactions were magnetically stirred and monitored by analytical thin layer chromatography (TLC) with Merck pre-coated silica gel plates with F254 indicator. Visualization was accomplished by UV light (254 nm), with combination of potassium permanganate ($KMnO_4$)

as indicator. All air-sensitive reactions were carried out in flame- or oven-dried glassware in a nitrogen-filled glove box. Stir bars and glassware utilized for studies involving gold complexes were washed with aqua regia. Flash column chromatography was carried out on Merck Silica Gel 60 Å, 230 X 400 mesh. ^{1}H NMR, ^{31}C NMR, ^{19}F-NMR and ^{31}P-NMR spectra were recorded on Bruker AV-300, AVQ-400, AVB-400, DRX-500 and AV-600 spectrometers and reported relative to residual solvent peaks. The proton spectra are reported as follows δ (position of proton, multiplicity, coupling constant *J,* number of protons). Multiplicities are reported using the following abbreviations: s = singlet, d = doublet, t = triplet, q = quartet, m = multiplet, br = broad. Enantiomeric excess was determined on a Shimadzu VP Series Chiral HPLC with a variable wavelength detector. Computational studies were carried out at Molecular Graphics and Computation at University of California, Berkeley. Facility Mass spectral data were obtained from QB3/Chemistry Mass Spectrometry Facility at University of California, Berkeley. X-Ray crystallographic analysis was carried out by X-Ray Crystallographic Facility at University of California, Berkeley.

2.5.2 Computational Studies on Thermodynamics of Chloride Binding from Gold(I)

Calculations were performed using the Gaussian 16 (Revision A.03)[1] on the Tiger Cluster supported by Molecular Graphics and Computation Facility, College of Chemistry, UC Berkeley. M06 functionals was used for all calculations shown here. For gold, SDD was used as both effective-core-potential (ECP) and basis set for all geometry optimizations and single-point electronic energy. All electrons of all other atoms were described using the 6-31G** basis set for geometry optimizations with subsequent frequency calculations and 6-311++G** basis set for electronic energies. All geometry optimizations and single-point electronic energy calculations were conducted with PCM implicit solvation model. Default geometric and SCF convergence criteria were used. In cases for which SCF convergence was difficult to achieve (energy circulates between two values), single-point electronic energy was based on the lower-energy geometry after at least 10 cycles. Control experiments including using ultrafine convergence criteria and different functionals (wB97X) didn't resolved difficulty in convergence of certain system. Though the origin of difficulty in convergence here is not validated, it was suggested that it might related to the PCM solvent correction or it's due to the nature of a flat potential energy surface of particular structure. All calculated energies were listed in Table S1 (the energy of state 1 was defined as 0).

Table S1 Relative electronic energies with M06 functionals and given basis sets (for details of states, see Figure 2.8)

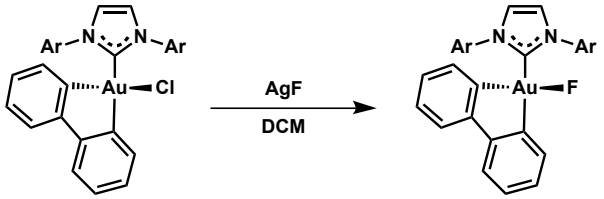
X	Ligand	Solvent	E(State 2) (kcal/mol)	E(State 3) (kcal/mol)	E(State 4) (kcal/mol)
C(CN)2	NHC	Benzene	58.69976994	20.00290005	-2.24824446
C(CN)2	NHC	DCM	34.87939056	2.56195485	-2.77795791
C(CN)2	NHC	Gas Phase	100.9254985	53.12516643	-11.29923963
C(CN)2	NHCMes	Benzene	55.5077124	19.1888613	-4.7835396
C(CN)2	NHCMes	DCM	34.656615	-1.08199413	-5.3786691
C(CN)2	NHCMes	Gas Phase	93.5180694	45.2049822	-9.0359766
C(CN)2	PMe3	Benzene	58.68856476	21.24127404	2.6091702
C(CN)2	PMe3	DCM	33.78438	2.82863889	1.2613482
C(CN)2	PMe3	Gas Phase	103.3498355	56.35362852	0.527499

C(CN)2	PPh3	Benzene	57.1958226	19.9618524	-19.6564536
C(CN)2	PPh3	DCM	34.9221789	2.57195547	-3.3090939
C(CN)2	PPh3	Gas Phase	95.6940516	52.2079929	-25.3798965
CF2	NHC	Benzene	57.51092214	18.81405225	-16.92803826
CF2	NHC	DCM	33.05240946	0.73497375	-15.32933451
CF2	NHC	Gas Phase	101.2545349	53.45420283	-19.97673993
CF2	NHCMes	Benzene	54.3188646	18.0000135	-14.8146264
CF2	NHCMes	DCM	32.8296339	-2.90897523	-15.9497982
CF2	NHCMes	Gas Phase	93.8471058	45.5340186	-13.0178286
CF2	PMe3	Benzene	57.49971696	20.05242624	-16.7135346
CF2	PMe3	DCM	31.9573989	1.00165779	-15.1288578
CF2	PMe3	Gas Phase	103.6788719	56.68266492	-19.7089263
CF2	PPh3	Benzene	56.0069748	18.7730046	-15.3384651
CF2	PPh3	DCM	33.0951978	0.74497437	-18.3043917
CF2	PPh3	Gas Phase	96.023088	52.5370293	-23.965704
SO2	NHC	Benzene	57.57099894	18.87412905	-5.34483306
SO2	NHC	DCM	33.99790716	1.68047145	-4.50405711
SO2	NHC	Gas Phase	99.33471702	51.53438493	-4.56928353
SO2	NHCMes	Benzene	54.3789414	18.0600903	-4.3154874
SO2	NHCMes	DCM	33.7751316	-1.96347753	-3.3438951
SO2	NHCMes	Gas Phase	91.9272879	43.6142007	-5.2718211
SO2	PMe3	Benzene	57.55979376	20.11250304	-2.4618762
SO2	PMe3	DCM	32.9028966	1.94715549	-1.5466626
SO2	PMe3	Gas Phase	101.759054	54.76284702	-2.2803165
SO2	PPh3	Benzene	56.0670516	18.8330814	-5.8790214
SO2	PPh3	DCM	34.0406955	1.69047207	0.1610406
SO2	PPh3	Gas Phase	94.1032701	50.6172114	-2.5111233
CS	NHC	Benzene	53.74699974	15.05012985	-14.61954816
CS	NHC	DCM	31.13934516	-1.17809055	-12.90657501
CS	NHC	Gas Phase	95.25328092	47.45294883	-21.19362903
CS	NHCMes	Benzene	50.5549422	14.2360911	-27.6714207
CS	NHCMes	DCM	30.9165696	-4.82203953	-23.7889575
CS	NHCMes	Gas Phase	87.8458518	39.5327646	-31.8674601
CS	PMe3	Benzene	53.73579456	16.28850384	-19.7762733
CS	PMe3	DCM	30.0443346	-0.91140651	-18.8651673
CS	PMe3	Gas Phase	97.67761794	50.68141092	-21.5642007
CS	PPh3	Benzene	52.2430524	15.0090822	-22.1745195
CS	PPh3	DCM	31.1821335	-1.16808993	-21.1458366
CS	PPh3	Gas Phase	90.021834	46.5357753	-26.5472298
CO	NHC	Benzene	55.88013564	17.18326575	-5.71280346

CO	NHC	DCM	32.04279036	-0.27464535	-6.38548911
CO	NHC	Gas Phase	98.87005422	51.06972213	-5.04918603
CO	NHCMes	Benzene	52.6880781	16.369227	-14.7595959
CO	NHCMes	DCM	31.8200148	-3.91859433	-8.7232887
CO	NHCMes	Gas Phase	91.4626251	43.1495379	-13.3193277
CO	PMe3	Benzene	55.86893046	18.42163974	-6.0774336
CO	PMe3	DCM	30.9477798	-0.00796131	-7.0657713
CO	PMe3	Gas Phase	101.2943912	54.29818422	-3.8221596
CO	PPh3	Benzene	54.3761883	17.1422181	-9.6863004
CO	PPh3	DCM	32.0855787	-0.26464473	-8.0796807
CO	PPh3	Gas Phase	93.6386073	50.1525486	-10.5388416

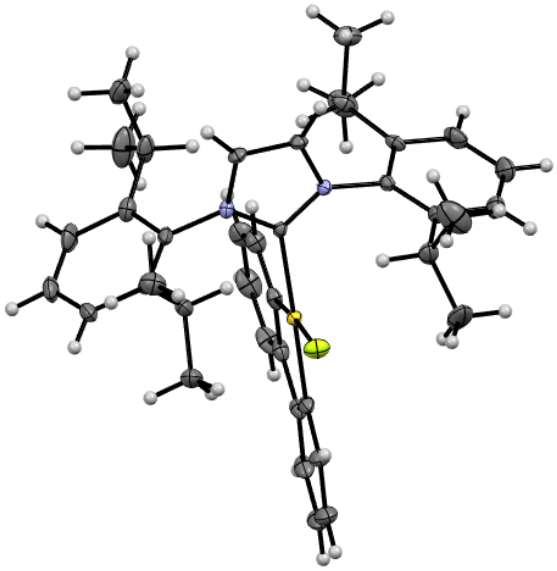
2.5.3 Synthetic Procedures

IPr(biphenyl)gold(III) fluoride (**61a**):



61a was prepared by salt metathesis from **61b**. **61a** (1.0 equiv., 0.13 mmol, 100 mg) was dissolved in DCM (2 mL) and added AgF (5.0 equiv. 0.65 mmol, 82 mg). Sonicated for 1 hour and repeated 5 times with an interval of 30 min (elevated temperature from sonication led to decomposition). The organic phase was then passed through glass fiber filter. Pentane was added to the filtrate and product precipitated out. After being collected and dried *in vacuo*, product is obtained as white solid (89 mg, 90%). ^{1}H NMR (600 MHz, Methylene Chloride-d_2, 23 °C) δ 7.49 (t, J = 7.8 Hz, 2H), 7.46 (dd, J = 7.8, 2.9 Hz, 1H), 7.39 (d, J = 9.1 Hz, 4H), 7.27 (d, J = 7.7 Hz, 2H), 7.19 (dd, J = 14.6, 7.5 Hz, 2H), 7.03 (t, J = 7.5 Hz, 2H), 6.95 (t, J = 7.4 Hz, 1H), 6.88 (dd, J = 7.8, 3.3 Hz, 1H), 6.73 (t, J = 7.5 Hz, 1H), 3.24 (p, J = 6.8 Hz, 2H), 3.04 (hept, J = 6.8 Hz, 2H), 1.47 (d, J = 6.6 Hz, 6H), 1.27 (d, J = 6.8 Hz, 6H), 1.10 (d, J = 6.9 Hz, 6H), 1.05 (d, J = 6.7 Hz, 6H). ^{13}C NMR (151 MHz, CD_2Cl_2, 23 °C) δ 159.94, 154.20, 151.78, 148.25, 147.36, 144.83, 134.42, 134.38, 133.87, 130.47, 129.84, 129.79, 127.05, 126.60, 126.45, 125.77, 124.91, 124.46, 124.08, 120.76, 119.73, 28.69, 28.56, 26.21, 25.92, 22.64, 22.40. ^{19}F NMR (376 MHz, CD_2Cl_2, 23 °C) δ -222.71. Compound ionized during ESI. **HRMS** (ESI): found 737.3181 C39H44N2Au requires 737.3165. X-ray crystallography data was shown in next section.

Crystallographic data of 61a



Bond precision: C-C = 0.0062 A Wavelength=0.71073

Cell: a=13.8036(8) b=14.8154(8) c=16.4447(8)
alpha=90 beta=90 gamma=90
Volume=3363.0(3)

Temperature: 100 K

	Calculated	Reported
Volume	3363.0(3)	3363.0(3)
Space group	P 21 21 21	P 21 21 21
Hall group	P 2ac 2ab	P 2ac 2ab
Moiety formula	C39 H44 Au F N2	0.1(C39 H44 Au F N2)
Sum formula	C39 H44 Au F N2	C H Au F N
Mr	756.73	242.99
Dx,g cm-3	1.495	4.799
Z	4	40
Mu (mm-1)	4.409	43.512
F000	1520.0	4080.0
F000'	1512.65	
h,k,lmax	21,22,25	21,22,25
Nref	12920[7073]	12861
Tmin,Tmax		0.427,0.747

Tmin'

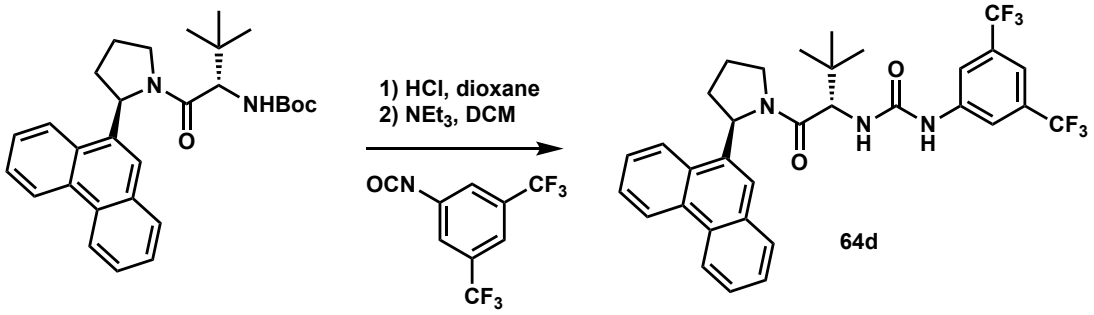
Correction method= # Reported T Limits: Tmin=0.427 Tmax=0.747
AbsCorr = NONE

Data completeness= 1.82/1.00 Theta(max)= 33.232

R(reflections)= 0.0287(11667) wR2(reflections)= 0.0567(12861)

S = 1.023 Npar= 396

Urea catalyst (**64**):



The procedure was adapted from a reported version of its thiourea counterpart.[10] The preparation of **64d** was described as an example. ((*S*)-3,3-dimethyl-1-oxo-1-((*R*)-2-(phenanthren-9-yl)pyrrolidin-1-yl) butan-2-yl) carbamate (2.1 mmol) was added HCl (4 M in dioxane, 10 mL) slowly at 0 ℃. The reaction was warmed to room temperature and stirred for 4 hours. The reaction mixture was then concentrated under vacuum, yielding a yellow oil that was used without further purification. To the yellow oil was added DCM (14 mL), followed by NEt_3 (0.86 mL, 6.2 mmol) dropwise. The mixture was stirred for 15 min before 3,5-bis(trifluoromethyl)phenyl isocyanate (0.36 mL, 2.1 mmol) was added dropwise. The reaction was stirred overnight, concentrated under vacuum, and purified by silica gel flash chromatography to obtain the desired product as pale yellow foam (900 mg, 69% over two steps). NMR showed rotamers, spectra were included in the corresponding section.

2.5.4 General Procedure for Catalytic Reactions (Lactonization, Conia-Ene Reaction, Enyne Isomerization and Hydroarylation of Allene with Indole)

All catalytic reactions were run in vials fitted with a screw cap and stirred using 8 mm magnetic stir bars. All gold precatalysts containing X-type ligand other than chloride or fluoride were made by salt metathesis described as following. Corresponding gold chloride was dissolved in DCM (0.02 M) and added 5 equiv. silver salt with desired X-type ligand. After 20-min. sonication, the mixture was passed through a glass fiber filter and the solvent of filtrate was then removed under reduced pressure. The resulting solid was used directly as desired precatalyst without further purification. Substrate(s) (0.1 mmol), hydrogen bond donor and solvent were added to the vial sequentially. The reaction mixture was then stirred for denoted time and at denoted temperature. When time was over, the mixture was passed through a glass fiber filter into an NMR tube and subjected to TLC and NMR analysis.

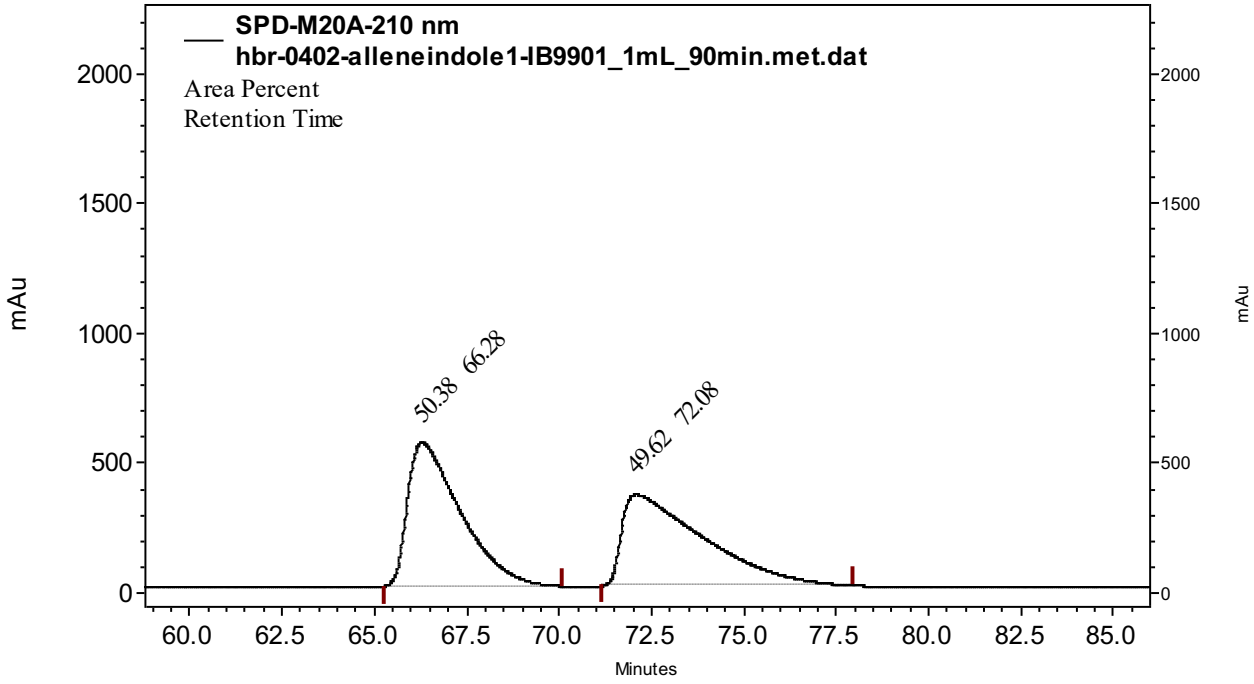
For hydroarylation of allene with indole, the reaction mixture was spotted on a 5 cm × 5 cm TLC plate and developed with hexane/DCM = 2:1. The product band was collected and suspended in hexane/isopropanol = 10:1. The solution was filtered and the filtrate was subjected to HPLC analysis.

2.5.5 Procedure for NMR Studies of Interaction Between 53, 54 and 55

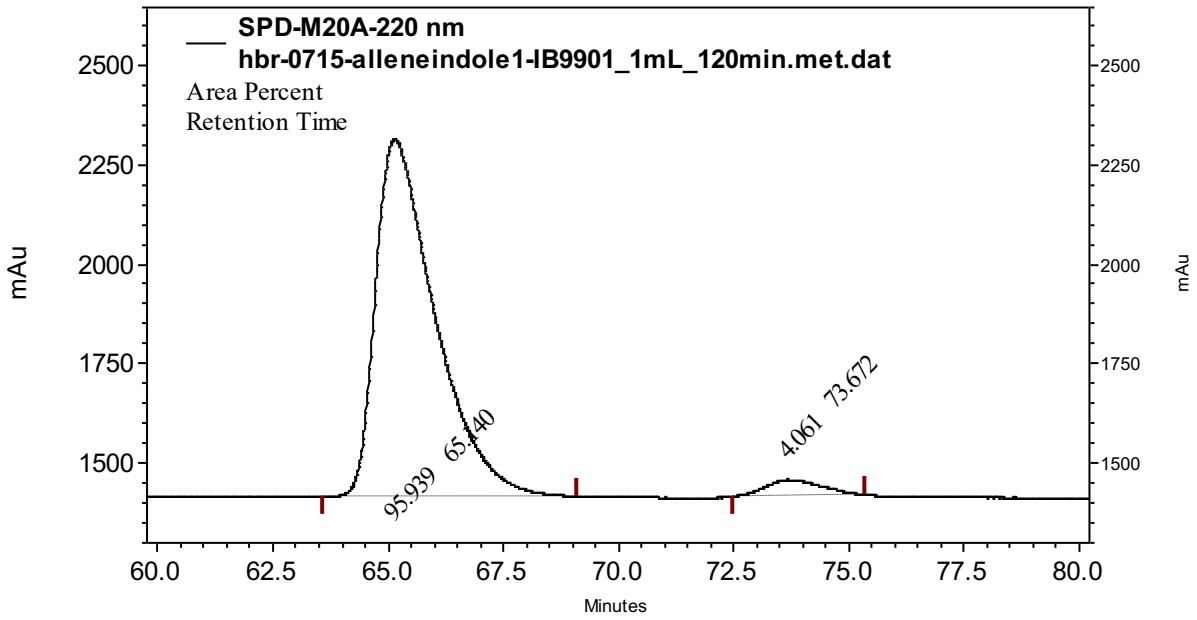
Three samples were prepared, each in DCM-d_2 (1 mL): 1. **55** (0.05 mmol, 8.4 mg); 2. **55** (0.05 mmol, 8.4 mg) and **53** (0.025 mmol, 11 mg); 3. **55** (0.05 mmol, 8.4 mg) and **54** (0.025 mmol, 12.5 mg).

2.5.6 HPLC Trace for Hydroarylation Product 65

HPLC Chiralpak IB column (99:1 hexanes:isopropanol, 1.0 mL/min, 210 nm); first enantiomer tr = 66.34 min, second enantiomer tr = 72.10 min.
Racemic trace:



Trace from optimized conditions:



2.5.7 Computational Details on the Origin of Enantioselectivities in Hydroarylation of Allene

All DFT calculations were performed using the *Gaussian 16* program[1] on Pitt CRC and FRONTERA supercomputers. Geometries of all stationary points were fully optimized using the dispersion-corrected[2] B3LYP functional,[3] i.e. B3LYP-D3, with the SDD[4] effective core potential basis set for Au and the 6-31G(d) basis set for other atoms. Vibrational frequency calculations at the same level of theory of the geometry optimization were performed to confirm the nature of stationary points as minima or transition states. Single-point energy calculations were carried out using ωB97X-D functional[5] with the SDD basis set for Au and 6-311+G(d,p) basis set for other atoms. Solvation energy corrections of methyl *tert*-butyl ether (MTBE) were calculated using the SMD solvation model[6] in the single-point energy calculations. Since the solvent parameters for MTBE are not available in *Gaussian 16*, the solvent parameters for dibutyl ether were used and the dielectric constant was modified to the value of MTBE (ε = 2.6).

Starting from initial optimized structures of relevant intermediates and transition states, conformational samplings were carried out using extensive metadynamics simulations and genetic z-matrix crossing (iMTD-GC) approach with the conformer–rotamer ensemble sampling (CREST) algorithm.[7] For these calculations, the semiempirical tight-binding based quantum chemistry method GFN2-xTB implemented in the xTB code[8] was used. For all conformational searches, the energy window was set to be 10 kcal/mol. Conformers that have RMSD less than 0.25 Å were discarded as duplicates. Other settings and thresholds were set to the default values. During TS samplings, the forming C–C bond distance was fixed to the value obtained from initial optimization.

The strengths of the π/CH-π interactions ($\Delta E_{\pi/\text{CH-}\pi}$) were calculated with Grimme's DFT-D4 method[9] using HF as the reference "functional". The π/CH-π stacking complexes were extracted from optimized structures of **TS-S** and **TS-R** by keeping the corresponding aryl/CH units. Additional hydrogen atoms were added to the dangling carbon atoms. The interaction energy was calculated from:

$$\Delta E_{\pi/\text{CH-}\pi} = E_{\text{dimer}} - E_{\pi/\text{CH}} - E_{\pi}$$

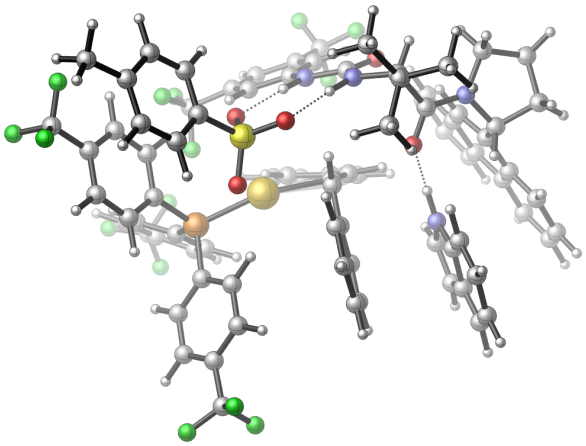


Figure S2.1 Optimized structure of reactant complex **RC**.

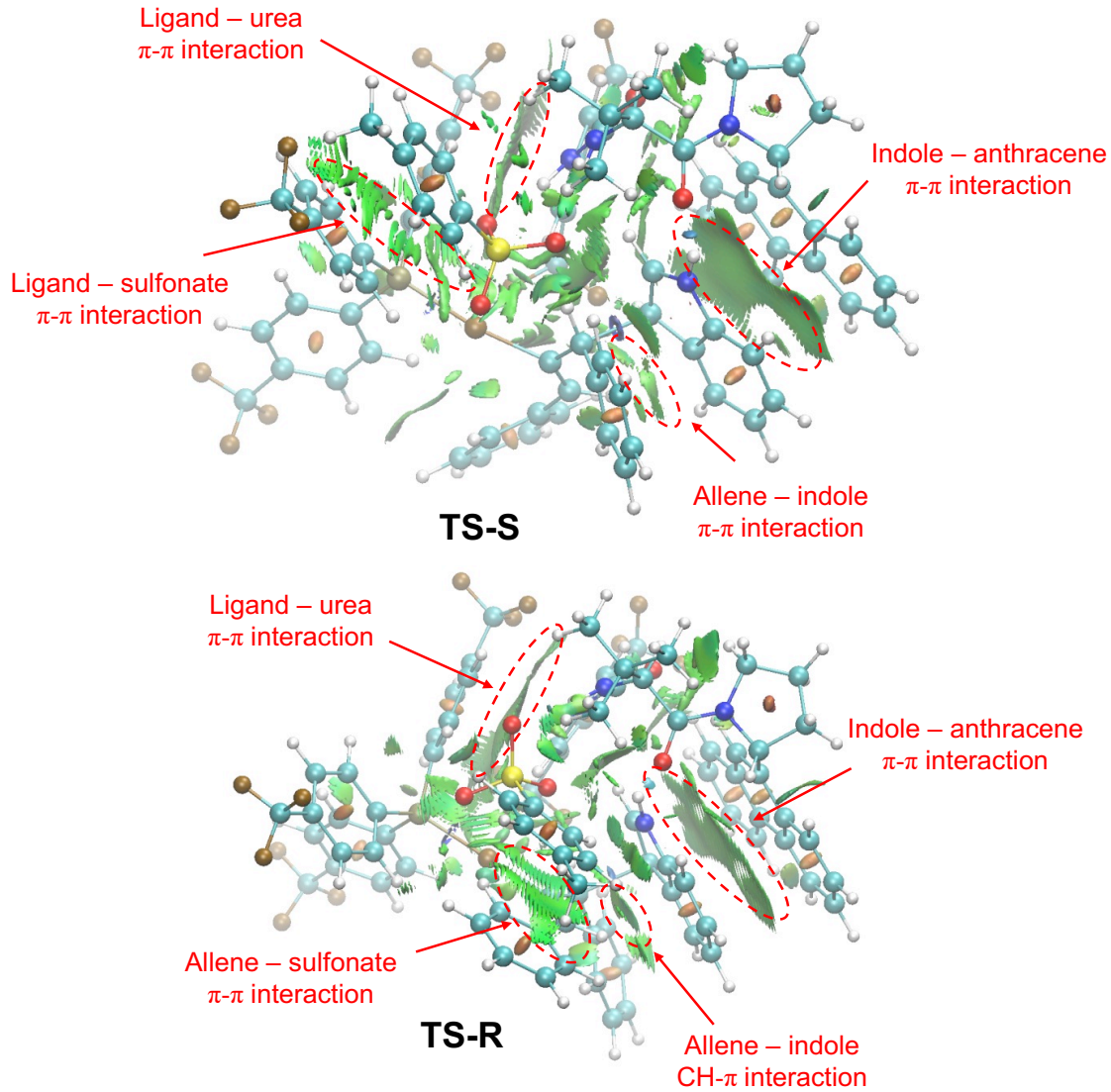


Figure S2.2 Non-covalent interactions in **TS-S** and **TS-R** (isovalue is 0.25).

Cartesian Coordinates

6-H$^+$

B3LYP-D3 SCF energy (au)	-2190.471692
B3LYP-D3 enthalpy (au)	-2189.824775
B3LYP-D3 free energy (au)	-2189.934538
ωB97X-D SCF energy in solution (au)	-2190.432363
ωB97X-D enthalpy in solution (au)	-2189.785446
ωB97X-D free energy in solution (au)	-2189.895209

Cartesian coordinates

ATOM	X	Y	Z
C	-1.33069600	5.03826900	-3.18381700
O	-2.49568300	5.20405700	-3.53249300
N	-0.29121900	5.50186300	-3.99222400
H	0.62390100	5.63928300	-3.58682100
N	-0.90279800	4.38886600	-2.05325500
H	0.08522600	4.17320900	-2.00829300
C	-0.66728300	6.39531200	-5.06672200
C	-1.68736200	3.68323200	-1.11440300
C	-3.08756000	3.66835100	-1.13452800
C	-0.99798800	2.93982300	-0.15071200
C	-3.76922100	2.89244300	-0.20003300
H	-3.62792100	4.21726200	-1.89031900
C	-1.70195700	2.16688000	0.76851000
H	0.08724600	2.92880000	-0.13586400
C	-3.09382600	2.13867400	0.75902100
H	-3.63849800	1.52140600	1.46331100
C	-1.44270100	5.65304200	-6.15179100
O	-2.37825400	6.41975000	-6.67762500
C	-1.92891900	3.93303500	-7.83185000
C	-0.22038000	3.45175600	-6.11788100
C	-1.28239600	2.56262400	-8.09425500
H	-1.74560100	4.63107800	-8.65753700
H	-3.00671800	3.86257600	-7.64543400
C	0.08765800	2.67019500	-7.40970000
H	0.64098600	4.00468900	-5.76739200
H	-1.87600800	1.77326700	-7.62687500
H	-1.21393100	2.35390200	-9.16375500
H	0.53002700	1.69737000	-7.18657800
H	0.79115200	3.23745400	-8.03157900
N	-1.22393900	4.45260100	-6.61906300
C	-0.77636100	2.58146200	-5.00420600
C	0.15109300	1.97367300	-4.06919600

C	-2.11523900	2.36406400	-4.86682700
C	1.54830000	2.20886400	-4.13281100
C	-0.35993300	1.15108700	-3.01418100
C	-2.66271000	1.52286900	-3.84874400
H	-2.82730000	2.86564300	-5.51479100
C	2.41368700	1.69557500	-3.18290000
H	1.96879300	2.78942700	-4.94789500
C	0.55209800	0.65006800	-2.05501900
C	-1.79016300	0.89014000	-2.91959700
C	-4.06037700	1.34015400	-3.74853500
C	1.90749400	0.91804900	-2.12776200
H	3.47945900	1.89133700	-3.25631300
H	0.18686000	0.06876100	-1.21804500
C	-2.36835300	0.06656600	-1.92639100
H	-4.71024500	1.85236700	-4.45358600
C	-4.59719500	0.53790000	-2.76188100
H	2.57762700	0.52214800	-1.37066400
C	-3.73938300	-0.10609300	-1.85124900
H	-1.74639000	-0.42142100	-1.18685200
H	-5.67193800	0.41885100	-2.67364400
H	-4.15880800	-0.72786400	-1.06652900
C	-5.27695700	2.85272100	-0.22538500
C	-0.93864100	1.24807300	1.68371400
F	-5.73314100	1.60251900	0.02504200
F	-5.80985900	3.66451800	0.70901600
F	-5.77196800	3.23172100	-1.42364000
F	-0.70987900	0.04870200	1.07056600
F	0.26998000	1.74829900	2.01053000
F	-1.60943300	0.98463800	2.81658800
H	-1.40136600	7.12331000	-4.70248700
C	0.54833000	7.22209600	-5.63374200
C	0.06398600	8.13313900	-6.77955400
H	-0.23549100	7.56208000	-7.66494600
H	-0.78414300	8.75399000	-6.47370200
H	0.87839900	8.79818400	-7.08247400
C	1.68904300	6.32800700	-6.15305900
H	2.51469300	6.95650800	-6.50151700
H	2.09493700	5.66674300	-5.37866900
H	1.37039300	5.71488100	-7.00397200
C	1.06754500	8.11753600	-4.48718700
H	1.49219400	7.54486500	-3.65482000
H	1.86381600	8.76710200	-4.86400300
H	0.27209500	8.75597200	-4.08795400
H	-2.91371500	5.98102800	-7.36229100

RC

B3LYP-D3 SCF energy (au)	-6210.941596
B3LYP-D3 enthalpy (au)	-6209.463814
B3LYP-D3 free energy (au)	-6209.719742
ωB97X-D SCF energy in solution (au)	-6210.688494
ωB97X-D enthalpy in solution (au)	-6209.210712
ωB97X-D free energy in solution (au)	-6209.466640

Cartesian coordinates

ATOM	X	Y	Z
C	-1.695965	-2.523076	2.151858
O	-2.753045	-3.050284	1.782690
N	-1.636436	-1.699519	3.240133
H	-0.783318	-1.183469	3.458396
N	-0.471209	-2.711390	1.527223
H	0.333915	-2.183587	1.876521
C	-2.876530	-1.374475	3.922061
C	-0.218900	-3.413885	0.350907
C	-1.175469	-4.184920	-0.335636
C	1.083169	-3.330978	-0.173388
C	-0.815671	-4.837096	-1.512085
H	-2.174870	-4.262653	0.062621
C	1.408811	-3.982629	-1.359122
H	1.827308	-2.743498	0.348429
C	0.470587	-4.747707	-2.045785
H	0.726206	-5.248056	-2.971697
C	-3.817255	-0.649365	2.936776
O	-3.377438	0.262734	2.219731
C	-5.740488	-2.169868	3.566578
C	-6.096444	-0.214805	2.134319
C	-7.215331	-2.092647	3.132686
H	-5.650852	-2.095489	4.653635
H	-5.241733	-3.085588	3.234596
C	-7.423068	-0.601017	2.828442
H	-5.853662	0.843562	2.257292
H	-7.371772	-2.679698	2.222412
H	-7.890135	-2.473947	3.904010
H	-8.294140	-0.406201	2.199307
H	-7.529613	-0.027469	3.757515
N	-5.123913	-0.994309	2.918282
C	-6.125669	-0.575905	0.653422
C	-6.902213	0.243395	-0.257700
C	-5.479864	-1.683715	0.189456
C	-7.504366	1.454103	0.163862
C	-7.022853	-0.142558	-1.628542

C	-5.607974	-2.126260	-1.168892
H	-4.844182	-2.265404	0.850446
C	-8.187561	2.266748	-0.719314
H	-7.399227	1.780084	1.191751
C	-7.741416	0.705096	-2.503584
C	-6.395192	-1.375126	-2.088470
C	-4.981159	-3.321961	-1.590419
C	-8.311344	1.885551	-2.065581
H	-8.611958	3.204634	-0.373545
H	-7.837413	0.439995	-3.550757
C	-6.526848	-1.873566	-3.406852
H	-4.376814	-3.873004	-0.877210
C	-5.133944	-3.787529	-2.881813
H	-8.844288	2.522261	-2.766373
C	-5.916119	-3.054725	-3.793519
H	-7.127473	-1.337016	-4.133239
H	-4.638103	-4.698866	-3.192694
H	-6.041986	-3.416261	-4.810736
O	2.138926	1.212703	2.198026
S	1.981653	-0.105081	2.866037
O	1.973168	-1.264064	1.905686
O	0.793675	-0.171317	3.774740
C	3.456141	-0.337523	3.855729
C	4.229436	0.765114	4.213751
C	3.821023	-1.625663	4.253360
C	5.378517	0.571828	4.979844
H	3.938835	1.753739	3.875899
C	4.970537	-1.801523	5.018985
H	3.218581	-2.475407	3.948771
C	5.766371	-0.708513	5.395018
H	5.992164	1.427520	5.248991
H	5.262230	-2.803394	5.324919
C	7.037748	-0.916944	6.180898
H	7.320250	-0.015713	6.734667
H	6.937348	-1.740633	6.895919
H	7.864373	-1.162208	5.504711
H	-3.955736	1.134533	0.616191
C	-4.454644	3.177864	0.704349
C	-4.400400	2.102422	-1.262697
C	-4.787473	4.116754	-0.315899
C	-4.380086	3.529902	2.056713
C	-4.743550	3.399433	-1.559822
C	-5.055127	5.446640	0.054921
C	-4.650545	4.852508	2.388885
H	-4.098266	2.793088	2.801793
H	-4.959064	3.789619	-2.544984

C	-4.984339	5.801596	1.397569
H	-5.309645	6.187103	-0.699792
H	-4.596146	5.164253	3.428808
H	-5.188192	6.827773	1.692924
N	-4.225557	1.966067	0.096733
H	-4.286340	1.251511	-1.917859
C	-1.840033	-5.614931	-2.290425
C	2.753546	-3.718389	-1.965930
F	-2.976622	-5.834674	-1.588063
F	-2.195520	-4.961957	-3.424355
F	-1.364672	-6.821696	-2.674861
F	3.731518	-3.607331	-1.033722
F	3.129974	-4.664273	-2.845816
F	2.751065	-2.529968	-2.646793
H	-3.336639	-2.319727	4.223486
C	-2.629402	-0.546450	5.230591
C	-3.961073	-0.420490	5.997300
H	-3.808002	0.166772	6.909251
H	-4.729884	0.085771	5.402786
H	-4.345437	-1.402003	6.299757
C	-2.081916	0.866690	4.952704
H	-2.759070	1.450299	4.324412
H	-1.954166	1.394996	5.905298
H	-1.106143	0.830718	4.466760
C	-1.624944	-1.315557	6.115464
H	-0.624562	-1.336548	5.674555
H	-1.544656	-0.824260	7.092364
H	-1.953240	-2.348894	6.282816
Au	0.974023	0.224821	-0.493709
P	3.070253	1.022025	-1.132888
C	4.476019	0.614403	-0.045074
C	5.391957	1.586855	0.381022
C	4.624424	-0.716111	0.368162
C	6.454028	1.225228	1.205521
H	5.270620	2.623000	0.082230
C	5.691251	-1.076151	1.187946
H	3.905606	-1.467179	0.068793
C	6.603604	-0.105889	1.603566
H	7.160801	1.974318	1.547561
H	5.797553	-2.101153	1.523082
C	2.884495	2.846772	-1.143698
C	2.982001	3.598317	-2.321138
C	2.475047	3.462595	0.053237
C	2.634833	4.950960	-2.314151
H	3.303011	3.133366	-3.247694
C	2.150860	4.813277	0.056788

H	2.372104	2.877584	0.960921
C	2.208084	5.550448	-1.129701
H	2.688833	5.533655	-3.227374
H	1.811311	5.283231	0.972127
C	3.561594	0.536578	-2.825702
C	4.905305	0.390196	-3.194791
C	2.550664	0.295353	-3.768909
C	5.233485	-0.003447	-4.491350
H	5.694477	0.569906	-2.471269
C	2.878865	-0.091311	-5.064322
H	1.505562	0.379877	-3.486537
C	4.220835	-0.244452	-5.422088
H	6.272062	-0.121854	-4.780955
H	2.094582	-0.286534	-5.787993
C	7.800926	-0.485704	2.431784
C	1.709970	6.969739	-1.122421
C	4.567217	-0.743621	-6.800772
F	5.800648	-0.348098	-7.183657
F	4.547360	-2.094416	-6.849940
F	3.687445	-0.300493	-7.725439
F	8.063547	0.435991	3.389039
F	8.914365	-0.575331	1.666990
F	7.644975	-1.678745	3.046346
F	2.096552	7.629190	-0.008073
F	2.146325	7.672638	-2.189165
F	0.353531	7.009185	-1.146739
C	-0.983492	0.719210	0.742308
H	-0.785801	0.215320	1.685082
C	-1.009518	2.188139	0.802300
C	-0.719451	2.810702	2.026696
C	-1.311752	2.975952	-0.323391
C	-0.777276	4.199543	2.132055
H	-0.438917	2.201222	2.877491
C	-1.358938	4.358808	-0.214780
H	-1.530712	2.492720	-1.269711
C	-1.098763	4.974363	1.015836
H	-0.571252	4.675325	3.086772
H	-1.603171	4.962933	-1.081626
H	-1.140466	6.056589	1.092857
C	-1.231233	-0.041945	-0.366668
C	-2.048104	-0.616953	-1.238972
H	-3.103523	-0.615026	-0.960911
C	-1.741970	-1.225088	-2.542971
C	-2.794681	-1.401213	-3.457007
C	-0.451041	-1.615915	-2.935840
C	-2.557704	-1.926046	-4.726391

H	-3.806339	-1.132955	-3.169734
C	-0.211640	-2.137701	-4.203812
H	0.368397	-1.551971	-2.229278
C	-1.265675	-2.292061	-5.108884
H	-3.392202	-2.061237	-5.408229
H	0.797037	-2.445270	-4.464978
H	-1.084236	-2.712665	-6.094264

TS-S

B3LYP-D3 SCF energy (au)	-6210.929915
B3LYP-D3 enthalpy (au)	-6209.452649
B3LYP-D3 free energy (au)	-6209.703776
ωB97X-D SCF energy in solution (au)	-6210.670247
ωB97X-D enthalpy in solution (au)	-6209.192981
ωB97X-D free energy in solution (au)	-6209.444108

Cartesian coordinates

ATOM	X	Y	Z
C	-2.414604	-2.128704	-1.759371
O	-3.238965	-2.000565	-2.673936
N	-2.504989	-3.099453	-0.792905
H	-2.045120	-2.903192	0.102861
N	-1.308445	-1.301986	-1.610398
H	-0.643027	-1.484141	-0.849385
C	-3.729178	-3.887428	-0.724967
C	-1.063441	-0.145458	-2.361222
C	-1.445887	-0.024428	-3.705764
C	-0.399106	0.923669	-1.738236
C	-1.179488	1.155274	-4.394973
H	-1.960989	-0.839674	-4.192275
C	-0.141237	2.093379	-2.451360
H	-0.088325	0.837003	-0.701191
C	-0.523099	2.222768	-3.785883
H	-0.316474	3.130198	-4.337757
C	-4.824141	-3.002064	-0.102947
O	-4.635772	-2.481367	1.011121
C	-6.297322	-3.268116	-2.149635
C	-6.981345	-1.869579	-0.249981
C	-7.579553	-2.493986	-2.498037
H	-6.479599	-4.348934	-2.115639
H	-5.477483	-3.063052	-2.842041
C	-8.209389	-2.197334	-1.127894
H	-7.135448	-2.143519	0.796412
H	-7.321370	-1.554387	-2.997143

H	-8.237272	-3.061666	-3.161917
H	-8.929510	-1.375716	-1.151662
H	-8.714585	-3.088991	-0.736271
N	-5.956932	-2.774193	-0.799386
C	-6.569562	-0.402349	-0.329763
C	-7.227892	0.573470	0.516509
C	-5.604114	0.005314	-1.202404
C	-8.283174	0.210727	1.390181
C	-6.808811	1.941788	0.480257
C	-5.159533	1.365096	-1.272428
H	-5.091619	-0.715461	-1.832658
C	-8.910657	1.144162	2.195237
H	-8.623196	-0.818560	1.424451
C	-7.477709	2.870700	1.308934
C	-5.717868	2.339527	-0.398135
C	-4.139307	1.732919	-2.180821
C	-8.505995	2.488355	2.149905
H	-9.720097	0.837801	2.852271
H	-7.182089	3.913202	1.292024
C	-5.169349	3.643078	-0.422700
H	-3.750610	0.982230	-2.860331
C	-3.642185	3.021377	-2.199723
H	-8.997744	3.228541	2.774909
C	-4.148632	3.975464	-1.296509
H	-5.531928	4.397756	0.266049
H	-2.861465	3.290061	-2.902374
H	-3.738474	4.981671	-1.287889
O	-1.196014	-2.265490	1.561918
S	0.308144	-2.312727	1.525563
O	0.931682	-1.790754	2.758311
O	0.799540	-1.685653	0.247745
C	0.770454	-4.040949	1.402849
C	0.798585	-4.817666	2.563335
C	1.085529	-4.599750	0.165358
C	1.148685	-6.162070	2.475011
H	0.566424	-4.361609	3.520494
C	1.440952	-5.946825	0.094265
H	1.064410	-3.979975	-0.724220
C	1.478697	-6.747226	1.243053
H	1.180465	-6.767695	3.377511
H	1.703925	-6.380865	-0.866945
C	1.920665	-8.188080	1.172320
H	1.776560	-8.604931	0.170238
H	2.986987	-8.266172	1.412887
H	1.371606	-8.812337	1.885633
H	-4.432041	-0.854841	1.694481

C	-4.380211	1.133957	2.623663
C	-2.975296	0.438391	1.023641
C	-3.519959	2.220312	2.349562
C	-5.404030	1.190920	3.560461
C	-2.508772	1.736402	1.403216
C	-3.721404	3.425907	3.021121
C	-5.582389	2.404204	4.224341
H	-6.053381	0.341366	3.741342
H	-1.991985	2.371060	0.695492
C	-4.760484	3.509340	3.950244
H	-3.083251	4.282900	2.827494
H	-6.382265	2.498238	4.952415
H	-4.932804	4.444049	4.476305
N	-3.994651	0.072678	1.787309
H	-2.547007	-0.249389	0.310083
C	-1.712183	1.314826	-5.792386
C	0.429730	3.280572	-1.726560
F	-2.982937	1.794079	-5.757091
F	-0.983499	2.185734	-6.521427
F	-1.751502	0.145520	-6.462977
F	-0.494230	3.795704	-0.865618
F	1.519702	2.973630	-0.989960
F	0.782440	4.278337	-2.563741
H	-3.995181	-4.131416	-1.753507
C	-3.528673	-5.240387	0.026455
C	-2.442907	-6.041267	-0.717993
H	-2.708767	-6.191456	-1.772232
H	-1.477306	-5.530308	-0.678194
H	-2.320725	-7.027829	-0.255581
C	-4.861551	-6.013279	-0.032516
H	-4.753135	-6.990361	0.451365
H	-5.665036	-5.475714	0.485373
H	-5.178837	-6.188938	-1.068449
C	-3.108262	-5.065048	1.498854
H	-3.869625	-4.532386	2.072912
H	-2.955941	-6.053812	1.948745
H	-2.173870	-4.507425	1.597109
Au	1.897149	0.993213	1.451409
P	3.651154	0.062177	0.205833
C	3.273327	0.149465	-1.595606
C	2.464097	-0.833101	-2.185799
C	3.674362	1.257312	-2.357842
C	2.072573	-0.714463	-3.518202
H	2.112644	-1.669560	-1.594208
C	3.268873	1.382094	-3.683220
H	4.289658	2.034454	-1.917761

C	2.466108	0.396628	-4.263559
H	1.431784	-1.466230	-3.964927
H	3.561957	2.251275	-4.263226
C	4.095262	-1.686727	0.519082
C	4.673279	-2.504231	-0.466936
C	3.813755	-2.220988	1.782522
C	4.952929	-3.839195	-0.192646
H	4.879637	-2.107247	-1.455945
C	4.097032	-3.559292	2.057361
H	3.310828	-1.617603	2.529172
C	4.658817	-4.365862	1.069274
H	5.381176	-4.477685	-0.958941
H	3.839444	-3.980728	3.021736
C	5.209293	1.025679	0.374990
C	5.099850	2.394559	0.669313
C	6.478991	0.460029	0.191450
C	6.240988	3.187646	0.764732
H	4.124851	2.843818	0.833489
C	7.621317	1.251128	0.299100
H	6.581005	-0.597857	-0.028814
C	7.500976	2.614434	0.581016
H	6.146165	4.246023	0.983239
H	8.604449	0.814918	0.156512
C	2.066196	0.538665	-5.706673
C	4.989188	-5.807867	1.340218
C	8.737325	3.455751	0.755808
F	9.766782	2.997287	0.009754
F	8.520106	4.743330	0.408039
F	9.152139	3.458512	2.043664
F	1.004390	-0.235471	-6.022418
F	3.075622	0.187119	-6.537432
F	1.742802	1.818019	-6.005716
F	4.610305	-6.605401	0.309968
F	6.321473	-5.989087	1.495484
F	4.389977	-6.277946	2.455489
C	-0.897778	1.060572	2.448533
H	-0.791584	0.122264	1.923703
C	-1.375262	0.829399	3.831234
C	-1.908734	-0.431593	4.160511
C	-1.360603	1.840476	4.808276
C	-2.437231	-0.660702	5.429699
H	-1.892137	-1.224068	3.420502
C	-1.893955	1.607165	6.072056
H	-0.926823	2.805226	4.569091
C	-2.441007	0.358158	6.384391
H	-2.844734	-1.638452	5.672928

H	-1.882473	2.398435	6.816818
H	-2.856100	0.178879	7.372965
C	0.216483	1.992217	2.180674
C	0.109341	3.337727	2.209050
H	-0.882549	3.794193	2.275865
C	1.215011	4.304475	2.077697
C	1.037825	5.477165	1.323449
C	2.460046	4.095686	2.698947
C	2.081215	6.386803	1.154855
H	0.083699	5.650827	0.833835
C	3.500961	5.011346	2.541034
H	2.597828	3.213057	3.315928
C	3.320132	6.156466	1.759957
H	1.927989	7.277104	0.550346
H	4.451816	4.833162	3.037520
H	4.130427	6.870488	1.637451

TS-R

B3LYP-D3 SCF energy (au)	-6210.922083
B3LYP-D3 enthalpy (au)	-6209.444431
B3LYP-D3 free energy (au)	-6209.696894
ωB97X-D SCF energy in solution (au)	-6210.662066
ωB97X-D enthalpy in solution (au)	-6209.184414
ωB97X-D free energy in solution (au)	-6209.436877

Cartesian coordinates

ATOM	X	Y	Z
C	2.499606	0.829072	2.860156
O	3.558937	1.471640	2.859232
N	2.361927	-0.375238	3.477896
H	1.468004	-0.871396	3.427973
N	1.338210	1.255760	2.212324
H	0.708011	0.502077	1.918732
C	3.564506	-1.074692	3.899602
C	1.208614	2.455003	1.521138
C	1.934954	3.609017	1.855854
C	0.289253	2.512877	0.455050
C	1.763384	4.773358	1.111924
H	2.626418	3.586423	2.684705
C	0.133149	3.692714	-0.265779
H	-0.302117	1.635940	0.211440
C	0.871290	4.835626	0.044683
H	0.745168	5.751842	-0.520067
C	4.324204	-1.519325	2.630911

O	3.728061	-2.106557	1.712734
C	6.446292	-0.431756	3.484205
C	6.405277	-1.608240	1.333649
C	7.798210	-0.272919	2.768313
H	6.560507	-0.969665	4.430637
H	5.954028	0.525854	3.676509
C	7.861694	-1.494346	1.838879
H	6.130693	-2.631914	1.066602
H	7.799307	0.644351	2.171020
H	8.633356	-0.221743	3.472268
H	8.577799	-1.375252	1.022814
H	8.125791	-2.396638	2.404402
N	5.643466	-1.236141	2.538674
C	6.134864	-0.683950	0.149281
C	6.616353	-1.045467	-1.169445
C	5.479018	0.497087	0.326448
C	7.320386	-2.253225	-1.399489
C	6.376626	-0.170765	-2.276645
C	5.211034	1.395293	-0.754213
H	5.095999	0.774281	1.302550
C	7.782850	-2.595395	-2.656226
H	7.503063	-2.932969	-0.574586
C	6.862672	-0.551954	-3.548145
C	5.639631	1.069854	-2.071471
C	4.491437	2.590558	-0.513903
C	7.554134	-1.733501	-3.741064
H	8.319902	-3.528676	-2.802140
H	6.693994	0.094594	-4.402119
C	5.304927	1.967901	-3.112074
H	4.180481	2.811861	0.502599
C	4.181713	3.449767	-1.550567
H	7.914557	-1.994430	-4.732319
C	4.589364	3.127770	-2.860435
H	5.598739	1.751676	-4.133596
H	3.639973	4.367937	-1.348197
H	4.347988	3.797081	-3.682191
O	0.214238	-1.020429	0.983147
S	-0.572151	-1.891565	1.924082
O	-2.023854	-1.959373	1.602309
O	-0.306704	-1.503159	3.348510
C	0.046109	-3.559964	1.707659
C	0.981160	-3.848159	0.717668
C	-0.463496	-4.572136	2.522013
C	1.406009	-5.161545	0.538509
H	1.335494	-3.057805	0.072807
C	-0.030084	-5.882630	2.331793

H	-1.187324	-4.334434	3.295305
C	0.902853	-6.198226	1.333482
H	2.113417	-5.386078	-0.255282
H	-0.428371	-6.674789	2.961497
C	1.318549	-7.626035	1.075129
H	1.068408	-8.281709	1.915566
H	0.808680	-8.016231	0.183889
H	2.396221	-7.704508	0.890787
H	2.710837	-1.300051	0.352506
C	3.170501	-1.786029	-1.681688
C	2.276367	0.173659	-1.084399
C	3.027303	-1.030578	-2.870760
C	3.705941	-3.068975	-1.652466
C	2.383006	0.217057	-2.497689
C	3.442509	-1.588601	-4.084439
C	4.105307	-3.607626	-2.875922
H	3.817795	-3.599878	-0.713106
H	2.481139	1.146864	-3.037645
C	3.976298	-2.877590	-4.072864
H	3.345951	-1.031121	-5.010799
H	4.541106	-4.601979	-2.903132
H	4.313720	-3.324399	-5.003698
N	2.688603	-1.006777	-0.628158
H	1.903309	0.930364	-0.417618
C	2.636057	5.960283	1.412286
C	-0.836375	3.788126	-1.406801
F	3.802414	5.880400	0.716754
F	2.049811	7.124747	1.058003
F	2.961568	6.041700	2.716686
F	-0.208676	4.117816	-2.566528
F	-1.495612	2.626587	-1.641325
F	-1.776288	4.738774	-1.196094
H	4.170848	-0.351223	4.447453
C	3.267118	-2.252029	4.882313
C	4.612549	-2.826611	5.368498
H	5.205633	-2.070701	5.897789
H	4.434370	-3.652818	6.065496
H	5.212804	-3.217498	4.538400
C	2.436734	-3.377276	4.240149
H	1.438684	-3.030356	3.970809
H	2.908413	-3.777814	3.339753
H	2.314577	-4.194517	4.961413
C	2.497714	-1.684106	6.091991
H	2.348499	-2.471062	6.840709
H	3.049311	-0.863534	6.567729
H	1.512957	-1.309238	5.798155

Au	-1.953381	-0.472135	-1.186363
P	-3.698770	0.408944	0.123318
C	-3.071506	1.590142	1.382203
C	-2.387373	1.096211	2.505995
C	-3.093174	2.970985	1.137506
C	-1.701300	1.969600	3.344932
H	-2.357256	0.032271	2.704889
C	-2.408455	3.842945	1.982155
H	-3.602425	3.369961	0.267540
C	-1.696616	3.340448	3.072449
H	-1.129508	1.571060	4.175644
H	-2.386194	4.904457	1.761837
C	-4.706167	-0.832615	1.010576
C	-5.303024	-0.575164	2.250611
C	-4.873680	-2.086918	0.406781
C	-6.060890	-1.560938	2.880946
H	-5.159948	0.383806	2.739082
C	-5.635559	-3.068538	1.031404
H	-4.387126	-2.302718	-0.539791
C	-6.226451	-2.804907	2.270092
H	-6.522475	-1.365606	3.842985
H	-5.765970	-4.039615	0.565391
C	-4.918473	1.393070	-0.840879
C	-4.592139	1.800840	-2.141864
C	-6.149370	1.778034	-0.286561
C	-5.479272	2.587487	-2.876539
H	-3.643233	1.504210	-2.577116
C	-7.036935	2.560010	-1.019772
H	-6.418311	1.463537	0.717106
C	-6.698694	2.966247	-2.314358
H	-5.222696	2.909063	-3.880319
H	-7.985998	2.862744	-0.589849
C	-0.913340	4.274304	3.955369
C	-6.985431	-3.894817	2.978301
C	-7.686655	3.762840	-3.125517
F	-7.073216	4.531704	-4.051302
F	-8.545023	2.952987	-3.786612
F	-8.432637	4.576085	-2.345199
F	0.198731	3.680351	4.444256
F	-1.640053	4.688089	5.019194
F	-0.521134	5.384694	3.288566
F	-7.610256	-4.717482	2.105697
F	-6.162115	-4.665500	3.725159
F	-7.924404	-3.394816	3.812570
C	0.246104	0.071671	-3.029364
H	0.086825	1.011897	-2.512836

C	0.379954	0.272327	-4.487002
C	0.598992	1.585125	-4.956783
C	0.313473	-0.772897	-5.425843
C	0.777984	1.839243	-6.311831
H	0.623330	2.404888	-4.242350
C	0.500563	-0.516249	-6.783944
H	0.091824	-1.779030	-5.092856
C	0.739265	0.784856	-7.231560
H	0.943692	2.856932	-6.654357
H	0.446917	-1.335186	-7.496015
H	0.878459	0.980590	-8.291262
C	-0.377656	-1.082494	-2.410429
C	0.060440	-2.350182	-2.643040
H	0.979606	-2.463802	-3.216238
C	-0.484807	-3.638843	-2.214710
C	-1.509413	-3.804712	-1.261529
C	0.089683	-4.801125	-2.770556
C	-1.954509	-5.072386	-0.902135
H	-1.912782	-2.941220	-0.744178
C	-0.359358	-6.070912	-2.414994
H	0.905116	-4.695914	-3.483046
C	-1.387392	-6.212419	-1.479111
H	-2.719065	-5.167869	-0.136170
H	0.099340	-6.950533	-2.859520
H	-1.728086	-7.201747	-1.185222

TS-S-F

B3LYP-D3 SCF energy (au)	-5497.506698
B3LYP-D3 enthalpy (au)	-5496.076922
B3LYP-D3 free energy (au)	-5496.307581
ωB97X-D SCF energy in solution (au)	-5497.219019
ωB97X-D enthalpy in solution (au)	-5495.789243
ωB97X-D free energy in solution (au)	-5496.019902

Cartesian coordinates

ATOM	X	Y	Z
C	-2.481187	-2.062302	-1.756881
O	-3.262431	-1.926465	-2.708235
N	-2.616077	-3.036903	-0.799249
H	-2.167102	-2.873912	0.109068
N	-1.386431	-1.237216	-1.552316
H	-0.745912	-1.425908	-0.768987
C	-3.839249	-3.828504	-0.783549
C	-1.056387	-0.124464	-2.336244

C	-1.289528	-0.075392	-3.718538
C	-0.430424	0.961889	-1.706831
C	-0.897463	1.046743	-4.444990
H	-1.762707	-0.912810	-4.211675
C	-0.067658	2.083072	-2.450084
H	-0.229443	0.926511	-0.640616
C	-0.294258	2.139521	-3.824739
H	0.002501	3.006157	-4.400372
C	-4.943052	-2.963895	-0.148599
O	-4.784672	-2.500496	0.994748
C	-6.360418	-3.114128	-2.247793
C	-7.058924	-1.760665	-0.320910
C	-7.607508	-2.288663	-2.606152
H	-6.575231	-4.189544	-2.257733
H	-5.514858	-2.909902	-2.908758
C	-8.269063	-2.016644	-1.245795
H	-7.254119	-2.063223	0.710493
H	-7.305525	-1.342081	-3.065964
H	-8.262294	-2.813005	-3.307566
H	-8.960629	-1.170626	-1.262670
H	-8.815422	-2.903039	-0.900197
N	-6.047221	-2.679203	-0.870701
C	-6.593473	-0.307064	-0.338216
C	-7.241194	0.664577	0.520821
C	-5.584230	0.091496	-1.164026
C	-8.333592	0.312263	1.351780
C	-6.771737	2.016863	0.543228
C	-5.083593	1.433329	-1.170116
H	-5.079760	-0.626388	-1.803854
C	-8.947844	1.240123	2.173183
H	-8.711639	-0.704192	1.340412
C	-7.426854	2.940436	1.388695
C	-5.640818	2.402419	-0.289079
C	-4.003088	1.782569	-2.014080
C	-8.491023	2.568077	2.188493
H	-9.785717	0.942019	2.797571
H	-7.090510	3.970133	1.420010
C	-5.046692	3.685572	-0.255634
H	-3.605151	1.029759	-2.686889
C	-3.453593	3.049101	-1.968721
H	-8.969965	3.303491	2.828878
C	-3.972329	4.000379	-1.069648
H	-5.413646	4.436103	0.435252
H	-2.617384	3.303302	-2.609965
H	-3.524300	4.988741	-1.013184
O	-1.321377	-2.370159	1.637683

S	0.182852	-2.339713	1.588914
O	0.798195	-1.850770	2.837981
O	0.628444	-1.623468	0.341411
C	0.750221	-4.027533	1.364944
C	0.952592	-4.833862	2.486096
C	1.026704	-4.508080	0.085609
C	1.465023	-6.118169	2.319970
H	0.744399	-4.437667	3.474768
C	1.542288	-5.794928	-0.065178
H	0.860352	-3.870340	-0.775628
C	1.787481	-6.610726	1.046948
H	1.643585	-6.740968	3.193339
H	1.778090	-6.162997	-1.060878
C	2.450819	-7.956385	0.887351
H	2.242216	-8.398634	-0.092620
H	3.538618	-7.843186	0.978818
H	2.126052	-8.663013	1.658643
H	-4.483027	-0.920225	1.745167
C	-4.440144	1.037124	2.735653
C	-3.031689	0.402434	1.114419
C	-3.587439	2.137243	2.494738
C	-5.470391	1.061850	3.667067
C	-2.579058	1.694525	1.526106
C	-3.796250	3.320100	3.203425
C	-5.658833	2.254261	4.365244
H	-6.114680	0.203007	3.820954
H	-2.087466	2.356488	0.825815
C	-4.839573	3.370402	4.130092
H	-3.160510	4.184953	3.038797
H	-6.463025	2.323049	5.091463
H	-5.017924	4.287417	4.684560
N	-4.045516	0.003399	1.869565
H	-2.602822	-0.255236	0.373587
C	-1.152102	1.068026	-5.927738
C	0.481219	3.282747	-1.727027
F	-2.441375	1.382833	-6.201378
F	-0.378790	1.974969	-6.562788
F	-0.916233	-0.137407	-6.490093
F	-0.442924	3.772650	-0.854854
F	1.587648	2.998142	-1.004445
F	0.802783	4.289954	-2.566250
H	-4.085246	-4.029298	-1.826155
C	-3.653795	-5.211982	-0.087509
C	-2.544412	-5.975829	-0.836372
H	-2.774523	-6.070284	-1.905403
H	-1.579935	-5.469639	-0.738222

H	-2.439062	-6.985522	-0.422265
C	-4.982828	-5.982524	-0.220407
H	-4.888151	-6.979645	0.223883
H	-5.801883	-5.467434	0.296125
H	-5.268995	-6.112435	-1.272142
C	-3.275678	-5.104470	1.402686
H	-4.054994	-4.601084	1.979022
H	-3.134454	-6.113305	1.809968
H	-2.346747	-4.548894	1.553351
Au	1.842833	0.982080	1.447400
P	3.589294	0.016811	0.210005
C	3.200389	0.010111	-1.587817
C	2.382728	-1.000559	-2.120406
C	3.597333	1.072936	-2.413523
C	1.970792	-0.952896	-3.450114
H	2.041420	-1.807065	-1.483116
C	3.175574	1.138312	-3.740822
H	4.225111	1.866313	-2.022112
C	2.360859	0.126027	-4.234554
H	1.323758	-1.713575	-3.872180
H	3.456209	1.963082	-4.387137
C	4.021030	-1.712872	0.613218
C	4.590151	-2.588509	-0.327096
C	3.738636	-2.181548	1.905398
C	4.859477	-3.913835	0.009881
H	4.797654	-2.246138	-1.336256
C	4.015380	-3.501854	2.255518
H	3.243051	-1.536241	2.621839
C	4.560500	-4.346831	1.297640
H	5.279600	-4.611657	-0.706589
H	3.769508	-3.889294	3.236928
C	5.140853	0.990401	0.326354
C	5.038909	2.368472	0.582760
C	6.409027	0.422376	0.131131
C	6.178066	3.170417	0.629771
H	4.067229	2.822158	0.755208
C	7.556226	1.212215	0.187772
H	6.506962	-0.642562	-0.055771
C	7.419493	2.575750	0.432273
H	6.109882	4.235046	0.826258
H	8.546499	0.791676	0.047979
C	-0.923851	1.033231	2.518208
H	-0.829534	0.097198	1.987423
C	-1.359026	0.802017	3.914634
C	-1.897327	-0.453403	4.256604
C	-1.297977	1.808215	4.894618

C	-2.384356	-0.681626	5.542092
H	-1.916509	-1.243504	3.514282
C	-1.787737	1.574808	6.176283
H	-0.859684	2.768279	4.644757
C	-2.339337	0.331616	6.502048
H	-2.796094	-1.655181	5.794798
H	-1.738157	2.361762	6.924155
H	-2.720438	0.151928	7.504175
C	0.171317	1.974341	2.212604
C	0.044027	3.318666	2.242996
H	-0.954216	3.756768	2.341086
C	1.121038	4.310396	2.074826
C	0.869741	5.501803	1.372588
C	2.408324	4.113865	2.607974
C	1.879130	6.441141	1.165178
H	-0.119448	5.669773	0.955192
C	3.416558	5.057145	2.409542
H	2.606185	3.217706	3.187761
C	3.160227	6.220932	1.678647
H	1.666477	7.346050	0.601654
H	4.401914	4.885620	2.836249
H	3.945672	6.956283	1.524496
F	4.794508	-5.637602	1.619920
F	1.918637	0.202659	-5.506364
F	8.527194	3.340530	0.485551

TS-R-F

B3LYP-D3 SCF energy (au)	-5497.502368
B3LYP-D3 enthalpy (au)	-5496.071501
B3LYP-D3 free energy (au)	-5496.299100
ωB97X-D SCF energy in solution (au)	-5497.215854
ωB97X-D enthalpy in solution (au)	-5495.784987
ωB97X-D free energy in solution (au)	-5496.012586

Cartesian coordinates

ATOM	X	Y	Z
C	2.877912	0.910257	2.843815
O	3.990227	1.325189	2.470278
N	2.742381	-0.159693	3.669565
H	1.811934	-0.505327	3.932597
N	1.673876	1.464103	2.430230
H	0.815512	0.919935	2.607852
C	3.934171	-0.881185	4.079883
C	1.489796	2.533462	1.559157

C	2.521555	3.388876	1.123905
C	0.179433	2.756100	1.082984
C	2.228594	4.421074	0.234227
H	3.526866	3.233328	1.483614
C	-0.076631	3.787402	0.184826
H	-0.621197	2.101298	1.403149
C	0.938126	4.639800	-0.246721
H	0.730035	5.442094	-0.944829
C	4.636218	-1.437829	2.825371
O	3.976355	-2.024122	1.948767
C	6.876505	-0.542163	3.604707
C	6.699524	-1.960555	1.615814
C	8.258092	-0.702592	2.944540
H	6.874752	-0.959914	4.614793
H	6.544332	0.499244	3.655089
C	8.138831	-2.026975	2.173671
H	6.259964	-2.949859	1.470104
H	8.438263	0.117664	2.242736
H	9.066482	-0.703730	3.680704
H	8.885262	-2.135204	1.383045
H	8.229282	-2.880465	2.856889
N	5.978322	-1.319815	2.726980
C	6.632583	-1.171240	0.313960
C	6.975071	-1.823607	-0.934461
C	6.287234	0.147259	0.315738
C	7.342572	-3.191283	-0.983301
C	6.922817	-1.083837	-2.158219
C	6.237554	0.927532	-0.884208
H	5.968299	0.626205	1.235703
C	7.636044	-3.820203	-2.179317
H	7.401016	-3.765994	-0.065653
C	7.230719	-1.757211	-3.362281
C	6.542406	0.321673	-2.136031
C	5.852903	2.288664	-0.833919
C	7.578783	-3.094994	-3.380540
H	7.912843	-4.870902	-2.186604
H	7.186564	-1.221546	-4.303205
C	6.432465	1.116843	-3.300455
H	5.616286	2.728972	0.129823
C	5.759509	3.041708	-1.988145
H	7.805100	-3.582571	-4.324682
C	6.046649	2.443427	-3.230730
H	6.636725	0.686378	-4.274105
H	5.455635	4.080027	-1.939981
H	5.964462	3.027818	-4.143190
O	-0.696505	0.069253	2.367738

S	-0.889792	-1.110558	3.294418
O	-2.280275	-1.268240	3.759275
O	0.142744	-1.069127	4.379276
C	-0.487336	-2.542058	2.290831
C	0.754839	-2.587645	1.651550
C	-1.367019	-3.619521	2.213861
C	1.113001	-3.725921	0.938783
H	1.452194	-1.762771	1.735746
C	-0.990049	-4.756357	1.495602
H	-2.327298	-3.560401	2.714567
C	0.248875	-4.827006	0.846968
H	2.083441	-3.763297	0.450350
H	-1.675445	-5.598437	1.433107
C	0.632964	-6.027612	0.018048
H	1.697350	-6.265978	0.127643
H	0.054742	-6.914464	0.298291
H	0.442749	-5.831779	-1.044880
H	3.637878	-1.719857	0.249129
C	3.564946	-1.630051	-1.933817
C	3.162482	0.110852	-0.584920
C	3.359855	-0.509427	-2.772967
C	3.838740	-2.901565	-2.425714
C	2.991107	0.606576	-1.907267
C	3.472972	-0.658603	-4.157642
C	3.934067	-3.032879	-3.810820
H	3.988389	-3.746827	-1.762261
H	3.217307	1.637127	-2.138107
C	3.762528	-1.926247	-4.663967
H	3.320994	0.190085	-4.816715
H	4.161362	-4.005284	-4.236789
H	3.856874	-2.065539	-5.737293
N	3.423872	-1.192883	-0.610056
H	3.121491	0.650685	0.347611
C	3.312017	5.332488	-0.266716
C	-1.440010	3.921356	-0.435488
F	4.533934	5.022715	0.220608
F	3.399545	5.271341	-1.628111
F	3.070741	6.624442	0.037327
F	-1.504374	3.230707	-1.611461
F	-2.422230	3.437038	0.349514
F	-1.740488	5.203897	-0.730531
H	4.602724	-0.166410	4.569495
C	3.613262	-2.002842	5.129129
C	4.941175	-2.605418	5.630970
H	5.526506	-3.049681	4.817501
H	5.559989	-1.853697	6.136061

H	4.732755	-3.398261	6.357347
C	2.741596	-3.133055	4.548741
H	2.564038	-3.882278	5.329674
H	1.768112	-2.766387	4.221348
H	3.225360	-3.626000	3.701679
C	2.888024	-1.357040	6.329562
H	3.458473	-0.508210	6.727713
H	1.885029	-1.013293	6.066818
H	2.781852	-2.096747	7.131819
Au	-1.564179	-0.000536	-0.541274
P	-3.781851	0.173592	0.268447
C	-4.271984	1.409638	1.528860
C	-3.423435	1.638131	2.624304
C	-5.474034	2.127494	1.425515
C	-3.775516	2.560086	3.607784
H	-2.492695	1.091970	2.713176
C	-5.828312	3.058666	2.400236
H	-6.137984	1.972575	0.581831
C	-4.970824	3.257956	3.477223
H	-3.135281	2.741840	4.464468
H	-6.749349	3.628360	2.336035
C	-4.385064	-1.441127	0.898643
C	-4.402461	-2.538353	0.020061
C	-4.768025	-1.624461	2.233168
C	-4.826670	-3.790115	0.457589
H	-4.083834	-2.418529	-1.011336
C	-5.176127	-2.879511	2.686542
H	-4.720389	-0.802101	2.935109
C	-5.203091	-3.939291	1.789985
H	-4.867078	-4.644535	-0.209280
H	-5.457149	-3.041208	3.721321
C	-4.871348	0.535418	-1.167243
C	-6.152523	-0.022086	-1.300639
C	-4.412031	1.435510	-2.144188
C	-6.961218	0.303450	-2.389529
H	-6.522726	-0.719075	-0.555555
C	-5.214021	1.773790	-3.232310
H	-3.425026	1.877634	-2.054688
C	-6.475704	1.197292	-3.338056
H	-7.951608	-0.122072	-2.512177
H	-4.873715	2.464665	-3.996367
C	0.903100	0.890748	-1.972826
H	0.951941	1.579944	-1.135715
C	0.812087	1.604426	-3.275928
C	1.294634	2.925911	-3.366386
C	0.268944	1.011967	-4.428069

C	1.254956	3.622574	-4.568169
H	1.720817	3.403098	-2.488917
C	0.229074	1.713047	-5.634818
H	-0.144758	0.012489	-4.369207
C	0.722749	3.016047	-5.712077
H	1.637336	4.638717	-4.613185
H	-0.199082	1.239650	-6.514286
H	0.687069	3.559920	-6.652170
C	0.131453	-0.327851	-1.722090
C	0.380083	-1.465609	-2.419818
H	1.236428	-1.460461	-3.087416
C	-0.346887	-2.735947	-2.491923
C	-1.284184	-3.193482	-1.548948
C	-0.073834	-3.562958	-3.603164
C	-1.958791	-4.396809	-1.743617
H	-1.448210	-2.631556	-0.635719
C	-0.751210	-4.763866	-3.799160
H	0.678703	-3.244269	-4.321126
C	-1.708260	-5.183392	-2.870771
H	-2.652853	-4.737597	-0.983124
H	-0.528885	-5.374786	-4.670366
H	-2.233599	-6.124593	-3.010339
F	-5.311639	4.158276	4.420418
F	-7.251607	1.512734	-4.393241
F	-5.602160	-5.154279	2.218407

TS-S-H

B3LYP-D3 SCF energy (au)	-5199.803139
B3LYP-D3 enthalpy (au)	-5198.351238
B3LYP-D3 free energy (au)	-5198.577261
ωB97X-D SCF energy in solution (au)	-5199.491818
ωB97X-D enthalpy in solution (au)	-5198.039917
ωB97X-D free energy in solution (au)	-5198.265940

Cartesian coordinates

ATOM	X	Y	Z
C	-2.454498	-2.092733	-1.752733
O	-3.247697	-1.970762	-2.696425
N	-2.573737	-3.058980	-0.784431
H	-2.122958	-2.877833	0.119992
N	-1.361362	-1.260093	-1.569853
H	-0.712386	-1.435113	-0.790453
C	-3.787628	-3.864621	-0.752351
C	-1.051619	-0.146982	-2.361788

C	-1.327097	-0.094592	-3.736666
C	-0.415280	0.942344	-1.747199
C	-0.970476	1.036592	-4.467108
H	-1.823690	-0.926341	-4.215634
C	-0.088831	2.072311	-2.494375
H	-0.183638	0.905060	-0.687032
C	-0.357268	2.132522	-3.860523
H	-0.101370	3.011750	-4.437132
C	-4.896194	-3.012048	-0.110059
O	-4.739535	-2.552025	1.034805
C	-6.322349	-3.172235	-2.203019
C	-7.024692	-1.829303	-0.270385
C	-7.579582	-2.359008	-2.553412
H	-6.527323	-4.249696	-2.212348
H	-5.482564	-2.959726	-2.868555
C	-8.236987	-2.097301	-1.189107
H	-7.210551	-2.135612	0.761651
H	-7.289537	-1.408124	-3.012093
H	-8.232291	-2.888349	-3.253050
H	-8.938305	-1.259259	-1.200436
H	-8.771231	-2.990663	-0.842463
N	-6.005648	-2.735082	-0.827470
C	-6.576652	-0.370315	-0.288076
C	-7.235729	0.593491	0.571147
C	-5.572780	0.040286	-1.114450
C	-8.320883	0.226999	1.405429
C	-6.785061	1.952165	0.590768
C	-5.089728	1.388498	-1.122011
H	-5.060038	-0.671779	-1.754399
C	-8.945520	1.147068	2.227730
H	-8.684396	-0.794763	1.396689
C	-7.450421	2.867423	1.437260
C	-5.661111	2.352097	-0.244171
C	-4.011834	1.749818	-1.964114
C	-8.507036	2.481189	2.240506
H	-9.777155	0.837941	2.855107
H	-7.127720	3.901505	1.467253
C	-5.086001	3.644011	-0.215275
H	-3.601078	0.999221	-2.631619
C	-3.479707	3.023799	-1.922034
H	-8.993993	3.210473	2.881876
C	-4.014796	3.971238	-1.028471
H	-5.464819	4.391802	0.472148
H	-2.643729	3.286793	-2.559781
H	-3.581054	4.966117	-0.974848
O	-1.286976	-2.309039	1.622925

S	0.219145	-2.303838	1.573447
O	0.837918	-1.829868	2.825476
O	0.675501	-1.598451	0.325231
C	0.727665	-4.010944	1.349348
C	0.814669	-4.846609	2.463621
C	1.008371	-4.496552	0.073032
C	1.188409	-6.177567	2.291530
H	0.606682	-4.446668	3.450916
C	1.385006	-5.829716	-0.083877
H	0.939806	-3.832095	-0.781072
C	1.483389	-6.688534	1.018841
H	1.257320	-6.830799	3.158441
H	1.609419	-6.208014	-1.078459
C	1.929845	-8.121135	0.844761
H	1.636532	-8.517097	-0.133451
H	3.022929	-8.203908	0.915051
H	1.504533	-8.771608	1.616548
H	-4.424964	-0.970479	1.777090
C	-4.411845	0.990579	2.758863
C	-2.999516	0.375006	1.133629
C	-3.579625	2.104528	2.510561
C	-5.439460	1.000969	3.693578
C	-2.568636	1.676961	1.537504
C	-3.805552	3.285705	3.216747
C	-5.646052	2.192357	4.388317
H	-6.068302	0.131636	3.852691
H	-2.098230	2.345484	0.828971
C	-4.846279	3.321314	4.146995
H	-3.184600	4.160334	3.047422
H	-6.449011	2.249986	5.116890
H	-5.037894	4.236841	4.699546
N	-4.002501	-0.039257	1.895094
H	-2.561361	-0.278716	0.395012
C	-1.152984	1.025945	-5.958885
C	0.454290	3.281221	-1.781263
F	-1.280695	2.271683	-6.466672
F	-0.079570	0.461080	-6.577076
F	-2.235073	0.314815	-6.337715
F	-0.472760	3.770397	-0.910603
F	1.563100	3.011029	-1.060980
F	0.762926	4.285157	-2.629827
H	-4.042381	-4.074129	-1.791110
C	-3.578766	-5.241891	-0.050320
C	-2.494235	-6.011185	-0.828940
H	-2.767706	-6.129564	-1.885387
H	-1.532148	-5.494263	-0.780003

H	-2.361377	-7.011213	-0.399390
C	-4.910276	-6.015192	-0.131210
H	-4.795617	-7.012295	0.308523
H	-5.709632	-5.502472	0.417315
H	-5.237157	-6.145814	-1.171003
C	-3.150743	-5.118956	1.425014
H	-3.907943	-4.604464	2.020475
H	-2.998933	-6.123295	1.839514
H	-2.214597	-4.566863	1.537296
Au	1.864992	1.046300	1.416416
P	3.630348	0.101399	0.187436
C	3.265514	0.117390	-1.616461
C	2.431308	-0.873537	-2.158439
C	3.709013	1.164362	-2.437344
C	2.052599	-0.813991	-3.499054
H	2.059589	-1.668118	-1.522294
C	3.315222	1.223431	-3.775063
H	4.351436	1.940594	-2.034493
C	2.482897	0.238114	-4.309941
H	1.392715	-1.576201	-3.903171
H	3.654680	2.047469	-4.397033
C	4.054923	-1.634752	0.575364
C	4.645504	-2.491365	-0.368285
C	3.748790	-2.121185	1.853698
C	4.915905	-3.818818	-0.035832
H	4.868956	-2.129169	-1.367437
C	4.022053	-3.450139	2.180102
H	3.240703	-1.485031	2.569404
C	4.600319	-4.300724	1.237404
H	5.360975	-4.479191	-0.775419
H	3.746001	-3.825879	3.160298
C	5.181056	1.073769	0.343672
C	5.071293	2.456401	0.565914
C	6.452113	0.496136	0.214337
C	6.216725	3.249533	0.641420
H	4.092903	2.912888	0.686692
C	7.595352	1.291906	0.303428
H	6.550036	-0.573253	0.053568
C	7.480318	2.668675	0.512528
H	6.114323	4.318087	0.809873
H	8.577061	0.835286	0.209509
C	-0.892308	1.060756	2.513261
H	-0.787531	0.120657	1.992431
C	-1.304556	0.837014	3.918593
C	-1.820259	-0.422264	4.280259
C	-1.243164	1.853226	4.887875

C	-2.285183	-0.644726	5.574905
H	-1.839849	-1.218963	3.545085
C	-1.710259	1.625329	6.179130
H	-0.821755	2.816626	4.622155
C	-2.239597	0.377985	6.524825
H	-2.679991	-1.621259	5.842878
H	-1.660132	2.419986	6.918834
H	-2.603095	0.202540	7.534251
C	0.181181	2.018072	2.183761
C	0.025290	3.359716	2.197515
H	-0.981681	3.776493	2.301383
C	1.075065	4.375008	2.002795
C	0.778848	5.557596	1.303034
C	2.378533	4.212017	2.506974
C	1.759506	6.521174	1.070742
H	-0.223547	5.699797	0.907789
C	3.358308	5.178800	2.282715
H	2.612382	3.322456	3.083399
C	3.056845	6.333941	1.555460
H	1.511859	7.418785	0.509733
H	4.357618	5.030939	2.684924
H	3.820698	7.087190	1.380469
H	8.373178	3.284589	0.580174
H	4.787781	-5.341516	1.486961
H	2.145300	0.301438	-5.339710

TS-R-H

B3LYP-D3 SCF energy (au)	-5199.796884
B3LYP-D3 enthalpy (au)	-5198.344358
B3LYP-D3 free energy (au)	-5198.567032
ωB97X-D SCF energy in solution (au)	-5199.489573
ωB97X-D enthalpy in solution (au)	-5198.037047
ωB97X-D free energy in solution (au)	-5198.259721

Cartesian coordinates

ATOM	X	Y	Z
C	-2.32937400	5.87614200	-3.37069400
O	-3.48350400	5.88991800	-3.83949000
N	-1.25314500	6.29492800	-4.09814200
H	-0.30991600	6.26837500	-3.68712700
N	-2.02934400	5.46997300	-2.09294200
H	-1.04806700	5.53186500	-1.78055800
C	-1.43492200	6.75520800	-5.46110600
C	-2.89945900	4.93112800	-1.14309400

C	-4.29147400	4.83014900	-1.31139800
C	-2.32096400	4.44988900	0.04538100
C	-5.06629800	4.24679300	-0.31262200
H	-4.74541100	5.15913200	-2.23000700
C	-3.12145300	3.86038900	1.02012900
H	-1.24706100	4.51844400	0.18174600
C	-4.50154100	3.75242900	0.86070400
H	-5.11460500	3.29002300	1.62366100
C	-1.57479800	5.65300400	-6.52996600
O	-2.31216200	5.88403400	-7.51513400
C	-0.96732700	3.59003500	-7.65592700
C	-0.08787000	3.90873600	-5.39357000
C	-0.12967100	2.36926700	-7.24669100
H	-0.56367700	4.10720700	-8.53353400
H	-2.01252300	3.35186700	-7.87531200
C	0.81372200	2.92060400	-6.16759700
H	0.50899500	4.67777200	-4.90681800
H	-0.77431400	1.59822000	-6.81286300
H	0.39956500	1.93024600	-8.09682000
H	1.22719300	2.14828000	-5.51585000
H	1.64525800	3.47282900	-6.62204200
N	-0.87925900	4.50039000	-6.49301700
C	-0.97042100	3.20074500	-4.36799400
C	-0.39085700	2.74983500	-3.11737600
C	-2.29464300	2.98710000	-4.61059200
C	0.96404500	2.99847600	-2.79402400
C	-1.21362200	2.07205300	-2.16263400
C	-3.16339800	2.35950700	-3.66160400
H	-2.74385300	3.34399200	-5.53180400
C	1.50465500	2.59711600	-1.58683600
H	1.59134700	3.56559900	-3.47036500
C	-0.62346400	1.65180100	-0.94972400
C	-2.63337700	1.88651000	-2.42908500
C	-4.54869300	2.24870200	-3.92139200
C	0.70530400	1.90703900	-0.66330000
H	2.52537100	2.86901400	-1.34595200
H	-1.22318300	1.14335300	-0.20673400
C	-3.53196600	1.30983200	-1.50112800
H	-4.93335200	2.62718200	-4.86657800
C	-5.40452000	1.68980500	-2.99210400
H	1.11958900	1.59390400	0.29102200
C	-4.88516900	1.21354200	-1.77357600
H	-3.17315500	0.97492300	-0.53481500
H	-6.47083000	1.63032500	-3.18994600
H	-5.55598200	0.79867400	-1.02782800
O	1.34906200	6.30378600	-3.10326500

S	1.66122800	6.17584000	-1.63165200
O	2.87618200	5.39201400	-1.35152700
O	0.44418500	5.76619000	-0.85699500
C	1.98338800	7.86194300	-1.08356000
C	1.78368900	8.18915700	0.25941900
C	2.45986600	8.82021200	-1.97782700
C	2.06727100	9.47869800	0.70329300
H	1.38494400	7.44048200	0.93583600
C	2.73107700	10.11239500	-1.52295400
H	2.60164700	8.55335300	-3.01969600
C	2.54577600	10.46029000	-0.17774400
H	1.90099300	9.73415300	1.74751300
H	3.09219700	10.86167200	-2.22403700
C	2.86788200	11.85087300	0.31794000
H	2.17722100	12.16521200	1.10872300
H	3.88161500	11.89480400	0.73794700
H	2.81732100	12.58851100	-0.49012100
C	-6.55140500	4.12380100	-0.49424400
C	-2.45992300	3.23320400	2.21425100
F	-7.00636100	2.90250700	-0.12638800
F	-7.22943600	5.02089800	0.28265400
F	-6.94916100	4.33692500	-1.76658800
F	-1.98549800	1.99179800	1.92582100
F	-1.40747400	3.95665800	2.65745000
F	-3.31153700	3.07796000	3.25645400
H	-2.40551600	7.25024800	-5.49825000
C	-0.37545000	7.83514600	-5.89846300
C	-0.89651200	8.55456000	-7.16084800
H	-1.00809900	7.87097200	-8.00584200
H	-1.87260400	9.02117300	-6.97733200
H	-0.19351000	9.34504200	-7.44797800
C	1.00614800	7.22158300	-6.20001300
H	1.69480900	8.01432400	-6.51621700
H	1.44065500	6.74373200	-5.31855500
H	0.95245500	6.49000900	-7.01430600
C	-0.23276900	8.87177800	-4.76575800
H	0.28517900	8.45376500	-3.90042700
H	0.35302300	9.72729200	-5.12264900
H	-1.20829300	9.24503800	-4.43403500
H	-3.88647200	6.58480900	-7.32785900
C	-5.85808000	7.53126600	-7.55435000
C	-5.39613400	5.92468500	-6.06390600
C	-7.05829000	7.28826500	-6.84609600
C	-5.75118700	8.48272700	-8.56367600
C	-6.73550600	6.32680100	-5.79036100
C	-8.20295800	8.01138400	-7.18838700

C	-6.90690800	9.19508600	-8.88476600
H	-4.80998800	8.66023800	-9.07459100
H	-7.44698900	5.65434700	-5.32929700
C	-8.11771800	8.95459800	-8.21338700
H	-9.13862500	7.85287700	-6.66045900
H	-6.86964200	9.94591200	-9.66848600
H	-9.00154900	9.52085400	-8.49290900
N	-4.87906600	6.67172400	-7.03595300
H	-4.77872900	5.22392100	-5.52061900
Au	-6.56355400	7.82329800	-1.30599100
P	-5.32213200	8.63851500	0.51040800
C	-3.66306400	9.17885300	-0.03638200
C	-3.02496900	8.43682800	-1.04252000
C	-2.98945500	10.25373500	0.56426400
C	-1.72213400	8.75052900	-1.42514700
H	-3.54328200	7.61244500	-1.51965100
C	-1.69390100	10.57716100	0.15728600
H	-3.47383600	10.83584000	1.34267600
C	-1.05723800	9.82529000	-0.83321300
H	-1.22501500	8.15330500	-2.17794600
H	-1.17580500	11.41191400	0.62185300
C	-5.02968000	7.45959000	1.87753000
C	-3.74368400	7.16269600	2.34763900
C	-6.14506600	6.83983500	2.46277100
C	-3.57843300	6.26050400	3.40002900
H	-2.87386200	7.61892700	1.88648600
C	-5.97449100	5.94948700	3.52049200
H	-7.14178500	7.04905700	2.08418600
C	-4.69035300	5.65814200	3.98935400
H	-2.57856900	6.00389400	3.73445800
H	-6.84159200	5.47108400	3.96744500
C	-6.09103000	10.09996100	1.30335800
C	-6.85939000	10.96849700	0.51215400
C	-5.90405100	10.38676500	2.66385600
C	-7.42464500	12.11305400	1.07435000
H	-7.01825500	10.74319400	-0.53949500
C	-6.47450900	11.53186500	3.22218500
H	-5.32042200	9.71364400	3.28494100
C	-7.23337900	12.39572200	2.42913700
H	-8.02146000	12.77803100	0.45635600
H	-6.32786200	11.74666800	4.27714700
C	-6.29999500	7.37663800	-4.05217100
H	-5.46550900	6.74656400	-3.76101600
C	-5.85910000	8.71722300	-4.51317800
C	-4.48934400	8.97522600	-4.67961700
C	-6.78551600	9.73772800	-4.78766400

C	-4.05453800	10.22056400	-5.13328300
H	-3.78001900	8.19819300	-4.42213200
C	-6.35130700	10.97395100	-5.25496900
H	-7.84200400	9.54653100	-4.63316500
C	-4.98472500	11.21733400	-5.43423400
H	-2.99216800	10.41366600	-5.24792000
H	-7.07645100	11.75148500	-5.47882100
H	-4.64776900	12.18514000	-5.79586600
C	-7.44422000	7.29806800	-3.14105300
C	-8.73622700	7.09554100	-3.44312600
H	-9.00803100	6.92180000	-4.48813600
C	-9.88604900	7.12308200	-2.52210300
C	-11.12855200	7.57598900	-3.00027100
C	-9.80216400	6.70977700	-1.18004700
C	-12.23677700	7.66182700	-2.15861700
H	-11.21724300	7.88022300	-4.04151400
C	-10.91129100	6.79323600	-0.33897800
H	-8.87605000	6.28625200	-0.80997200
C	-12.13096000	7.27680000	-0.81965600
H	-13.18367500	8.02693200	-2.54819000
H	-10.82566200	6.46150700	0.69288000
H	-12.99448400	7.33721200	-0.16267200
H	-0.04473300	10.06633100	-1.13754500
H	-4.55375200	4.94335900	4.79472400
H	-7.67979200	13.28416600	2.86737300

TS-S-Me

B3LYP-D3 SCF energy (au)	-5317.768442
B3LYP-D3 enthalpy (au)	-5316.228682
B3LYP-D3 free energy (au)	-5316.469317
ωB97X-D SCF energy in solution (au)	-5317.441847
ωB97X-D enthalpy in solution (au)	-5315.902087
ωB97X-D free energy in solution (au)	-5316.142722

Cartesian coordinates

ATOM	X	Y	Z
C	-2.745645	1.673019	-2.036493
O	-3.611485	2.556907	-2.027821
N	-2.782548	0.599717	-2.900066
H	-2.291764	-0.253364	-2.613655
N	-1.633466	1.659584	-1.209349
H	-0.901094	0.973129	-1.427548
C	-3.914158	0.479654	-3.808816
C	-1.177981	2.728609	-0.428022

C	-2.028605	3.714024	0.095522
C	0.197290	2.800697	-0.156086
C	-1.501434	4.739070	0.876145
H	-3.078974	3.681091	-0.140402
C	0.701433	3.839407	0.625766
H	0.862160	2.048939	-0.567096
C	-0.134752	4.821678	1.151222
H	0.263741	5.619908	1.763537
C	-5.108786	-0.066526	-3.022087
O	-4.996306	-1.135022	-2.390670
C	-6.569393	1.926168	-3.605614
C	-7.338311	0.138068	-2.094786
C	-7.912583	2.329182	-2.967946
H	-6.664614	1.798298	-4.690600
H	-5.771375	2.644543	-3.399652
C	-8.544463	0.991481	-2.543174
H	-7.483263	-0.916230	-2.326229
H	-7.737644	2.956802	-2.089010
H	-8.541672	2.895320	-3.660627
H	-9.288480	1.101138	-1.749976
H	-9.028689	0.511097	-3.402169
N	-6.259509	0.631717	-2.972316
C	-6.972937	0.293328	-0.618413
C	-7.321542	-0.728570	0.349564
C	-6.279009	1.396014	-0.208483
C	-8.034453	-1.897684	-0.015017
C	-6.885039	-0.594655	1.707457
C	-5.908756	1.611709	1.155857
H	-5.922456	2.122073	-0.931390
C	-8.267966	-2.917592	0.887146
H	-8.404508	-2.009232	-1.027476
C	-7.128028	-1.663806	2.600430
C	-6.186213	0.611038	2.129203
C	-5.231582	2.795458	1.533232
C	-7.796521	-2.806439	2.205056
H	-8.803961	-3.808290	0.571462
H	-6.770194	-1.601584	3.621596
C	-5.742907	0.838299	3.454685
H	-5.052330	3.559091	0.783015
C	-4.812871	2.990970	2.834482
H	-7.951393	-3.615997	2.912264
C	-5.065998	1.995521	3.799478
H	-5.932969	0.099696	4.225443
H	-4.292740	3.902971	3.105183
H	-4.735559	2.140646	4.824545
O	1.025493	-2.358723	-1.020544

S	0.245012	-1.409131	-1.847035
O	0.622042	0.032501	-1.679402
O	-1.243571	-1.586980	-1.709167
C	0.638509	-1.790958	-3.558260
C	0.904860	-3.108354	-3.929255
C	0.641549	-0.771385	-4.508846
C	1.166400	-3.402392	-5.267010
H	0.927435	-3.882641	-3.169300
C	0.893449	-1.079938	-5.844168
H	0.475908	0.251764	-4.190333
C	1.156512	-2.397224	-6.245241
H	1.383431	-4.427877	-5.557631
H	0.895994	-0.283992	-6.585055
C	1.400855	-2.726884	-7.699317
H	1.886970	-1.896564	-8.223498
H	2.032131	-3.615061	-7.810492
H	0.455929	-2.931199	-8.220557
H	-4.221706	-0.934875	-0.813837
C	-4.170003	-2.531322	0.575265
C	-3.448843	-0.480020	1.114809
C	-3.681321	-2.615895	1.897752
C	-4.729696	-3.608880	-0.104469
C	-3.140449	-1.306621	2.225755
C	-3.746407	-3.841040	2.568877
C	-4.795349	-4.816480	0.588897
H	-5.098037	-3.490677	-1.117388
H	-2.990865	-0.939742	3.230476
C	-4.309109	-4.930698	1.905237
H	-3.349314	-3.943924	3.574356
H	-5.227970	-5.686836	0.103449
H	-4.367962	-5.890623	2.410966
N	-3.992985	-1.216971	0.144002
H	-3.223491	0.566657	0.972150
C	-2.423588	5.770521	1.462063
C	2.191472	3.927225	0.803170
F	-2.641834	5.568175	2.793747
F	-1.921027	7.019426	1.352426
F	-3.644751	5.768039	0.877597
F	2.734711	2.755494	1.226495
F	2.810081	4.208847	-0.376333
F	2.561843	4.879404	1.681936
H	-4.137501	1.489346	-4.155787
C	-3.581101	-0.377880	-5.070461
C	-4.866534	-0.524851	-5.908618
H	-4.644946	-1.046180	-6.846707
H	-5.631211	-1.105787	-5.380151

H	-5.293558	0.453049	-6.166071
C	-3.045369	-1.777937	-4.713960
H	-3.767022	-2.337649	-4.114686
H	-2.842949	-2.335446	-5.636536
H	-2.111182	-1.731624	-4.149813
C	-2.529879	0.389804	-5.893544
H	-1.636646	0.587620	-5.297147
H	-2.228517	-0.196755	-6.769183
H	-2.926580	1.350461	-6.246378
Au	1.490728	-0.223390	1.387631
P	3.631072	-0.600365	0.521543
C	3.809155	-0.230213	-1.256472
C	3.908293	-1.249844	-2.208986
C	3.723327	1.103484	-1.685506
C	3.938800	-0.936155	-3.567298
H	3.928342	-2.287821	-1.895621
C	3.761504	1.403597	-3.043134
H	3.617579	1.907074	-0.964098
C	3.872078	0.390396	-4.006661
H	3.982866	-1.740146	-4.297696
H	3.688896	2.441691	-3.360032
C	4.154015	-2.340660	0.745827
C	5.505879	-2.709381	0.668834
C	3.189421	-3.329399	0.989196
C	5.880795	-4.040802	0.831367
H	6.267012	-1.955294	0.487954
C	3.577548	-4.658339	1.153091
H	2.137822	-3.070005	1.028118
C	4.923759	-5.036058	1.080616
H	6.932244	-4.312731	0.768099
H	2.813053	-5.407339	1.344287
C	4.920324	0.397128	1.361417
C	6.056456	0.884804	0.702812
C	4.762190	0.674477	2.728212
C	7.005570	1.636141	1.397078
H	6.194428	0.692697	-0.356934
C	5.716053	1.420446	3.414430
H	3.882768	0.309999	3.252663
C	6.850737	1.920918	2.759233
H	7.879136	2.011116	0.868523
H	5.573502	1.626877	4.472925
C	-1.049665	-1.285796	1.697855
H	-1.218066	-1.288788	0.622396
C	-0.640842	-2.616626	2.204617
C	-0.652221	-3.710780	1.325056
C	-0.223842	-2.800758	3.533148

C	-0.244049	-4.968407	1.768911
H	-0.957303	-3.557658	0.295600
C	0.178181	-4.058785	3.973451
H	-0.200944	-1.945226	4.202378
C	0.171816	-5.145808	3.090561
H	-0.251325	-5.808704	1.080169
H	0.506014	-4.193778	5.000751
H	0.490969	-6.126210	3.434987
C	-0.433423	-0.083880	2.226077
C	-0.954551	0.863918	3.022929
H	-2.010884	0.793096	3.291512
C	-0.301854	2.055222	3.594481
C	-1.109561	3.117400	4.035382
C	1.089865	2.184237	3.749175
C	-0.551633	4.274387	4.578284
H	-2.187007	3.042360	3.920337
C	1.651636	3.339466	4.284645
H	1.732532	1.369428	3.433839
C	0.833772	4.393828	4.701746
H	-1.200483	5.089744	4.883132
H	2.732512	3.417352	4.367668
H	1.272310	5.296934	5.118100
C	7.856116	2.771926	3.497755
H	8.837238	2.749212	3.011879
H	7.531124	3.820318	3.531852
H	7.980535	2.437391	4.533626
C	3.924799	0.724733	-5.478005
H	3.286256	1.583396	-5.715035
H	4.945833	0.983587	-5.789594
H	3.593714	-0.121330	-6.087938
C	5.340762	-6.471400	1.297443
H	5.582631	-6.654331	2.353144
H	4.541404	-7.167197	1.021016
H	6.231547	-6.724841	0.712081

TS-R-Me

B3LYP-D3 SCF energy (au)	-5317.763466
B3LYP-D3 enthalpy (au)	-5316.222376
B3LYP-D3 free energy (au)	-5316.456384
ωB97X-D SCF energy in solution (au)	-5317.443772
ωB97X-D enthalpy in solution (au)	-5315.902682
ωB97X-D free energy in solution (au)	-5316.136690

Cartesian coordinates

ATOM	X	Y	Z
C	-2.40588700	5.83319300	-3.31994900
O	-3.53335200	5.77904200	-3.84357200
N	-1.31585500	6.28279200	-4.00268900
H	-0.38409100	6.25087000	-3.57197900
N	-2.14157500	5.45941200	-2.02423200
H	-1.18484500	5.60836200	-1.67264900
C	-1.45991700	6.75708400	-5.36273100
C	-3.01077000	4.85706100	-1.11651600
C	-4.38172000	4.64500400	-1.35190000
C	-2.45531200	4.43628200	0.10494600
C	-5.15204700	4.00148000	-0.38851000
H	-4.81608200	4.94122800	-2.29135600
C	-3.24828700	3.77818100	1.04215000
H	-1.39898700	4.60089500	0.29400000
C	-4.60202500	3.54666900	0.80916100
H	-5.21093900	3.03155300	1.54090700
C	-1.54208500	5.67456600	-6.45530200
O	-2.21684600	5.93128900	-7.47884400
C	-0.87032700	3.63467200	-7.58631000
C	-0.14267700	3.89221100	-5.26276100
C	-0.07048400	2.39723500	-7.15154900
H	-0.40391800	4.16944400	-8.42139600
H	-1.89932200	3.41019000	-7.88297600
C	0.80120300	2.91446500	-5.99784600
H	0.42768700	4.64216200	-4.72006100
H	-0.74842100	1.62144400	-6.78167800
H	0.51198900	1.97448100	-7.97473900
H	1.16382300	2.12423400	-5.33689100
H	1.66578600	3.46972600	-6.38120100
N	-0.85633000	4.51641900	-6.39825400
C	-1.09656800	3.16312600	-4.31782300
C	-0.61551400	2.68833900	-3.03389300
C	-2.39819300	2.95471100	-4.66433900
C	0.69814900	2.96334600	-2.58456600
C	-1.50429100	1.97612600	-2.16691700
C	-3.32853600	2.28000700	-3.81191500
H	-2.77983400	3.34222200	-5.60311400
C	1.12904900	2.57398100	-1.32923500
H	1.37382900	3.54576200	-3.19769700
C	-1.02471600	1.57124900	-0.90172200
C	-2.88699300	1.75419500	-2.56648500
C	-4.68615700	2.15690100	-4.18679600
C	0.25981800	1.86706200	-0.48378400
H	2.11607300	2.86979000	-0.99377500
H	-1.68656400	1.06425300	-0.21139300

C	-3.83560900	1.08430700	-1.75929200
H	-5.00466300	2.58116200	-5.13705900
C	-5.59644600	1.52171000	-3.36464000
H	0.57918900	1.57814000	0.51342600
C	-5.15918500	0.97001500	-2.14554300
H	-3.53635900	0.66428600	-0.80590400
H	-6.64124700	1.44826300	-3.65232100
H	-5.86946000	0.47390100	-1.49191300
O	1.30765900	6.12882000	-3.02272900
S	1.55124200	6.21533900	-1.53662900
O	2.62535600	5.32934500	-1.05743000
O	0.25908300	6.12048700	-0.77204100
C	2.09860000	7.91081700	-1.26949400
C	1.82565100	8.54131900	-0.05380700
C	2.83086300	8.57076900	-2.25747900
C	2.28773600	9.83742900	0.16676200
H	1.23998200	8.01997500	0.69596900
C	3.28526600	9.86898400	-2.02449600
H	3.02597400	8.07070800	-3.20038400
C	3.02064300	10.52214900	-0.81299200
H	2.06818000	10.33033500	1.11125200
H	3.85025700	10.38511700	-2.79753200
C	3.46788600	11.94687600	-0.58584800
H	2.67595300	12.65535900	-0.86568300
H	3.70914400	12.12958700	0.46702500
H	4.35128100	12.19264100	-1.18473000
C	-6.62386000	3.80663400	-0.60970500
C	-2.59822900	3.24254100	2.28643400
F	-7.02953600	2.55971300	-0.27516300
F	-7.35837800	4.65348400	0.17895200
F	-7.00793400	4.03597100	-1.88084000
F	-1.86772700	2.12577200	2.03646400
F	-1.75101600	4.13642200	2.84600600
F	-3.50780400	2.90030600	3.23163000
H	-2.43515500	7.24169800	-5.42111500
C	-0.39748600	7.85653200	-5.74337100
C	-0.93164400	8.66205000	-6.94630000
H	-1.08793100	8.02870600	-7.82295400
H	-1.88631400	9.14605200	-6.70162700
H	-0.21483400	9.44805200	-7.21135300
C	0.97395500	7.25088500	-6.10075800
H	1.67721800	8.05812300	-6.33867400
H	1.39480500	6.68466500	-5.26582300
H	0.91218300	6.59913700	-6.97962300
C	-0.23009300	8.81167800	-4.54691400
H	0.32137400	8.34305000	-3.73009700

H	0.33168200	9.69981500	-4.85875100
H	-1.19736300	9.13940500	-4.15305400
H	-3.75085800	6.74572200	-7.30596500
C	-5.65538400	7.83836300	-7.46107600
C	-5.32212400	6.06445300	-6.13528300
C	-6.88375300	7.59517000	-6.80267400
C	-5.47259200	8.87925000	-8.36606500
C	-6.64374000	6.51101600	-5.84931700
C	-7.97776500	8.41484400	-7.08777800
C	-6.57896600	9.68661100	-8.63182000
H	-4.51157700	9.05255000	-8.84043300
H	-7.40279700	5.83000300	-5.48766300
C	-7.81634900	9.45075200	-8.00878600
H	-8.93185900	8.25780600	-6.59314700
H	-6.48173100	10.50947500	-9.33385200
H	-8.65999300	10.09365800	-8.24314000
N	-4.73997800	6.87328600	-7.01795000
H	-4.76040800	5.27398700	-5.65980400
Au	-6.55469800	7.54209700	-1.22765300
P	-5.35656700	8.45401900	0.56744200
C	-3.84898200	9.22113900	-0.13376000
C	-2.74789400	8.41746000	-0.46479100
C	-3.81368200	10.58705200	-0.45055200
C	-1.61961000	8.97448500	-1.06551600
H	-2.75351100	7.35776400	-0.23541600
C	-2.68640800	11.13181100	-1.06042800
H	-4.66072100	11.22516300	-0.21770800
C	-1.56783200	10.34275500	-1.36523200
H	-0.77342600	8.33064800	-1.27973300
H	-2.66971700	12.19427400	-1.29420400
C	-4.80164600	7.38538600	1.93869800
C	-3.58164400	7.58590300	2.60553200
C	-5.66822800	6.38345900	2.39381600
C	-3.25079000	6.80455900	3.70796400
H	-2.88474100	8.34032100	2.25451900
C	-5.33147500	5.61774200	3.50991800
H	-6.59586100	6.18885700	1.86560600
C	-4.12371400	5.81724600	4.18829200
H	-2.29457600	6.95676800	4.20244500
H	-6.01048100	4.83846700	3.84659700
C	-6.26138600	9.82620700	1.37795900
C	-7.45707300	10.30493700	0.82539500
C	-5.75522900	10.43860600	2.53569300
C	-8.12725100	11.37668500	1.41741900
H	-7.86654400	9.83982300	-0.06761700
C	-6.43109600	11.50589300	3.11865000

H	-4.83397400	10.07659200	2.98331100
C	-7.62892000	11.99231800	2.57120200
H	-9.05394000	11.73487900	0.97539700
H	-6.02597200	11.97052500	4.01478000
C	-6.23504000	7.33232800	-3.98300600
H	-5.41412700	6.66003800	-3.75562800
C	-5.76819200	8.71811700	-4.25414800
C	-4.39179500	8.98819000	-4.31021100
C	-6.67835500	9.77517600	-4.42471300
C	-3.93497600	10.28405500	-4.55040200
H	-3.69303900	8.18280800	-4.12278700
C	-6.22123200	11.06390200	-4.68106200
H	-7.74145500	9.57310500	-4.34980500
C	-4.84753200	11.32147100	-4.74850100
H	-2.86843400	10.48435200	-4.57414100
H	-6.93443500	11.87108700	-4.82424600
H	-4.49209300	12.33021600	-4.94160400
C	-7.40203900	7.16007500	-3.11693100
C	-8.68993000	7.01632800	-3.46729800
H	-8.93785800	6.96342800	-4.53166800
C	-9.86543100	6.97665900	-2.58051600
C	-11.09517900	7.45658100	-3.06606300
C	-9.82074000	6.48235700	-1.26412700
C	-12.22868400	7.48784500	-2.25468200
H	-11.15429400	7.82454300	-4.08872300
C	-10.95451700	6.51168900	-0.45326000
H	-8.90380600	6.04222000	-0.89126400
C	-12.16166100	7.02118200	-0.93955600
H	-13.16486200	7.87416000	-2.64978800
H	-10.89742400	6.11856800	0.55877300
H	-13.04456000	7.03913900	-0.30616600
C	-0.34043700	10.96880400	-1.98141100
H	0.07060500	11.74766500	-1.32723300
H	0.44684600	10.23357800	-2.15255800
H	-0.57868400	11.44391500	-2.94129600
C	-8.37121100	13.12868700	3.23273200
H	-8.98070700	12.76250800	4.06949200
H	-7.68029700	13.87600200	3.63849300
H	-9.04507100	13.63167700	2.53166900
C	-3.74217400	4.98859400	5.38973700
H	-2.78648900	4.48367600	5.21746200
H	-3.63090100	5.61798600	6.28135900
H	-4.49197000	4.22207100	5.60572500

TS-S-OMe

B3LYP-D3 SCF energy (au) -5543.392144

B3LYP-D3 enthalpy (au)	-5541.833684
B3LYP-D3 free energy (au)	-5542.073771
ωB97X-D SCF energy in solution (au)	-5543.066947
ωB97X-D enthalpy in solution (au)	-5541.508487
ωB97X-D free energy in solution (au)	-5541.748574

Cartesian coordinates

ATOM	X	Y	Z
C	-2.363179	-2.044463	-1.730251
O	-3.150463	-1.923080	-2.679385
N	-2.501602	-2.999185	-0.755582
H	-2.060016	-2.823112	0.154178
N	-1.262606	-1.220487	-1.547331
H	-0.604953	-1.421826	-0.781359
C	-3.703986	-3.821235	-0.753094
C	-0.970260	-0.091575	-2.323621
C	-1.276859	-0.011325	-3.689698
C	-0.326877	0.989754	-1.700653
C	-0.959963	1.144016	-4.401674
H	-1.762617	-0.843221	-4.179250
C	-0.024102	2.135382	-2.431664
H	-0.068591	0.931989	-0.647436
C	-0.340693	2.229700	-3.787182
H	-0.112333	3.127108	-4.346361
C	-4.842901	-2.974214	-0.158519
O	-4.728611	-2.503385	0.986909
C	-6.201628	-3.155710	-2.293999
C	-6.972627	-1.811316	-0.386704
C	-7.442380	-2.338767	-2.690998
H	-6.410054	-4.232736	-2.304122
H	-5.338482	-2.949274	-2.930590
C	-8.149433	-2.074494	-1.351990
H	-7.196332	-2.128076	0.634431
H	-7.131986	-1.389022	-3.138730
H	-8.070541	-2.865838	-3.414468
H	-8.846663	-1.233729	-1.389152
H	-8.700296	-2.965865	-1.026727
N	-5.931062	-2.711158	-0.911687
C	-6.528112	-0.351087	-0.370695
C	-7.204382	0.594193	0.495945
C	-5.512121	0.078370	-1.172804
C	-8.304906	0.210349	1.302184
C	-6.755684	1.952389	0.552289
C	-5.034303	1.428724	-1.147464

H	-4.985221	-0.620943	-1.815585
C	-8.944703	1.112486	2.132604
H	-8.669045	-0.810477	1.264214
C	-7.437090	2.849504	1.405541
C	-5.618976	2.371304	-0.255393
C	-3.950355	1.814110	-1.971254
C	-8.507317	2.446210	2.181772
H	-9.787757	0.789933	2.737614
H	-7.116195	3.883012	1.462356
C	-5.046701	3.662996	-0.187753
H	-3.532970	1.084660	-2.657533
C	-3.422813	3.088422	-1.892888
H	-9.006463	3.161762	2.829255
C	-3.967553	4.012133	-0.980770
H	-5.434109	4.392481	0.514341
H	-2.582703	3.369410	-2.517307
H	-3.536171	5.006035	-0.897668
O	-1.253463	-2.292441	1.681854
S	0.251937	-2.362359	1.630219
O	0.892602	-1.888738	2.871532
O	0.750094	-1.717031	0.368572
C	0.641275	-4.108734	1.455357
C	0.215036	-4.998541	2.443009
C	1.369117	-4.566075	0.357550
C	0.511260	-6.354890	2.317651
H	-0.344510	-4.631366	3.297528
C	1.666584	-5.923566	0.248532
H	1.717168	-3.859458	-0.386115
C	1.237998	-6.838631	1.219239
H	0.174889	-7.049133	3.084256
H	2.253287	-6.274633	-0.596541
C	1.548928	-8.309572	1.074893
H	0.864631	-8.788859	0.362451
H	2.567103	-8.464461	0.700023
H	1.452699	-8.838221	2.029052
H	-4.391703	-0.939121	1.725325
C	-4.374056	1.007724	2.733976
C	-2.937070	0.398162	1.128517
C	-3.523160	2.114373	2.519872
C	-5.421665	1.017174	3.646100
C	-2.497634	1.689096	1.560249
C	-3.748811	3.287343	3.239462
C	-5.628127	2.200580	4.354560
H	-6.065972	0.154349	3.776513
H	-2.012601	2.363237	0.867051
C	-4.808741	3.322320	4.148041

H	-3.113364	4.156288	3.096804
H	-6.446221	2.257799	5.066152
H	-5.000164	4.231702	4.710742
N	-3.960105	-0.014335	1.863086
H	-2.491476	-0.248769	0.388295
C	-1.340418	1.207153	-5.854435
C	0.534407	3.332049	-1.710852
F	-2.678085	1.341486	-6.010214
F	-0.760320	2.256074	-6.490191
F	-0.979561	0.088536	-6.520983
F	-0.385100	3.825649	-0.835283
F	1.642651	3.045541	-0.996043
F	0.852317	4.339458	-2.553394
H	-3.918722	-4.048878	-1.797379
C	-3.501366	-5.185506	-0.023526
C	-2.279618	-5.886524	-0.649741
H	-2.386484	-5.979077	-1.738021
H	-1.355806	-5.338895	-0.445313
H	-2.172776	-6.894629	-0.231943
C	-4.763410	-6.035440	-0.273649
H	-4.667707	-7.010555	0.217165
H	-5.661751	-5.550378	0.128294
H	-4.921913	-6.214293	-1.344956
C	-3.280659	-5.043411	1.495412
H	-4.173312	-4.663214	1.997179
H	-3.035438	-6.026974	1.915052
H	-2.459058	-4.362717	1.727865
Au	1.912800	1.014395	1.433690
P	3.669304	0.091670	0.171587
C	3.257451	0.062882	-1.617747
C	2.444810	-0.965391	-2.131436
C	3.630417	1.107191	-2.470712
C	2.025609	-0.944716	-3.452391
H	2.114106	-1.764650	-1.479751
C	3.198769	1.145753	-3.798694
H	4.256549	1.914224	-2.103928
C	2.382665	0.120450	-4.293095
H	1.386149	-1.725336	-3.850975
H	3.495124	1.977359	-4.427374
C	4.128199	-1.624307	0.575549
C	4.746479	-2.485088	-0.351308
C	3.789059	-2.127682	1.836594
C	5.003025	-3.809661	-0.024761
H	4.998318	-2.124266	-1.344469
C	4.041676	-3.456892	2.174139
H	3.258554	-1.502873	2.545926

C	4.638463	-4.308578	1.237169
H	5.461965	-4.488462	-0.736831
H	3.716244	-3.820561	3.140821
C	5.188073	1.109078	0.276182
C	5.054321	2.498208	0.465858
C	6.473188	0.572354	0.145355
C	6.170977	3.320680	0.505926
H	4.069541	2.938833	0.591672
C	7.605095	1.388870	0.196846
H	6.604145	-0.497468	0.012026
C	7.456165	2.771556	0.373248
H	6.070588	4.391326	0.652496
H	8.586654	0.939184	0.101688
C	-0.845434	1.049524	2.548519
H	-0.747764	0.105395	2.032788
C	-1.271515	0.832609	3.952170
C	-1.811522	-0.417889	4.308427
C	-1.197774	1.844973	4.924447
C	-2.288483	-0.634958	5.599578
H	-1.839782	-1.212137	3.570821
C	-1.676419	1.622412	6.212603
H	-0.756091	2.800834	4.664918
C	-2.230269	0.384343	6.552474
H	-2.702505	-1.604844	5.862930
H	-1.615619	2.414304	6.954521
H	-2.602770	0.213110	7.559356
C	0.244234	1.992359	2.226939
C	0.103839	3.336040	2.261237
H	-0.898687	3.761608	2.374615
C	1.160669	4.345788	2.078925
C	0.864601	5.549416	1.415254
C	2.470072	4.159204	2.558968
C	1.849826	6.510588	1.193501
H	-0.142519	5.710742	1.039660
C	3.454962	5.123073	2.344806
H	2.705601	3.252623	3.107446
C	3.152836	6.299472	1.652858
H	1.601471	7.424930	0.660434
H	4.459854	4.954485	2.723681
H	3.921050	7.050029	1.485532
O	8.485972	3.660303	0.436625
O	4.880369	-5.632494	1.437904
O	1.874396	0.067757	-5.553992
C	9.812321	3.167265	0.320521
H	10.463791	4.039559	0.399476
H	10.052667	2.460825	1.126580

H	9.977980	2.677569	-0.648773
C	4.476390	-6.207326	2.675191
H	4.745971	-7.263571	2.613047
H	5.003551	-5.747973	3.521892
H	3.393665	-6.115779	2.822097
C	2.162204	1.133885	-6.447536
H	3.237026	1.195852	-6.664218
H	1.610751	0.909144	-7.360926
H	1.812621	2.094392	-6.050124

TS-R-OMe

B3LYP-D3 SCF energy (au)	-5543.386680
B3LYP-D3 enthalpy (au)	-5541.827385
B3LYP-D3 free energy (au)	-5542.067111
ωB97X-D SCF energy in solution (au)	-5543.062419
ωB97X-D enthalpy in solution (au)	-5541.503124
ωB97X-D free energy in solution (au)	-5541.742850

Cartesian coordinates

ATOM	X	Y	Z
C	-2.09200400	6.11355500	-3.25125400
O	-3.28681100	6.10641800	-3.59540200
N	-1.08725500	6.41490000	-4.12168500
H	-0.10962200	6.35454700	-3.81712300
N	-1.67008200	5.84738800	-1.97176300
H	-0.67362600	5.99915600	-1.75629800
C	-1.38776000	6.93648700	-5.43785700
C	-2.43366600	5.35200900	-0.91646100
C	-3.78097800	4.96416100	-1.02723700
C	-1.78472700	5.21614500	0.32044000
C	-4.43988700	4.44412000	0.08304000
H	-4.28710100	5.04122700	-1.97460200
C	-2.46548900	4.67983900	1.41016500
H	-0.73945700	5.49795700	0.40501300
C	-3.79922300	4.28820200	1.31263700
H	-4.32637300	3.88825500	2.16950900
C	-1.41604300	5.92936800	-6.60583600
O	-2.09074500	6.24797400	-7.61104500
C	-0.66573000	3.99751500	-7.87799300
C	-0.12933700	4.02902100	-5.48628700
C	-0.04279800	2.65441400	-7.46938800
H	-0.06020900	4.53538600	-8.61685300
H	-1.67351600	3.90567700	-8.29306000
C	0.76147500	2.99418300	-6.20651600

H	0.48392900	4.68124900	-4.87187600
H	-0.83032400	1.93447200	-7.22399100
H	0.57023000	2.22577500	-8.26698400
H	0.96773000	2.12831200	-5.57267100
H	1.71668700	3.46485000	-6.46724100
N	-0.69382200	4.78920700	-6.62702300
C	-1.23021100	3.37568100	-4.65087300
C	-0.95379400	2.94740200	-3.29342500
C	-2.48192500	3.19877000	-5.16610500
C	0.32142600	3.12611300	-2.70508000
C	-2.00623900	2.38706500	-2.49995800
C	-3.56232800	2.64545200	-4.40859400
H	-2.70705100	3.52561000	-6.17684500
C	0.55897600	2.79973900	-1.38244300
H	1.13084600	3.57000100	-3.27040800
C	-1.71975100	2.03269100	-1.16156300
C	-3.34257900	2.24596800	-3.06126600
C	-4.85582800	2.53685000	-4.97276100
C	-0.47116700	2.24302500	-0.60643700
H	1.53292100	3.01421100	-0.95741200
H	-2.50242900	1.61869400	-0.53613400
C	-4.45240500	1.77270600	-2.32379200
H	-5.00037500	2.83585500	-6.00897900
C	-5.92173500	2.07174500	-4.22596600
H	-0.30029000	2.01285000	0.44135700
C	-5.71403700	1.69454500	-2.88590600
H	-4.33833600	1.50070100	-1.28187700
H	-6.91284000	2.00158600	-4.66608900
H	-6.54887300	1.35915600	-2.27834400
O	1.66307700	6.08864800	-3.53116500
S	2.09641500	6.14117300	-2.09045100
O	2.86608300	4.96972600	-1.63410400
O	0.92734300	6.49808000	-1.20704300
C	3.19894400	7.55742200	-1.97607500
C	3.96090700	7.71945700	-0.81628100
C	3.23769200	8.51700100	-2.98630500
C	4.75068300	8.85649700	-0.66829800
H	3.93100300	6.95739600	-0.04404300
C	4.03590200	9.65123700	-2.82607900
H	2.65214900	8.37138400	-3.88655700
C	4.79994300	9.84146000	-1.66785300
H	5.34034000	8.98494100	0.23662300
H	4.06443600	10.40018500	-3.61442200
C	5.68277100	11.05690600	-1.50726100
H	6.72118700	10.82808700	-1.78163500
H	5.35021700	11.88307200	-2.14452400

H	5.69294600	11.41051100	-0.47018100
C	-5.87278600	4.00482500	-0.02786100
C	-1.71432600	4.53569500	2.70143600
F	-6.01468900	2.68457700	0.26190600
F	-6.66889600	4.66677400	0.85474800
F	-6.39620000	4.20447600	-1.25420600
F	-0.53130100	3.90658800	2.52705500
F	-1.42928700	5.74272800	3.25916700
F	-2.40894900	3.83055300	3.62994800
H	-2.41479700	7.29912100	-5.39140000
C	-0.48521300	8.18139300	-5.79944600
C	-1.15928000	9.00897000	-6.91260600
H	-1.25427800	8.43900700	-7.83880000
H	-2.16321000	9.33427000	-6.61266300
H	-0.56149500	9.90532700	-7.11693500
C	0.91686600	7.74561100	-6.26630100
H	1.54065100	8.63103700	-6.44033700
H	1.41837800	7.11949000	-5.52379700
H	0.86564900	7.19093800	-7.21024000
C	-0.36414700	9.06681800	-4.54129200
H	0.22288100	8.58486200	-3.75615900
H	0.13326700	10.00897000	-4.80059100
H	-1.34938600	9.30888900	-4.12356500
H	-3.76809400	6.77658700	-7.30413500
C	-5.86386500	7.41431100	-7.39977300
C	-5.07866900	5.89185600	-5.95431500
C	-6.97290400	6.97665400	-6.63784600
C	-5.96059300	8.37855100	-8.39815000
C	-6.45094300	6.06498900	-5.61790200
C	-8.23270300	7.51559600	-6.90888800
C	-7.22868900	8.90286600	-8.64878900
H	-5.08702000	8.70691000	-8.95274400
H	-7.01334600	5.26699600	-5.15041400
C	-8.34970000	8.47033300	-7.91985900
H	-9.10207700	7.20905700	-6.33506100
H	-7.35065600	9.65690300	-9.42075700
H	-9.32437800	8.89465800	-8.14335300
N	-4.73572900	6.71815800	-6.94209300
H	-4.34011300	5.28865500	-5.44789200
Au	-6.51061000	7.57422900	-1.12984300
P	-5.57780600	8.61420800	0.74890200
C	-3.87645400	9.19984600	0.48259900
C	-3.07483600	8.62901000	-0.51532100
C	-3.31937100	10.19301500	1.31208500
C	-1.74199800	9.00946700	-0.67708700
H	-3.48642900	7.87203500	-1.17539400

C	-2.00124500	10.58634700	1.15401400
H	-3.92597800	10.66056400	2.08262900
C	-1.19557300	9.99195100	0.16401700
H	-1.14017100	8.52322900	-1.43421300
H	-1.55929700	11.35040300	1.78564100
C	-5.54451600	7.58077300	2.25142500
C	-4.36558700	7.28798100	2.94220100
C	-6.75256200	7.01142600	2.70000200
C	-4.37819200	6.45670500	4.06473100
H	-3.41554300	7.68670400	2.60253300
C	-6.77663600	6.18737600	3.81274600
H	-7.67635800	7.20609700	2.16051400
C	-5.58491700	5.89952800	4.50251000
H	-3.44295700	6.23490200	4.56000900
H	-7.69934200	5.73489600	4.16160000
C	-6.54047700	10.10032400	1.20742500
C	-7.07476400	10.90400700	0.18139900
C	-6.73378500	10.49185500	2.53622800
C	-7.77021100	12.06496000	0.48140500
H	-6.94555700	10.61173900	-0.85803500
C	-7.43753700	11.65729700	2.85029200
H	-6.34067000	9.88096700	3.34359400
C	-7.95773800	12.45087700	1.81966100
H	-8.18947100	12.69011000	-0.30042900
H	-7.57338800	11.92962300	3.89040200
C	-6.17661000	7.12304800	-3.86383100
H	-5.26291800	6.60788200	-3.58862500
C	-5.93265700	8.52738500	-4.28694200
C	-4.61559400	8.98436500	-4.45091700
C	-6.99720700	9.41683200	-4.50962400
C	-4.36684700	10.30035900	-4.84172100
H	-3.79924800	8.30594400	-4.23482600
C	-6.74819700	10.72421800	-4.91614000
H	-8.01388800	9.06980100	-4.35801100
C	-5.43218700	11.16943700	-5.08616200
H	-3.34277500	10.64723600	-4.94747400
H	-7.57904200	11.40056000	-5.09758100
H	-5.24020200	12.19291200	-5.39701700
C	-7.28611700	6.85673400	-2.95276400
C	-8.51408600	6.38656600	-3.21712200
H	-8.77026500	6.13933900	-4.25148400
C	-9.61956400	6.19127000	-2.26090400
C	-10.94217100	6.37168700	-2.70248900
C	-9.41407700	5.82247500	-0.91857200
C	-12.01939400	6.23891600	-1.82693300
H	-11.12238500	6.63694200	-3.74259000

C	-10.49108700	5.68798600	-0.04335200
H	-8.41129000	5.60440600	-0.57202900
C	-11.79791600	5.90311000	-0.48892400
H	-13.03212900	6.39612700	-2.18946300
H	-10.30718200	5.39476600	0.98747400
H	-12.63595600	5.79406000	0.19433300
O	-5.70818500	5.06439800	5.56748600
O	-8.65904900	13.60125000	2.00517600
O	0.07728700	10.44055800	0.10496600
C	-4.52634000	4.69285700	6.26996400
H	-4.04966500	5.56406100	6.73910700
H	-4.84870400	3.99634100	7.04584700
H	-3.80545800	4.20054800	5.60713100
C	-8.89216200	14.04536200	3.33434300
H	-9.46480000	14.97007200	3.24412200
H	-9.47459800	13.31189000	3.90792600
H	-7.95084300	14.25124300	3.86146000
C	0.96468400	9.83283000	-0.83943200
H	0.64971800	10.05202700	-1.86745900
H	1.94539900	10.27507600	-0.66211200
H	1.01483400	8.75001500	-0.69896500

2.5.8 NMR spectra

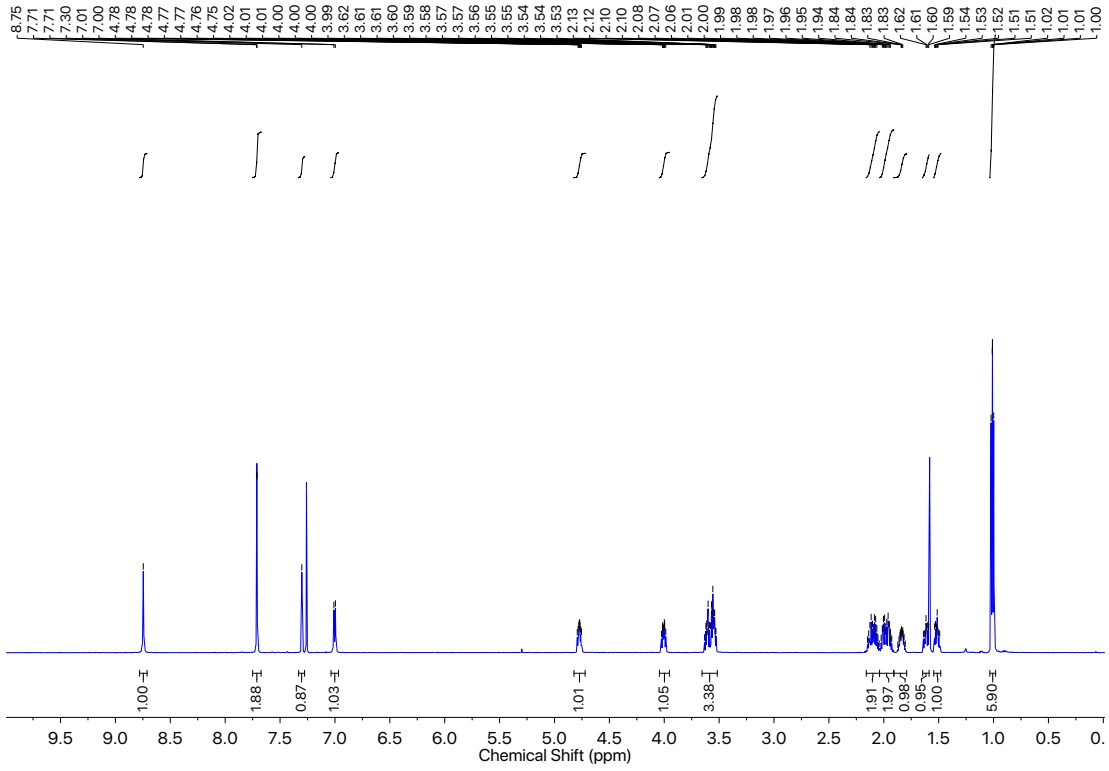


Figure S2.3 ^{1}H NMR (600 MHz, Chloroform-*d,* 23 °C) spectrum of **53**

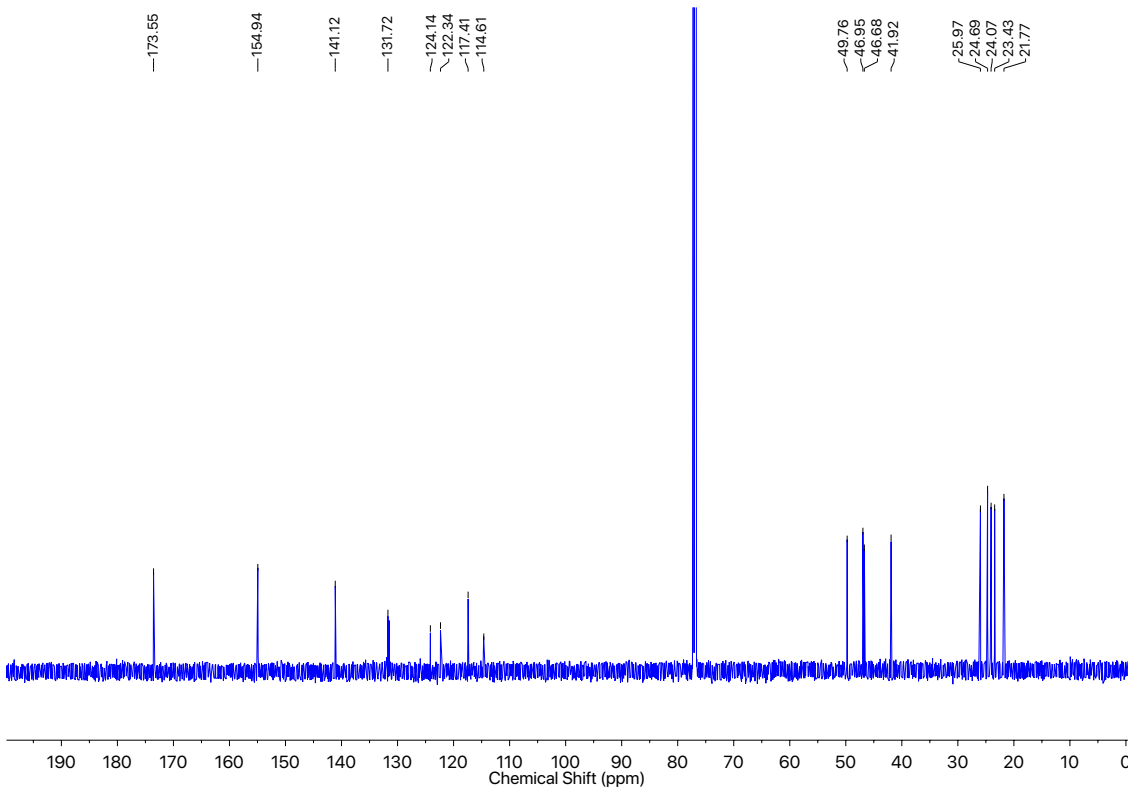


Figure S2.4 ^{13}C NMR (151 MHz, $CDCl_3$, 23 °C) spectrum of **53**

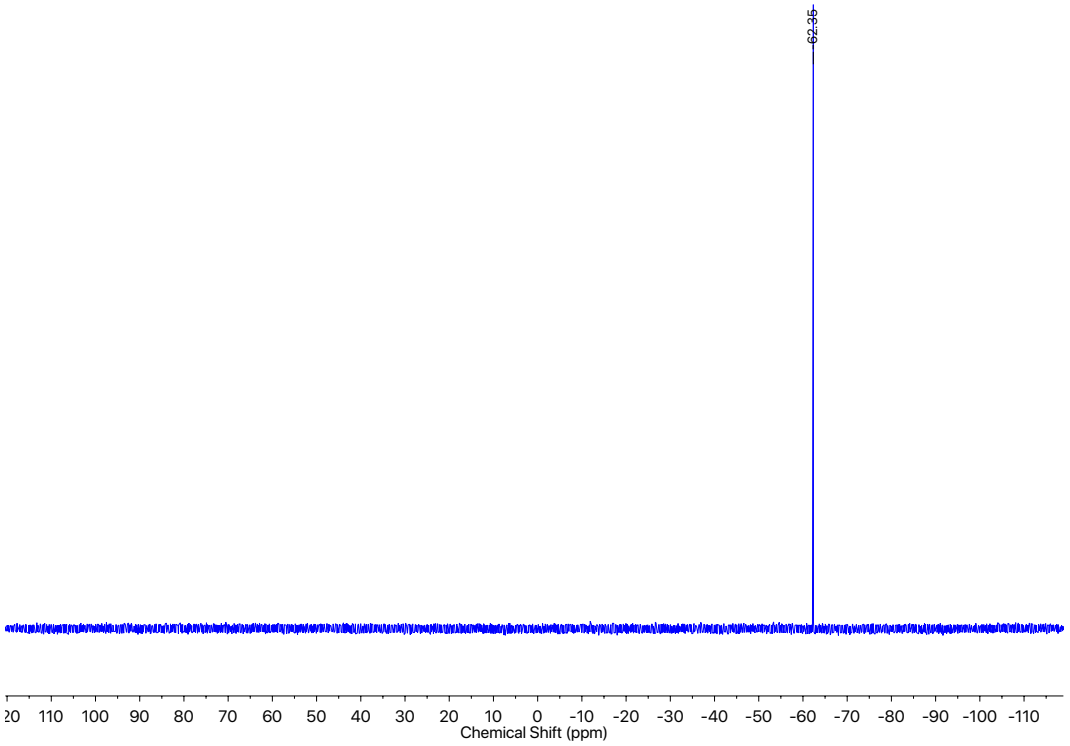


Figure S2.5 ^{19}F NMR (376 MHz, CDCl3, 23 °C) spectrum of **53**

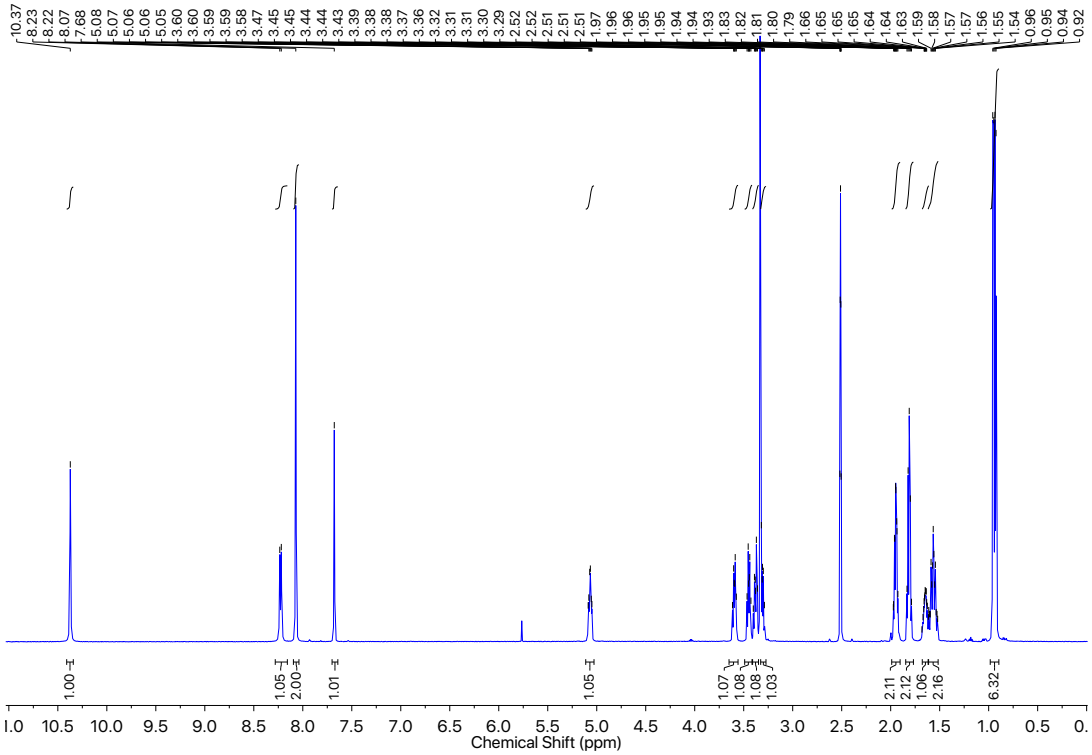


Figure S2.6 ^{1}H NMR (600 MHz, DMSO-d_6, 23 °C) spectrum of **54**

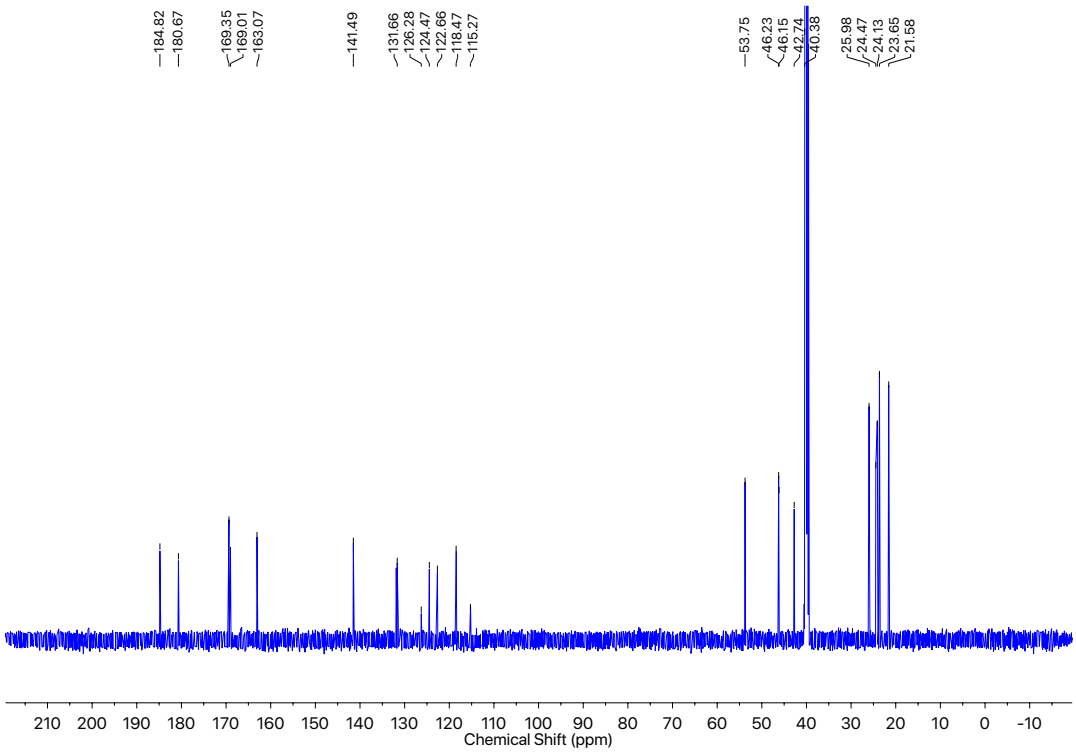


Figure S2.7 ^{13}C NMR (151 MHz, DMSO-d_6, 23 °C) spectrum of **54**

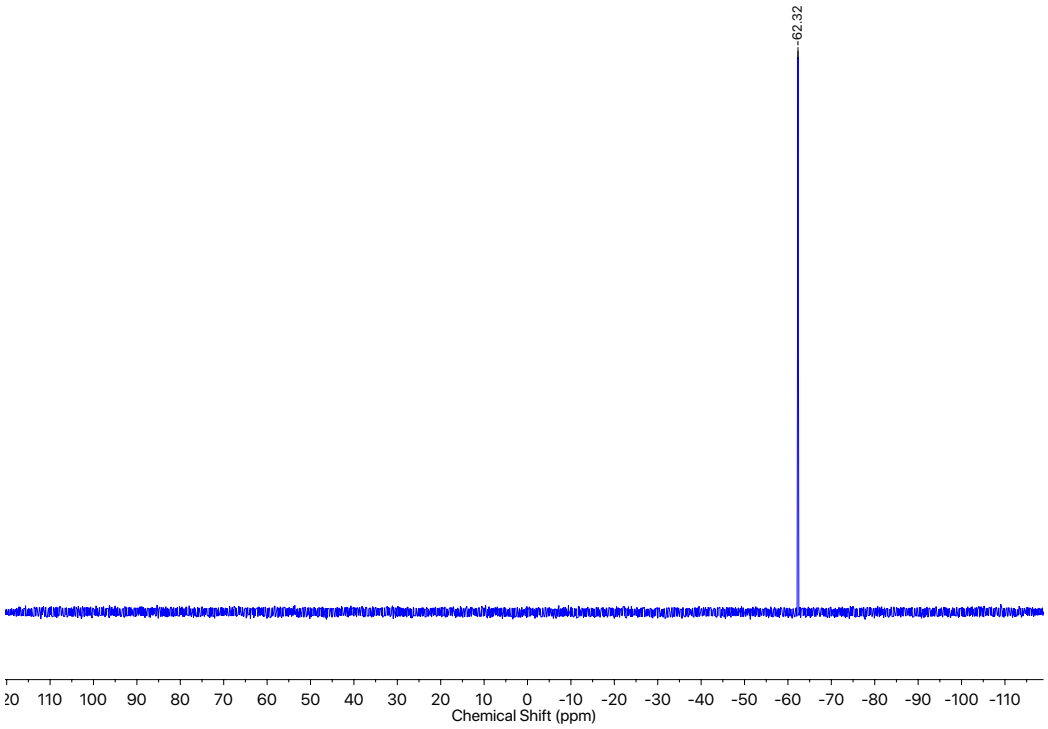


Figure S2.8 ^{19}F NMR (376 MHz, DMSO-d_6, 23 °C) spectrum of **54**

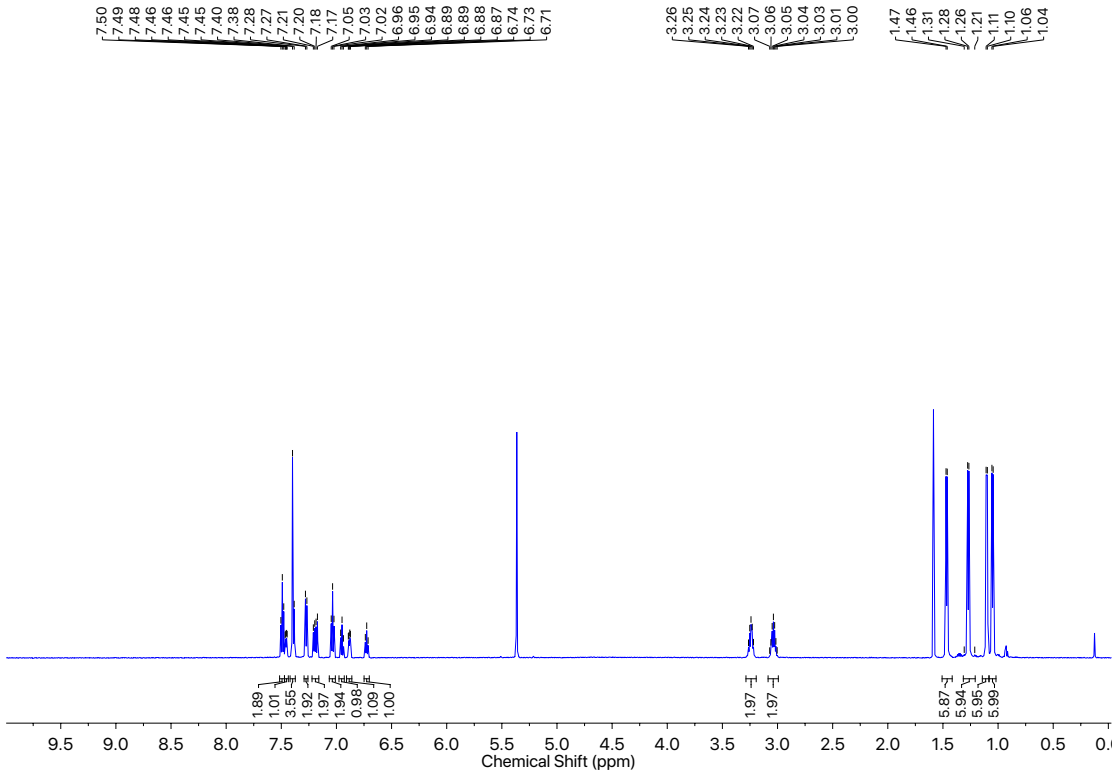


Figure S2.9 ^{1}H NMR (600 MHz, Methylene Chloride-d_2, 23 °C) spectrum of **61a**

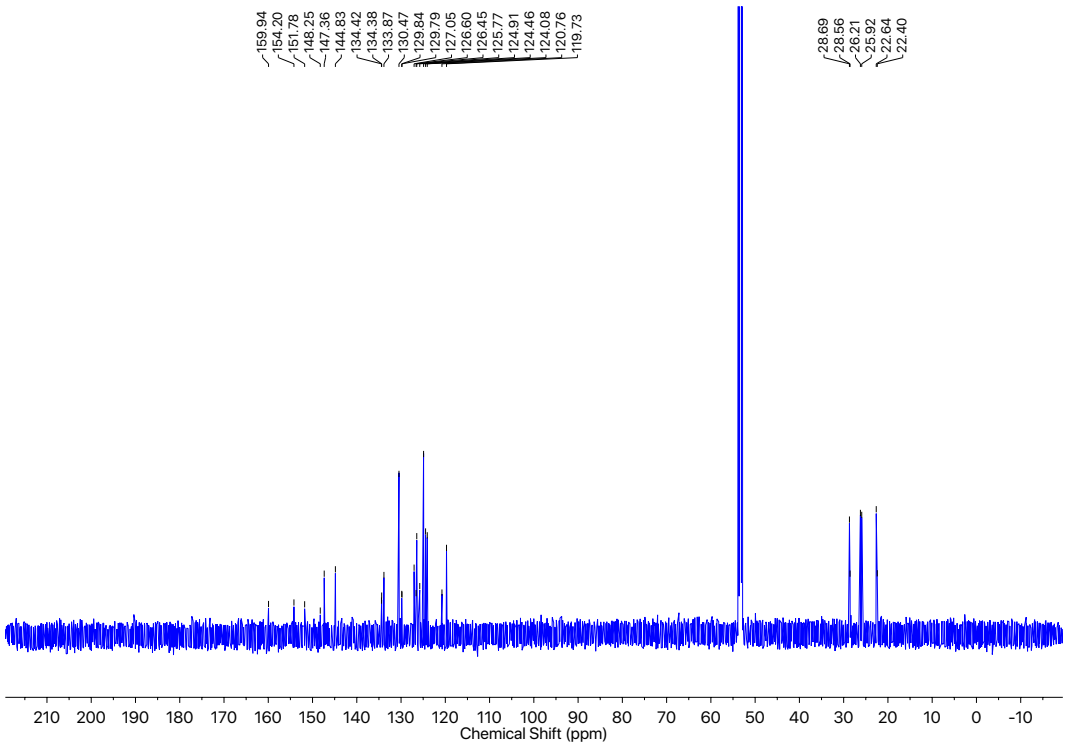


Figure S2.10 ^{13}C NMR (151 MHz, Methylene Chloride-d_2, 23 °C) spectrum of **61a**

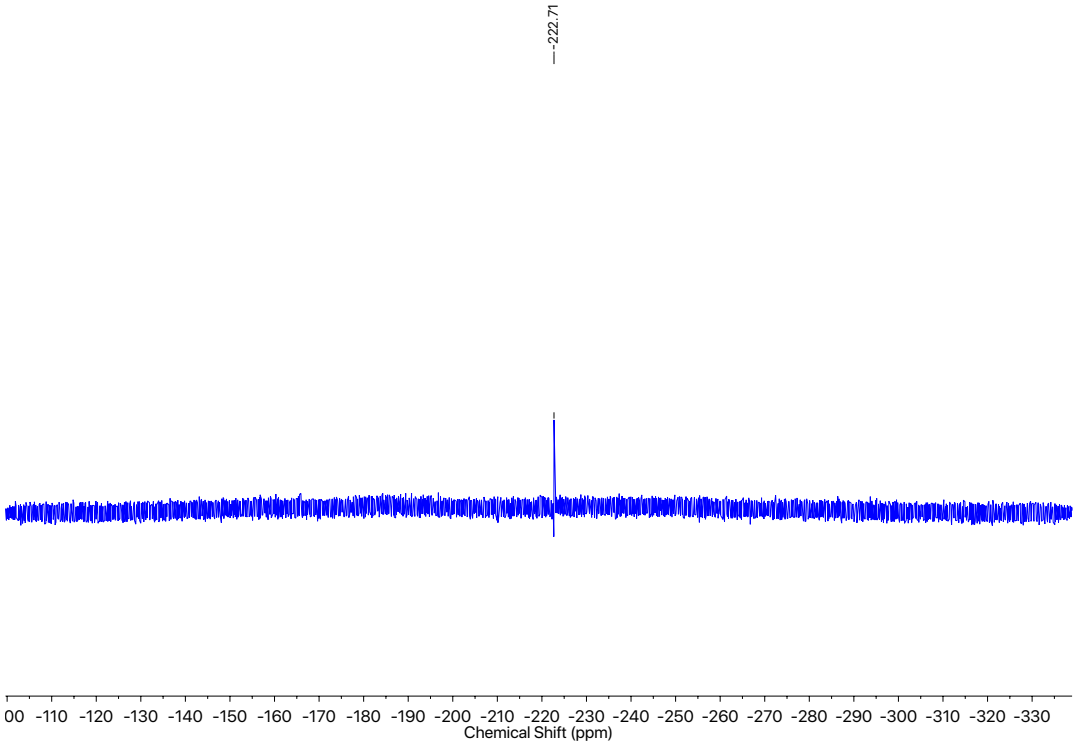


Figure S2.11 ^{19}F NMR (376 MHz, Methylene Chloride-d_2, 23 °C) spectrum of **61a**

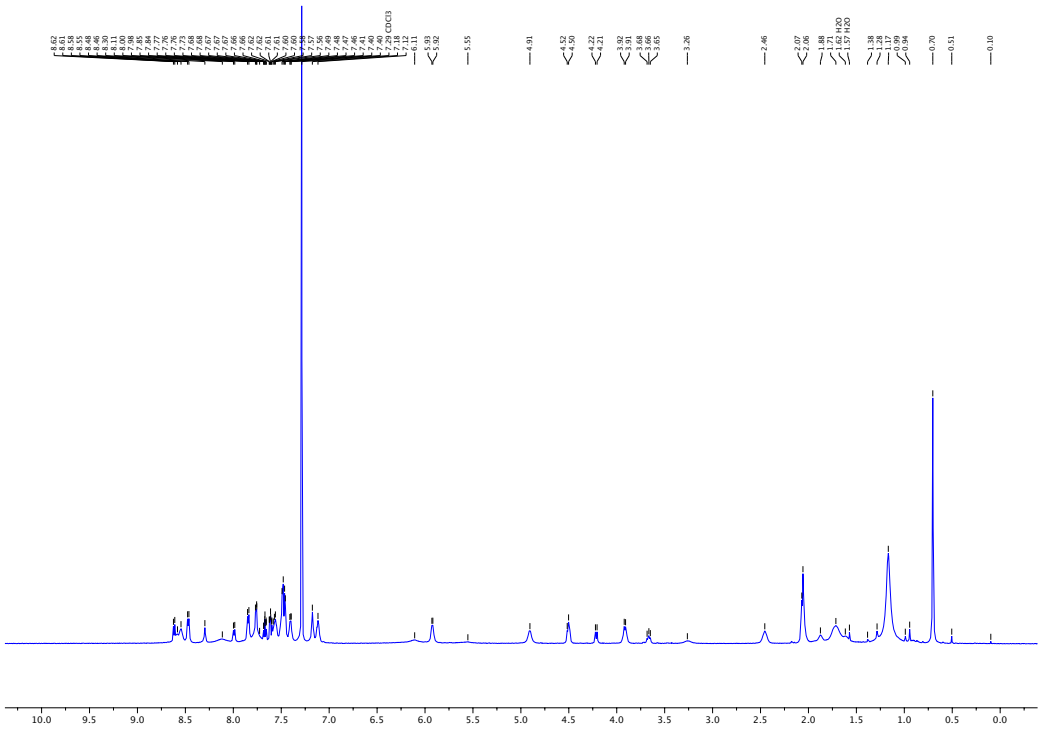


Figure S2.12 ^{1}H NMR (151 MHz, $CDCl_3$, 23 °C) spectrum of **64d**

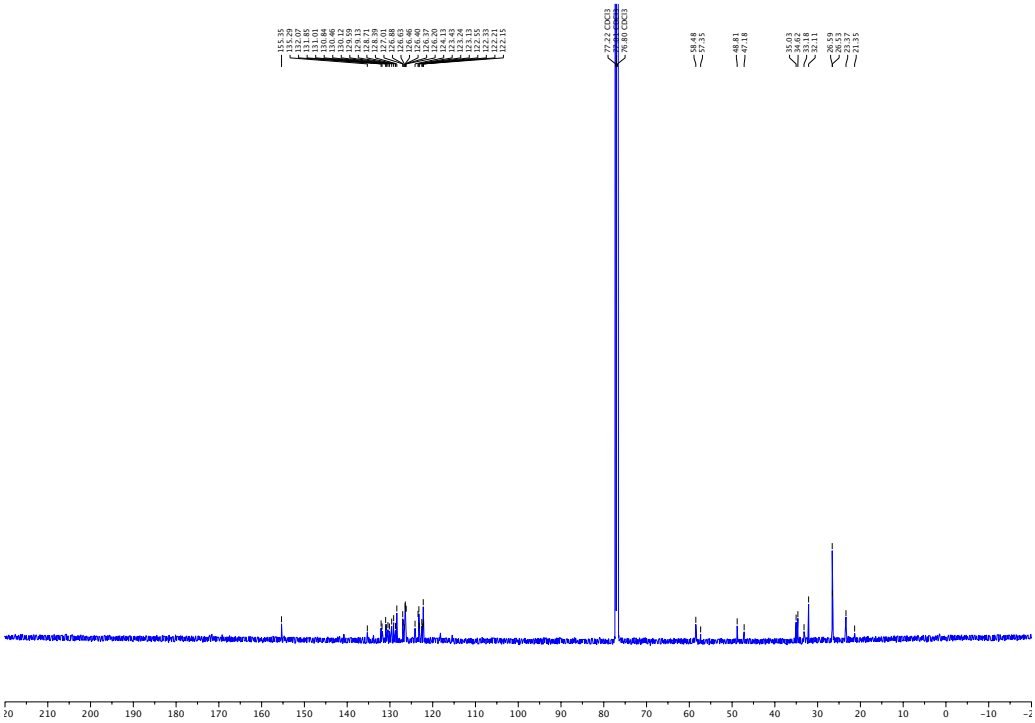


Figure S2.13 ^{13}C NMR (600 MHz, $CDCl_3$, 23 °C) spectrum of **64d**

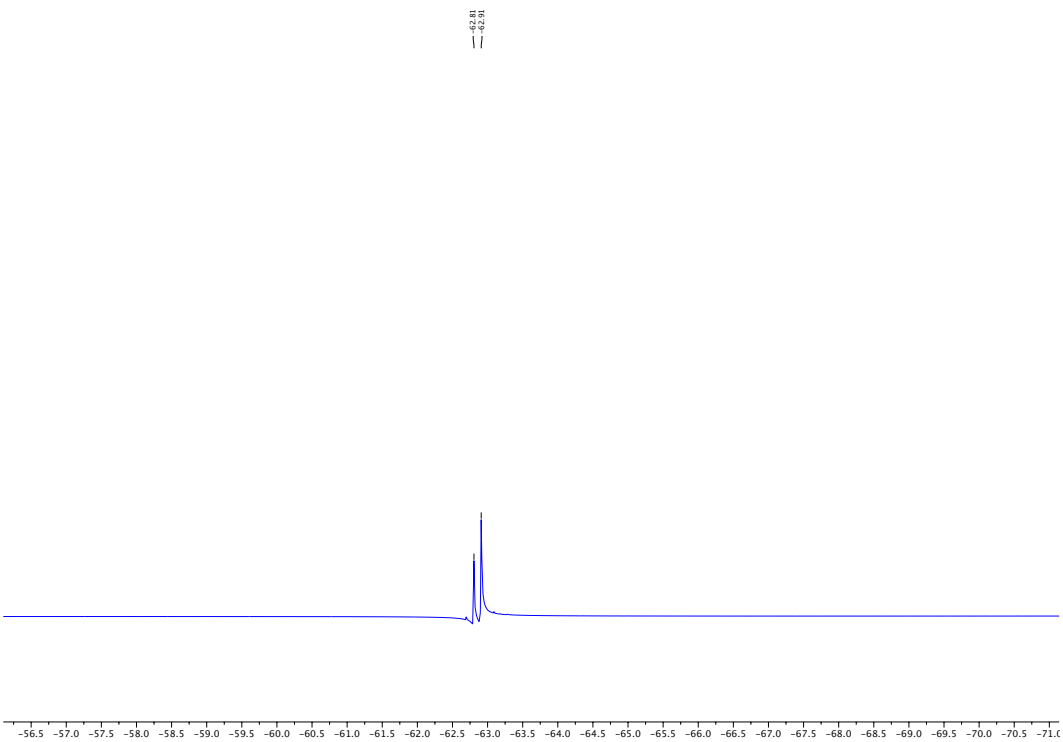


Figure S2.14 ^{19}F NMR (376 MHz $CDCl_3$, 23 °C) spectrum of **64d**

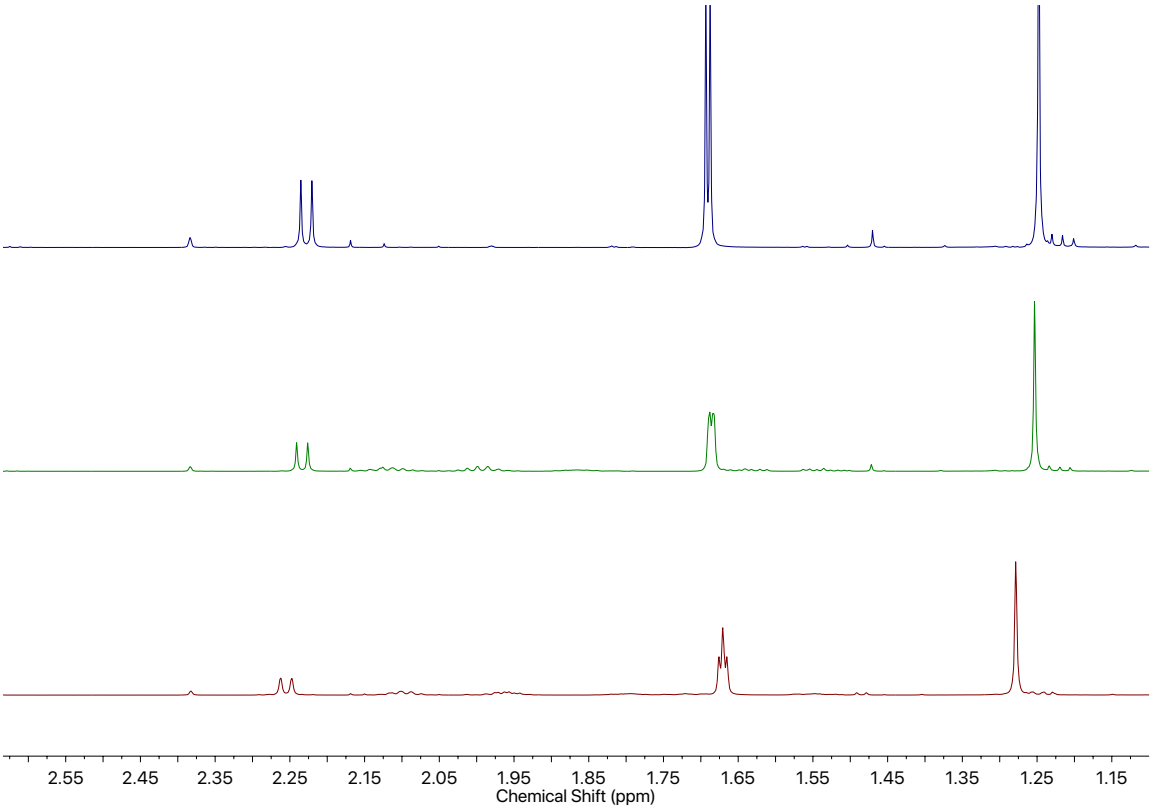


Figure S2.15 ^{1}H NMR (600 MHz, Methylene Chloride-d_2, 23 °C) spectrum for studies of interaction between **53, 54** and **55** (sample 1-3 from top to bottom)

2.5.9 References

[1]. Frisch, M. J.*, et al. Gaussian 16 Rev. C.01*, Wallingford, CT, 2016.
[2]. Grimme, S.; Antony, J.; Ehrlich, S.; Krieg, H. *J. Chem. Phys.* **2010**, *132*, 154104.
[3]. (a) Lee, C.; Yang, W.; Parr, R. G. *Phys. Rev. B* **1988**, *37*, 785-789; (b) Becke, A. D. *J. Chem. Phys.* **1993**, *98*, 5648-5652.
[4]. Andrae, D.; Häußermann, U.; Dolg, M.; Stoll, H.; Preuß, H. *Theor. Chem. Acc.* **1990**, *77*, 123-141.
[5]. Chai, J.-D.; Head-Gordon, M. *Phys. Chem. Chem. Phys.* **2008**, *10*, 6615-6620.
[6]. Marenich, A. V.; Cramer, C. J.; Truhlar, D. G. *J. Phys. Chem. B* **2009**, *113*, 6378-6396.
[7]. Pracht, P.; Bohle, F.; Grimme, S. *Phys. Chem. Chem. Phys.* **2020**, *22*, 7169-7192.
[8]. Bannwarth, C.; Ehlert, S.; Grimme, S. *J. Chem. Theory Comput.* **2019**, *15*, 1652-1671.
[9]. Caldeweyher, E.; Ehlert, S.; Hansen, A.; Neugebauer, H.; Spicher, S.; Bannwarth, C.; Grimme, S. *J. Chem. Phys.* **2019**, *150*, 154122.
[10]. Lin, S.; Jacobsen, E. N. *Nature Chem.* **2012**, *4,* 817–824.

Chapter 3

Mechanism-Guided Discoveries of Backbone-Degradable Polymers Based on New Cyclic Acylsilane Compounds

3.1 Introduction

Backbone-degradable polymers have been pursued for many biomedical, nanomaterials and environmental applications.[1–7] The past few years have witnessed research efforts aimed at developing ruthenium-catalyzed ring-opening metathesis polymerization (ROMP) generated macromolecules with degradable backbones. The excellent functional group tolerance of the ROMP has resulted in its application towards a wide range of functional materials; however, there remains a lack of ROMP-generated polymers bearing degradable units embedded within carbon-carbon bonded backbone of these materials.[8–10] Recently, monomer designs have produced polymers with degradable functionalities within the backbone, most notably enol ethers,[11–13] acetals,[14–16] aminals,[17] silyl ethers,[18,19] and other functionalities (Figure 3.1A).[20–24] While these elegant examples demonstrated efficient acid- and/or base-triggered polymer degradation, the scope and applicability of these materials would be expanded by the development of other stimuli that trigger polymer degradation.

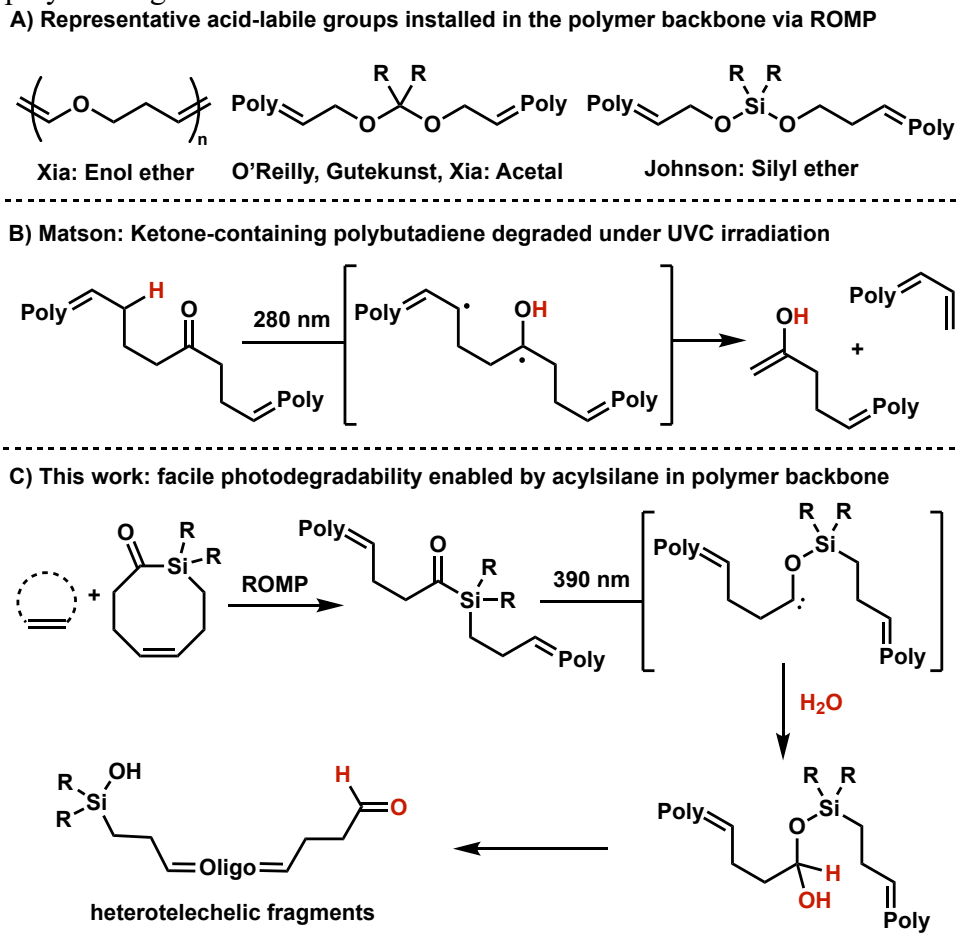


Figure 3.1 Design of backbone-degradable polymers via ROMP

Given the high spatial and temporal tunability as well as the non-invasive nature of light, photodegradability is a highly desired trait. In 2017, Matson and coworkers reported the ROMP of an unsaturated cyclic ketone and 1,5-cyclooctadiene.[25] The resulting polymer was degraded through a Norrish photocleavage using UVC light with a peak emission at 280 nm (Figure 3.1B). Inspired by this study, ROMP monomers were designed for polymers that degrade under less invasive, longer-wavelength irradiation, which would potentially be compatible with biomedical

applications. Common photolabile scaffolds that absorb >300 nm light,[26] such as o-nitrobenzyl derivatives, have been incorporated into cross-linkers for core-degradable complex polymer architecture synthesized using ROMP.[27–30] However, it remains challenging to design cyclic monomers containing these large scaffolds while maintaining the requisite strain energies for efficient ROMP with widely used monomers (e.g. cyclooctene-type and norbornene-type monomers).

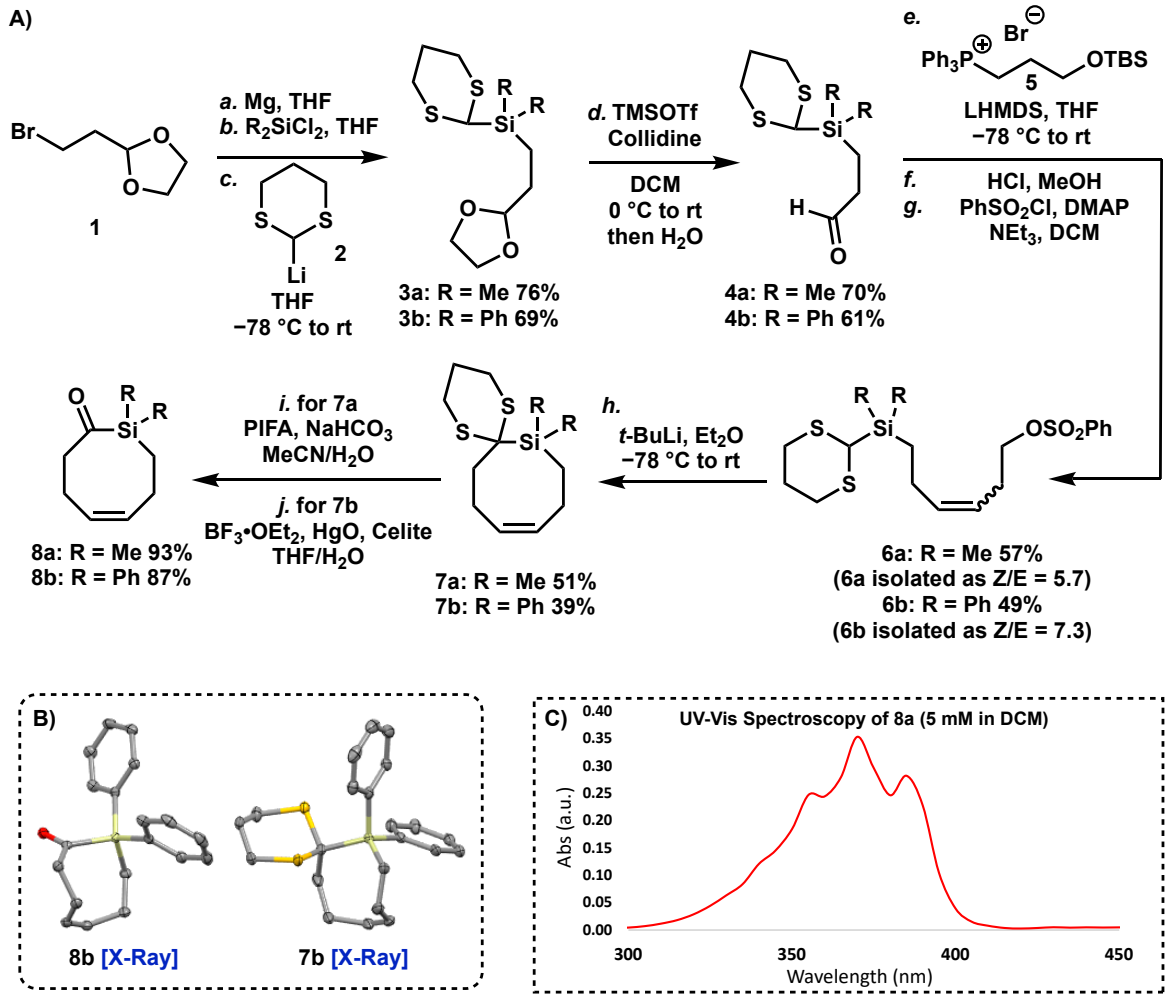
Acylsilanes are attractive for such photolabile polymers, because of their long wavelength UV-absorption profile (350–420 nm) and potential cleavage mechanisms. These silicon-based moieties can be cleaved through either a Norrish-type homolysis or through the insertion of an α-siloxy carbene, generated via a 1,2-photo Brook rearrangement, into water followed by collapse of the hemiacetal (Figure 3.1C).[31,32] Either degradation mechanism can enable access to end-functionalized fragments for further chemical modifications. Additionally, polymers prepared by radical polymerization,[33] with acylsilane in their sidechains, underwent chemical changes upon UV irradiation.[34,35] Moreover, the small size of the acylsilanes was expected to enable straightforward design and synthetic planning of the proposed monomers. Thus, it was envisioned that eight-membered-ring acylsilane-based cyclic olefins would undergo efficient ROMP with other monomers and render a photodegradable polymer backbone.

3.2 Results and Discussion

3.2.1 Synthetic Routes of Unsaturated Acylsilane Monomers for ROMP

Reports of unsaturated cyclic acylsilanes are rare as they are reported to be extremely challenging to access.[36] Spirodithianes **7a** and **7b** were successfully synthesized through classical chemical transformations (Scheme 3.1A). Subjecting **7a** to oxidative cleavage with PIFA yielded cyclic acylsilane **8a** in 93% yield. However, the same oxidative conditions led to complete decomposition of **7b**. Alternative conditions using mercury oxide were thus employed for **7b**, which generated acylsilane **8b** in 87% yield. These synthetic routes afforded cyclic acylsilane monomers **8a** and **8b** in 14% and 7% overall yields, respectively. Finally, the structure of **8b** was determined by X-ray crystallography (Scheme 3.1B). Monomer **8a** absorbs at a long-wavelength UV λmax between 350–390 nm (Scheme 3.1C). Unsuccessful synthetic attempts of unsaturated acylsilanes can be found in the supporting information.

Scheme 3.1 (A) Synthetic routes to cyclic acylsilane monomers[a]; (B) Crystal structures of **7b** and **8b** determined by X-ray crystallography; (C) UV-Vis spectrum of **8a** that has a broad absorption in the range of 300–400 nm.



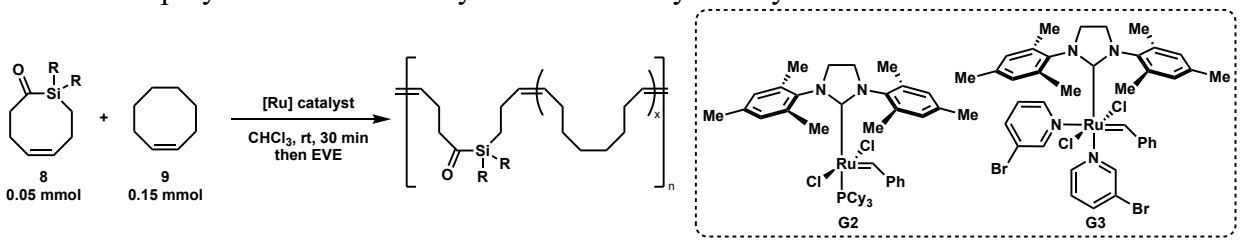
[a]Hydrogen atoms and solvents are omitted for clarity in the crystal structure of **7b** and **8b**; thermal ellipsoid plot is drawn at 50% probability.

3.2.2 Copolymerization of Acylsilane Monomers via ROMP

The calculated strain energies of **8a** and **8b** are –0.97 kcal/mol and –5.05 kcal/mol, respectively (See Supporting Information, Figure S3.1). Thus, homopolymerization of **8a** and **8b** are not thermodynamically favorable and were unsuccessful experimentally. Without homopolymerization, it becomes feasible to insert and modulate the distribution of cleaving points along a long polymer chain by copolymerizing these monomers with common ROMP monomers (cis-cyclooctene and norbornene-type monomers). Thus, polymer backbones can be cleaved when only a very small fraction of foreign monomers is added to minimize alteration of the polymer composition and properties. A 1:3 ratio monomers **8a/b**: cis-cyclooctene (**9**) underwent efficient copolymerization within 30 min using 2nd-generation Grubbs' catalyst (**G2**) in chloroform (Table 3.1). Catalyst loadings were varied with the $([8]_0+[9]_0)/[Ru]_0$ ratio ranging from 100 to 1000 (Table 3.1, entries 1−3 and 5−9). Copolymers from **8a** or **8b** (**P1-9**) consisting of >20 mol% acylsilane were generated in high yields in all cases. When $([8]_0+[9]_0)/[Ru]_0 = 400$, **P3** was obtained in 79% yield with M_n = 52.3 kDa, $Đ$ = 2.01, and 22% acylsilane incorporation (Table 3.1, entry 3). The same catalyst loading of 3rd-generation Grubbs' catalyst (**G3**) delivered **P4** in 72% yield with $Đ$

= 1.86 and similar M_n and acylsilane ratio (Table 3.1, entry 4). For future studies, potential inhibitory effects of acylsilanes on ROMP catalysts **G2** and/or **G3** need to be examined, which may lead to more controlled copolymerization of acylsilane monomers.

Table 3.1 Copolymerization of cis-cyclooctene and cyclic acylsilane monomers via ROMP



entry	polymer	acylsilane monomer	[Ru]	$[8]_0+[9]_0$ (M)	$([8]_0+[9]_0)/[Ru]_0$	M_n[b] (kDa)	$Đ$[b]	Yield (%)[c]	acylsilane mol%[d]
1	**P1**	**8a**	**G2**	1.0	100	38.0	1.73	83	22
2	**P2**	**8a**	**G2**	1.0	200	40.4	1.75	84	20
3	**P3**	**8a**	**G2**	1.0	400	52.3	2.01	79	22
4	**P4**	**8a**	**G3**	1.0	400	44.3	1.86	72	21
5	**P5**	**8a**	**G2**	1.0	1000	76.5	2.08	77	20
6	**P6**	**8b**	**G2**	1.0	100	48.8	1.82	85	24
7	**P7**	**8b**	**G2**	1.0	200	60.8	1.99	85	21
8	**P8**	**8b**	**G2**	1.0	400	85.9	1.81	82	20
9	**P9**	**8b**	**G2**	1.0	1000	99.2	1.78	79	20

[a]Conditions: $CHCl_3$, room temperature, N_2 atmosphere, 30 min, then quenched with ethyl vinyl ether (EVE). [b]Determined by GPC-RI detector in THF with polystyrene standard. [c]Polymer precipitated with methanol and dried *in vacuo*. [d]Mole percentage of acylsilane units in the copolymers as determined by ^{1}H NMR spectroscopy.

3.2.3 Photodegradation Studies in Solution

Photodegradation reactions of the copolymers were then examined. As a control experiment, the homopolymer of **9** was subjected to irradiation conditions (1 mg/mL in $CHCl_3$, irradiated with a 52 W Kessil PR160L LED lamp with a peak emission at 390 nm). As expected, no degradation was observed by gel permeation chromatography (GPC) analysis (Figure S3.4). In contrast, exposure of a chloroform solution of dimethyl acylsilane-containing **P5** to the irradiation using the same LED source resulted in gradual decreases in molecular weight with increased irradiation periods (Figure 3.2A). Significant decreases in molecular weight and broadened molar mass distributions were observed after 15 min of irradiation: M_n = 6.0 kDa, $Đ$ = 3.86 (peak cutoff at 19 min) compared to M_n = 76.5 kDa, $Đ$ = 2.08 before irradiation. Notably, no significant degradation was observed in rigorously dried and degassed $CHCl_3$, suggesting that the initial photochemical reaction was reversible in absence of water and air (Figure S3.8). When diphenyl acylsilane-containing **P9** was subjected to the same conditions in benchtop chloroform, the molecular weight decreased from M_n = 99.2 kDa to M_n = 13.9 kDa after 15-min irradiation (Figure 3.2B). In contrast to **P5**, the molar mass distribution of **P9** broadened only slightly ($Đ$ changes from 1.78 to 1.88 after 15-min irradiation), consistent with a more block-like copolymerization in **P9**.

Following the efficient photodegradation of the copolymers of cyclic acylsilanes and cis-cyclooctene, copolymerization reactions of **8a** and norbornene-type monomers were tested. When the copolymer **P10**, prepared from a 1:1 molar ratio of **8a** and norbornene dimethyl carbate (**10**), was subjected to 390 nm irradiation, nearly complete degradation of the pristine polymer was

achieved after 15 min of irradiation, accompanied by the emergence of low-molecular-weight peaks eluting after 20 min. (Figure 3.2C). Finally, 15 min of irradiation resulted in a decrease in peak degree of polymerization (DP) from about 30 to 5 for bottlebrush copolymer **P11** containing methyl polyethylene glycol sidechains, (Figure 3.2D, DP of copolymers were estimated from homopolymerization of the macromonomer with targeted DP, see supporting information for details).

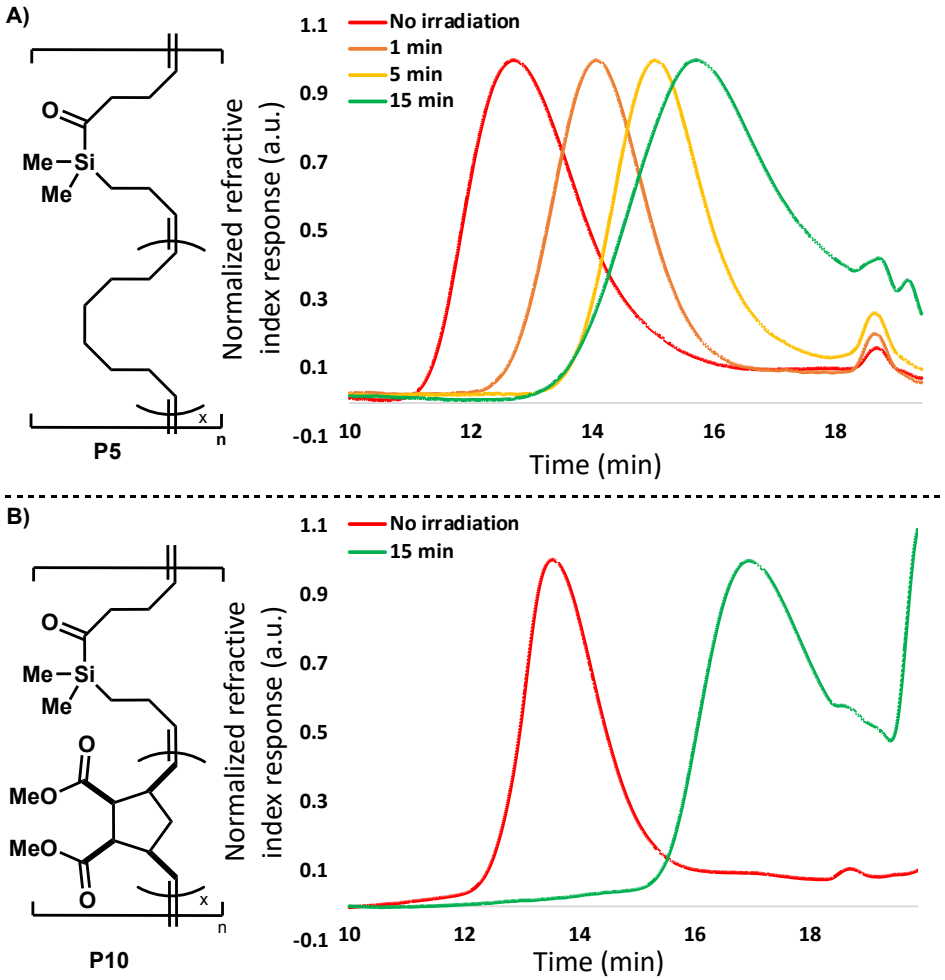


Figure 3.2 (first part)

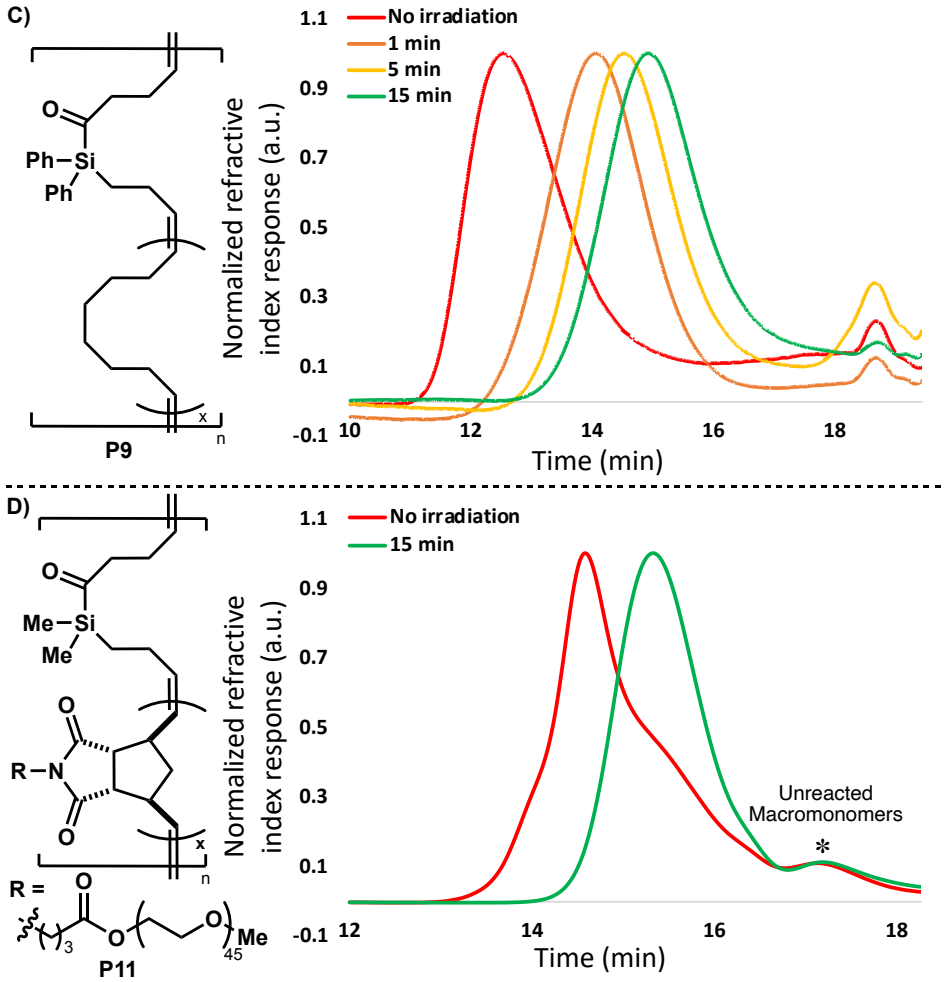


Figure 3.2 (Continued) Photodegradation of acylsilane copolymers (A) **P5**; (B) **P9**; (C) **P10**; (D) **P11** in solution and GPC traces in THF; all irradiation studies were conducted on polymer solutions with a 52 W Kessil PR160L-390 nm LED lamp.

3.2.4 Mechanistic Studies of the Photodegradation Process in Solution

Mechanistic investigation was conducted to provide in-sights into the photodegradation process of the acylsilane units in the solution. Pathways that involve a photogenerated radical[37–40] or carbene[41–45] are possible (Figure 3.3A). In pathway I, the acylsilane undergoes a Norrish type-I frag-mentation to effect acyl and silyl radicals upon irradiation. The acyl radical can abstract a hydrogen atom from C−H bonds with low bond dissociation energies (BDE) (such as allylic C−H bonds) and lead to aldehyde products. In pathway II, an α-siloxy carbene is generated via a 1,2-photo Brook rearrangement of the acylsilane followed by subsequent insertion into water and cleavage of the hemiacetal. ^{1}H-NMR spectroscopy revealed the formation of aldehydes during the irradiation of acylsilane-containing polymers. However, this observation alone cannot distinguish one mechanism from the other as both pathways produce aldehyde products. Thus, a D_2O-saturated polymer solution was selected for photodegradation. If pathway I is operative, the aldehyde hydrogen would be a proton, whereas deuterium incorporation would occur if pathway II is operative. Due to the existence of multiple aldehyde peaks in the ^{1}H-NMR spectra and low signal-to-noise ratio of the degraded polymer samples, studies were carried out using model compound **11**. Two samples with the same concentration were prepared using 1) H_2O-saturated $CDCl_3$ and 2)

D_2O-saturated $CHCl_3$ as solvents. After irradiation, 4-pentenal was obtained as the major product in 1). In 2); however, only C1-deuterated 4-pentenal was observed, which is evident from the disappearance of the C1 proton peak (indicated by a red star, Figure 3.3B) and loss of J-coupling between C1 and C2 protons (indicated by a green triangle, Figure 3.3B) in the ^{1}H-NMR spectra. Moreover, cyclopropanation product was not observed in the post-irradiation mixture. In contrast, photolysis of **11** in the presence of an electron-deficient alkene, dimethyl fumarate, led to **12** as the major product (Figure 3.3C). Again, the intramolecular cyclopropanation product was not observed in the post-irradiation mixture, likely the result of unfavorable cyclopropanation reaction of nucleophilic α-siloxy carbenes and unactivated alkenes. Collectively, these results support pathway II as the operative mechanism of acylsilane photo-degradation in $CHCl_3$.

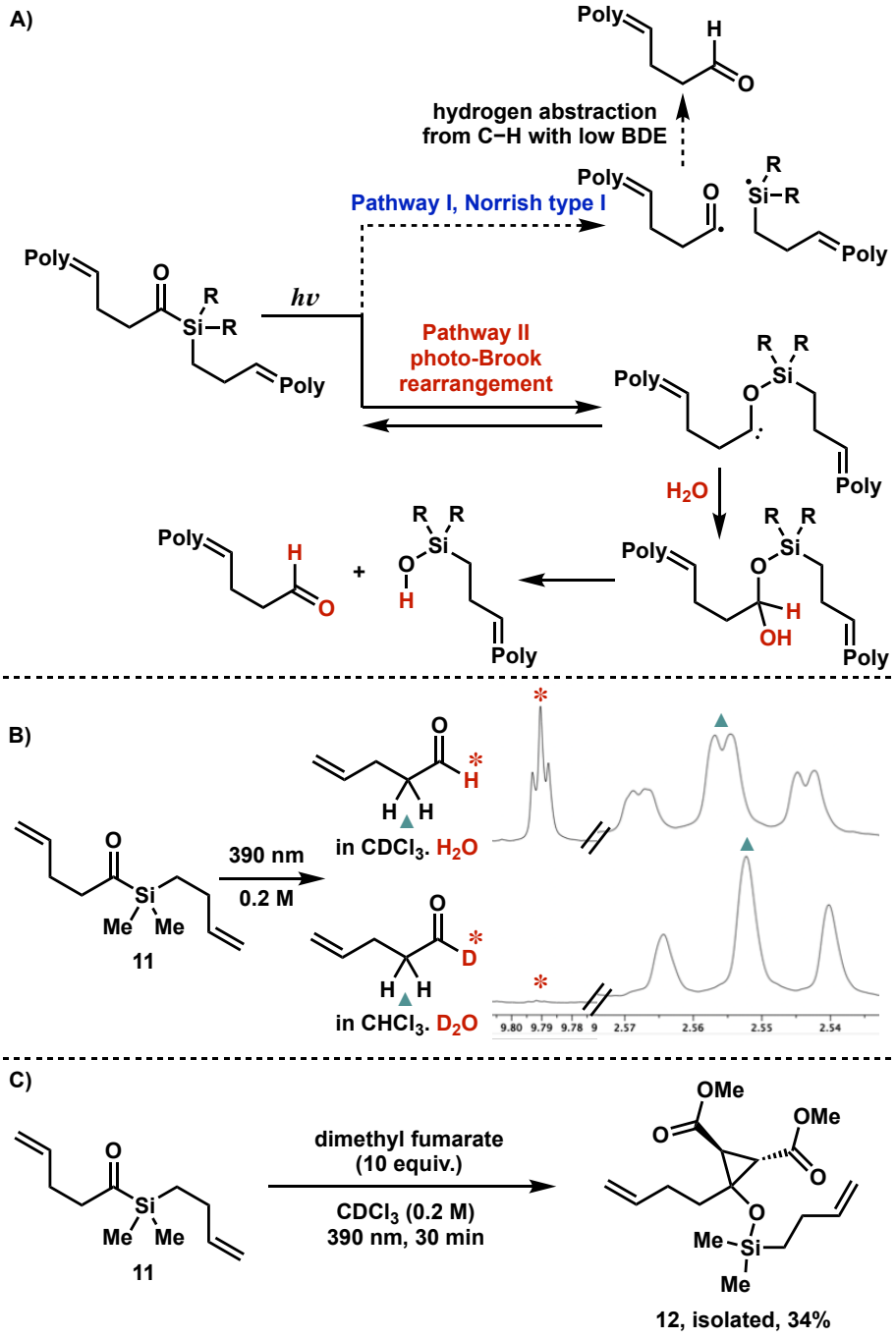


Figure 3.3 (A) Possible photodegradation mechanisms of acylsilane polymers; (B) Deuteration experiments in support of pathway II; (C) Photolysis of **11** in the presence of dimethyl fumarate led to cycloproponation product.

3.2.5 Photodegradation Studies in Solid

Following the studies conducted in solution, photodegradation was probed in the solid state. Films of the copolymer of **8a** and 9, 0.14 mm in thickness, were prepared through solution casting and exposed to 390 nm LED irradiation. Consistent with the results in solution degradation studies, gradual decreases in molecular weight and broadened molar mass distributions were observed after increased irradiation time (Figure 3.4A). The copolymer from **8a** and dicyclopentadiene (**13**) was also prepared (Figure 3.4B). Thermogravimetric analysis (TGA) of the polymer sample revealed the onset of thermal degradation (5% weight loss) occurred above 240 °C (Figure S3.13), indicating the complete incorporation of monomers into the polymer networks. The copolymer was then irradiated under 390 nm light for 30 min. and its surface morphology was characterized by scanning electron microscope (SEM). Before irradiation, SEM showed smooth areas along with wrinkles on the surface of the sample (Figures 3.4C and S3.14). In stark contrast, noticeable cracks and cavities emerged on the surface after irradiation (Figures 3.4D and S3.15). The post-irradiation sample was subjected to sonication in THF, resulting in fracturing after the sonication. The supernatant was analyzed by GPC, UPLC-MS and NMR (Figures S3.17-S3.19), which showed polymer fragments dissolved in THF (Figure 3.4D). The remaining solids were dried *in vacuo*, and a weight loss of 28% was noted compared to the pristine sample. Control experiments with polymer samples that underwent no irradiation showed no weight loss after sonication. The photo-degradation shown here would potentially be utilized to upcycle the highly crosslinked and mechanically strong polydicyclopentadiene at the end of its lifecycle.

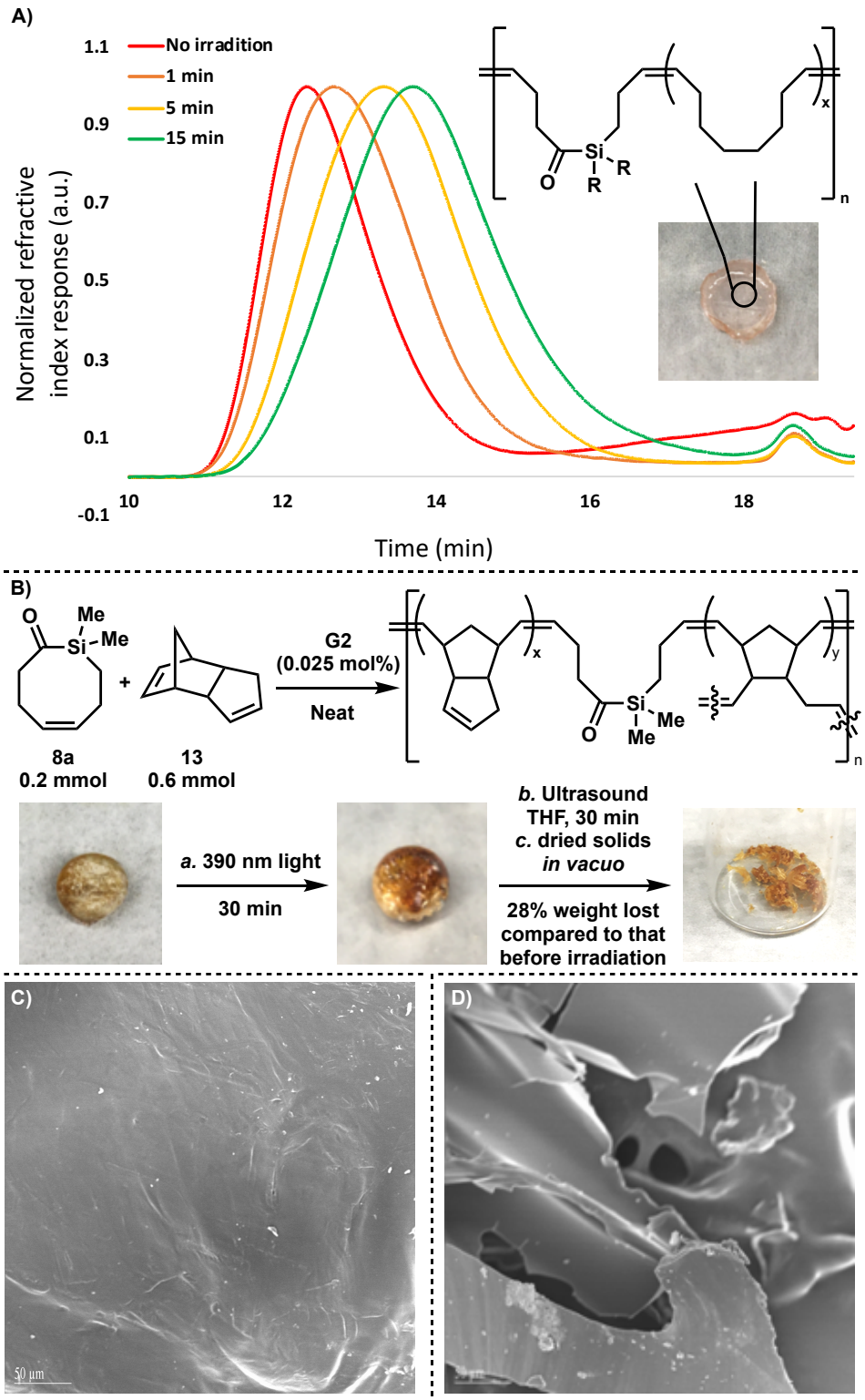


Figure 3.4 Photodegradation of acylsilane copolymers in the solid state; all irradiation studies were conducted with a 52 W Kessil PR160L-390 nm LED lamp: (A) Irradiation studies of polymer films and GPC traces in THF; (B) Irradiation studies of polydicyclopentadiene containing acylsilane; (C) SEM image of the copolymer sample before irradiation showed smooth surface; (D) Holes and

cracks emerged from the surface as shown by SEM image of the copolymer sample after 30 min irradiation.

3.2.6 Initial Studies on Photochemical Ring Expansion Reactions of Cyclic Acylsilane Precursors to Access Unsaturated Cyclic Siloxyacetal Compounds

To further utilize the cyclic acylsilanes **8a/b** in the context of polymer chemistry, it was envisioned that photochemical ring expansion reactions can provide entry to unsaturated cyclic siloxyacetal compounds as potential monomers for ROMP (Figure 3.5A). Importantly, siloxyacetal compounds were reported as potential pH-sensitized prodrugs for treatment of tumors.[46] Thus, polymers with such backbones were suggested to bear controlled release properties.

Initial studies of the ring expansion reactions were conducted with **8b** under irradiation with various compounds bearing X–H bonds (Figure 3.5B). Alcohol **13** was found to form desired adduct in high yield. In contrast, acetylated amines, including several protected amino acids, led to only decomposition without forming the desired adduct. These initial results can serve as the foundation for future research including the polymerization of the adduct of **13**.

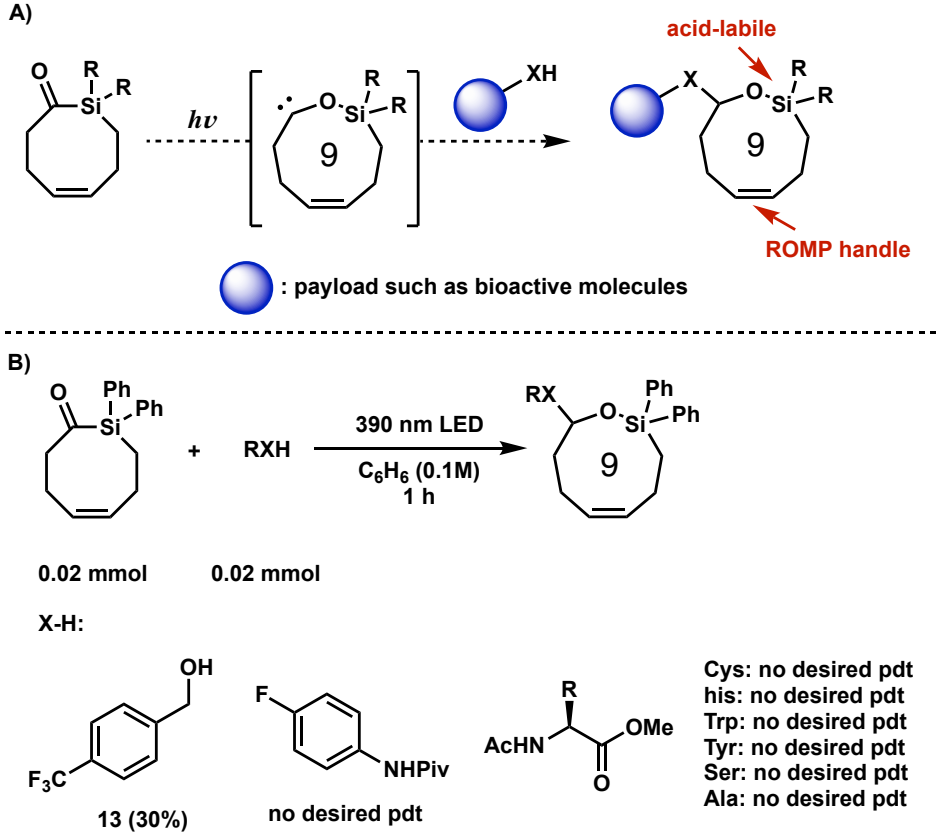


Figure 3.5 A) Proposed photochemical ring expansion reactions of cyclic acylsilane precursors to access functionalized siloxyacetal monomers for ROMP; B) Initial studies of the ring expansion reactions.

3.3 Conclusion

In conclusion, cyclic acylsilane monomers for ROMP were successfully designed and synthesized. Efficient copolymerization of acylsilane monomers with common ROMP monomers was achieved. The resulting polymers were easily degraded under 390 nm irradiation both in solution and solid states, highlighting the untapped potential of acylsilanes as photocleavable

groups. Low-molecular-weight fragments, with asymmetrically functionalized aldehyde and silanol end-groups, were generated from the photodegradation processes. The formation of the heterotelechilic fragments provides opportunities for post-degradation chemical upcycling. Mechanistic investigation revealed the α-siloxy carbene as a key intermediate in the degradation and adventitious water as a reaction component. These results will inform the synthesis of photoresponsive materials for use in sustainable materials and biomedical applications. The mechanistic insights garnered here also pave the way for α-siloxy carbene-mediated diversification of acylsilane-containing polymers in the future.

3.4 References and Notes

[1]. Hillmyer, M. A.; Tolman, W. B. *Acc. Chem. Res.* **2014**, *47*(8), 2390–2396.
[2]. Nishida, H. *Polym. J.* **2011**, *43*(5), 435–447.
[3]. Hong, M.; Chen, E. Y. X. *Green Chem.* **2017**, *19*(16), 3692–3706.
[4]. Wei, M.; Gao, Y.; Li, X.; Serpe, M. J. *Polym. Chem.* **2017**, *8*(1), 127–143.
[5]. Shieh, P.; Hill, M. R.; Zhang, W.; Kristufek, S. L.; Johnson, J. A. *Chem. Rev.* **2021**, *121*(12), 7059–7121.
[6]. Pasparakis, G.; Manouras, T.; Argitis, P.; Vamvakaki, M. *Macromol. Rapid Commun.* **2012**, *33*(3), 183–198.
[7]. Becker, G.; Wurm, F. R. *Chem. Soc. Rev.* **2018**, *47*(20), 7739–7782.
[8]. Ogba, O. M.; Warner, N. C.; O'Leary, D. J.; Grubbs, R. H. *Chem. Soc. Rev.* **2018**, 47(12), 4510–4544.
[9]. Sutthasupa, S.; Shiotsuki, M.; Sanda, F. *Polym. J.* **2010**, *42* (12), 905–915.
[10]. Martinez, H.; Ren, N.; Matta, M. E.; Hillmyer, M. A. *Polym. Chem.* **2014**, *5*(11), 3507–3532.
[11]. Feist, J. D.; Xia, Y. *J. Am. Chem. Soc.* **2020**, *142*(3), 1186–1189.
[12]. Feist, J. D.; Lee, D. C.; Xia, Y. *Nat. Chem.* **2021**, *14*(1), 53–58.
[13]. Yang, J.; Xia, Y. *Chem. Sci.* **2021**, *12*(12), 4389–4394.
[14]. Moatsou, D.; Nagarkar, A.; Kilbinger, A. F. M.; O'Reilly, R. K. *J. Polym. Sci. Part A Polym. Chem.* **2016**, *54*(9), 1236–1242.
[15]. Elling, B. R.; Su, J. K.; Xia, Y. *ACS Macro Lett.* **2020**, *9*(2), 180–184.
[16]. Fu, L.; Sui, X.; Crolais, A. E.; Gutekunst, W. R. *Angew. Chem. Int. Ed.* **2019**, *58*(44), 15726–15730.
[17]. Bhaumik, A.; Peterson, G. I.; Kang, C.; Choi, T. L. *J. Am. Chem. Soc.* **2019**, *141*(31), 12207–12211.
[18]. Shieh, P.; Nguyen, H. V. T.; Johnson, J. A. *Nat. Chem.* **2019**, *11*(12), 1124–1132.
[19]. Shieh, P.; Zhang, W.; Husted, K. E. L.; Kristufek, S. L.; Xiong, B.; Lundberg, D. J.; Lem, J.; Veysset, D.; Sun, Y.; Nelson, K. A.; Plata, D. L.; Johnson, J. A. *Nature* **2020**, *583*, 542–547.
[20]. Mallick, A.; Xu, Y.; Lin, Y.; He, J.; Chan-Park, M. B.; Liu, X. W. *Polym. Chem.* **2018**, *9*(3), 372–377.
[21]. Fishman, J. M.; Kiessling, L. L. *Angew. Chem. Int. Ed.* **2013**, *52*(19), 5061–5064.
[22]. Haider, T.; Shyshov, O.; Suraeva, O.; Lieberwirth, I.; Von Delius, M.; Wurm, F. R. *Macromolecules* **2019**, *52*(6), 2411–2420.
[23]. Steinbach, T.; Alexandrino, E. M.; Wurm, F. R. *Polym. Chem.* **2013**, *4*(13), 3800–3806.
[24]. Chang, C. C.; Emrick, T. *Macromolecules* **2014**, *47*(4), 1344–1350.
[25]. Arrington, K. J.; Waugh, J. B.; Radzinski, S. C.; Matson, J. B. *Macromolecules* **2017**, *50*(11), 4180–4187.

[26]. Klán, P.; Šolomek, T.; Bochet, C. G.; Blanc, A.; Givens, R.; Rubina, M.; Popik, V.; Kostikov, A.; Wirz, J. *Chem. Rev.* **2013**, *113*(1), 119–191.
[27]. Johnson, J. A.; Finn, M. G.; Koberstein, J. T.; Turro, N. J. *Macromolecules* **2007**, *40*(10), 3589–3598.
[28]. Johnson, J. A.; Baskin, J. M.; Bertozzi, C. R.; Koberstein, J. T.; Turro, N. J. *Chem. Commun.* **2008**, *26*, 3064–3066.
[29]. Liu, J.; Burts, A. O.; Li, Y.; Zhukhovitskiy, A. V.; Ottaviani, M. F.; Turro, N. J.; Johnson, J. A. *J. Am. Chem. Soc.* **2012**, *134*(39), 16337–16344.
[30]. Burts, A. O.; Gao, A. X.; Johnson, J. A. *Macromol. Rapid Commun.* **2014**, *35*(2), 168–173.
[31]. Zhang, H. J.; Priebbenow, D. L.; Bolm, C. *Chem. Soc. Rev.* **2013**, *42*(21), 8540–8571.
[32]. Holownia, A.; Apte, C. N.; Yudin, A. K. *Chem. Sci.* **2021**, *12*(15), 5346–5360.
[33]. Gozdz, A. S.; Reich, H. J.; Bowe, M. D. *Macromolecules* **1987**, *20*(8), 2031–2034.
[34]. Gozdz, A. S.; Reich, H. J.; Bowe, M. D. *Adv. Chem. Ser.* **1989**, *224*, 693–704.
[35]. Stuckhardt, C.; Wissing, M.; Studer, A. *Angew. Chem. Int. Ed.* **2021**, *60*(34), 18605–18611.
[36]. Hammaecher, C.; Bouillon, J. P.; Portella, C. *Tetrahedron* **2009**, *65*(82), 5527–5534.
[37]. Brook, A. G.; Duff, J. M. *J. Am. Chem. Soc.* **1969**, *91*(8), 2118–2119.
[38]. Brook, A. G.; Dillon, P. J.; Pearce, R. *Can. J. Chem.* **1971**, *49*(1), 133−135.
[39]. Brook, A. G.; Duff, J. M. *Can. J. Chem.* **1973**, *51*(3), 352–360.
[40]. Alberti, A.; Seconi, G.; Pedulli, G. F.; Degl'innocenti, A. *J. Organomet. Chem.* **1983**, *253*(3), 291–299.
[41]. Duff, J. M.; Brook, A. G. *Can. J. Chem.* **1973**, *51*(17), 2869–2883.
[42]. Bourque, R. A.; Davis, P. D.; Dalton, J. C. *J. Am. Chem. Soc.* **1981**, *103*(3), 697–699.
[43]. Brook, A. G.; Kucera, H. W.; Pearce, R. *Can. J. Chem.* **1971**, *49*(10), 1618−1621.
[44]. Brook, A. G.; Pearce, R.; Pierce, J. B. *Can. J. Chem.* **1971**, *49*(10), 1622−1628.
[45]. Perrin, H. M.; White, W. R.; Platz, M. S. *Tetrahedron Lett.* **1991**, *32*(35), 4443–4446.
[46]. Svarovsky, S. A.; Taraban, M. B.; Barchi Jr., J. J. *Org. Biomol. Chem.* **2004**, *2*(21), 3155–3161.

3.5 Supporting Information

3.5.1 General Information

Unless otherwise noted, all reagents were purchased from commercial suppliers and used without further purification. Tetrahydrofuran, dichloromethane, diethyl ether, toluene, trimethylamine, and N,N-dimethylformamide were purified by passage through an activated alumina column under argon. Thin-layer chromatography (TLC) analysis of reaction mixtures was performed using Merck silica gel 60 F254 TLC plates and visualized under UV or by staining with $KMnO_4$ or panisaldehyde. Column chromatography was performed on Merck Silica Gel 60 Å, 230 X 400 mesh. Nuclear magnetic resonance (NMR) spectra were recorded using Bruker AV-600, AV-500, Neo-500, AVB-400, AVQ-400, and AV-300 spectrometers. These CoC-NMR instruments at UC Berkeley are funded in part by the NIH (S10OD024998). ^{1}H and ^{13}C chemical shifts are reported in ppm downfield of tetramethylsilane and referenced to residual solvent peak ($CHCl_3$; $\delta H = 7.268$ ppm and $\delta C = 77.16$ppm). Multiplicities are reported using the following abbreviations: s = singlet, d = doublet, t = triplet, q = quartet, p = pentet, hept = heptet/septet, m = multiplet, br = broad, dt = doublet of triplet resonance. Mass spectral data for EMM were obtained from the QB3 mass spectral facility at the University of California, Berkeley on a Thermo LTQFTICR (7T, ESI) and in the Center of Catalysis at the University of California, Berkeley. Solvent abbreviations are reported as follows: EtOAc = ethyl acetate, hex = hexanes, DCM = dichloromethane, Et_2O =

diethyl ether, MeOH = methanol, THF = tetrahydrofuran, DMSO = dimethylsulfoxide, Et_3N = trimethylamine, MeCN = acetonitrile.

UV-Vis spectroscopic measurements were performed in DCM. Absorption spectra were recorded using a Varian Cary 50 spectrophotometer and samples for absorption measurements were prepared in 1 cm × 0.5 cm quartz cuvettes (1.4 mL volume, Starna).

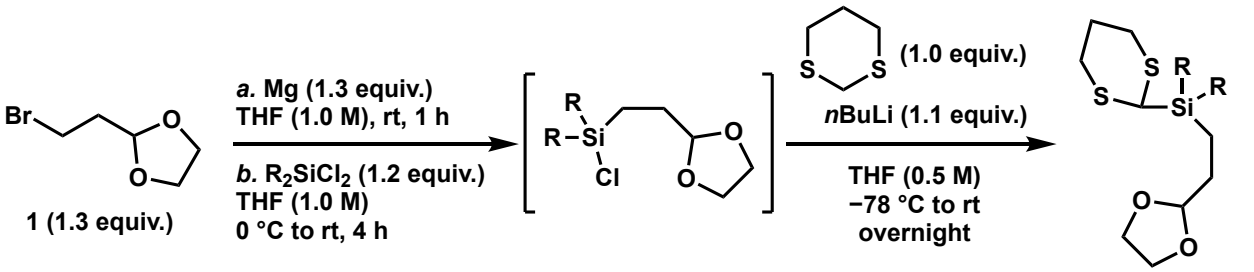
Number-average (M_n) and weight-average (M_w) molar mass and dispersity (D= Mw/Mn) of copolymers were obtained from gel permeation chromatography (GPC) carried out using an Agilent 1260 Infinity series instrument (including pump, autosampler, and RI detector) outfitted with an Agilent PolyPore,7.5 mm × 300 mm column. THF was used as eluent at 1 mL/ min at room temperature. Polystyrene standards were used to calibrate the GPC system. Analyte samples at 2 mg mL−1 were filtered through a polytetrafluoroethylene (PTFE) membrane with 0.2 μm pore before injection (20 μL). Data was analyzed using Agilent GPC/SEC Software.

All irradiation studies were conducted with a Kessil PR160L-390 nm LED light. Kessil PR160 Rig with Fan Kit was used in photodegradation studies to maintain the sample temperature around room temperature.

Thermogravimetric analysis (TGA) curves were recorded on a TA Q500 thermal analysis system under dry N_2 flow with a heat-up rate of 3 ˚C/min.

Scanning electron microscope (SEM) studies were conducted on a Hitachi S-5000 Scanning Electron Microscope to characterize surface morphology. The polymer samples were mounted onto stubs by using conductive carbon tape. A gold layer of ~3-5 nm was deposited on all samples via Tousimis Sputter Coater before SEM analysis. Scanning electron microscopy was performed with the beam accelerating voltage of 10 kV.

3.5.2 Monomer Synthesis

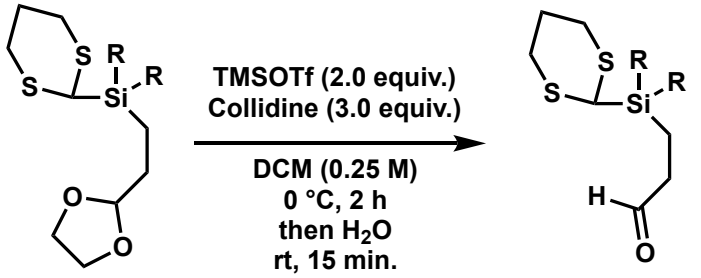


(2-(1,3-dioxolan-2-yl)ethyl)(1,3-dithian-2-yl)dimethylsilane (3a) and **(2-(1,3-dioxolan-2-yl)ethyl)(1,3-dithian-2-yl)dimethylsilane (3b)**: A flame-dried 100 mL round bottom flask cooled under vacuum was charged with a stir bar, Mg turnings (1.58 g, 66.0 mmol), and dry THF (66 mL). The addition of 2-(2-bromoethyl)-1,3-dioxolane (**1**) (11.95 g, 66.0 mmol) to the suspension was followed by placing the flask into a room temperature water bath to prevent overheating. The mixture was stirred for one hour at which point the Mg turnings were consumed and the Grignard reagent was prepared. A separate flame-dried 250 mL round bottom flask cooled under vacuum

was charged with a stir bar, corresponding R_2SiCl_2 (60 mmol), and dry THF (60 mL). The reaction vessel was cooled to 0 ˚C. To this vigorously stirring mixture was added the aforementioned Grignard reagent solution via cannula transfer. The reaction mixture was then allowed to warm to room temperature and stirred for 4 h. The resulting chlorosilane solution was used directly without further purification. A separate flame-dried 500 mL round bottom flask cooled under vacuum was charged with a stir bar, 1,3-dithiane (6.01 g, 50 mmol) and dry THF (100 mL). The reaction vessel was cooled to −78 ˚C and a solution of *n*BuLi (55 mmol, 1.1 equiv.) was added dropwise. The solution was stirred at −78 ˚C for 1 h before the aforementioned chlorosilane solution was added via cannula transfer at −78 ˚C. The reaction mixture was allowed to warm to room temperature overnight and the resulting orange solution was quenched by addition of sat. aqueous NH_4Cl solution. The organic solvents were evaporated *in vacuo* and the resulting oil was dissolved in diethyl ether (250 mL). The organic layer was washed with water (twice) and saturated brine, dried over Na_2SO4, and concentrated *in vacuo*. The crude product was purified by silica gel column chromatography (ethyl acetate/hexane = 1:10) to afford compound **3**.

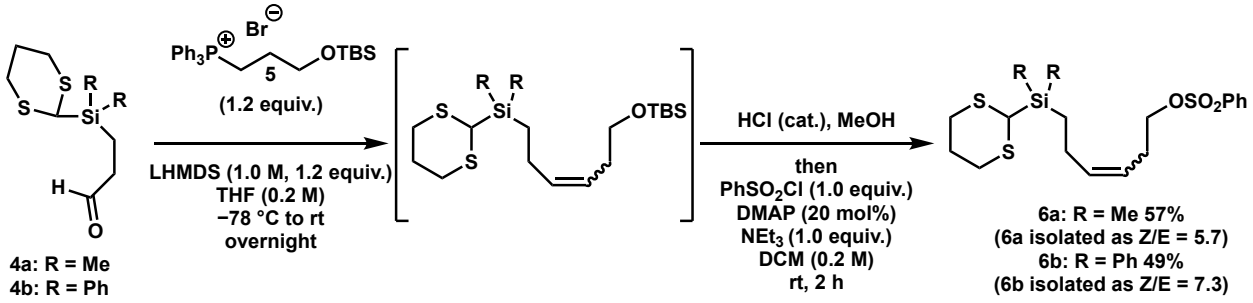
Compound **3a** was obtained as a colorless oil (10.6 g, 76%). **^{1}H NMR** (600 MHz, Chloroform-d) δ 4.86 (t, J = 4.5 Hz, 1H), 4.08 – 3.94 (m, 2H), 3.94 – 3.81 (m, 2H), 3.76 (s, 1H), 2.94 – 2.83 (m, 2H), 2.74 (m, 2H), 2.14 (m, 1H), 2.03 (m, 1H), 1.80 – 1.69 (m, 2H), 0.86 – 0.74 (m, 2H), 0.18 (s, 6H). **^{13}C NMR** (151 MHz, CDCl3) δ 105.79, 64.97, 33.46, 31.12, 28.00, 26.21, 7.25, -4.95. **HRMS** (ESI+): calculated for $[C_{11}H_{22}O_2S_2Si+Na]^+$ required m/z 301.0728, found m/z 301.0740.

Compound **3b** was obtained as a colorless oil (13.8 g, 69%). **^{1}H NMR** (600 MHz, Chloroform-*d*) δ 7.69 (m, 4H), 7.50 – 7.37 (m, 6H), 4.90 (t, J = 4.4 Hz, 1H), 4.28 (s, 1H), 4.02 – 3.94 (m, 2H), 3.93 – 3.83 (m, 2H), 2.93 (ddd, J = 14.6, 12.2, 2.7 Hz, 2H), 2.73 (ddd, J = 14.0, 4.2, 2.9 Hz, 2H), 2.17 – 1.99 (m, 2H), 1.84 (ddd, J = 9.4, 8.1, 4.3 Hz, 2H), 1.44 – 1.37 (m, 2H). **^{13}C NMR** (151 MHz, CDCl3) δ 135.67, 132.05, 130.02, 127.86, 105.62, 64.99, 32.36, 31.66, 28.03, 26.03, 5.29. **HRMS** (ESI+): calculated for $[C_{21}H_{26}O_2S_2Si+Na]^+$ required m/z 425.1041, found m/z 425.1037.

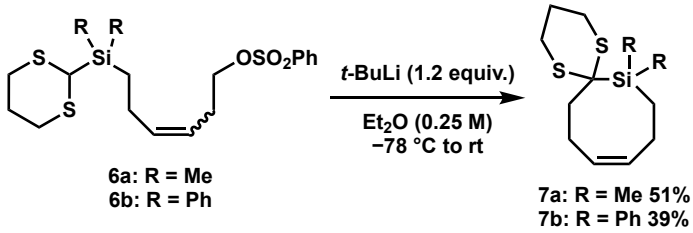


3-((1,3-dithian-2-yl)dimethylsilyl)propanal (4a) and **3-((1,3-dithian-2-yl)diphenylsilyl)propanal (4b)**: The procedure was modified from a reported example.[1] A flame-dried 250 mL round bottom flask cooled under vacuum was charged with a stir bar, **3** (31 mmol), 2,4,6-trimethylpyridine (11.27 g, 93 mmol) and dry DCM (120 mL). The reaction vessel was cooled to 0 ˚C. To this vigorously stirring mixture was slowly added trimethylsilyl trifluoromethanesulfonate (TMSOTf) (13.78 g, 62 mmol). The solution was stirred at 0 ˚C for 2 h followed by addition of water (20 mL). The reaction mixture was allowed to warm to room temperature and stirred for 15 min. The mixture was washed with 2M HCl solution (twice) and saturated brine, dried over Na_2SO4, and concentrated *in vacuo*. The crude product was purified by silica gel column chromatography (ethyl acetate/hexane = 1:10) to afford compound **4**.

Compound **4a** was obtained as a colorless oil (5.0 g, 70%). **^{1}H NMR** (600 MHz, Chloroform-d) δ 9.78 (t, J = 1.5 Hz, 1H), 3.76 (s, 1H), 2.94 – 2.85 (m, 2H), 2.79 – 2.71 (m, 2H), 2.57 – 2.52 (m, 2H), 2.18 – 1.98 (m, 2H), 1.02 – 0.94 (m, 2H), 0.19 (s, 6H). **^{13}C NMR** (151 MHz, CDCl3) δ 202.49, 38.25, 33.35, 31.08, 26.12, 5.47, -4.85. **HRMS** (ESI+): calculated for $[C_9H_{18}OS_2Si+Na]^+$ required m/z 257.0466, found m/z 257.0463.
Compound **4b** was obtained as a colorless oil (6.8 g, 61%). **^{1}H NMR** (600 MHz, Chloroform-d) δ 9.77 (t, J = 1.4 Hz, 1H), 7.71 – 7.62 (m, 4H), 7.51 – 7.36 (m, 6H), 4.30 (s, 1H), 2.95 (ddd, J = 14.7, 12.3, 2.6 Hz, 2H), 2.75 (ddd, J = 14.1, 4.3, 2.9 Hz, 2H), 2.65 – 2.57 (m, 2H), 2.17 – 2.02 (m, 2H), 1.61 – 1.53 (m, 2H). **^{13}C NMR** (151 MHz, CDCl3) δ 202.13, 135.56, 131.48, 130.30, 128.02, 38.34, 32.14, 31.60, 25.95, 3.56. **HRMS** (ESI+): calculated for $[C_{19}H_{22}OS_2Si+Na]^+$ required m/z 381.0779, found m/z 381.0765.



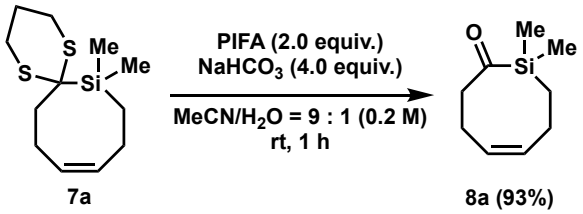
6-((1,3-dithian-2-yl)dimethylsilyl)hex-3-en-1-yl benzenesulfonate (6a) and **6-((1,3-dithian-2-yl)diphenylsilyl)hex-3-en-1-yl benzenesulfonate (6b)**: A flame-dried 250 mL round bottom flask cooled under vacuum was charged with a stir bar, phosphonium **5** (10.30 g, 20.0 mmol), and dry THF (100 mL). The reaction vessel was cooled to 0 ˚C. To this stirring mixture was slowly added LHMDS (20.0 mmol, 1.0 M in THF). The mixture was stirred at 0 ˚C for 30 min and cooled to −78 ˚C. Compound **4** (16.6 mmol, 1.0 M in THF) was added dropwise. The reaction mixture was allowed to warm to room temperature overnight and was quenched by addition of sat. aqueous NH_4Cl solution. The organic solvent was evaporated *in vacuo*. The crude product was loaded onto a silica plug and was eluted with ethyl acetate/hexane = 1:10. The eluent was concentrated *in vacuo* and the resulting oil was added 40 mL of methanol containing 1% concentrated hydrochloric acid. The mixture was stirred at room temperature for 15 min before being sparged with N_2 for 15 min. The organic solvent was evaporated *in vacuo*. The crude product was loaded onto a silica plug and was eluted with diethyl ether. The eluent was concentrated *in vacuo*. The resulting oil was dissolved in dry DCM (83 mL) and transfer to a round bottom flask charged with a stir bar, DMAP (405.6 mg, 3.32 mmol), benzenesulfonyl chloride (2.93 g, 16.6 mmol), triethylamine (2.31 mL, 16.6 mmol). The solution was stirred at room temperature for 2 h and was concentrated *in vacuo*. The crude product was purified by silica gel column chromatography (ethyl acetate/hexane = 1:4) to afford compound **6**.
Compound **6a**, a mixture of Z/E isomers (Z/E = 5.7), was obtained as a colorless oil (3.9 g, 57%). **^{1}H NMR** and **^{13}C NMR** spectra were shown in the spectra section. **HRMS** (ESI+): calculated for $[C_{18}H_{28}O_3S_3Si+Na]^+$ required m/z 439.0868, found m/z 439.0849.
Compound **6b**, a mixture of Z/E isomers (Z/E = 7.3), was obtained as a colorless oil (4.4 g, 49%). **^{1}H NMR** and **^{13}C NMR** spectra were shown in the spectra section. **HRMS** (ESI+): calculated for $[C_{28}H_{32}O_3S_3Si+Na]^+$ required m/z 563.1181, found m/z 563.1191.



(Z)-7,7-dimethyl-1,5-dithia-7-silaspiro[5.7]tridec-10-ene (7a) and **(Z)-7,7-diphenyl-1,5-dithia-7-silaspiro[5.7]tridec-10-ene (7b)**: A flame-dried 500 mL round bottom flask cooled under vacuum was charged with a stir bar, **6** (5.0 mmol), and diethyl ether (200 mL). The reaction vessel was cooled to −78 ˚C and a solution of *t*BuLi (6.0 mmol, 1.2 equiv.) was added dropwise. The reaction mixture was allowed to warm to room temperature overnight and was quenched by addition of sat. aqueous NH_4Cl solution. The organic solvents were evaporated *in vacuo*. The crude product was purified by silica gel column chromatography (ethyl acetate/hexane = 1:10) to afford compound **7**.

Compound **7a** was obtained as a colorless oil (660 mg, 51%). **^{1}H NMR** (600 MHz, Chloroform-d) δ 5.74 – 5.68 (m, 1H), 5.59 (m, 1H), 3.14 – 3.05 (m, 2H), 2.46 – 2.37 (m, 6H), 2.29 (q, J = 7.6 Hz, 2H), 2.11 – 2.02 (m, 1H), 1.99 – 1.88 (m, 1H), 1.04 (t, J = 7.1 Hz, 2H), 0.18 (s, 6H). **^{13}C NMR** (151 MHz, CDCl3) δ 133.60, 130.18, 40.78, 35.49, 25.24, 24.46, 22.63, 22.05, 18.95. **HRMS** (ESI+): calculated for $[C_{12}H_{22}S_2Si+Na]^+$ required m/z 281.0830, found m/z 281.0842.

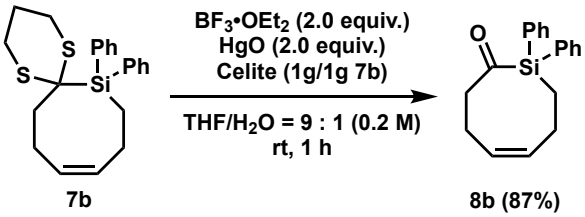
Compound **7b** was obtained as a white solid (746 mg, 39%). Crystals of **7b** suitable for X-ray diffraction were grown by layer diffusion of pentane to a saturated DCM solution of **7b** at –20 ˚C. **^{1}H NMR** (600 MHz, Chloroform-d) δ 7.74 (d, J = 6.5 Hz, 4H), 7.37 (dt, J = 29.3, 7.2 Hz, 6H), 5.64 (q, J = 9.0 Hz, 1H), 5.22 (q, J = 9.0 Hz, 1H), 3.11 (ddd, J = 14.7, 11.8, 3.3 Hz, 2H), 2.66 – 2.58 (m, 2H), 2.54 (q, J = 7.5 Hz, 2H), 2.41 (tt, J = 8.4, 3.4 Hz, 4H), 2.02 – 1.85 (m, 2H), 1.70 (t, J = 6.9 Hz, 2H). **^{13}C NMR** (151 MHz, CDCl3) δ 136.21, 135.41, 133.85, 129.65, 129.10, 127.31, 40.91, 35.96, 25.09, 24.59, 23.36, 21.97, 15.56. **HRMS** (ESI+): calculated for $[C_{22}H_{26}S_2Si+Na]^+$ required m/z 405.1143, found m/z 405.1161.



(Z)-1,1-dimethyl-3,4,7,8-tetrahydrosilocin-2(1H)-one (8a):

A 20 mL scintillation vial was charged with a stir bar, **7a** (517 mg, 2.0 mmol), sodium bicarbonate (672 mg, 4.0 equiv.), and MeCN/H_2O = 9 : 1 (10 mL). To this vigorously stirring mixture was added (bis(trifluoroacetoxy)iodo)benzene (PIFA) (1.72 g, 2.0 equiv.). The reaction mixture was stirred at room temperature for 1 h. The mixture was then diluted with diethyl ether and washed with 1 M HCl and saturated brine, dried over Na_2SO4, and concentrated *in vacuo*. The crude product was purified by silica gel column chromatography (diethyl ether/petane = 1:10) to afford compound **8a** as a colorless oil (312 mg, 93%). **^{1}H NMR** (600 MHz, Chloroform-d) δ 5.68 – 5.61 (m, 1H), 5.53 – 5.44 (m, 1H), 2.61 – 2.49 (m, 4H), 2.33 – 2.25 (m, 2H), 0.76 – 0.69 (m, 2H), 0.25 (s, 6H). **^{13}C NMR** (151 MHz, CDCl3) δ 250.28, 131.59, 128.81, 49.67, 21.31, 20.78, 13.89, -4.01. **HRMS** (ESI+): calculated for $[C_9H_{16}OSi+Na]^+$ required m/z 191.0868, found m/z 191.0867.

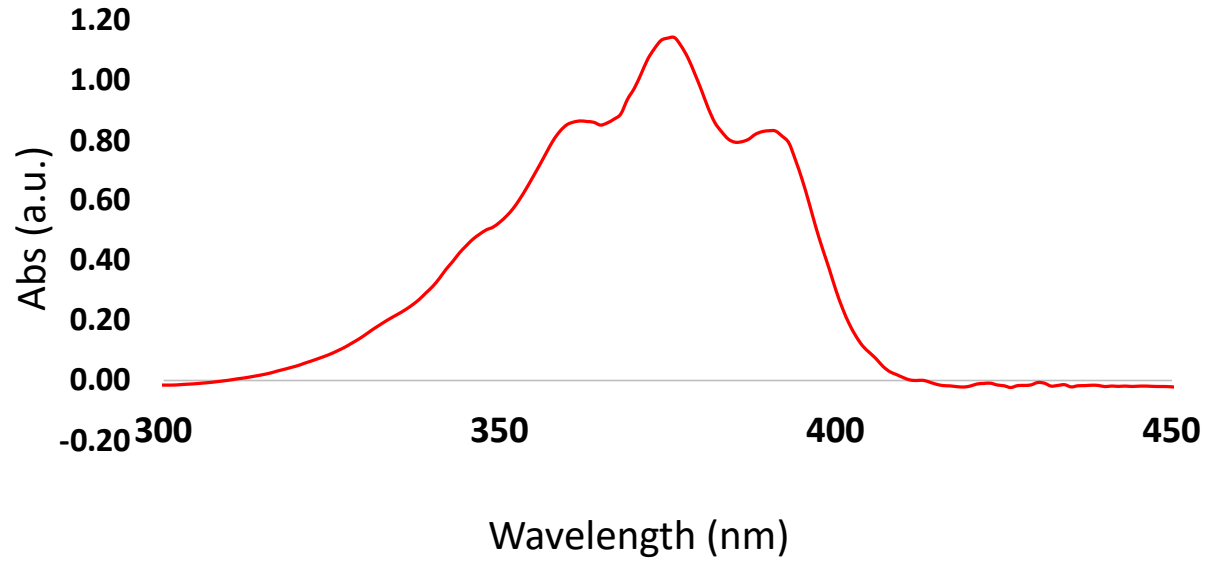
(Z)-1,1-diphenyl-3,4,7,8-tetrahydrosilocin-2(1H)-one (8b):



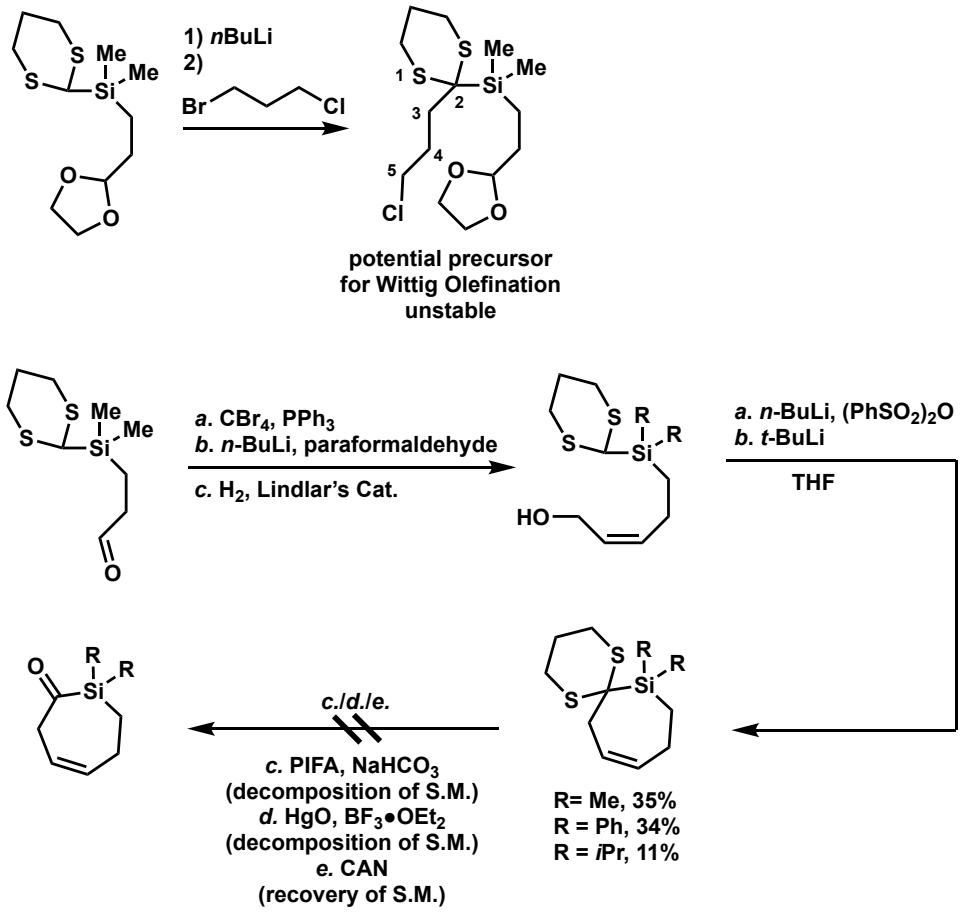
7b 8b (87%)

A 20 mL scintillation vial was charged with a stir bar, **7b** (765mg, 2.0 mmol), mercury oxide (866 mg, 4.0 mmol), Celite (765 mg), and THF/H_2O = 9 : 1 (10 mL). To this vigorously stirring mixture was added boron trifluoride diethyl etherate (BF3•OEt_2) (568 mg, 4.0 mmol) dropwise. The reaction mixture was stirred at room temperature for 1 h. The mixture was then loaded onto a silica plug and was eluted with diethyl ether. The eluent was concentrated *in vacuo*. The crude product was purified by silica gel column chromatography (ethyl acetate/hexane = 1:10) to afford compound **8b** as a white solid (509 mg, 87%). Crystals of **8b** suitable for X-ray diffraction were grown by layer diffusion of pentane to a saturated DCM solution of **8b** at –20 ˚C **^{1}H NMR** (600 MHz, Chloroform-d) δ 7.68 – 7.55 (m, 4H), 7.52 – 7.38 (m, 6H), 5.74 (dt, J = 10.6, 8.2 Hz, 1H), 5.47 (dt, J = 10.7, 8.5 Hz, 1H), 2.69 – 2.62 (m, 2H), 2.60 – 2.50 (m, 2H), 2.41 (tt, J = 8.7, 5.0 Hz, 2H), 1.42 – 1.33 (m, 2H). **^{13}C NMR** (151 MHz, CDCl3) δ 246.51, 132.73, 130.86, 129.97, 129.62, 128.17, 50.32, 21.18, 20.95, 11.63. **HRMS** (ESI+): calculated for $[C_{19}H_{20}OSi+Na]^+$ required m/z 315.1181, found m/z 315.1182.

UV-Vis Spectrum (5 mM in DCM):



Unsuccessful synthetic routes of cyclic acylsilanes:



3.5.3 Strain Energy Calculations in ROMP

Geometry optimization and frequency calculation were conducted with B3LYP/6-31G(d). Strain energies were calculated by subtracting the heats of formation of the cyclic monomer and ethylene from that of corresponding ring-opened product as shown in Figure S3.1.

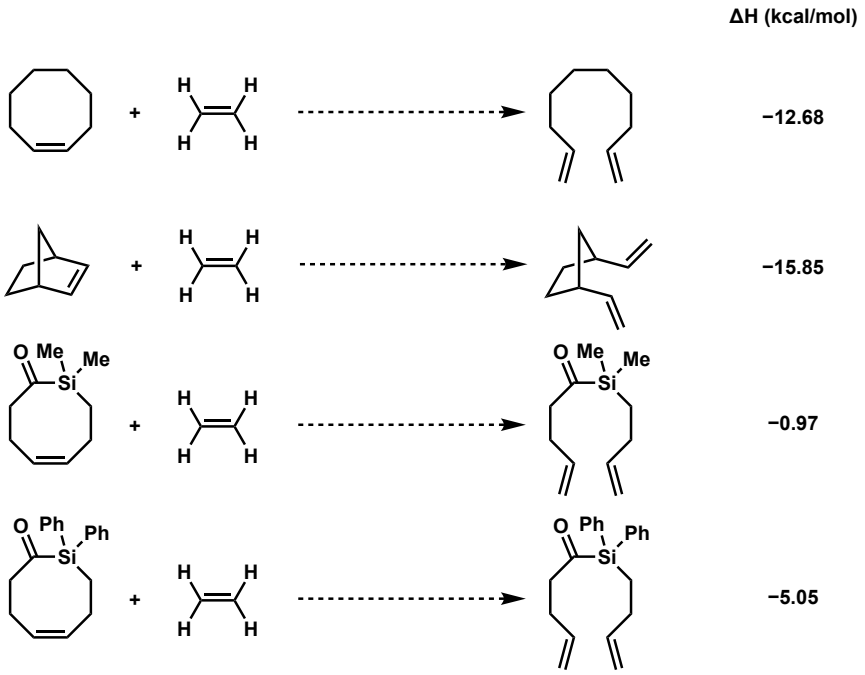


Figure S3.1 Calculated reaction enthalpy of hypothetical ring opening metathesis reactions

3.5.4 Polymer Synthesis and Solution Photodegradation Protocols

P1–P9: An oven-dried 1-dram vial with septum cap was charged with a stir bar, **8** (0.05 mmol), **9** (0.15 mmol), and $CHCl_3$ (200 μL). The solution was sparged with N_2 for 1 min. Designated ruthenium catalyst was then added as a $CHCl_3$ solution (50 mM) into the vigorously stirring solution. The reaction was stirred at room temperature for 30 min and before quenched with 2 drops of ethyl vinyl ether. Methanol was added 5 min after quenching to precipitate the polymer. The polymer was collected and dried *in vacuo*. The dry sample was dissolved in THF for THF GPC analyses. Mole percentage of acylsilane units in the copolymers were determined by ^{1}H NMR spectroscopy (time interval between data acquisition equals 30 s, relative integration remains the same for single-scan spectrum). Photodegradation studies of **P5** and **P9** were conducted on the 1 mg/mL $CHCl_3$ solution of the polymers in a 1-dram vial charged with a stir bar (Figure S3.5).

A homopolymer of **9** was prepared and subjected to the irradiation conditions following the same procedure. GPC traces were shown in Figure S3.4.

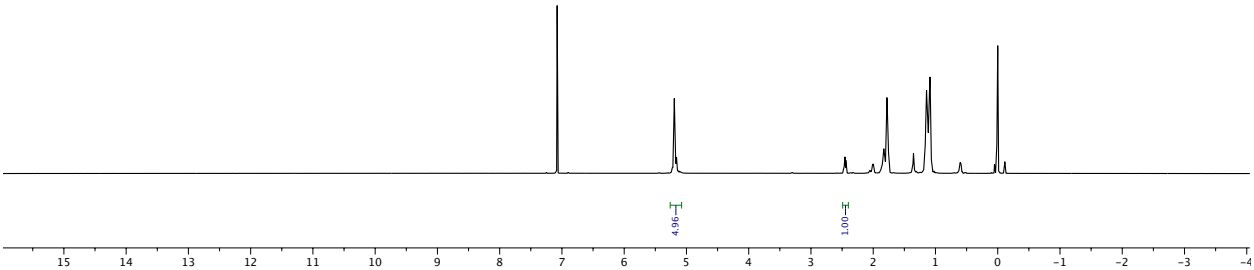


Figure S3.2 ^{1}H NMR spectrum of **P5** in $CDCl_3$ for the determination of mole percentage of acylsilane units.

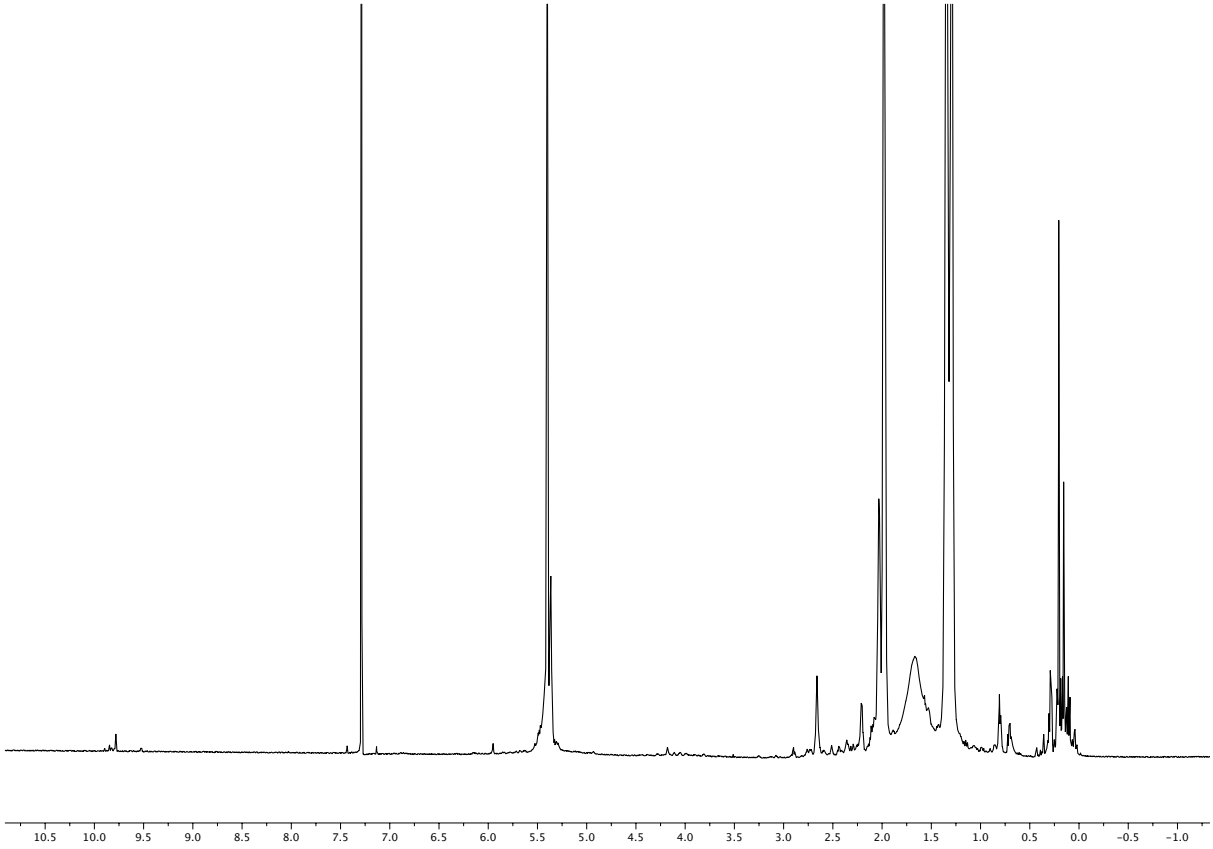


Figure S3.3 ^{1}H NMR spectrum of post-degradation **P5** in $CDCl_3$.

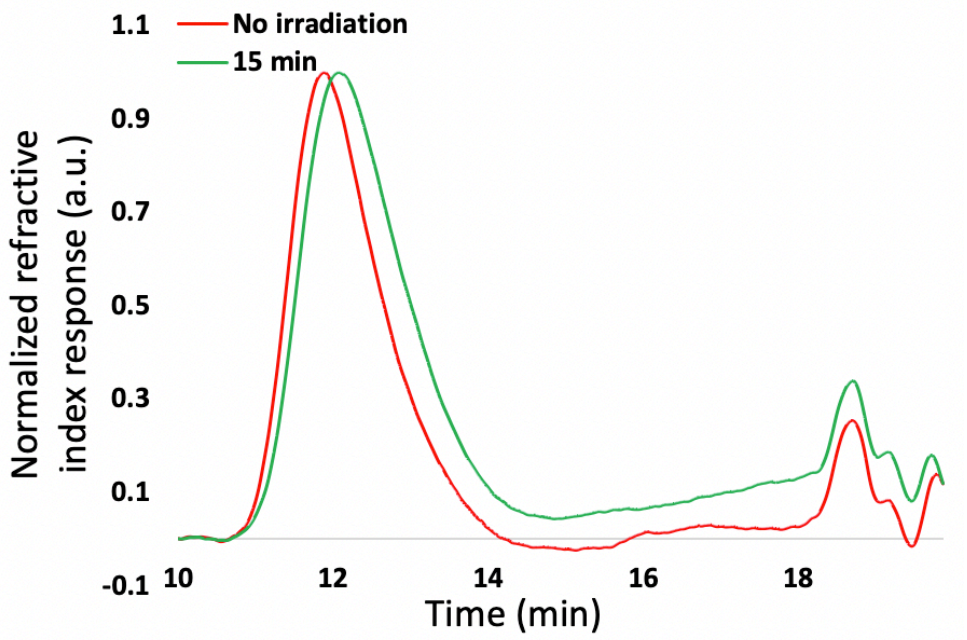


Figure S3.4 GPC traces of homopolymer of **9** before and after irradiation.

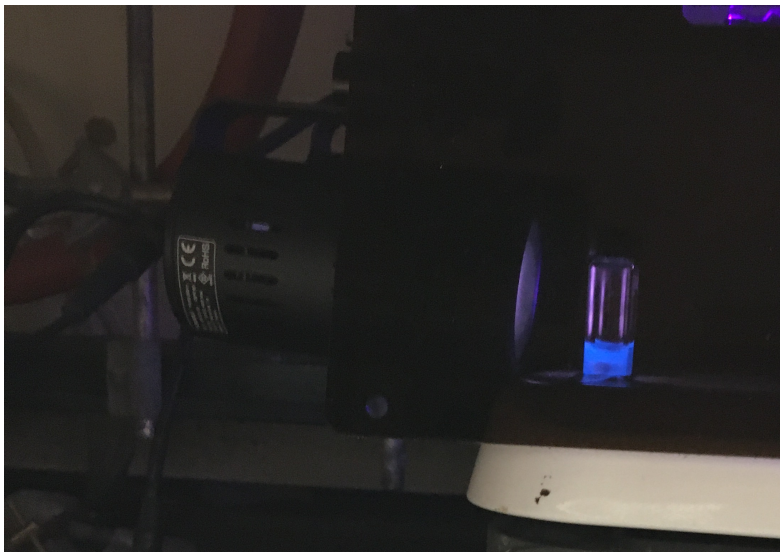


Figure S3.5 Solution photodegradation setup.

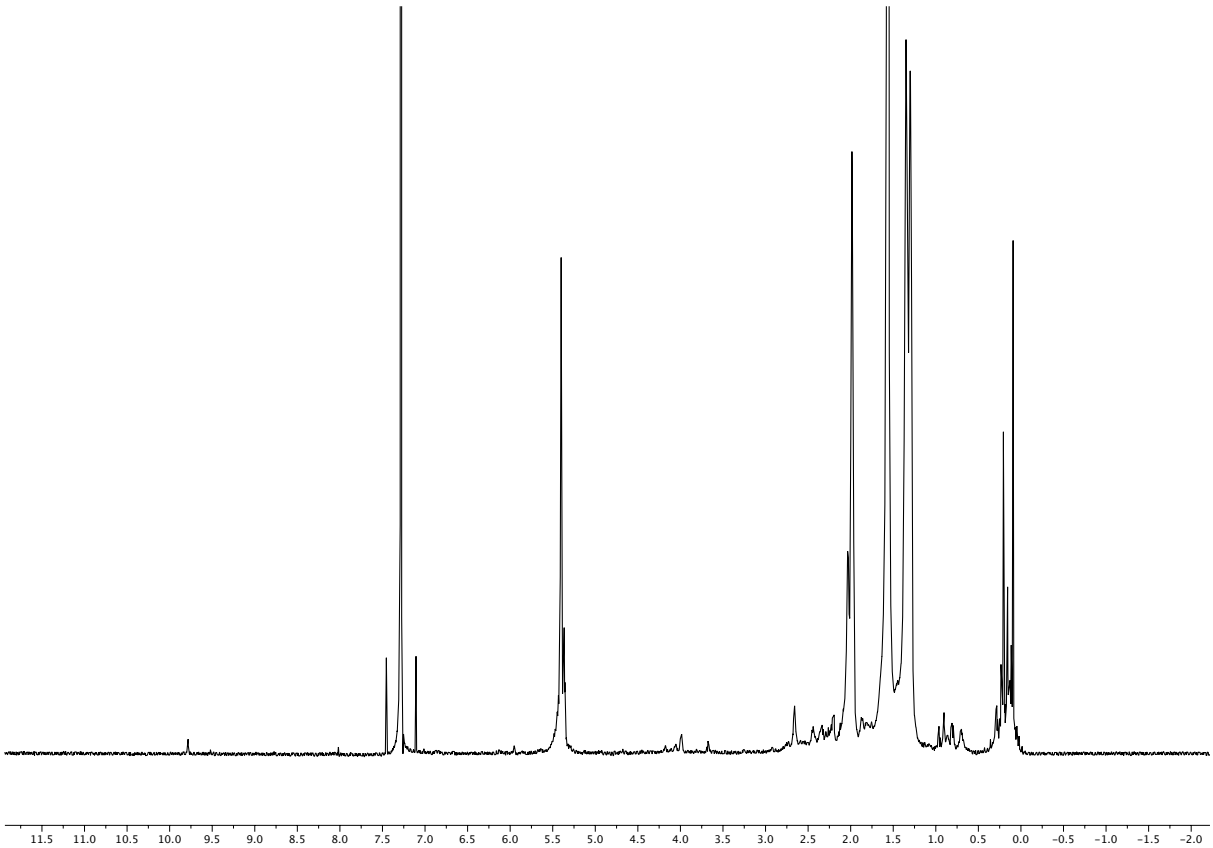


Figure S3.6 ^{1}H NMR spectrum of post-degradation polymer film in $CDCl_3$.

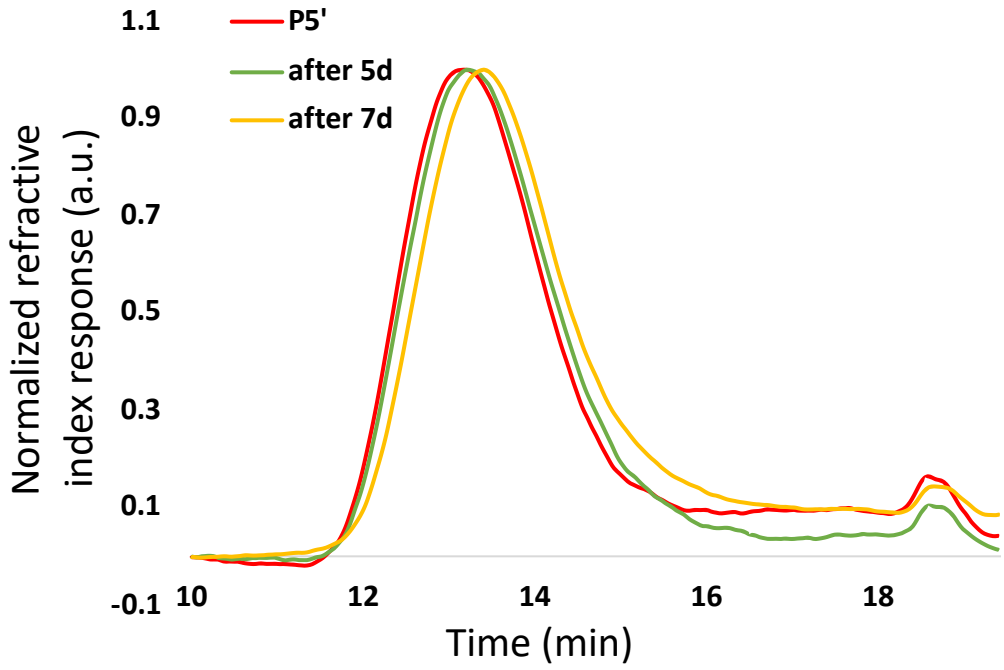


Figure S3.7 GPC traces from stability test with **P5'** (synthesized under the same conditions as **P5**) in degassed anhydrous $CHCl_3$ (1 mg/mL) in the dark.

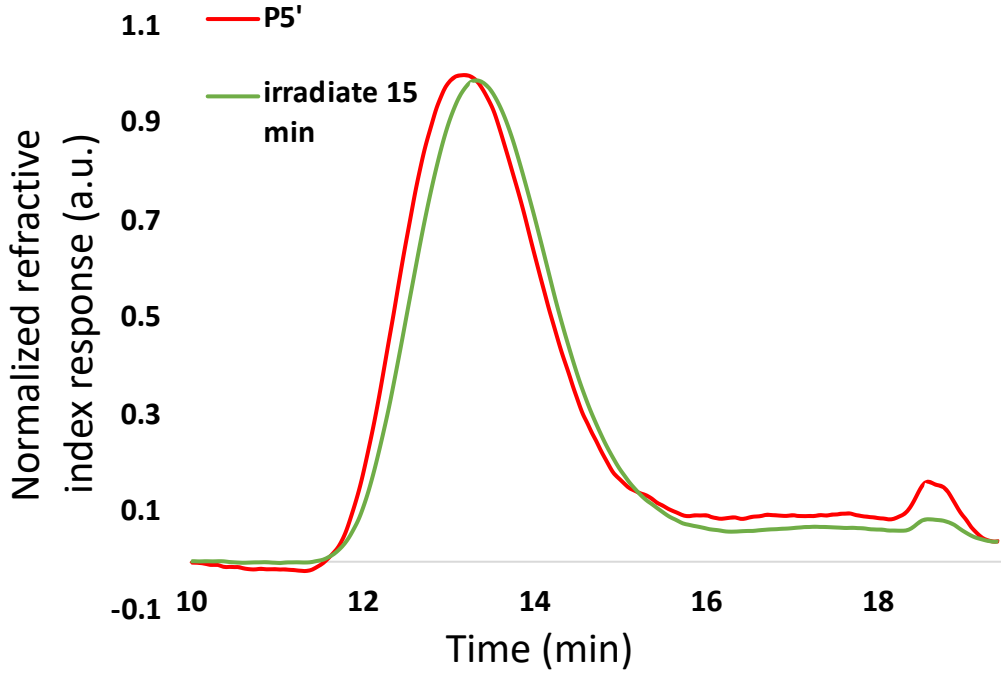


Figure S3.8 GPC traces from irradiation study of **P5'** in degassed anhydrous $CHCl_3$ (1 mg/mL).

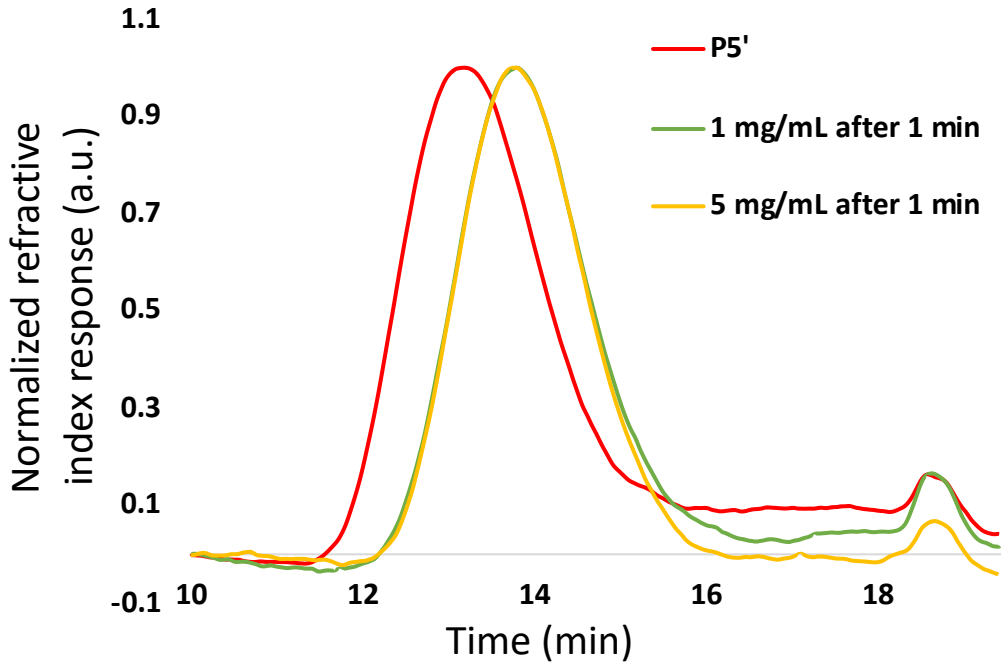


Figure S3.9 GPC traces from irradiation studies of **P5'** in benchtop $CHCl_3$ (different concentrations).

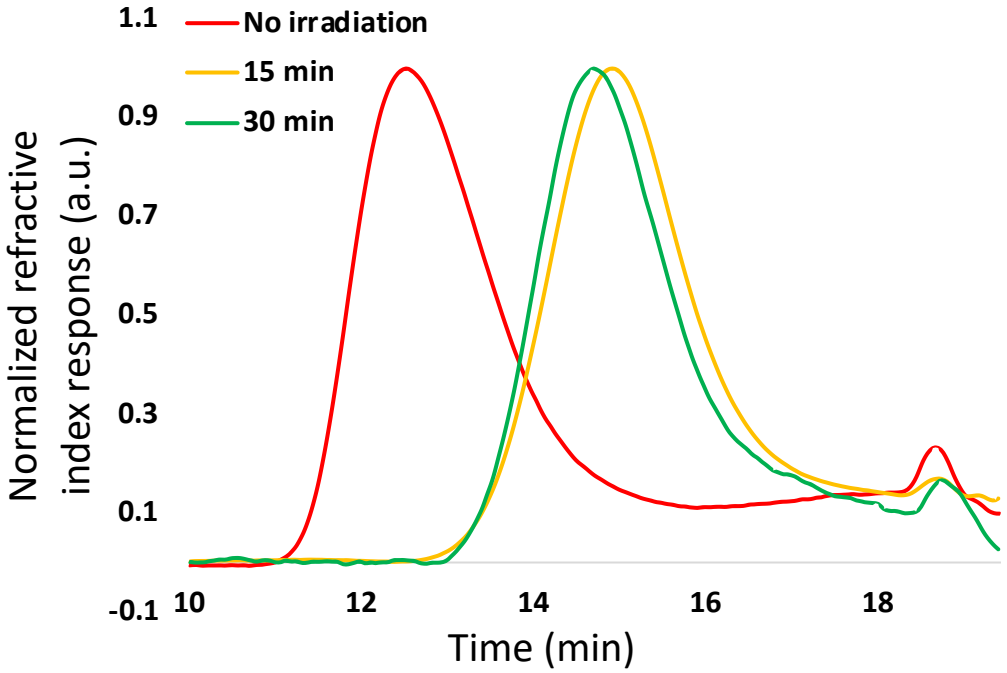


Figure S3.10 GPC traces of photodegradation of **P9** beyond 15 min (shift between 15-min and 30-min traces are likely caused by run-to-run variability).

P10: An oven-dried 1-dram vial with septum cap was charged with a stir bar, **8a** (0.1 mmol), dimethyl carbate (0.1 mmol), and $CHCl_3$ (400 µL). The solution was sparged with N_2 for 1 min. Catalyst **G3** was then added as a $CHCl_3$ solution (20 µL, 50 mM) into the vigorously stirring solution. The reaction was stirred at room temperature for 30 min and before quenched with 2 drops of ethyl vinyl ether. An aliquot was taken for THF GPC analysis. The rest of the solution was used directly for photodegradation study.

P11: The macromonomer (**PEGMM**) was prepared following a reported procedure.[2] An oven-dried 1-dram vial with septum cap was charged with a stir bar, **8a** (0.03 mmol), **PEGMM** (0.03 mmol), and $CHCl_3$ (300 µL). The solution was sparged with N_2 for 1 min. Catalyst G3 was then added as a $CHCl_3$ solution (20 µL, 50 mM) into the vigorously stirring solution. The reaction was stirred at room temperature for 30 min and before quenched with 2 drops of ethyl vinyl ether. An aliquot was taken for THF GPC analysis. The rest of the solution was used directly for photodegradation study.

Different catalyst loadings targeting various degree of polymerization (DP) in a similar procedure without **8a** was used to estimate the DP of **P11** and the degradation product.

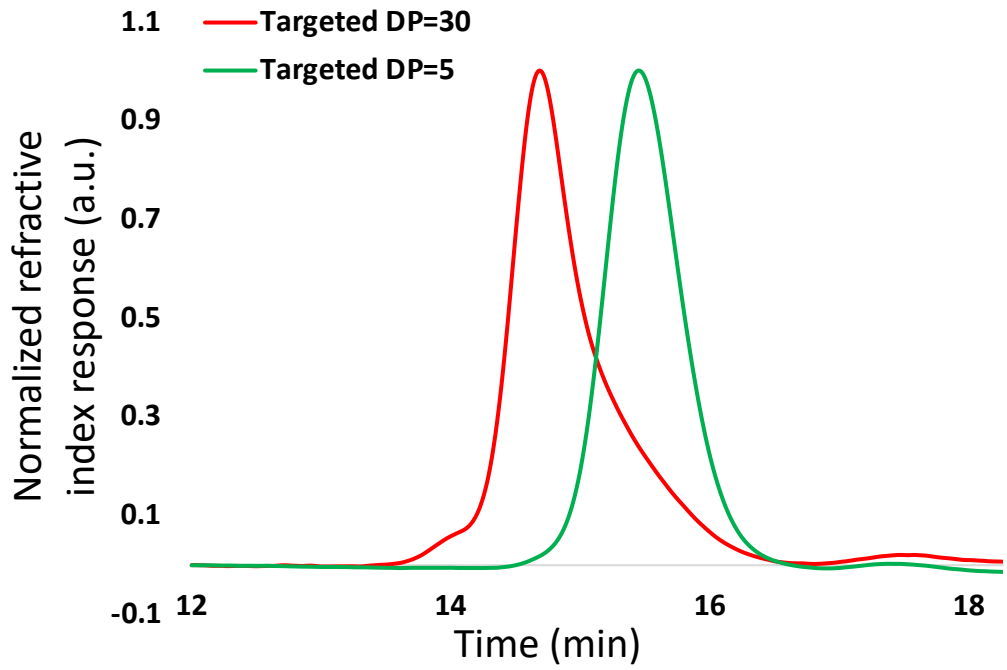


Figure S3.11 GPC traces of PEGMM homopolymer with targeted DPs.

3.5.5 Photodegradation Protocols in Solid State

3.5.5.1 Preparation of polymer film and its photodegradation studies

An oven-dried 1-dram vial with septum cap was charged with a stir bar, **8a** (0.1 mmol), **9** (0.3 mmol), and $CHCl_3$ (400 µL). The solution was sparged with N_2 for 1 min. Catalyst **G2** was then added as a $CHCl_3$ solution (4 µL, 50 mM) into the vigorously stirring solution. The reaction was stirred at room temperature for 30 min and before quenched with 2 drops of ethyl vinyl ether. A Teflon beaker was added 150 µL of the polymer solution and treated with N_2 flow for 1 h. Liquid N_2 was then added to the beaker to facilitate the demolding process. The film was further dried *in vacuo* for 1 h. The thickness of the film was measured by a caliper to be 0.135 ± 0.032 mm. The

film was placed in a Pyrex dish with lid and under the LED lamp. After each designated period of irradiation, a quarter of the film was cut and dissolved in THF for THF GPC analysis.

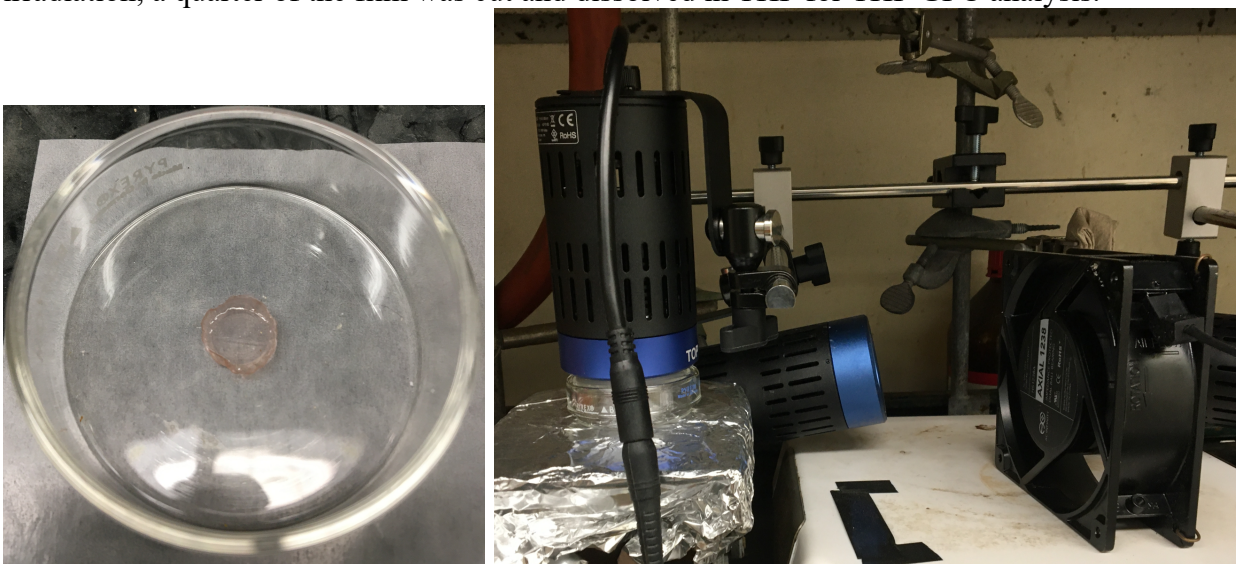


Figure S3.12 Polymer film in a Pyrex dish (left) and the photodegradation setup (right).

3.5.5.2 Preparation of 8a and dicyclopentadiene copolymer and its photodegradation studies
A Teflon beaker was charged with **8a** (0.2 mmol), **13** (0.6 mmol), and **G2** (4 μL, 50 mM). The polymerization was initiated with heat. The polymer sample was then demolded. The samples were weighed and subjected to TGA (Figure S3.13), SEM analysis (Figure S3.14). Photodegradation studies of the samples were conducted with the same setup as shown in Figure S6 for 30 min. A post-irradiation sample was characterized by SEM (Figure S3.15). Also, a post-irradiation sample was placed in a 20 mL scintillation vial containing 6 mL THF. The vial was sonicated for 30 min, after which fractured sample was filtered and dried *in vacuo* (Figure S3.16). The residual solid was weighed and a 28% weight loss was observed (from 100.5 mg to 72.3 mg). In control experiments, samples underwent no irradiation showed no weight loss. The components dissolved in THF supernatant were analyzed by GPC (Figure S3.17), UPLC-MS (Figure S3.18), and ^{1}H NMR (Figure S3.19), revealing oligomer fragments formed during the photodegradation.

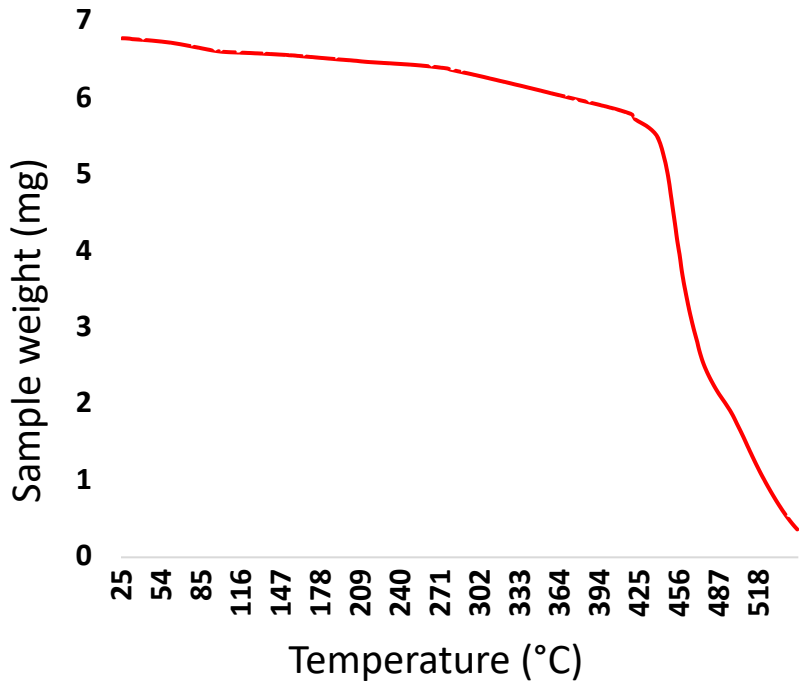


Figure S3.13 TGA analysis of polymer sample from **8a** and **13**.

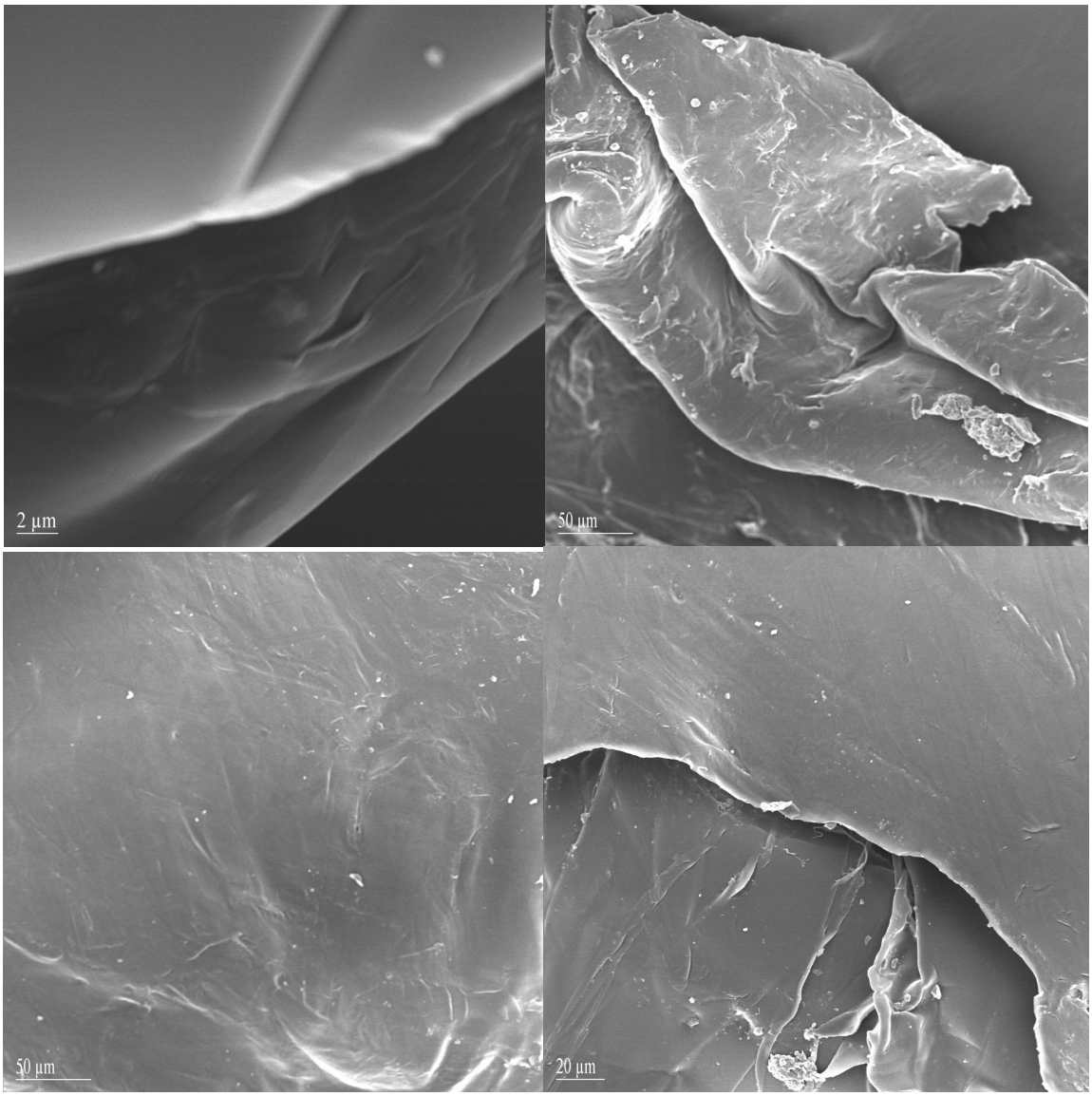


Figure S3.14 SEM images of polymer sample from **8a** and **13** before irradiation.

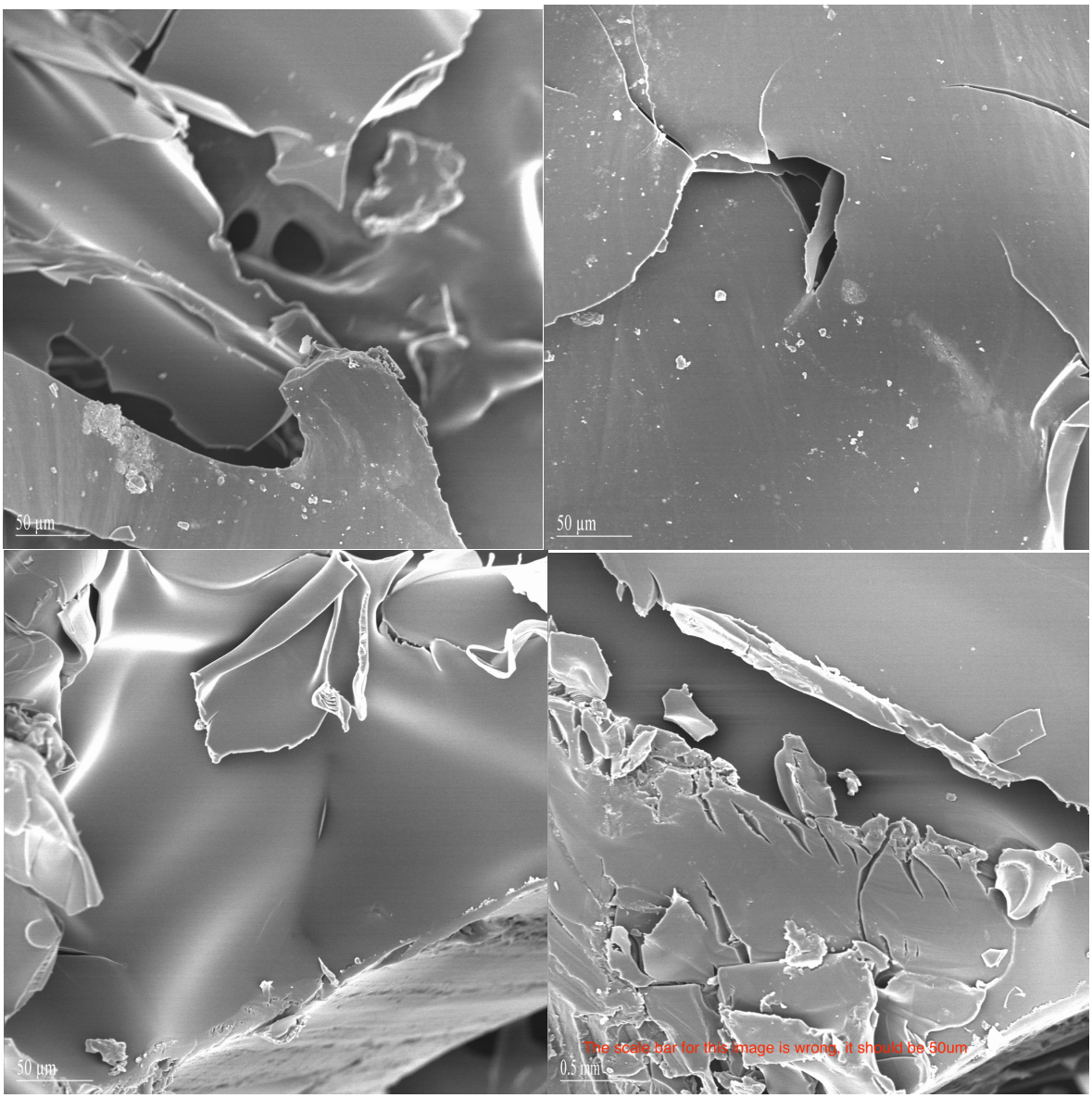


Figure S3.15 SEM images of polymer sample from **8a** and **13** after irradiation.

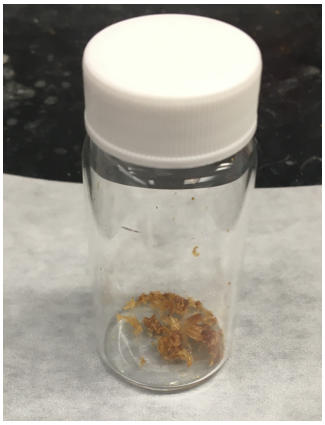


Figure S3.16 Picture of dry residual solids after sonication of post-irradiation polymer sample from **8a** and **13**.

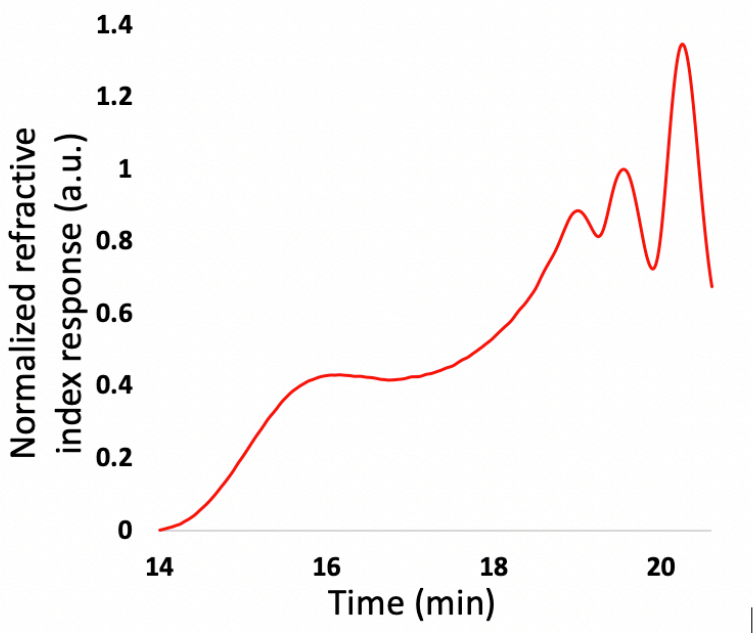


Figure S3.17 GPC analysis of the THF supernatant after sonication of post-irradiation polymer sample from **8a** and **13**.

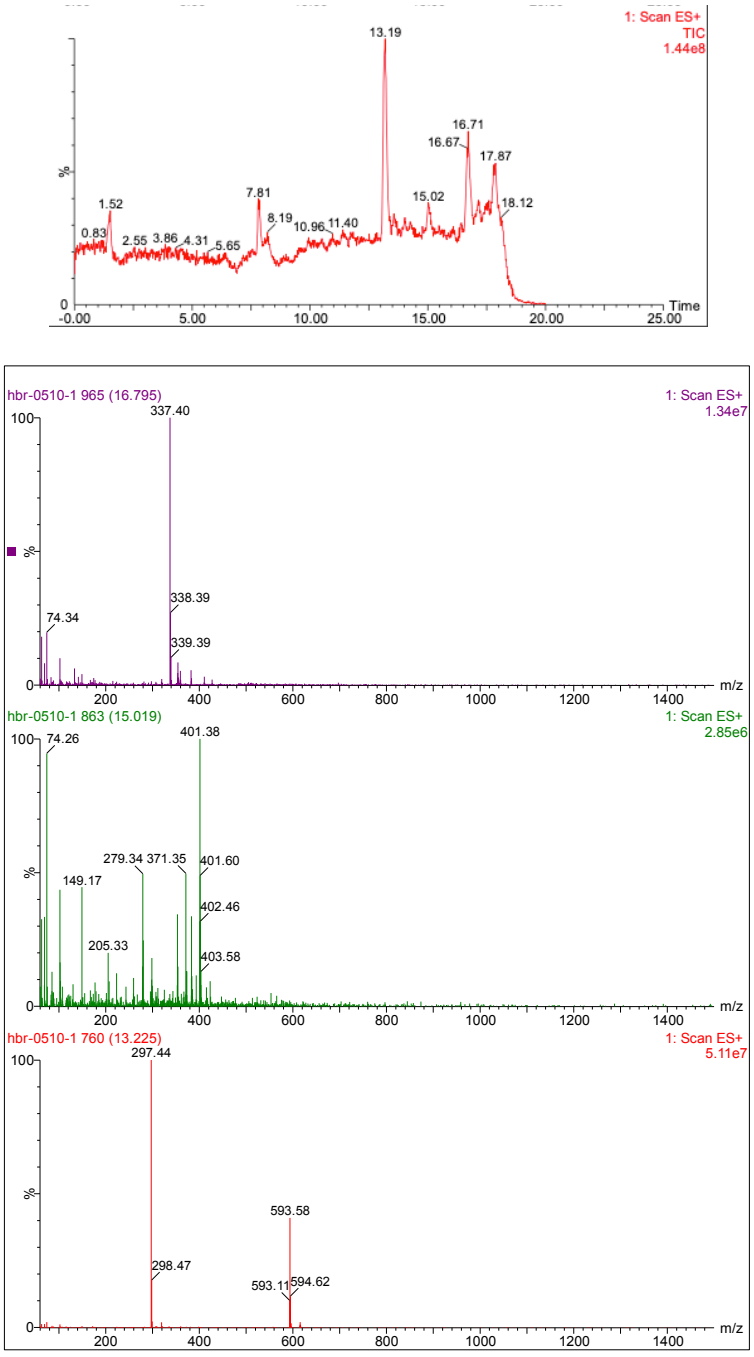


Figure S3.18 C18-UPLC chromatogram (top trace) and representative mass spectrometry data (bottom three traces) of the THF supernatant after sonication of post-irradiation polymer sample from **8a** and **13**.

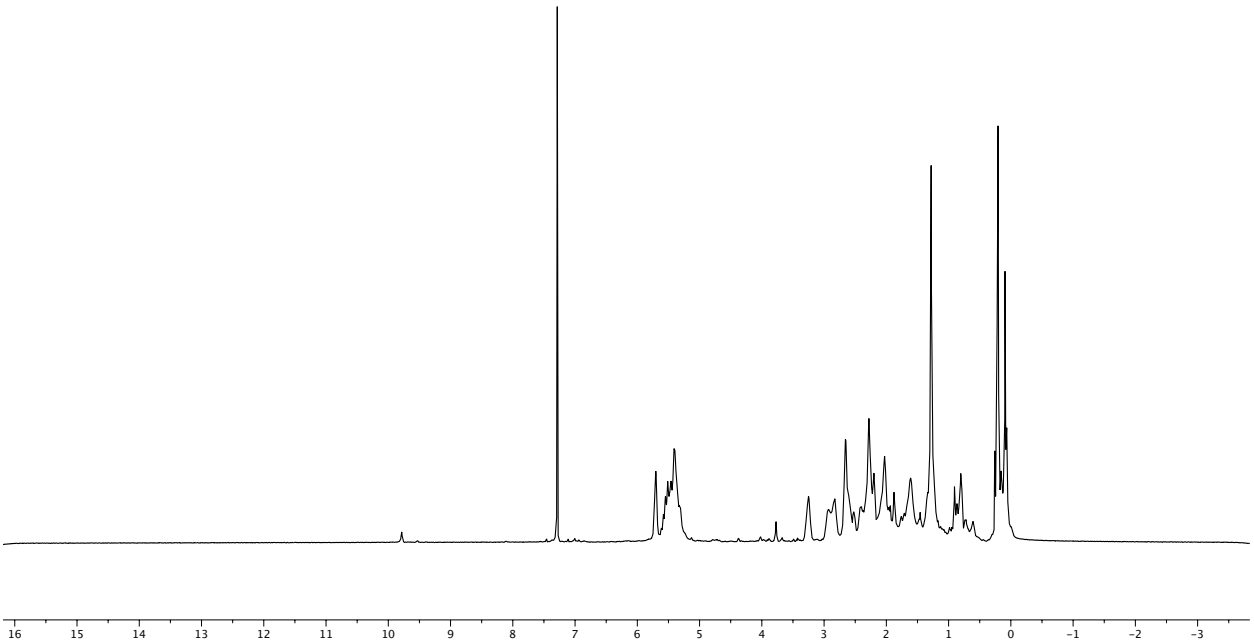


Figure S3.19 ^{1}H NMR spectrum of components from the THF supernatant after sonication of post-irradiation polymer sample from **8a** and **13** in $CDCl_3$.

3.5.6 Mechanistic Studies

3.5.6.1 Measurements of initial rate constants

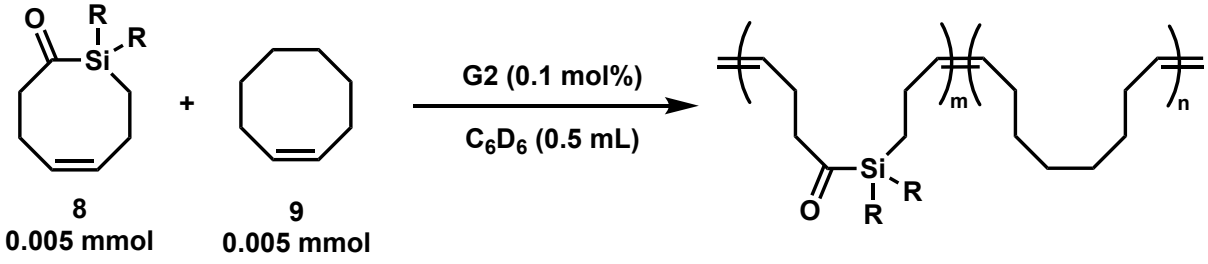
Initial rate constants were measured in oven-dried glassware using degassed solvents using standard NMR techniques on AV-600 with an Avance III console and a 5 mm 1H/BB Prodigy cryo-probe at 25 ± 0.5 °C. A solution of **G2** (50 mM, 8 µL) was added into a NMR tube containing **8a** (0.02 mmol), **10** (0.02 mmol), and 1,4-dinitrobenzene (0.0125 mmol) in $CDCl_3$ (0.5 mL), sealed with a rubber septum and secured with vinyl tape. The tube was quickly inverted and inserted into the NMR spectrometer. ^{1}H NMR spectra were collected at regular intervals. The measurements were conducted in triplicates. The reactivity ratio of **10** (M1) was calculated from Mayo-Lewis Equation, assuming r_2 of monomer **8a** (M2) is 0 (due to the low strain energy and no observed homopolymerization).

unit = s^-1 x 1000				
Run1	*k*(11)	0.06436285	*k*(8a)	0.04007494
Run2	*k*(11)	0.06127016	k(8a)	0.03179861
Run3	*k*(11)	0.06943228	k(8a)	0.0385916
	AVG	0.06502176	AVG	0.03682172
	STDEV	0.00412076	STDEV	0.00441291

Mayo-Lewis Equation: $$\frac{d[M_1]}{d[M_2]} = \frac{[M_1]\,(r_1\,[M_1] + [M_2])}{[M_2]\,([M_1] + r_2\,[M_2])}$$

When $[M_1]_0 = [M_2]_0$ and $r_2 = 0$, the equation can be simplified to : $k_1/k_2 = r_1 + 1$. k_1, k_2 are initial rate constants. Reactivity ratio r(10, with 8a) was derived to be 0.76.

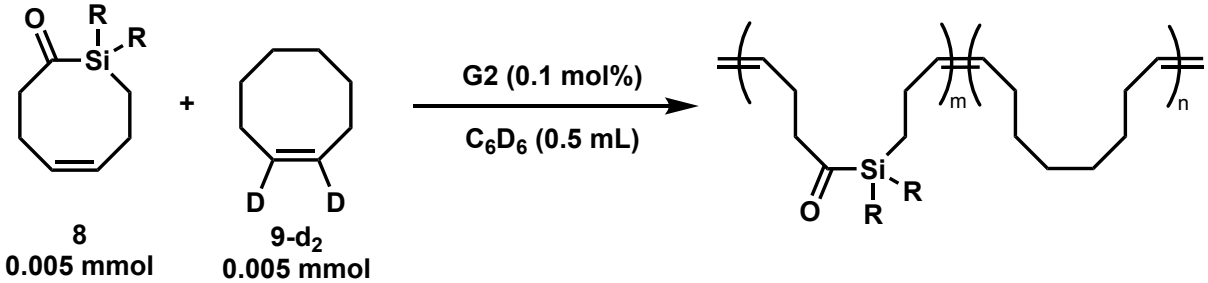
The measurements of reactivity data for **8** and **9** were challenging because of the overlapping olefin peaks of **8**, **9** and their copolymers in ^{1}H-NMR spectrum with $CDCl_3$. Benzene-d_6 was identified to resolve the olefin peaks of **8** and **9** so that the initial rates of **9** in the copolymerization can be measured. However, partial overlap between the olefin peaks of **8** and copolymers were still observed, preventing the initial rates of **8** being measured. To address the partial overlap, *cis*-1,2-dideuterio-cyclooctene (**9-d_2**, 95% D) was synthesized and used to conducted initial rates measurements of **8** in the copolymerization. The data were summarized below, from which reactivity ratios were also derived.



8
0.005 mmol

9
0.005 mmol

k_{obs} (9, with 8a) (s^{-1} x 10^3) = 0.144 ± 0.035
k_{obs} (9, with 8b) (s^{-1} x 10^3) = 0.072 ± 0.034



8
0.005 mmol

9-d_2
0.005 mmol

k_{obs} (8a, with 9) (s^{-1} x 10^3) = 0.0094 ± 0.0017
k_{obs} (8b, with 9) (s^{-1} x 10^3) = 0.0153 ± 0.0027

Assuming r(8) = 0 and no secondary kinetic isotope effect of 9-d_2:

reactivity ratio	r(9, with 8a)	r(9, with 8b)
	14.3	3.71

3.5.6.2 Isotope labeling studies

A 1-dram vial was charged with a stir bar, **11** (0.1 mmol), $CDCl_3$ (0.5 mL), and H_2O (2 drops). A separate 1-dram vial was charged with a stir bar, **11** (0.1 mmol), $CHCl_3$ (0.5 mL), and D_2O (2 drops). Both vials were irradiated under 390-nm LED lamp for 30 min, after which organic solvents were evaporated *in vacuo*. The residue in two vials were separately dissolved in CDCl3 (0.5 mL) and transferred into two NMR tubes. ^{1}H NMR spectra were recorded (Figure S3.20).

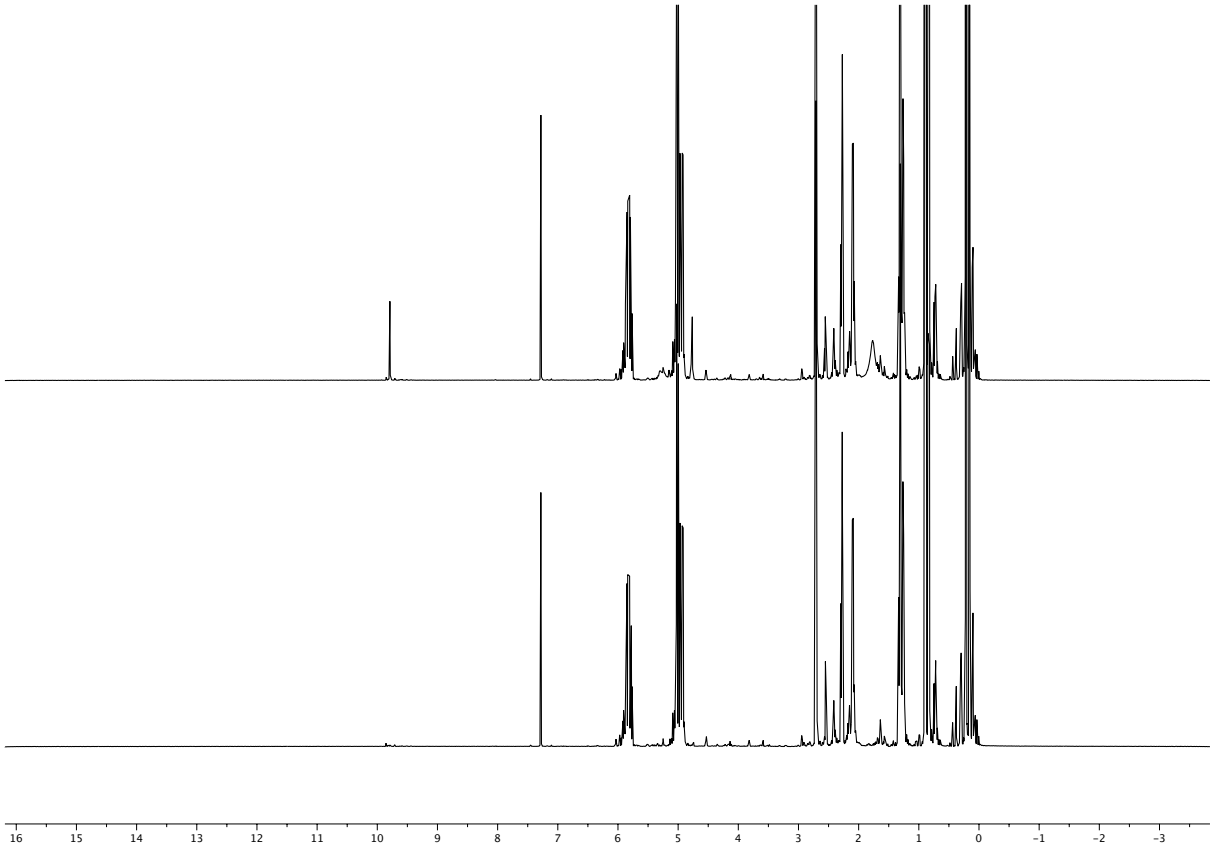


Figure S3.20 ^{1}H NMR spectra of **11** after irradiation in $CDCl_3/H_2O$ (top spectra) and $CHCl_3/D_2O$ (bottom spectra).

3.5.6.3 Additional Irradiation Studies of 11

Model compound **11** was irradiated for 30 min under anhydrous inert atmosphere and was dissolved in anhydrous degassed $CDCl_3$ (to prevent any decomposition in the solution). The ^{1}H-NMR spectrum showed no substantial formation of new specie. This indicated that the nucleophilic α-siloxy carbene intermediate did not react with simple terminal alkenes even at very high concentration. And the reversible Photo-Brook Rearrangement led to recovery of the starting materials due to the lack of downstream reaction partner.

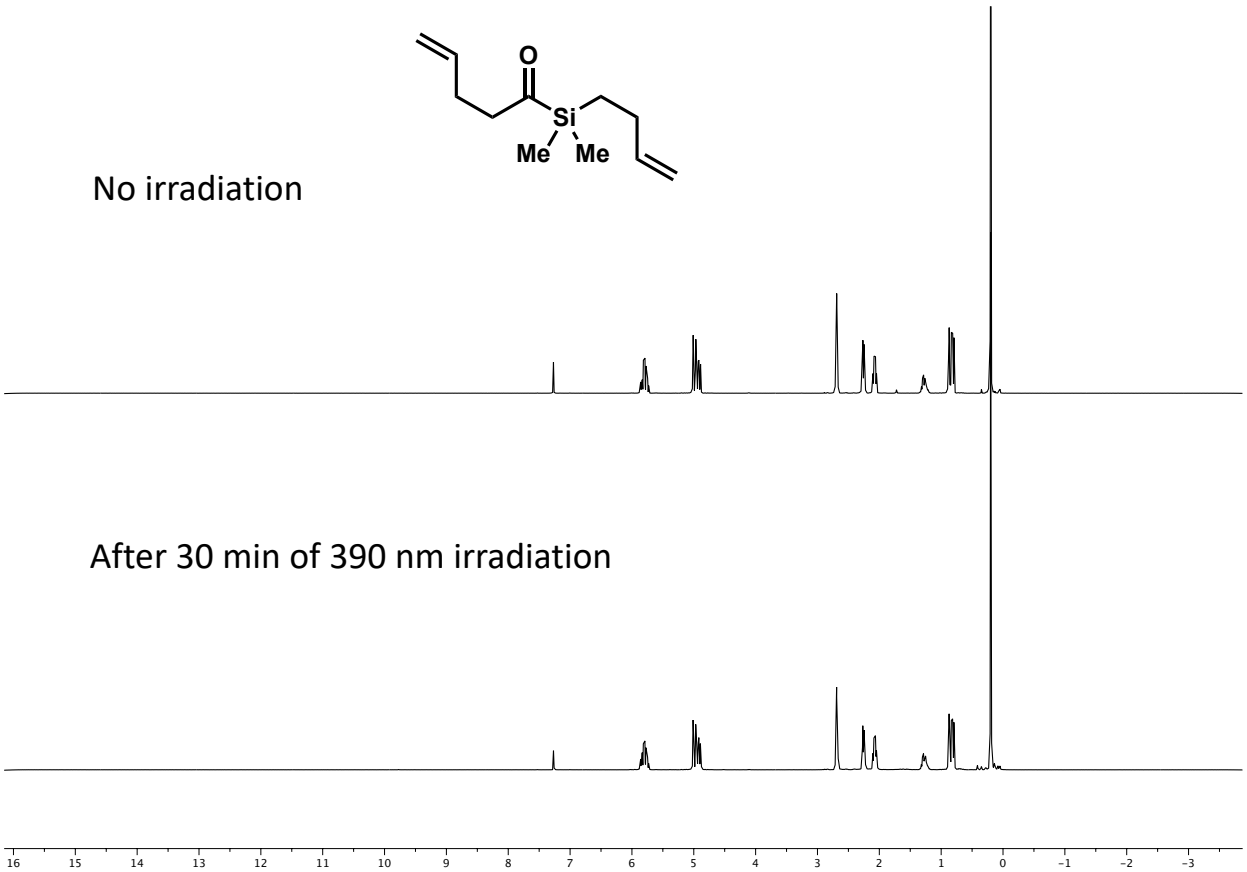
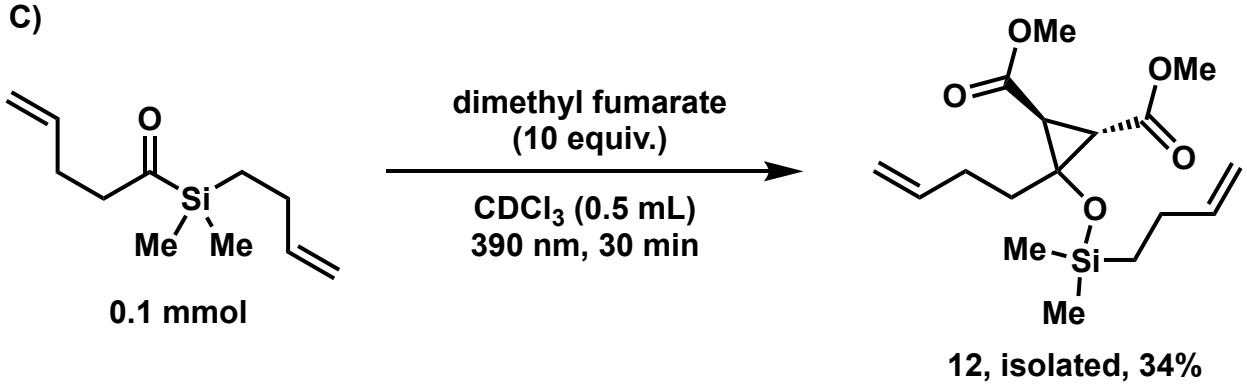


Figure S3.21 ^{1}H NMR spectrum of compound **11** in the irradiation study under anhydrous inert atmosphere.

To provide further evidence that the electronics of the olefins differentiates their reactivities with α-siloxy carbene, compound **11** was irradiated with an electron-deficient alkene, dimethyl fumarate, in benchtop $CDCl_3$. Only trace amount of aldehyde was observed in the crude mixture by ^{1}H NMR. The cyclopropanation product was isolated as the only major product (34% yield) and characterized by ^{1}H, ^{13}C, ^{1}H-^{13}C HSQC NMR spectroscopy, as well as HRMS. The observation is consistent with the literature report of cyclopropanation between a cyclic acylsilane and dimethyl fumurate.[3]

C)



Scheme S3.1 Irradiation study of compound **11** in the presence of dimethyl fumarate.

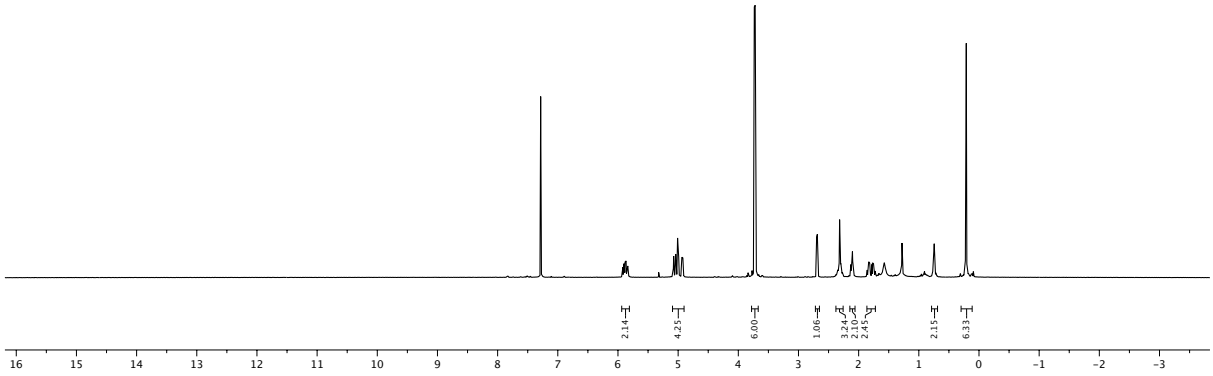


Figure S3.22 ^{1}H NMR spectrum of **12**.

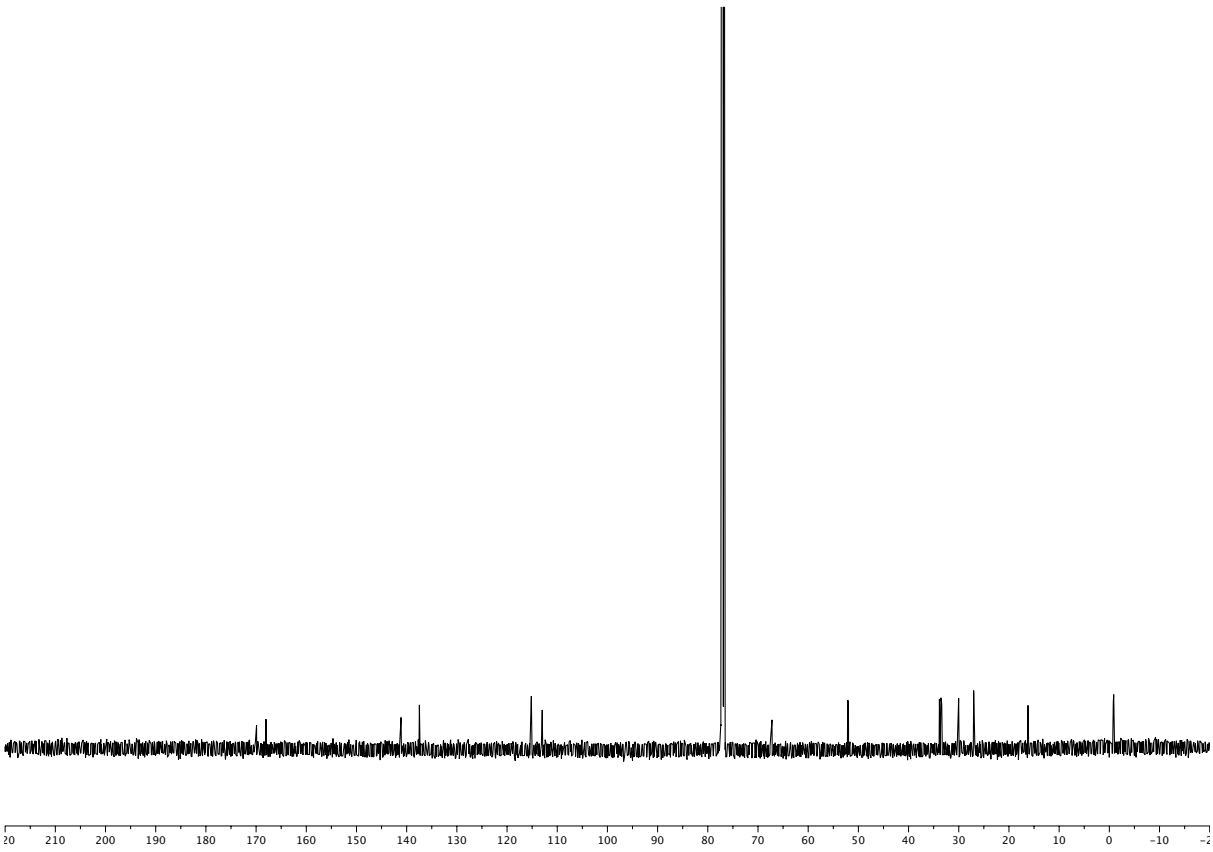


Figure S3.23 ^{13}C NMR spectrum of **12**.

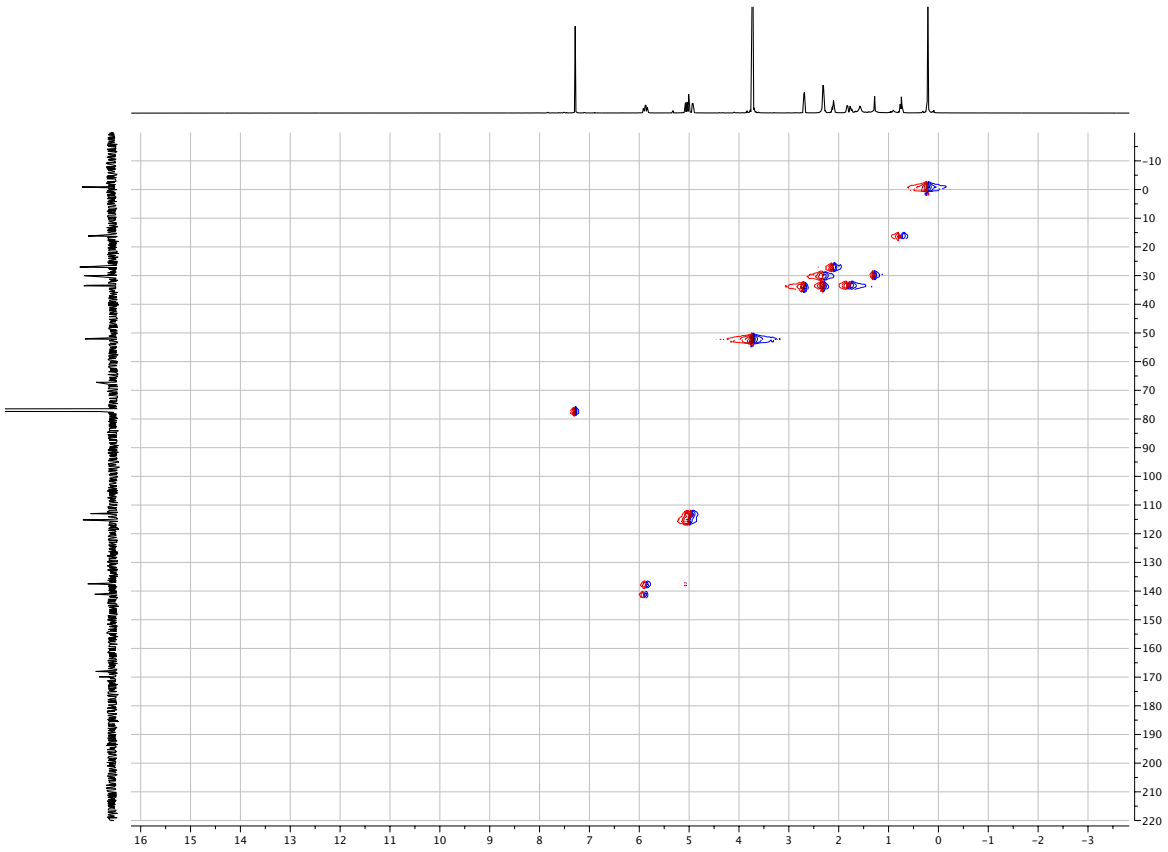


Figure S3.24 ^{1}H-^{13}C HSQC NMR spectrum of **12**.

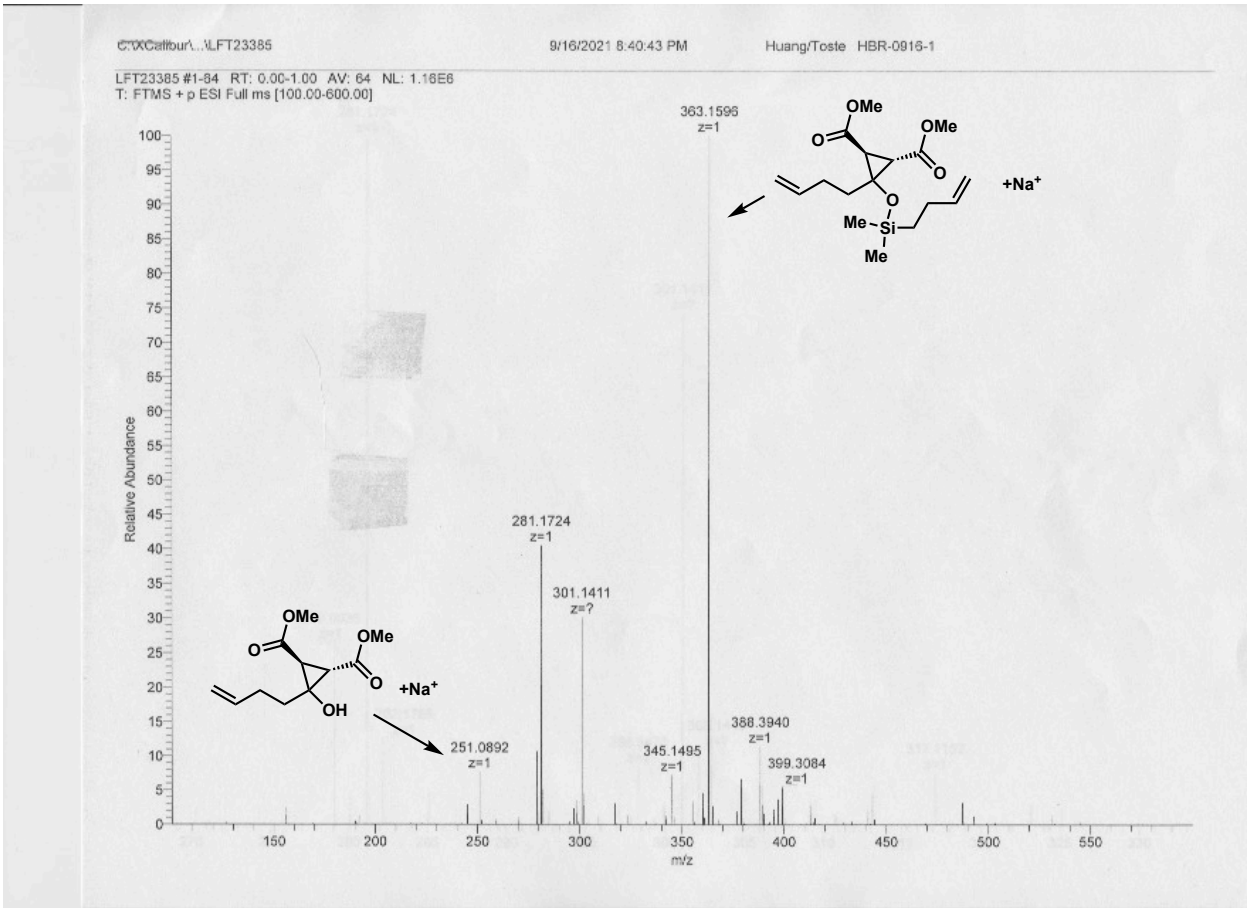


Figure S3.25 HRMS spectrum of **12**.

3.5.7 Protocol of Photochemical Ring Expansion Reactions

An oven-dried 1-dram vial with septum cap was charged with a stir bar, **8b** (0.02 mmol), reaction partner (0.02 mmol), and benzene (200 µL). The vial was irradiated with a 52 W Kessil PR160L LED lamp with a peak emission at 390 nm for 1 h. The reaction mixtures were analyzed by both analytical and preparative TLC, as well as NMR spectroscopy.

3.5.8 References

[1]. Zhong, J.; Chen, K.; Qiu, Y.; He, H.; Gao, S. *Org. Lett.* **2019**, *21* (10), 3741–3745.
[2]. Bates, C. M.; Chang, A. B.; Jones, S. C.; Grubbs, R. H. *Marcromolecules* **2015**, *48* (14), 4967–4973.
[3]. Brook, A. G.; Kucera, H. W.; Pearce, R. *Can. J. Chem.* **1971**, *49*, 1618−1621.

3.5.9 Crystallographic Data

Table S3.1 Crystal data and structure refinement for **7b**.

Identification code	BHuang03_Toste
Empirical formula	C22 H26 S2 Si
Formula weight	382.64
Temperature	100(2) K
Wavelength	1.54184 Å
Crystal system	Monoclinic
Space group	P 21/c

Unit cell dimensions	a = 9.47430(10) Å	□= 90°.
	b = 10.0189(2) Å	□= 93.4880(10)°.
	c = 20.8876(3) Å	□ = 90°.
Volume	1979.02(5) Å^3	
Z	4	
Density (calculated)	1.284 Mg/m^3	
Absorption coefficient	3.013 mm^{-1}	
F(000)	816	
Crystal size	0.230 x 0.170 x 0.080 mm^3	
Theta range for data collection	4.241 to 74.470°.	
Index ranges	-11<=h<=11, -12<=k<=12, -26<=l<=25	
Reflections collected	21264	
Independent reflections	4046 [R(int) = 0.0472]	
Completeness to theta = 74.000°	100.0 %	
Absorption correction	Semi-empirical from equivalents	
Max. and min. transmission	1.00000 and 0.60986	
Refinement method	Full-matrix least-squares on F^2	
Data / restraints / parameters	4046 / 1 / 254	
Goodness-of-fit on F^2	1.090	
Final R indices [I>2sigma(I)]	R1 = 0.0364, wR2 = 0.1003	
R indices (all data)	R1 = 0.0383, wR2 = 0.1015	
Extinction coefficient	n/a	
Largest diff. peak and hole	0.449 and -0.524 e.Å^{-3}	

Table S3.2 Atomic coordinates (x 10^4) and equivalent isotropic displacement parameters ($Å^2$x 10^3) for **7b**. U(eq) is defined as one third of the trace of the orthogonalized U^{ij} tensor.

	x	y	z	U(eq)
S(1)	4798(1)	6672(1)	4419(1)	27(1)
S(2)	6412(1)	9083(1)	4003(1)	22(1)
Si(1)	7839(1)	6460(1)	4254(1)	19(1)
C(1)	6120(2)	7288(2)	3887(1)	23(1)
C(2)	3298(2)	7767(2)	4243(1)	28(1)
C(3)	3612(2)	9230(2)	4367(1)	25(1)
C(4)	4645(2)	9796(2)	3907(1)	29(1)
C(5)	5701(2)	7007(2)	3172(1)	35(1)
C(6A)	5312(3)	5518(3)	3003(1)	34(1)
C(6B)	6187(13)	5957(14)	2779(6)	34(1)
C(7A)	6586(2)	4625(2)	2954(1)	32(1)
C(7B)	5342(17)	4844(17)	2995(7)	32(3)
C(8A)	7153(2)	3830(2)	3413(1)	30(1)
C(8B)	5756(12)	3861(12)	3388(6)	30(1)
C(9A)	6681(2)	3733(2)	4081(1)	28(1)
C(9B)	7166(15)	3739(14)	3719(9)	28(1)
C(10A)	7560(2)	4684(2)	4532(1)	23(1)
C(10B)	7470(17)	4660(17)	4292(7)	23(1)
C(11)	8450(2)	7338(2)	5020(1)	21(1)
C(12)	7740(2)	7183(2)	5589(1)	27(1)
C(13)	8251(2)	7782(2)	6158(1)	35(1)
C(14)	9478(2)	8533(2)	6178(1)	36(1)
C(15)	10192(2)	8702(2)	5626(1)	33(1)
C(16)	9683(2)	8109(2)	5055(1)	24(1)
C(17)	9271(2)	6592(2)	3669(1)	21(1)
C(18)	9418(2)	7699(2)	3270(1)	26(1)
C(19)	10455(2)	7738(2)	2828(1)	28(1)
C(20)	11382(2)	6675(2)	2778(1)	26(1)
C(21)	11274(2)	5583(2)	3178(1)	26(1)
C(22)	10236(2)	5540(2)	3618(1)	24(1)

Table S3.3 Bond lengths [Å] and angles [°] for **7b**.

S(1)-C(2)	1.8157(16)
S(1)-C(1)	1.8318(16)
S(2)-C(4)	1.8193(16)
S(2)-C(1)	1.8331(17)
Si(1)-C(10B)	1.839(17)
Si(1)-C(17)	1.8843(16)
Si(1)-C(11)	1.8848(16)
Si(1)-C(10A)	1.894(2)
Si(1)-C(1)	1.9435(16)
C(1)-C(5)	1.549(2)
C(2)-C(3)	1.514(2)
C(3)-C(4)	1.523(2)
C(5)-C(6B)	1.428(12)
C(5)-C(6A)	1.571(4)
C(6A)-C(7A)	1.511(3)
C(6B)-C(7B)	1.46(2)
C(7A)-C(8A)	1.334(4)
C(7B)-C(8B)	1.327(15)
C(8A)-C(9A)	1.494(3)
C(8B)-C(9B)	1.472(18)
C(9A)-C(10A)	1.548(3)
C(9B)-C(10B)	1.52(2)
C(11)-C(16)	1.399(2)
C(11)-C(12)	1.411(2)
C(12)-C(13)	1.391(3)
C(13)-C(14)	1.383(3)
C(14)-C(15)	1.382(3)
C(15)-C(16)	1.392(2)
C(17)-C(18)	1.399(2)
C(17)-C(22)	1.404(2)
C(18)-C(19)	1.389(2)
C(19)-C(20)	1.388(2)
C(20)-C(21)	1.385(2)
C(21)-C(22)	1.386(2)

C(2)-S(1)-C(1)	103.22(8)
C(4)-S(2)-C(1)	103.89(8)
C(10B)-Si(1)-C(17)	104.1(5)
C(10B)-Si(1)-C(11)	118.1(5)
C(17)-Si(1)-C(11)	108.74(7)
C(17)-Si(1)-C(10A)	112.56(8)
C(11)-Si(1)-C(10A)	102.72(8)
C(10B)-Si(1)-C(1)	106.2(5)
C(17)-Si(1)-C(1)	109.45(7)
C(11)-Si(1)-C(1)	110.00(6)
C(10A)-Si(1)-C(1)	113.11(8)
C(5)-C(1)-S(1)	112.32(12)
C(5)-C(1)-S(2)	109.46(13)
S(1)-C(1)-S(2)	110.71(8)
C(5)-C(1)-Si(1)	117.56(11)
S(1)-C(1)-Si(1)	101.78(8)
S(2)-C(1)-Si(1)	104.54(7)
C(3)-C(2)-S(1)	114.01(11)
C(2)-C(3)-C(4)	112.29(13)

C(3)-C(4)-S(2)	114.02(11)
C(6B)-C(5)-C(1)	128.0(5)
C(1)-C(5)-C(6A)	115.53(19)
C(7A)-C(6A)-C(5)	113.56(19)
C(5)-C(6B)-C(7B)	100.5(11)
C(8A)-C(7A)-C(6A)	126.4(2)
C(8B)-C(7B)-C(6B)	127.7(14)
C(7A)-C(8A)-C(9A)	125.39(18)
C(7B)-C(8B)-C(9B)	125.3(13)
C(8A)-C(9A)-C(10A)	110.33(16)
C(8B)-C(9B)-C(10B)	116.2(13)
C(9A)-C(10A)-Si(1)	118.19(15)
C(9B)-C(10B)-Si(1)	126.0(12)
C(16)-C(11)-C(12)	117.11(15)
C(16)-C(11)-Si(1)	120.98(11)
C(12)-C(11)-Si(1)	121.80(12)
C(13)-C(12)-C(11)	120.91(16)
C(14)-C(13)-C(12)	120.62(17)
C(15)-C(14)-C(13)	119.58(16)
C(14)-C(15)-C(16)	120.09(17)
C(15)-C(16)-C(11)	121.69(16)
C(18)-C(17)-C(22)	117.40(14)
C(18)-C(17)-Si(1)	122.94(11)
C(22)-C(17)-Si(1)	119.66(12)
C(19)-C(18)-C(17)	121.25(15)
C(20)-C(19)-C(18)	120.27(16)
C(21)-C(20)-C(19)	119.39(15)
C(20)-C(21)-C(22)	120.36(15)
C(21)-C(22)-C(17)	121.30(15)

Symmetry transformations used to generate equivalent atoms:

Table S3.4 Anisotropic displacement parameters ($Å^2 x\ 10^3$)for **7b**. The anisotropic displacement factor exponent takes the form: $-2\pi^2[\ h^2 a^{*2} U^{11} + ... + 2\ h\ k\ a^*\ b^*\ U^{12}\ ]$

	U^{11}	U^{22}	U^{33}	U^{23}	U^{13}	U^{12}
S(1)	14(1)	22(1)	44(1)	-7(1)	4(1)	2(1)
S(2)	18(1)	23(1)	25(1)	0(1)	1(1)	5(1)
Si(1)	13(1)	18(1)	26(1)	-3(1)	1(1)	1(1)
C(1)	16(1)	27(1)	27(1)	-9(1)	-1(1)	4(1)
C(2)	14(1)	32(1)	38(1)	-10(1)	-2(1)	4(1)
C(3)	18(1)	26(1)	30(1)	-4(1)	0(1)	9(1)
C(4)	24(1)	33(1)	29(1)	3(1)	-1(1)	11(1)
C(5)	24(1)	53(1)	28(1)	-18(1)	-8(1)	14(1)
C(6A)	19(1)	46(2)	36(1)	-21(1)	-6(1)	8(1)
C(6B)	19(1)	46(2)	36(1)	-21(1)	-6(1)	8(1)
C(7A)	20(1)	44(1)	31(1)	-22(1)	-2(1)	3(1)
C(7B)	25(7)	40(9)	30(7)	-12(7)	3(5)	3(8)
C(8A)	19(1)	30(1)	40(1)	-20(1)	5(1)	0(1)
C(8B)	19(1)	30(1)	40(1)	-20(1)	5(1)	0(1)
C(9A)	22(1)	23(1)	41(1)	-10(1)	9(1)	-4(1)
C(9B)	22(1)	23(1)	41(1)	-10(1)	9(1)	-4(1)
C(10A)	18(1)	21(1)	31(1)	-4(1)	3(1)	0(1)
C(10B)	18(1)	21(1)	31(1)	-4(1)	3(1)	0(1)
C(11)	19(1)	19(1)	24(1)	3(1)	-2(1)	5(1)
C(12)	28(1)	25(1)	28(1)	6(1)	2(1)	6(1)
C(13)	51(1)	31(1)	23(1)	5(1)	2(1)	17(1)
C(14)	48(1)	30(1)	29(1)	-5(1)	-16(1)	14(1)
C(15)	31(1)	27(1)	39(1)	-3(1)	-14(1)	5(1)
C(16)	20(1)	23(1)	30(1)	0(1)	-4(1)	4(1)
C(17)	15(1)	24(1)	24(1)	-5(1)	-3(1)	2(1)
C(18)	22(1)	29(1)	26(1)	0(1)	0(1)	8(1)
C(19)	25(1)	36(1)	23(1)	4(1)	1(1)	7(1)
C(20)	18(1)	37(1)	23(1)	-6(1)	0(1)	2(1)
C(21)	16(1)	26(1)	35(1)	-7(1)	0(1)	2(1)
C(22)	15(1)	23(1)	33(1)	-2(1)	1(1)	0(1)

Table S3.5 Hydrogen coordinates (x 10^4) and isotropic displacement parameters ($Å^2$x 10^3) for **7b**.

	x	y	z	U(eq)
H(2A)	2972	7655	3786	34
H(2B)	2515	7491	4506	34
H(3A)	4012	9339	4812	30
H(3B)	2718	9742	4323	30
H(4A)	4713	10773	3971	34
H(4B)	4264	9637	3461	34
H(5AA)	6497	7279	2914	42
H(5AB)	4881	7578	3039	42
H(5BC)	4840(170)	7400(170)	3070(80)	42
H(5BD)	6220(170)	7590(180)	2960(80)	42
H(6AA)	4718	5160	3338	41
H(6AB)	4742	5497	2590	41
H(6BA)	7212	5793	2861	41
H(6BB)	5984	6146	2317	41
H(7A)	7026	4630	2557	38
H(7B)	4382	4822	2835	38
H(8A)	7921	3280	3306	36
H(8B)	5088	3179	3462	36
H(9AA)	6795	2803	4236	34
H(9AB)	5667	3970	4083	34
H(9BA)	7883	3910	3404	34
H(9BB)	7291	2806	3868	34
H(10A)	8503	4275	4620	28
H(10B)	7099	4724	4944	28
H(10C)	8287	4262	4541	28
H(10D)	6651	4569	4561	28
H(12)	6901	6663	5585	32
H(13)	7753	7675	6536	42
H(14)	9828	8930	6569	44
H(15)	11031	9223	5636	39
H(16)	10186	8231	4680	29
H(18)	8798	8437	3302	31
H(19)	10531	8496	2559	34
H(20)	12084	6697	2472	31
H(21)	11915	4858	3151	31
H(22)	10176	4784	3889	28

Table S3.6 Torsion angles [°] for **7b**.

C(2)-S(1)-C(1)-C(5)	-68.86(13)
C(2)-S(1)-C(1)-S(2)	53.85(9)
C(2)-S(1)-C(1)-Si(1)	164.52(7)
C(4)-S(2)-C(1)-C(5)	71.18(12)
C(4)-S(2)-C(1)-S(1)	-53.17(10)
C(4)-S(2)-C(1)-Si(1)	-162.05(7)
C(1)-S(1)-C(2)-C(3)	-59.63(13)
S(1)-C(2)-C(3)-C(4)	67.27(16)
C(2)-C(3)-C(4)-S(2)	-65.88(16)
C(1)-S(2)-C(4)-C(3)	57.43(14)
S(1)-C(1)-C(5)-C(6B)	-99.7(8)
S(2)-C(1)-C(5)-C(6B)	136.9(8)
Si(1)-C(1)-C(5)-C(6B)	17.9(8)
S(1)-C(1)-C(5)-C(6A)	-52.50(19)
S(2)-C(1)-C(5)-C(6A)	-175.91(14)
Si(1)-C(1)-C(5)-C(6A)	65.1(2)
C(1)-C(5)-C(6A)-C(7A)	-79.0(2)
C(1)-C(5)-C(6B)-C(7B)	78.1(10)
C(5)-C(6A)-C(7A)-C(8A)	97.0(3)
C(5)-C(6B)-C(7B)-C(8B)	-102.8(16)
C(6A)-C(7A)-C(8A)-C(9A)	-3.8(3)
C(6B)-C(7B)-C(8B)-C(9B)	4(2)
C(7A)-C(8A)-C(9A)-C(10A)	-93.5(2)
C(7B)-C(8B)-C(9B)-C(10B)	75(2)
C(8A)-C(9A)-C(10A)-Si(1)	46.8(2)
C(17)-Si(1)-C(10A)-C(9A)	-79.35(16)
C(11)-Si(1)-C(10A)-C(9A)	163.89(14)
C(1)-Si(1)-C(10A)-C(9A)	45.36(17)
C(8B)-C(9B)-C(10B)-Si(1)	-74.7(18)
C(17)-Si(1)-C(10B)-C(9B)	-50.5(14)
C(11)-Si(1)-C(10B)-C(9B)	-171.1(11)
C(1)-Si(1)-C(10B)-C(9B)	65.0(14)
C(10B)-Si(1)-C(11)-C(16)	127.2(6)
C(17)-Si(1)-C(11)-C(16)	9.06(14)
C(10A)-Si(1)-C(11)-C(16)	128.52(13)
C(1)-Si(1)-C(11)-C(16)	-110.79(13)
C(10B)-Si(1)-C(11)-C(12)	-48.9(6)
C(17)-Si(1)-C(11)-C(12)	-167.01(12)
C(10A)-Si(1)-C(11)-C(12)	-47.55(14)
C(1)-Si(1)-C(11)-C(12)	73.14(14)
C(16)-C(11)-C(12)-C(13)	0.3(2)
Si(1)-C(11)-C(12)-C(13)	176.52(12)
C(11)-C(12)-C(13)-C(14)	-0.7(2)
C(12)-C(13)-C(14)-C(15)	0.8(3)
C(13)-C(14)-C(15)-C(16)	-0.6(3)
C(14)-C(15)-C(16)-C(11)	0.2(2)
C(12)-C(11)-C(16)-C(15)	-0.1(2)
Si(1)-C(11)-C(16)-C(15)	-176.31(12)
C(10B)-Si(1)-C(17)-C(18)	148.8(5)
C(11)-Si(1)-C(17)-C(18)	-84.52(14)
C(10A)-Si(1)-C(17)-C(18)	162.36(13)
C(1)-Si(1)-C(17)-C(18)	35.67(15)
C(10B)-Si(1)-C(17)-C(22)	-30.5(5)
C(11)-Si(1)-C(17)-C(22)	96.21(13)

C(10A)-Si(1)-C(17)-C(22)	-16.91(15)
C(1)-Si(1)-C(17)-C(22)	-143.60(12)
C(22)-C(17)-C(18)-C(19)	1.7(2)
Si(1)-C(17)-C(18)-C(19)	-177.57(12)
C(17)-C(18)-C(19)-C(20)	-0.6(2)
C(18)-C(19)-C(20)-C(21)	-0.8(2)
C(19)-C(20)-C(21)-C(22)	1.1(2)
C(20)-C(21)-C(22)-C(17)	0.1(2)
C(18)-C(17)-C(22)-C(21)	-1.4(2)
Si(1)-C(17)-C(22)-C(21)	177.87(12)

Symmetry transformations used to generate equivalent atoms:

Table S3.7 Crystal data and structure refinement for **8b**.

Identification code	BHuang02_Toste	
Empirical formula	C19 H20 O Si	
Formula weight	292.44	
Temperature	100(2) K	
Wavelength	1.54184 Å	
Crystal system	Monoclinic	
Space group	P 21/c	
Unit cell dimensions	a = 8.33350(10) Å	□= 90°.
	b = 18.3215(3) Å	□= 108.141(2)°.
	c = 11.0655(2) Å	□ = 90°.
Volume	1605.52(5) $Å^3$	
Z	4	
Density (calculated)	1.210 Mg/m^3	
Absorption coefficient	1.245 mm^{-1}	
F(000)	624	
Crystal size	0.210 x 0.200 x 0.070 mm^3	
Theta range for data collection	4.849 to 74.465°.	
Index ranges	-10<=h<=10, -22<=k<=22, -13<=l<=13	
Reflections collected	17100	
Independent reflections	3278 [R(int) = 0.0400]	
Completeness to theta = 74.000°	99.8 %	
Absorption correction	Semi-empirical from equivalents	
Max. and min. transmission	1.00000 and 0.93651	
Refinement method	Full-matrix least-squares on F^2	
Data / restraints / parameters	3278 / 0 / 190	
Goodness-of-fit on F^2	1.105	
Final R indices [I>2sigma(I)]	R1 = 0.0358, wR2 = 0.0971	
R indices (all data)	R1 = 0.0367, wR2 = 0.0979	
Extinction coefficient	n/a	
Largest diff. peak and hole	0.348 and -0.298 $e.Å^{-3}$	

Table S3.8 Atomic coordinates (x 10^4) and equivalent isotropic displacement parameters ($Å^2$x 10^3) for **8b**. U(eq) is defined as one third of the trace of the orthogonalized U^{ij} tensor.

	x	y	z	U(eq)
Si(1)	5354(1)	5283(1)	2368(1)	15(1)
O(1)	6596(1)	4667(1)	4704(1)	20(1)
C(1)	6320(1)	5270(1)	4207(1)	17(1)
C(2)	6807(2)	5959(1)	4987(1)	20(1)
C(3)	7968(2)	6433(1)	4464(1)	21(1)
C(4)	9471(2)	6001(1)	4401(1)	22(1)
C(5)	9674(2)	5709(1)	3356(1)	22(1)
C(6)	8488(2)	5778(1)	2020(1)	22(1)
C(7)	7139(2)	5164(1)	1686(1)	20(1)
C(8)	3885(2)	4483(1)	1984(1)	17(1)
C(9)	2130(2)	4564(1)	1455(1)	19(1)
C(10)	1056(2)	3963(1)	1257(1)	23(1)
C(11)	1715(2)	3269(1)	1586(1)	24(1)
C(12)	3453(2)	3175(1)	2101(1)	24(1)
C(13)	4520(2)	3775(1)	2295(1)	20(1)
C(14)	4174(1)	6146(1)	1747(1)	18(1)
C(15)	4357(2)	6492(1)	667(1)	23(1)
C(16)	3463(2)	7124(1)	184(1)	31(1)
C(17)	2348(2)	7416(1)	756(2)	33(1)
C(18)	2130(2)	7080(1)	1817(1)	30(1)
C(19)	3042(2)	6453(1)	2315(1)	23(1)

Table S3.9 Bond lengths [Å] and angles [°] for **8b**.

Si(1)-C(8)	1.8718(12)
Si(1)-C(14)	1.8754(12)
Si(1)-C(7)	1.8784(13)
Si(1)-C(1)	1.9415(12)
O(1)-C(1)	1.2237(15)
C(1)-C(2)	1.5115(17)
C(2)-C(3)	1.5393(17)
C(3)-C(4)	1.5016(18)
C(4)-C(5)	1.3320(19)
C(5)-C(6)	1.5061(17)
C(6)-C(7)	1.5517(17)
C(8)-C(13)	1.4022(17)
C(8)-C(9)	1.4035(17)
C(9)-C(10)	1.3928(18)
C(10)-C(11)	1.3887(19)
C(11)-C(12)	1.3919(19)
C(12)-C(13)	1.3882(18)
C(14)-C(15)	1.4024(18)
C(14)-C(19)	1.4041(18)
C(15)-C(16)	1.3907(19)
C(16)-C(17)	1.383(2)
C(17)-C(18)	1.388(2)
C(18)-C(19)	1.3921(19)
C(8)-Si(1)-C(14)	110.21(5)
C(8)-Si(1)-C(7)	111.21(6)
C(14)-Si(1)-C(7)	109.93(6)
C(8)-Si(1)-C(1)	104.88(5)
C(14)-Si(1)-C(1)	113.17(5)
C(7)-Si(1)-C(1)	107.34(5)
O(1)-C(1)-C(2)	121.18(11)
O(1)-C(1)-Si(1)	116.16(9)
C(2)-C(1)-Si(1)	122.56(8)
C(1)-C(2)-C(3)	110.17(10)
C(4)-C(3)-C(2)	110.55(10)
C(5)-C(4)-C(3)	125.81(12)
C(4)-C(5)-C(6)	126.61(12)
C(5)-C(6)-C(7)	112.20(10)
C(6)-C(7)-Si(1)	115.19(9)
C(13)-C(8)-C(9)	117.68(11)
C(13)-C(8)-Si(1)	119.88(9)
C(9)-C(8)-Si(1)	122.33(9)
C(10)-C(9)-C(8)	121.15(12)
C(11)-C(10)-C(9)	120.02(12)
C(10)-C(11)-C(12)	119.80(12)
C(13)-C(12)-C(11)	119.98(12)
C(12)-C(13)-C(8)	121.36(11)
C(15)-C(14)-C(19)	117.79(12)
C(15)-C(14)-Si(1)	120.66(9)
C(19)-C(14)-Si(1)	121.51(10)
C(16)-C(15)-C(14)	121.07(13)
C(17)-C(16)-C(15)	120.19(14)
C(16)-C(17)-C(18)	119.88(13)
C(17)-C(18)-C(19)	120.12(14)

C(18)-C(19)-C(14)	120.93(13)

Symmetry transformations used to generate equivalent atoms:

Table S3.10 Anisotropic displacement parameters ($Å^2 x\ 10^3$)for **8b**. The anisotropic displacement factor exponent takes the form: $-2\pi^2[h^2 a^{*2} U^{11} + ... + 2\ h\ k\ a^*\ b^*\ U^{12}]$

	U^{11}	U^{22}	U^{33}	U^{23}	U^{13}	U^{12}
Si(1)	14(1)	15(1)	16(1)	1(1)	4(1)	0(1)
O(1)	18(1)	20(1)	22(1)	3(1)	4(1)	0(1)
C(1)	12(1)	20(1)	19(1)	1(1)	6(1)	-1(1)
C(2)	22(1)	20(1)	18(1)	-1(1)	6(1)	-2(1)
C(3)	22(1)	18(1)	22(1)	1(1)	4(1)	-3(1)
C(4)	17(1)	21(1)	24(1)	5(1)	2(1)	-5(1)
C(5)	15(1)	24(1)	27(1)	5(1)	5(1)	-2(1)
C(6)	17(1)	27(1)	23(1)	3(1)	8(1)	-1(1)
C(7)	17(1)	23(1)	20(1)	-1(1)	7(1)	1(1)
C(8)	19(1)	18(1)	15(1)	-2(1)	6(1)	-1(1)
C(9)	18(1)	21(1)	17(1)	-1(1)	5(1)	1(1)
C(10)	17(1)	28(1)	22(1)	-3(1)	5(1)	-3(1)
C(11)	24(1)	21(1)	26(1)	-6(1)	7(1)	-8(1)
C(12)	26(1)	18(1)	27(1)	-3(1)	6(1)	0(1)
C(13)	18(1)	20(1)	22(1)	-3(1)	5(1)	1(1)
C(14)	14(1)	17(1)	19(1)	-1(1)	1(1)	-1(1)
C(15)	22(1)	22(1)	21(1)	2(1)	2(1)	-1(1)
C(16)	33(1)	24(1)	27(1)	6(1)	-4(1)	-1(1)
C(17)	28(1)	19(1)	39(1)	0(1)	-9(1)	5(1)
C(18)	19(1)	27(1)	38(1)	-10(1)	0(1)	5(1)
C(19)	17(1)	23(1)	26(1)	-4(1)	4(1)	0(1)

Table S3.11 Hydrogen coordinates (x 10^4) and isotropic displacement parameters ($Å^2$x 10^3) for **8b**.

	x	y	z	U(eq)
H(2A)	7399	5831	5884	24
H(2B)	5778	6238	4957	24
H(3A)	7330	6610	3604	25
H(3B)	8353	6862	5021	25
H(4)	10356	5929	5176	26
H(5)	10667	5428	3464	27
H(6A)	9147	5761	1415	26
H(6B)	7914	6258	1924	26
H(7A)	7705	4694	1991	24
H(7B)	6661	5133	749	24
H(9)	1667	5037	1228	23
H(10)	-129	4028	897	27
H(11)	983	2859	1460	29
H(12)	3909	2700	2320	29
H(13)	5704	3705	2645	24
H(15)	5104	6291	258	27
H(16)	3617	7356	-539	37
H(17)	1734	7847	422	40
H(18)	1357	7277	2205	36
H(19)	2897	6231	3049	27

Table S3.12 Torsion angles [°] for **8b**.

O(1)-C(1)-C(2)-C(3)	123.83(12)
Si(1)-C(1)-C(2)-C(3)	-52.45(13)
C(1)-C(2)-C(3)-C(4)	-54.70(13)
C(2)-C(3)-C(4)-C(5)	102.08(15)
C(3)-C(4)-C(5)-C(6)	3.0(2)
C(4)-C(5)-C(6)-C(7)	-89.56(16)
C(5)-C(6)-C(7)-Si(1)	77.21(12)
C(8)-Si(1)-C(7)-C(6)	-176.54(8)
C(14)-Si(1)-C(7)-C(6)	61.12(10)
C(1)-Si(1)-C(7)-C(6)	-62.35(10)
C(14)-Si(1)-C(8)-C(13)	176.24(9)
C(7)-Si(1)-C(8)-C(13)	54.07(11)
C(1)-Si(1)-C(8)-C(13)	-61.65(11)
C(14)-Si(1)-C(8)-C(9)	-7.61(12)
C(7)-Si(1)-C(8)-C(9)	-129.78(10)
C(1)-Si(1)-C(8)-C(9)	114.51(10)
C(13)-C(8)-C(9)-C(10)	0.58(17)
Si(1)-C(8)-C(9)-C(10)	-175.66(9)
C(8)-C(9)-C(10)-C(11)	0.09(19)
C(9)-C(10)-C(11)-C(12)	-0.7(2)
C(10)-C(11)-C(12)-C(13)	0.6(2)
C(11)-C(12)-C(13)-C(8)	0.1(2)
C(9)-C(8)-C(13)-C(12)	-0.68(18)
Si(1)-C(8)-C(13)-C(12)	175.65(10)
C(8)-Si(1)-C(14)-C(15)	-105.91(10)
C(7)-Si(1)-C(14)-C(15)	17.02(12)
C(1)-Si(1)-C(14)-C(15)	137.01(10)
C(8)-Si(1)-C(14)-C(19)	71.94(11)
C(7)-Si(1)-C(14)-C(19)	-165.13(10)
C(1)-Si(1)-C(14)-C(19)	-45.14(11)
C(19)-C(14)-C(15)-C(16)	0.81(18)
Si(1)-C(14)-C(15)-C(16)	178.74(10)
C(14)-C(15)-C(16)-C(17)	-1.1(2)
C(15)-C(16)-C(17)-C(18)	0.4(2)
C(16)-C(17)-C(18)-C(19)	0.6(2)
C(17)-C(18)-C(19)-C(14)	-0.9(2)
C(15)-C(14)-C(19)-C(18)	0.18(18)
Si(1)-C(14)-C(19)-C(18)	-177.73(10)

Symmetry transformations used to generate equivalent atoms:

3.5.10 NMR Spectra

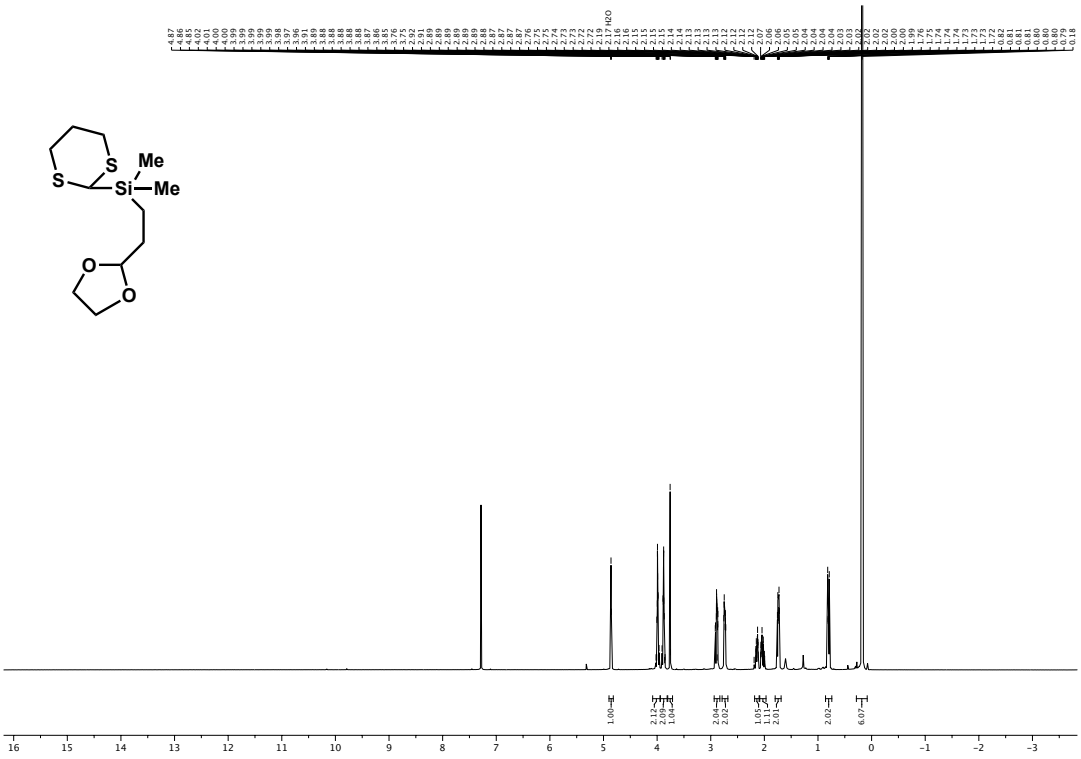


Figure S3.26 ^{1}H NMR spectrum of **3a**

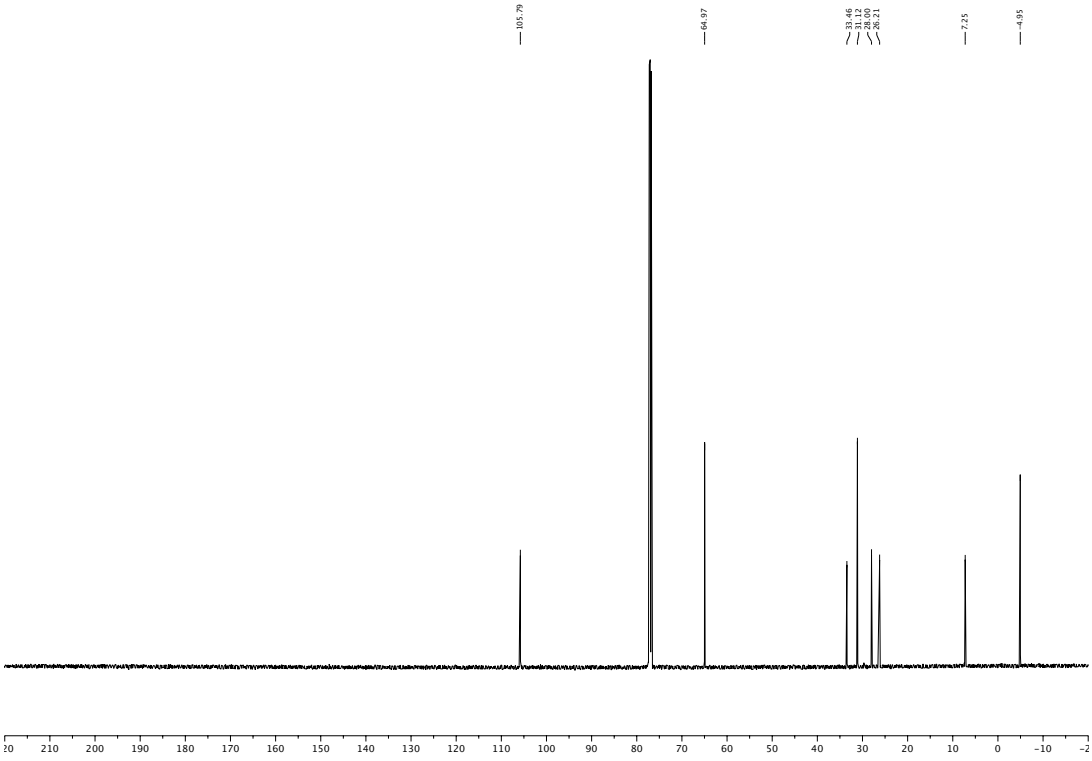


Figure S3.27 ^{13}C NMR spectrum of **3a**

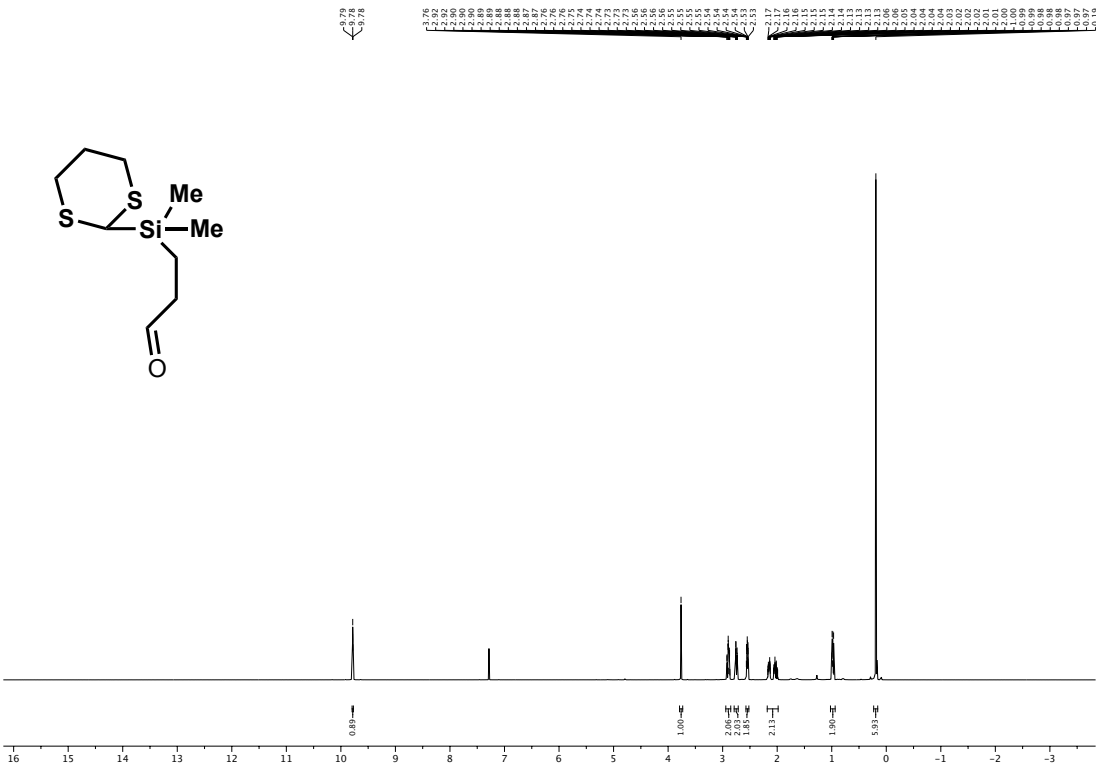


Figure S3.28 ^{1}H NMR spectrum of **4a**

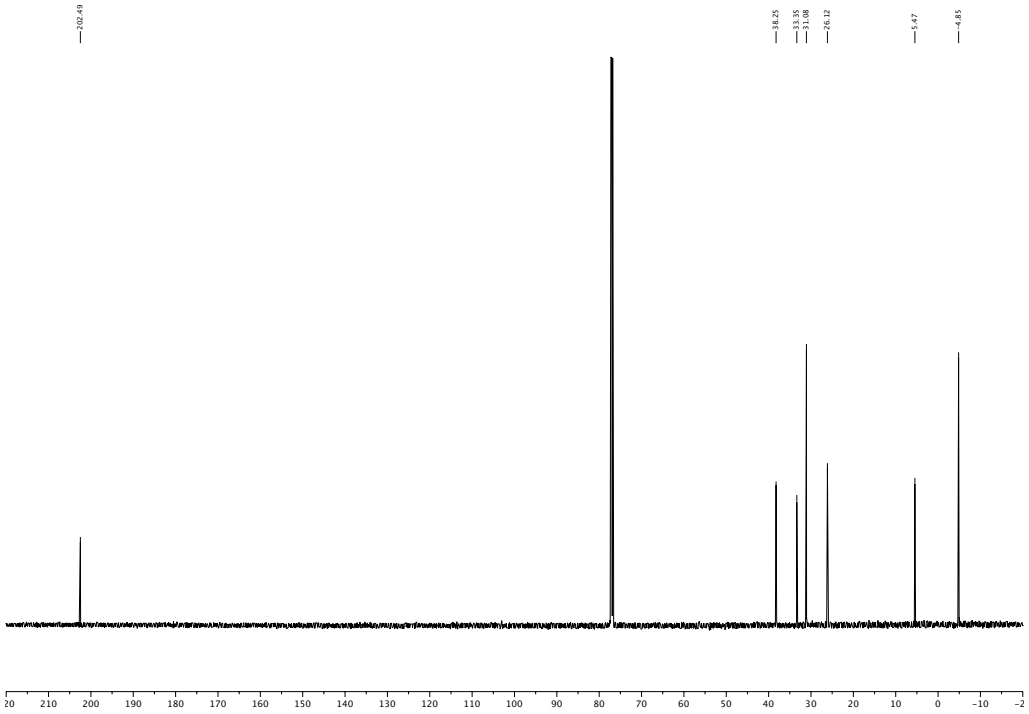


Figure S3.29 ^{13}C NMR spectrum of **4a**

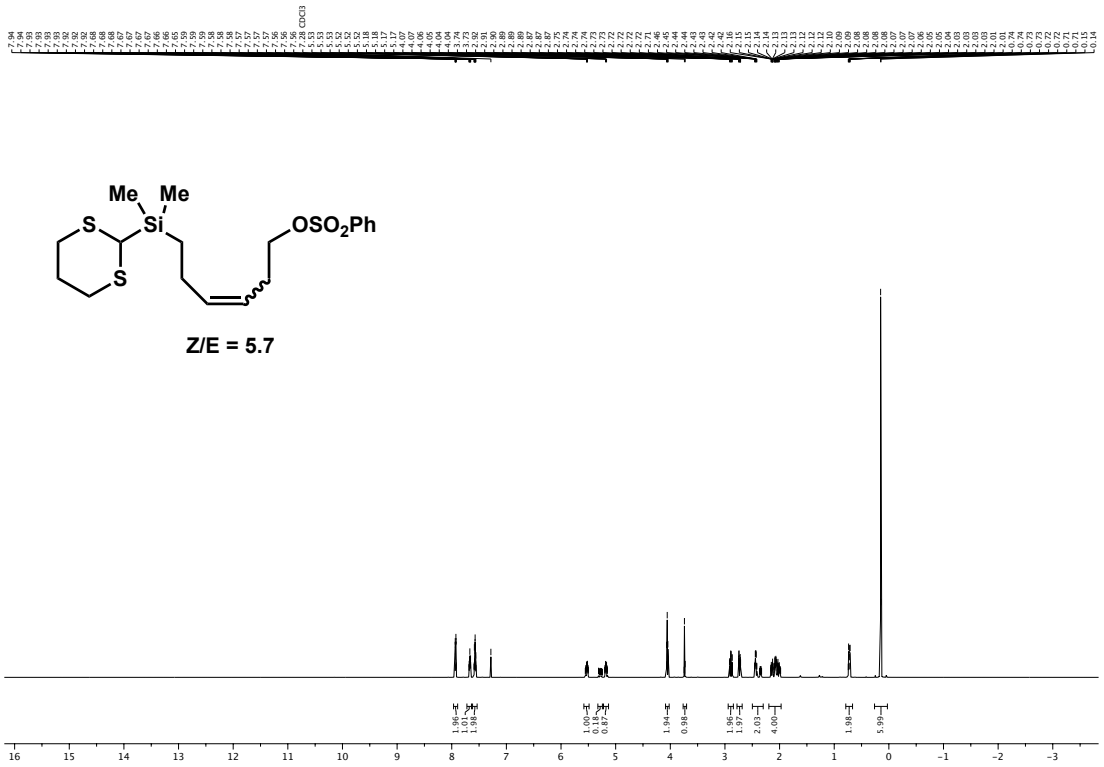


Figure S3.30 ^{1}H NMR spectrum of **6a**

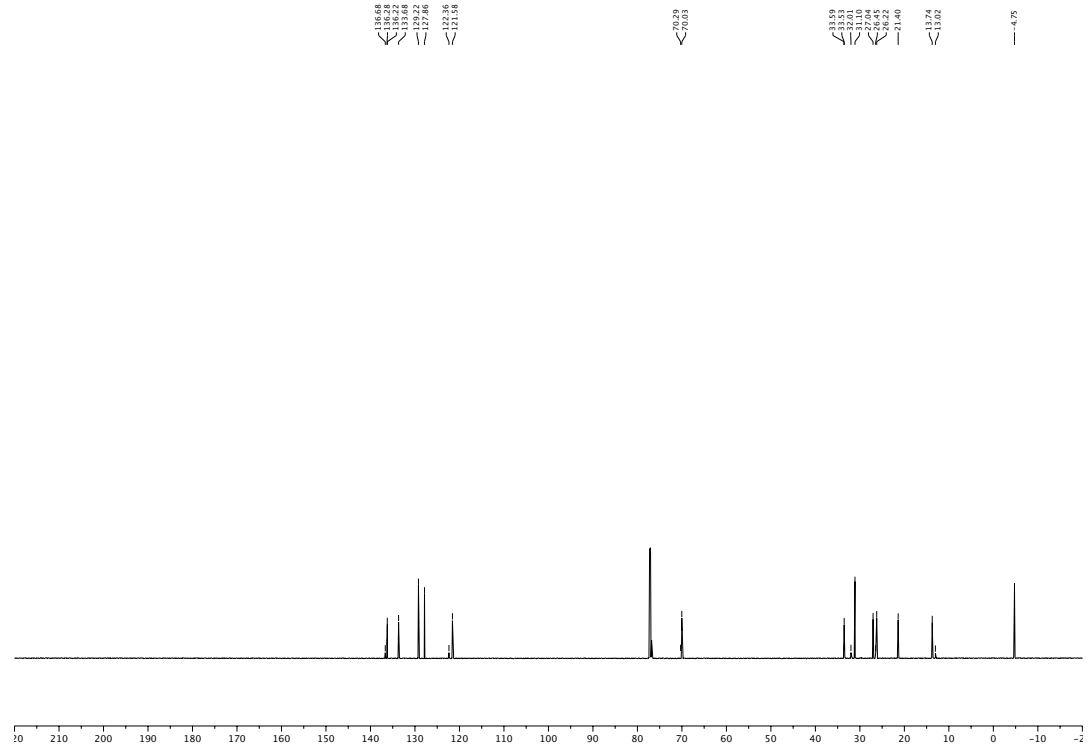


Figure S3.31 ^{13}C NMR spectrum of **6a**

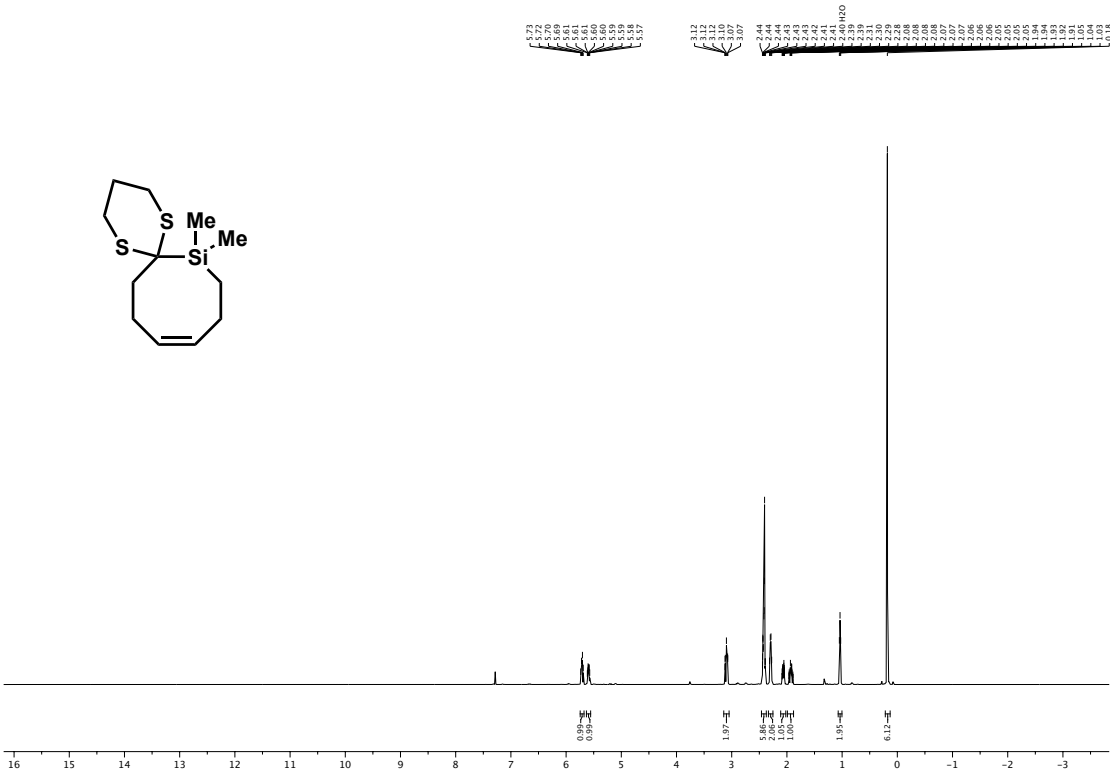


Figure S3.32 ^{1}H NMR spectrum of **7a**

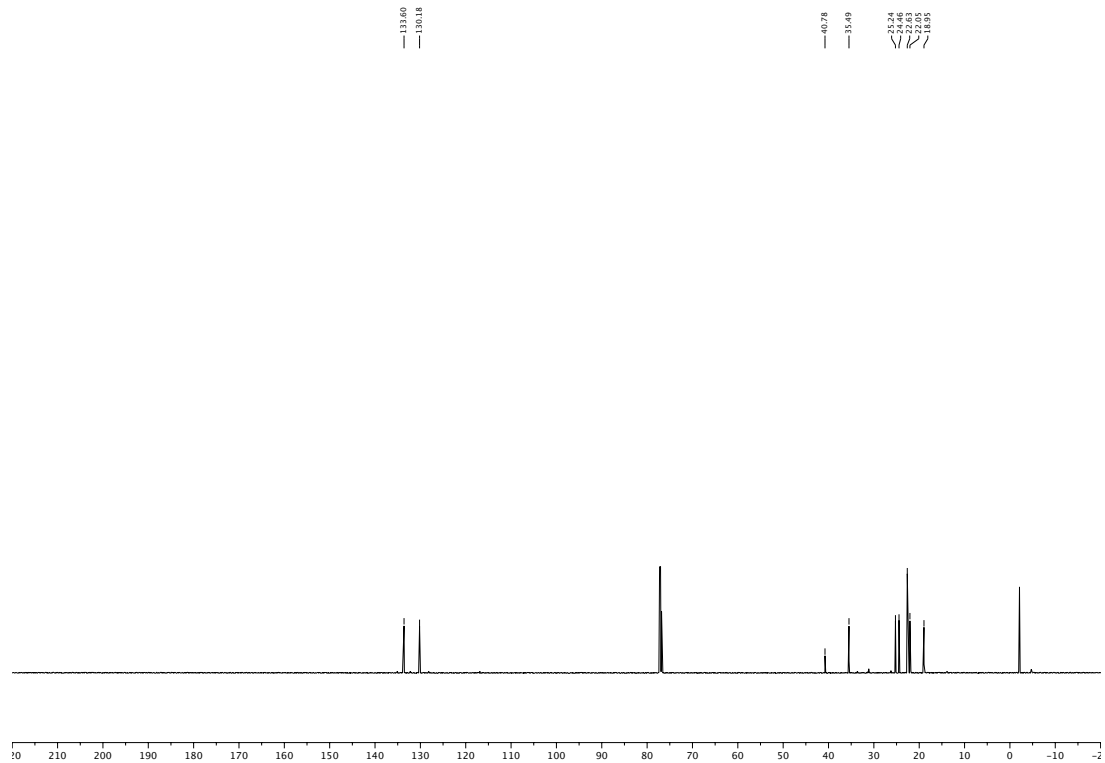


Figure S3.33 ^{13}C NMR spectrum of **7a**

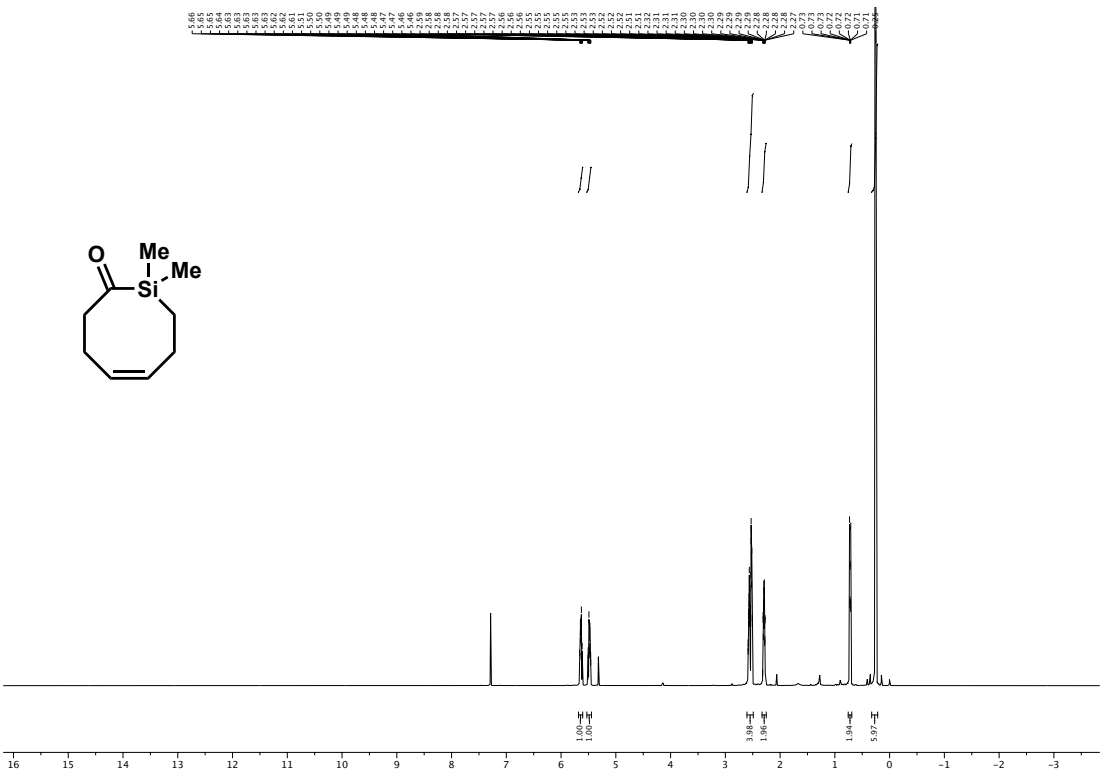


Figure S3.34 ^{1}H NMR spectrum of **8a**

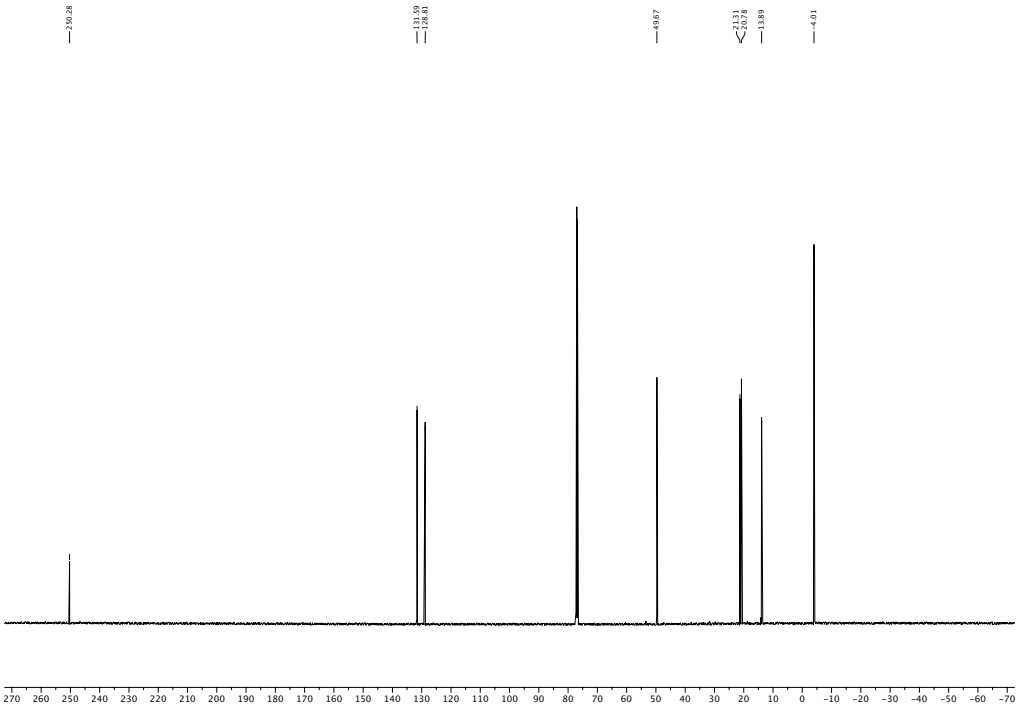


Figure S3.35 ^{13}C NMR spectrum of **8a**

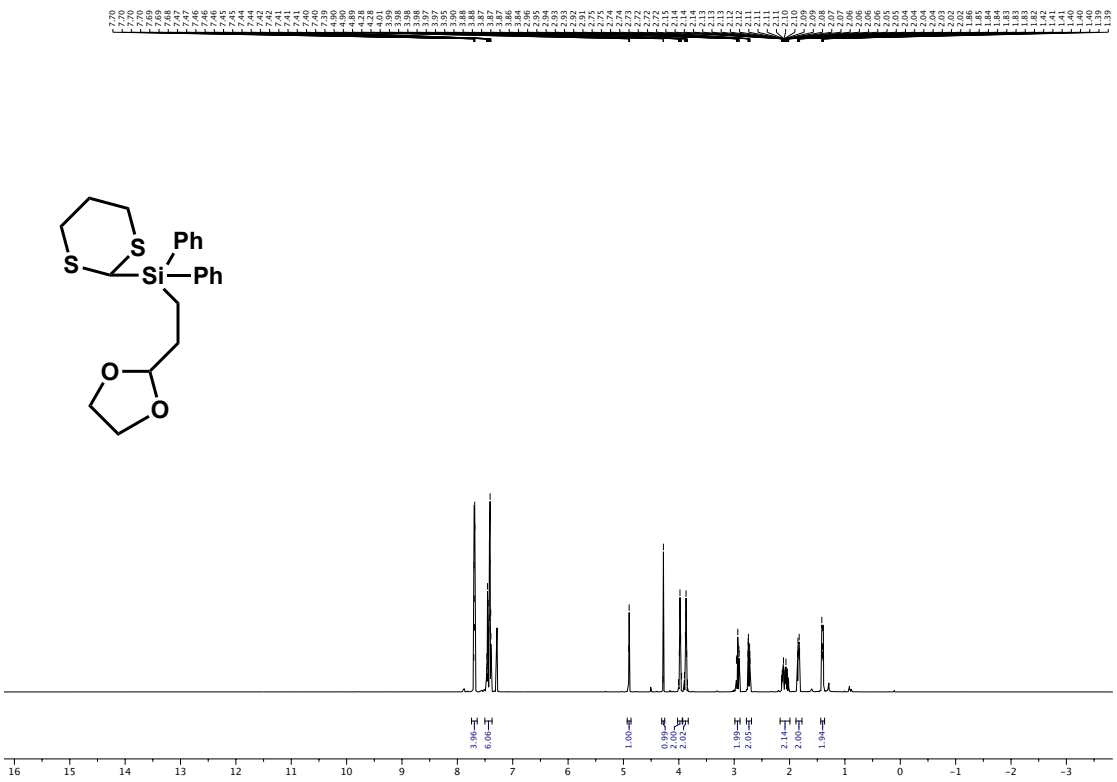


Figure S3.36 ^{1}H NMR spectrum of **3b**

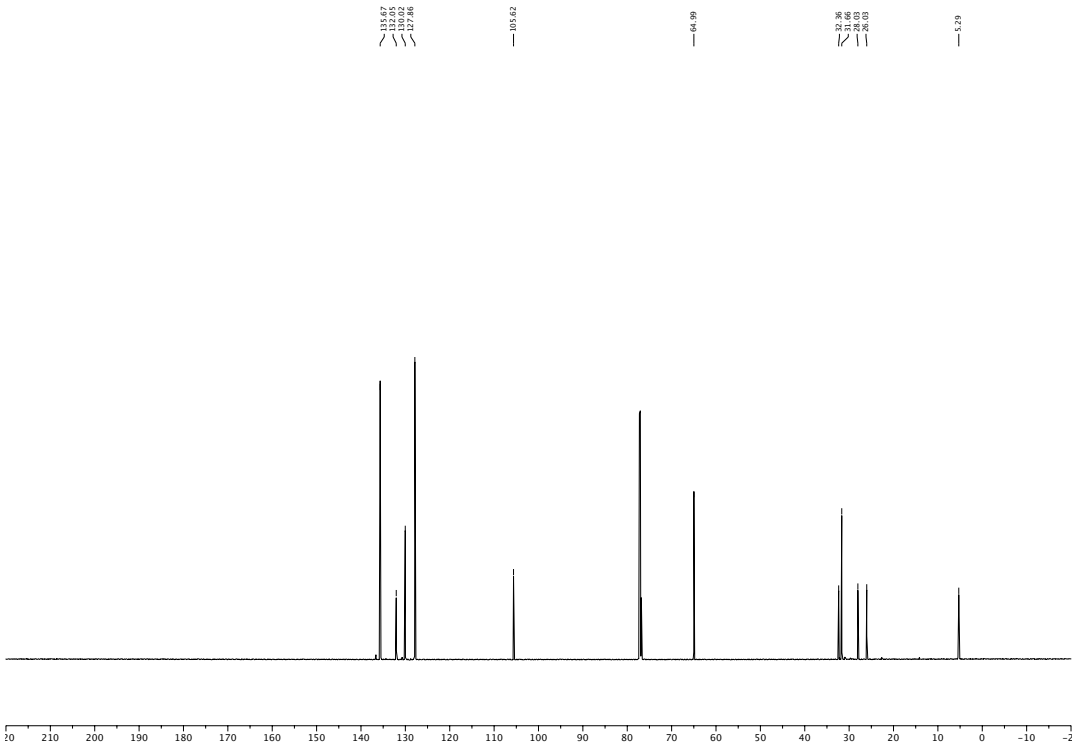


Figure S3.37 ^{13}C NMR spectrum of **3b**

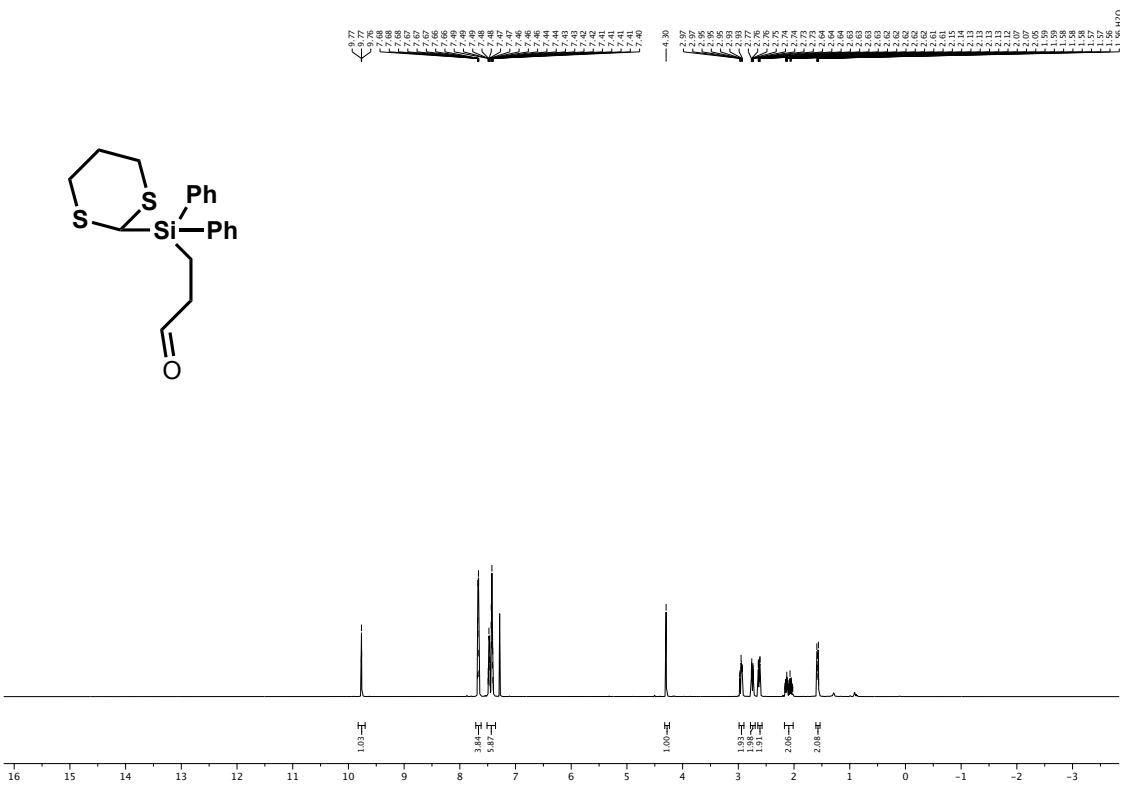


Figure S3.38 ^{1}H NMR spectrum of **4b**

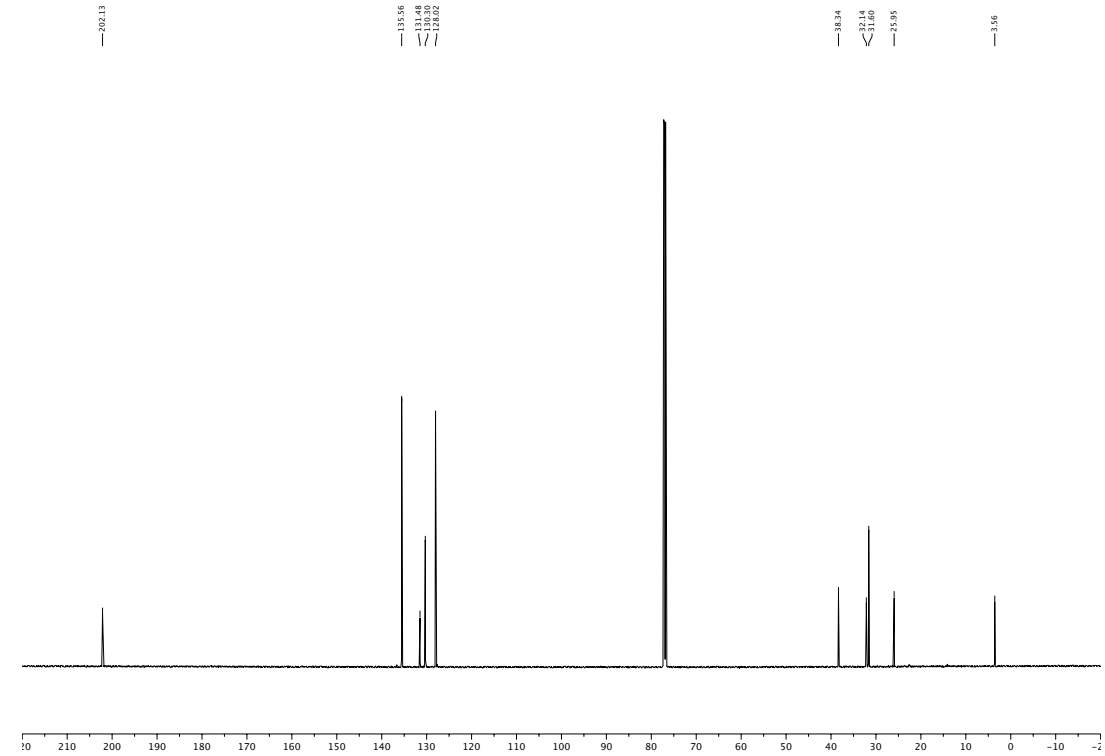


Figure S3.39 ^{13}C NMR spectrum of **4b**

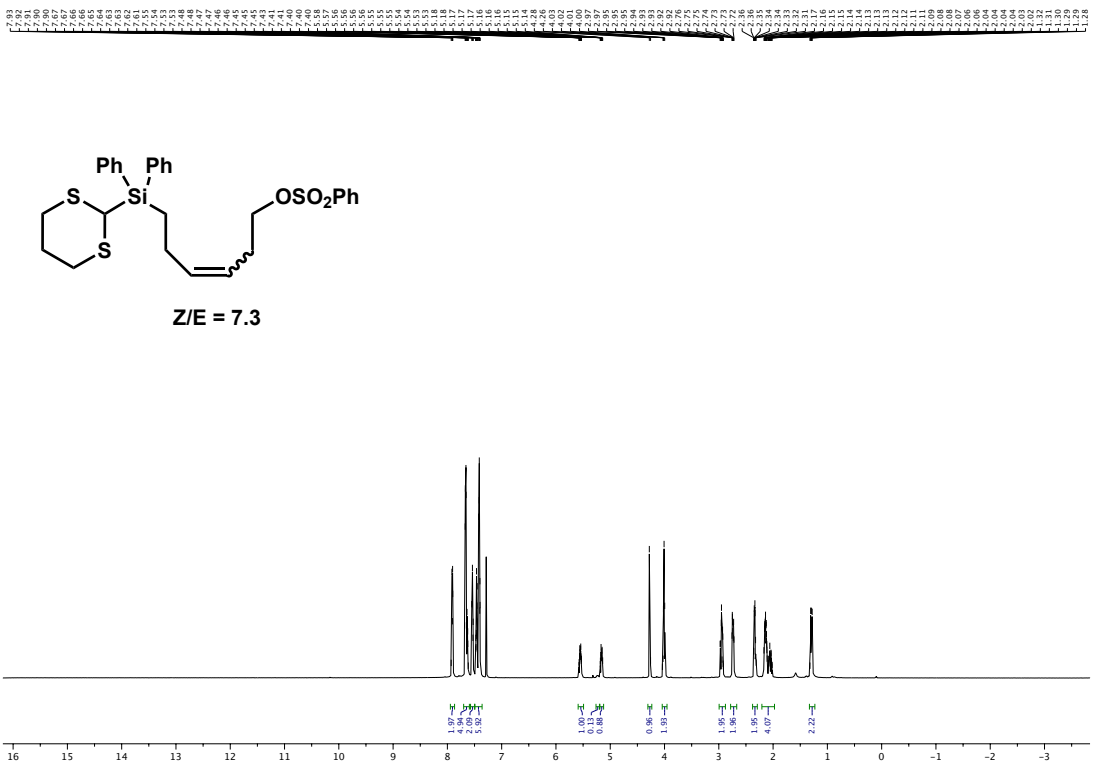


Figure S3.40 ^{1}H NMR spectrum of **6b**

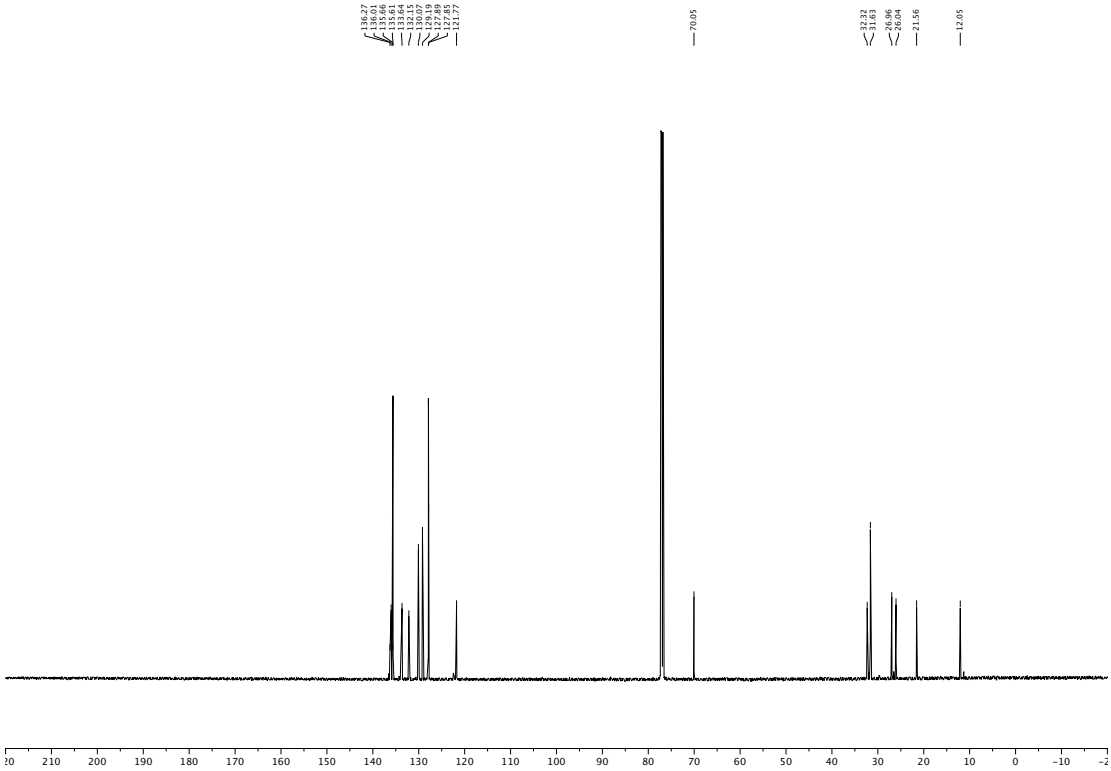


Figure S3.41 ^{13}C NMR spectrum of **6b**

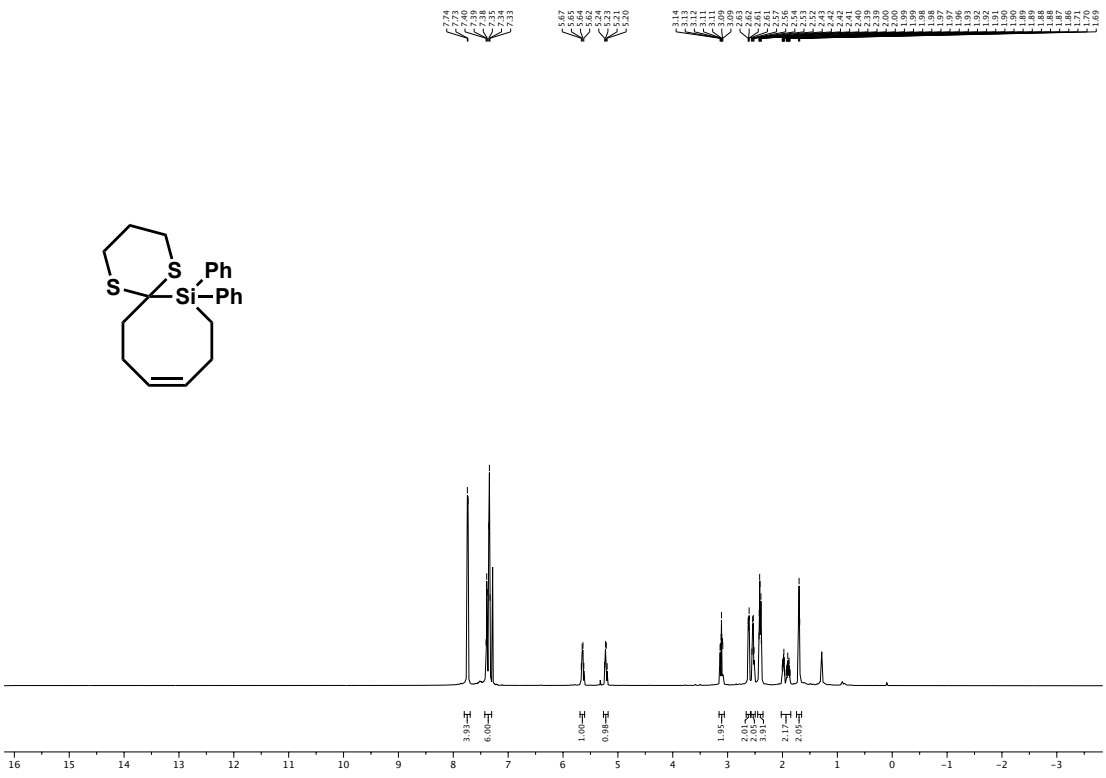


Figure S3.42 ^{1}H NMR spectrum of **7b**

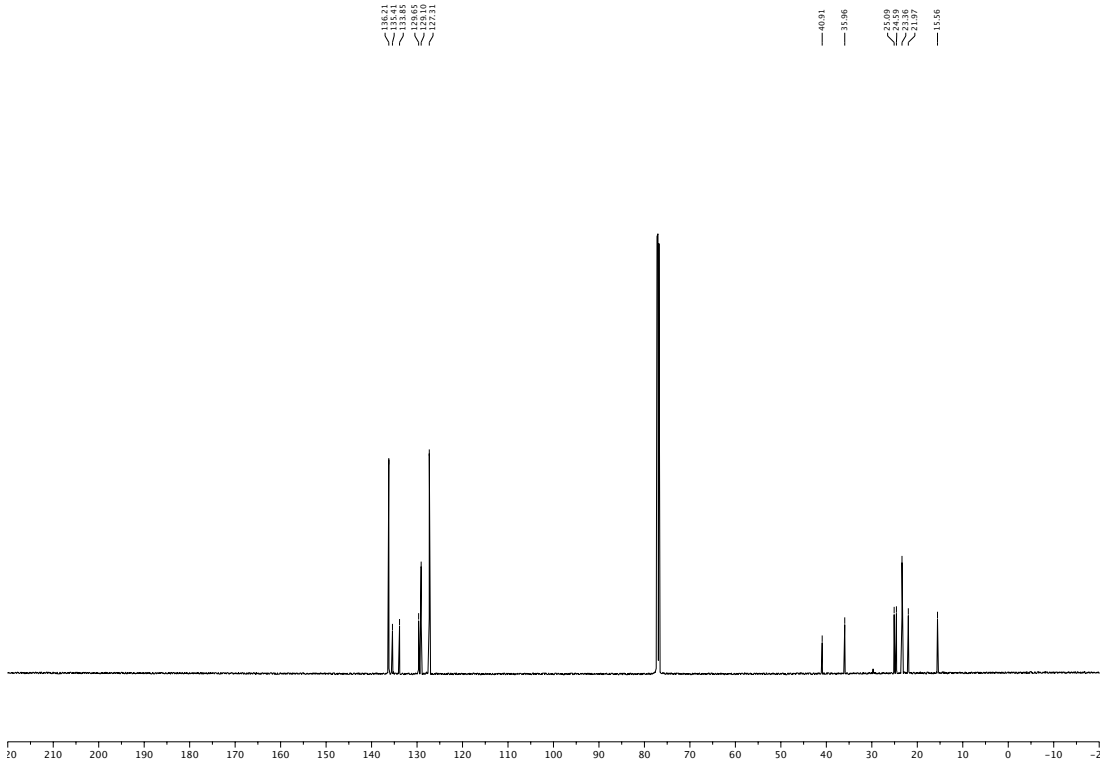


Figure S3.43 ^{13}C NMR spectrum of **7b**

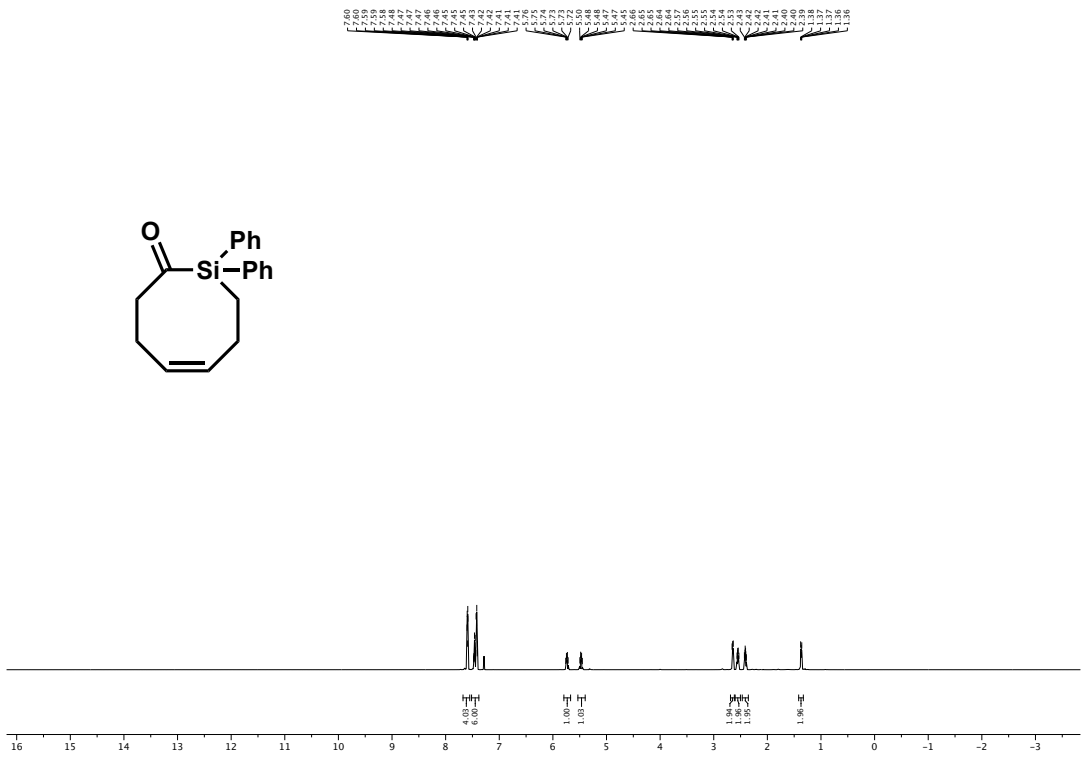


Figure S3.44 ^{1}H NMR spectrum of **7b**

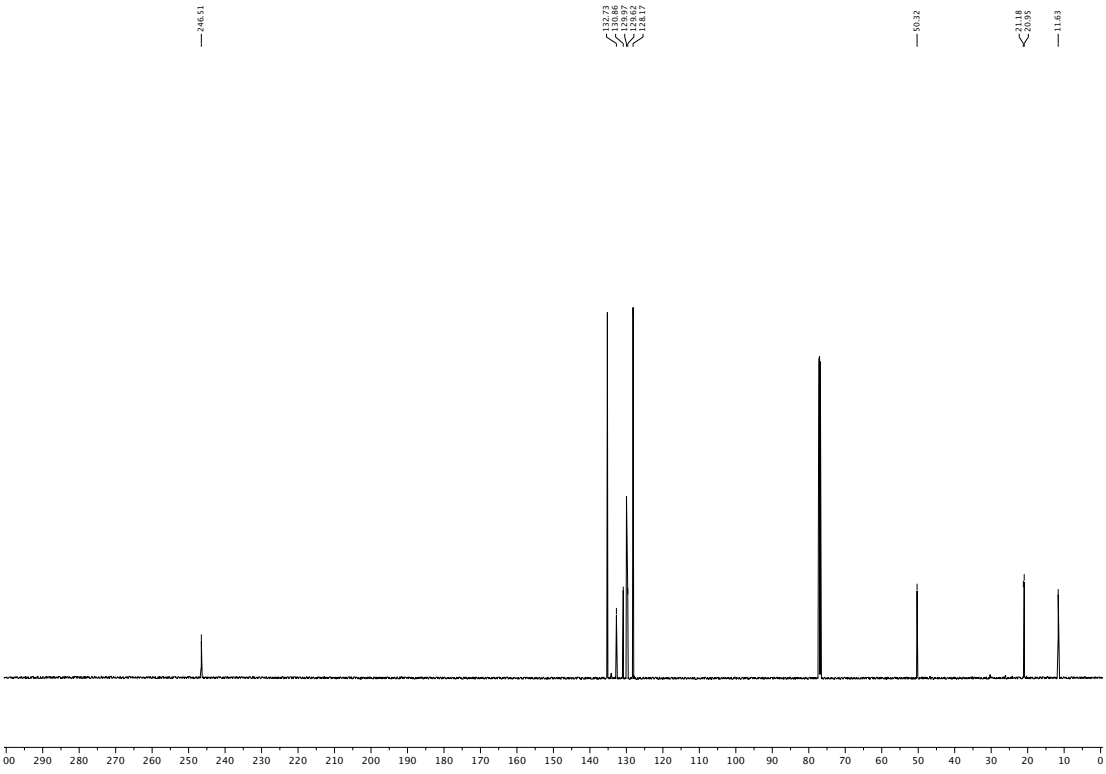


Figure S3.45 ^{13}C NMR spectrum of **8b**

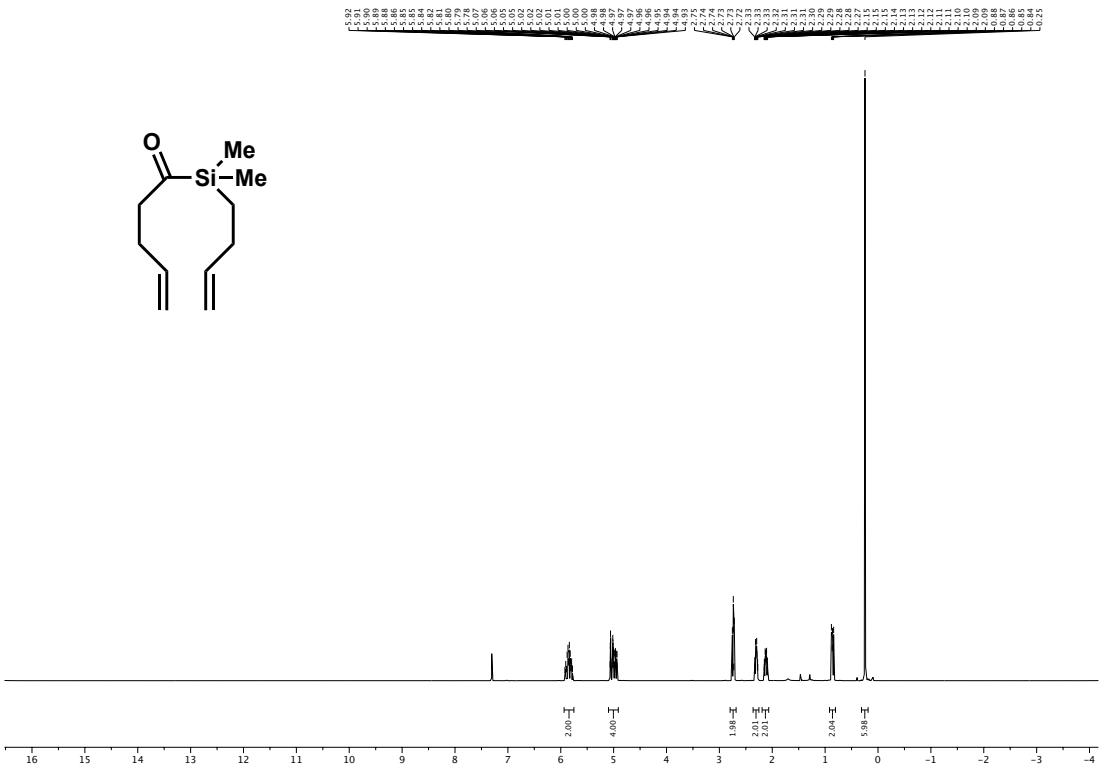


Figure S3.46 ^{1}H NMR spectrum of **11**

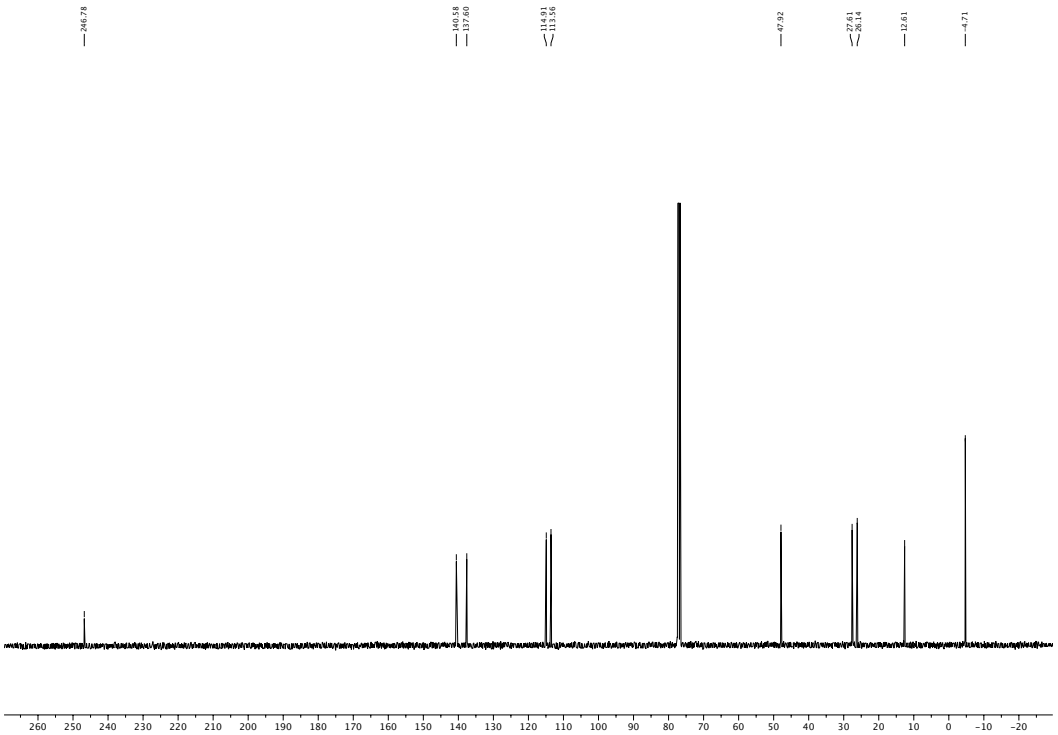


Figure S3.47 ^{13}C NMR spectrum of **11**

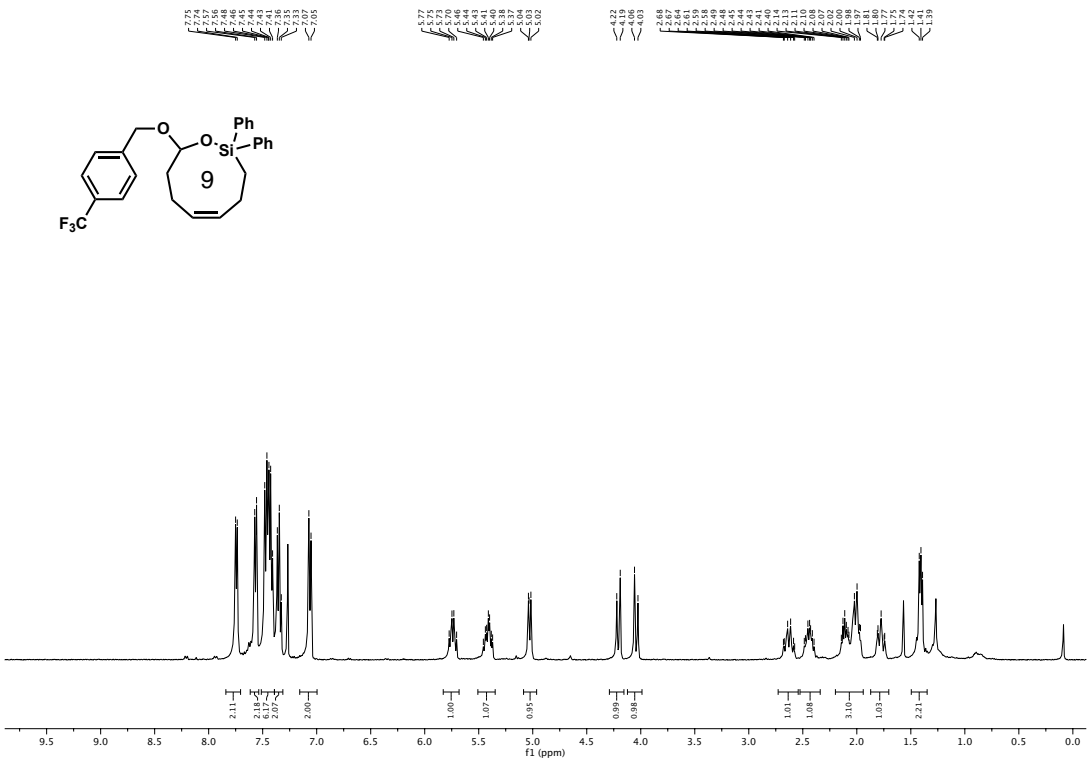


Figure S3.48 ^{1}H NMR spectrum of **14**

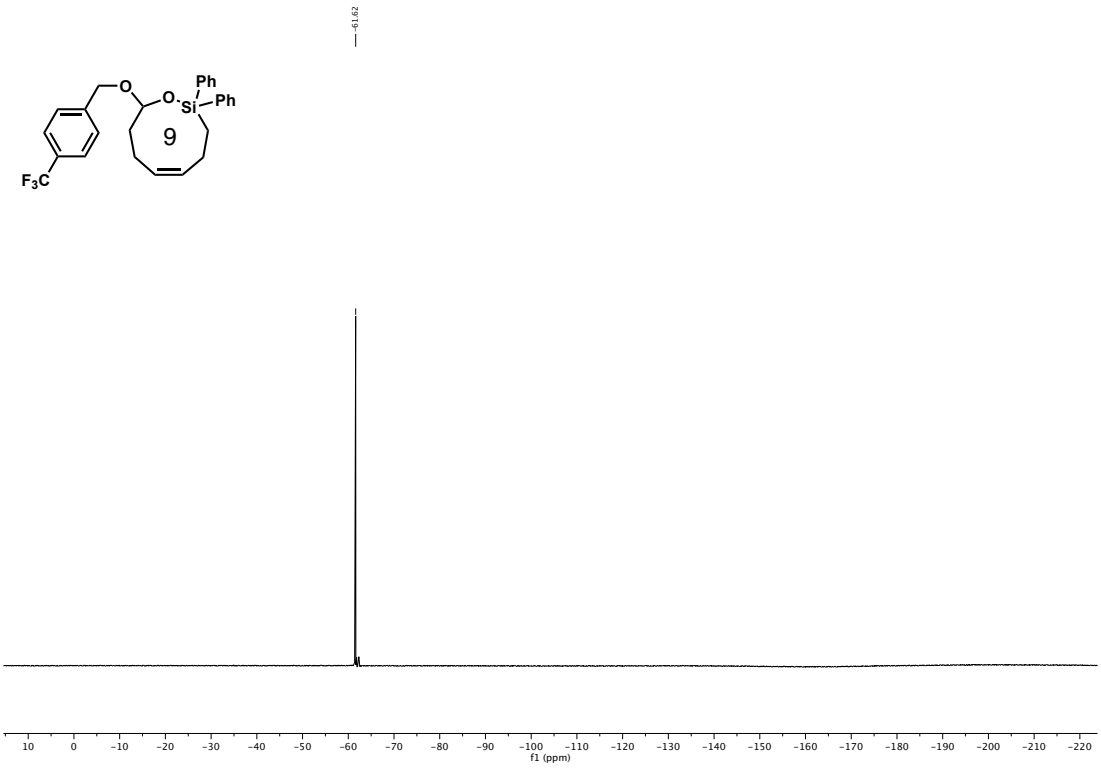


Figure S3.49 ^{19}F NMR spectrum of **14**

Chapter 4

Discovery of Porous Crystalline Nitrone-Linked Covalent Organic Framework

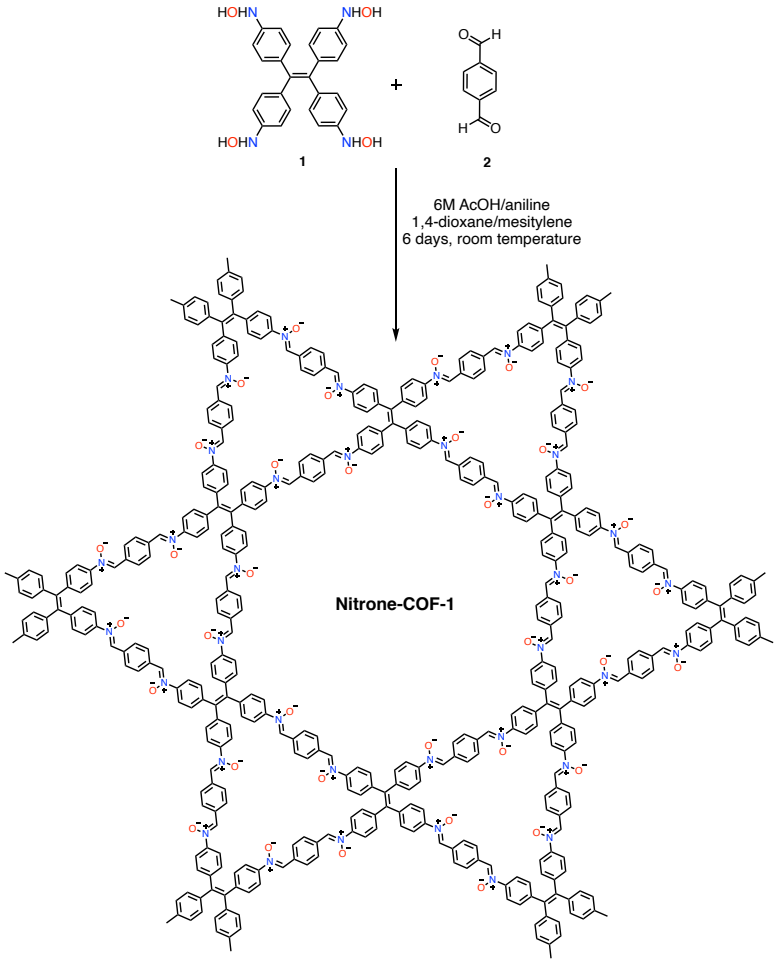
4.1 Introduction

Development of new linkages to broaden the scope of covalent organic frameworks (COFs) has been one of the major drivers of this research field.[1,2] The diversity of linkage functionalities plays a critical role in tunning the material properties including its chemical stability,[3] adsorption behavior,[4] and catalytic activity[5]. Despite the ubiquitous usage of the imine linkage in various studies, its oxidized counterpart, the nitrone functionality, remains elusive as a linkage in COFs.[2] Nitrone compounds, featuring 1,3-dipolar structures, are versatile synthetic intermediates that can undergo nucleophilic addition, cycloaddition reactions, photochemical rearrangements, etc. Additionally, nitrones can serve as spin traps to detect short-lived radicals and their therapeutic potential against oxidative stress is currently being actively studied.[6] Thus, synthesis of porous, crystalline nitrone-linked frameworks will provide an invaluable opportunity to expand the linkage chemistry of COFs and, potentially result in novel applications using extended structures.

4.2 Results and Discussion

4.2.1 Preparation of Nitrone-Linked Covalent Organic Framework

Despite being widely utilized in side chains in polymer chemistry, the nitrone functionality has never been reported to constitute backbones of polymers.[7] This can partially be attributed to the difficulty of synthesizing multidentate hydroxy-amine monomers.[8] Herein, an easy synthetic route (see SI) to access *N*, *N*', *N*', *N*'''-(ethene-1,1,2,2-tetrayltetrakis(benzene-4,1-diyl))tetrakis(hydroxylamine) (**1**) and to reticulate it with terephthaladehyde (**2**) via a condensation reaction leading to Nitrone-COF-1 (Scheme 4.1) is presented. Studies showing reversibility of a condensation reaction between aromatic hydroxylamines and aldehydes[9] suggested that a successful framework crystallization is feasible. However, due to thermal sensitivity of the nitrone functionality,[7a] the typical conditions for the crystallization of imine-linked COFs (120 °C, 3 days) would be unsuitable for COFs bearing nitrone linkages. After comprehensive screening of the reaction conditions, Nitrone-COF-1 was synthesized in a 1,4-dioxane/mesitylene mixture at room temperature for 6 days using an aqueous solution of acetic acid as a catalyst. Furthermore, the use of aniline as a modulator was essential for the high crystallinity of the target COF. The material was found to be sensitive to moisture, therefore anhydrous 1,4-dioxane and acetone were used for the washing procedure to remove any impurities within the COF pores. After supercritical CO_2 drying and activation, Nitrone-COF-1 required storage under inert atmosphere.



Scheme 4.1 Synthesis of the first nitrone-linked COF, Nitrone-COF-1, by linking *N*, *N*', *N*', *N*'''-(ethene-1,1,2,2-tetrayltetrakis(benzene-4,1-diyl))tetrakis(hydroxylamine) (1) and terephthaladehyde (2) via a condensation reaction.

4.2.2 Characterization of Nitrone-Linked Covalent Organic Framework

The structure of Nitrone-COF-1 was evaluated by powder X-ray diffraction (PXRD) analysis (Figure 4.1a). The PXRD pattern confirmed phase-purity and absence of starting materials. The structure of Nitrone-COF-1 was modeled in the *P*6 space group (No. 168), with the layers assuming the **kgm** topology stacked in an eclipsed fashion. Using this structural model, a Pawley refinement was performed against the experimental pattern to provide the unit cell parameters (a = 38.27 Å, and c = 6.89 Å) with reasonable agreement (R_p = 3.37%, Rwp = 4.33%).

The presence of the nitrone functionality in the framework was first assessed by Fourier transform infrared (FT-IR) spectroscopy (Figure 4.1b). The prominent peak at 1075 cm^{-1}, which is absent in the FT-IR spectrum of the isoreticular imine-linked COF,[10] was assigned to the N−O stretch.[11] The C=N stretch of the nitrone appeared at 1597 cm^{-1}, that is shifted to a lower frequency compared to the imine C=N stretch.[11] The absence of the C=O band at 1689 cm^{-1}, which is present in the reactant terephthalaldehyde (**2**), indicated the absence of dangling aldehyde functionalities in Nitrone-COF-1. The C=N band around 1623 cm^{-1} that has a weak intensity in the FT-IR spectrum of Nitrone-COF-1 was attributed to the presence of imine defects in the framework.[12]

Next, the ^{13}C-labeled Nitrone-COF-1 was synthesized via a condensation reaction between a ^{13}C-labeled terephthaladehyde (**2'**) and the hydroxylamine linker **1**. The resulting product was analyzed by solid-state ^{13}C multi cross-polarization magic angle spinning (multiCP-MAS) NMR spectroscopy. The major peak at 135.1 ppm evidently showed that the COF is mainly connected via the nitrone linkage[7a] (Figure 4.1c). Based on a previous report,[10b] the minor peaks at 159.4 ppm and 192.1 ppm were assigned to the imine and aldehyde defects (8% each), respectively. The aldehyde peak at 192.1 ppm possibly appeared due to handling the material in air before and during the NMR measurement.

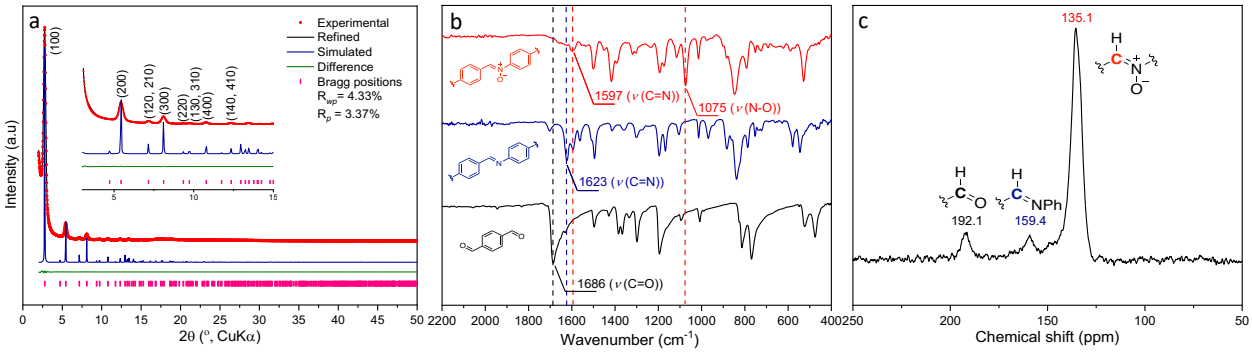


Figure 4.1 Characterization of Nitrone-COF-1. (a) Pawley refinement of Nitrone-COF-1 (eclipsed, AA-H) against the experimental PXRD pattern. (b) FT-IR spectra of Nitrone-COF-1 (red), its isoreticular imine-linked COF (blue), and terephthalaldehyde (black). (c) Solid-state ^{13}C multiCP-MAS NMR spectrum of the ^{13}C-labeled Nitrone-COF-1.

The porosity of Nitrone-COF-1 was studied via nitrogen sorption analysis at 77 K (Figure 4.2). A Type IV adsorption isotherm was observed, thus indicating the presence of mesopores in the framework structure. A surface area of 1368 m^2/g was estimated using the Brunauer–Emmett–Teller (BET) model. DFT analysis of the pore size distribution further confirmed the dual-pore structure of Nitrone-COF-1 with presence of micro- and mesopores (Figure 4.2, insert).

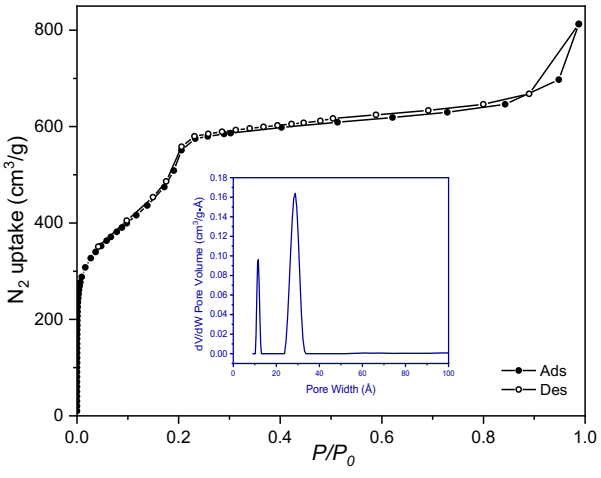
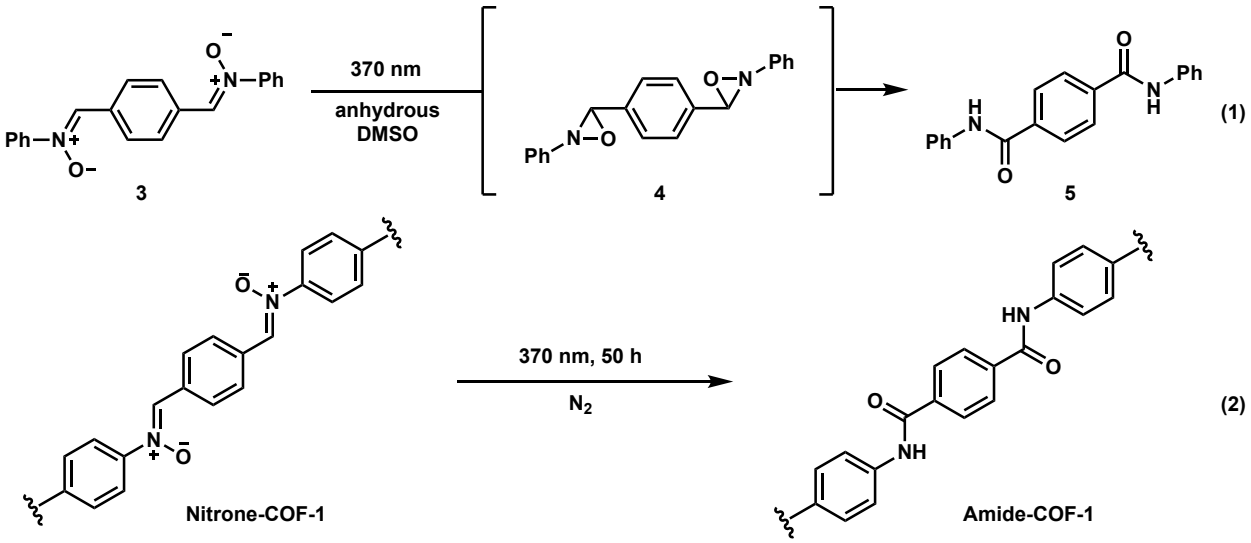


Figure 4.2 N_2 sorption isotherm of Nitrone-COF-1 at 77 K and its pore size distribution (insert).

4.2.3 Studies of Photochemical Properties of Nitrone-Linked Covalent Organic Framework

Following the sorption studies, the photochemical properties of the nitrone-linked COF were explored. It has been reported that small-molecule nitrone compounds can undergo photoisomerization reactions to afford amide products through an oxaziridine intermediate.[6a,13] Indeed, irradiation of model compound **3** in anhydrous DMSO led to quantitative conversion into amide product **5**. To study the photoreactivity of the nitrone functionality in a framework, Nitrone-COF-1 was subjected to irradiation conditions (Scheme 4.2, with a 52 W Kessil PR160L LED lamp with a peak emission at 370 nm, under N_2 atmosphere). MultiCP ssNMR indicated 55% conversion of the nitrone linkage into amide linkage. Another 16% conversion into aldehyde was observed as the result of undesired hydrolytic reaction. Further optimization of the irradiation conditions is in progress to achieve higher conversion into amide while avoid the hydrolysis. PXRD analysis of the microcrystalline powder confirmed retention of crystallinity after irradiation and did not reveal additional diffraction peaks. The skeletal rearrangement represents a rare example of a post-synthetic COF modification induced by light.[3a,3c,14]



Scheme 4.2 Photoinduced isomerization reactions of model compound **3** (1) and Nitrone-COF-1 (2).

4.3 Conclusion

In conclusion, this report reflects the synthesis of the first crystalline, porous COF with nitrone linkages. It will open possibilities for other nitrone-linked COFs of different topologies. In addition, the material was found to undergo photochemical isomerization to furnish an isostructural amide-linked COF.

4.4 References and Notes

[1]. (a) Côte, A. P.; Benin, A. I.; Ockwig, N. W.; O'Keeffe, M.; Matzger, A. J.; Yaghi, O. M. *Science* **2005**, *310*, 1166–1170. (b) El-Kaderi, H. M.; Hunt, J. R.; Mendoza-Cortes, J. L.; Côte, A. P.; Taylor, R. E.; O'Keeffe, M.; Yaghi, O. M. *Science* **2007**, *316*, 268–272.

[2]. Selected reviews: (a) Ding, S.-Y.; Wang, W. *Chem. Soc. Rev.* **2013**, *42*, 548–568. (b) Waller, P. J.; Gandara, F.; Yaghi, O. M. *Acc. Chem. Res.* **2015**, *48*, 3053–3063. (c) Huang, N.; Wang, P.; Jiang, D. *Nat. Rev. Mater.* **2016**, *1*, 1–19. (d) Diercks, C. S.; Yaghi, O. M. *Science* **2017**, *355*, eaal1585. (e) Lohse, M. S.; Bein, T. *Adv. Funct. Mater.* **2018**, *28*, 1705553. (f) Geng, K.; He, T.; Liu, R.; Dalapati, S.; Tan, K. T.; Li, Z.; Tao, S.; Gong, Y.; Jiang, Q.; Jiang, D. *Chem. Rev.* **2020**, *120*, 8814–8933.

[3]. (a) Waller, P. J.; Lyle, S. J.; Osborn Popp, T. M.; Diercks, C. S.; Reimer, J. A.; Yaghi, O. M. *J. Am. Chem. Soc.* **2016**, *138*, 15519–15522. (b) Waller, P. J.; AlFaraj, Y. S.; Diercks, C. S.; Jarenwattananon, N. N.; Yaghi, O. M. *J. Am. Chem. Soc.* **2018**, *140*, 9099–9103. (c) Zhou, Z. B.; Han, X. H.; Qi, Q. Y.; Gan, S. X.; Ma, D. L.; Zhao, X. *J. Am. Chem. Soc.* **2022**, *144*, 1138–1143.

[4]. (a) Doonan, C. J.; Tranchemontagne, D. J.; Glover, T. G.; Hunt, J. R.; Yaghi, O. M. *Nat. Chem.* **2010**, *2*, 235–238. (b) Pyles, D. A.; Crowe, J. W.; Baldwin, L. A.; McGrier, P. L. *ACS Macro Lett.* **2016**, *5*, 1055–1058.

[5]. (a) Li, H.; Pan, Q.; Ma, Y.; Guan, X.; Xue, M.; Fang, Q.; Yan, Y.; Valtchev, V.; Qiu, S. *J. Am. Chem. Soc.* **2016**, *138*, 14783–14788. (b) Han, X.; Xia, Q.; Huang, J.; Liu, Y.; Tan, C.; Cui, Y. *J. Am. Chem. Soc.* **2017**, *139*, 8693–8697.

[6]. Selected reviews: (a) Spence, G. G.; Taylor, E. C.; Buchardt, O. *Chem. Rev.* **1970**, *70*, 231–265. (b) Rosselin, M.; Poeggeler, B.; Durand, G. *Curr. Top. Med. Chem.* **2017**, *17*, 2006–2022. (c) Murahashi, S.-I.; Imada, Y. *Chem. Rev.* **2019**, *119*, 4684–4716.

[7]. (a) Selected papers on polymeric nitrones: Heinenberg, M.; Ritter, H. *Macromol. Chem. Phys.* **1999**, *200*, 1792–1805. (b) Heinenberg, M.; Menges, B.; Mittler, S.; Ritter, H. *Macromolecules* **2002**, *35*, 3448–3455. (c) Cinar, H.; Tabatabai, M.; Ritter, H. *Polym. Int.* **2012**, *61*, 692–695.

[8]. Beaudoin, D.; Maris, T.; Wuest, J. *Nat. Chem.* **2013***, 5***,** 830–834.

[9]. Turega, S. M.; Lorenz, C.; Sadownik, J. W.; Philp, D. *Chem. Commun.* **2008**, 4076–4078.

[10]. (a) Zhou, T.-Y.; Xu, S.-Q.; Wen, Q.; Pang, Z.-F.; Zhao X. *J. Am. Chem. Soc.* **2014**, *136*, 15885–15888. (b) Waller, P. J.; Lyle, S. J.; Osborn Popp, T. M., Diercks, C. S.; Reimer, J. A.; Yaghi, O. M. *J. Am. Chem. Soc.* **2016**, *138*, 15519–15522.

[11]. Shindo, H.; Umezawa, B. *Chem. Pharm. Bull.* **1962**, *10*, 492–503.

[12]. The presence of the imine defects is likely due to the partial retainment of the modulator (aniline) in the structure via condensation with terephthalaldehyde.

[13]. (a) Splitter, J. S.; Calvin, M. *J. Org. Chem.* **1958**, *23*, 651–651. (b) Splitter, J. S.; Calvin, M. *J. Org. Chem.* **1965**, *30*, 3427–3436. (c) Zeng, Y.; Smith, B. T.; Hershberger, J.; Aubé, J. *J. Org. Chem.* **2003**, *68*, 8065–8067. (d) Zhang, Y.; Blackman, M. L.; Leduc, A. B.; Jamison, T. F. *Angew. Chem. Int. Ed.* **2013**, *52*, 4251–4255. (e) Cai, B. G.; Luo, S.S.; Li, L.; Li, L.; Xuan, J.; Xiao, W. J. *CCS Chem.* **2021**, *3*, 2764–2771.

[14]. Selected reviews: (a) Segura, J. L.; Royuela, S.; Ramos, M.M. *Chem. Soc. Rev.* **2019**, *48*, 3903–3945. (b) Yusran, Y.; Guan, X.; Li, H.; Fang, Q.; Qiu, S. *Natl. Sci. Rev.* **2020**, *7*, 170–190.

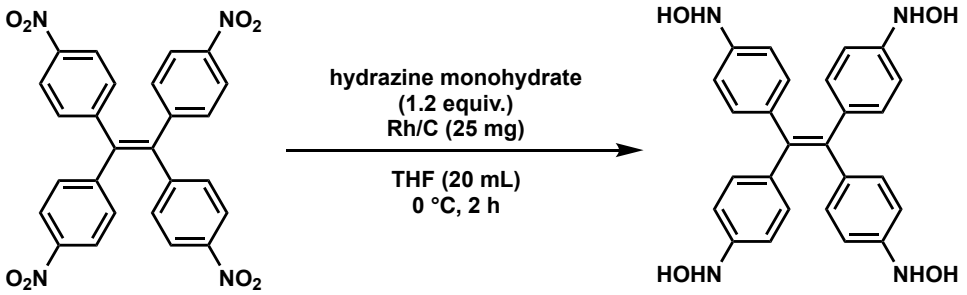
4.5 Supporting Information

4.5.1 General Information

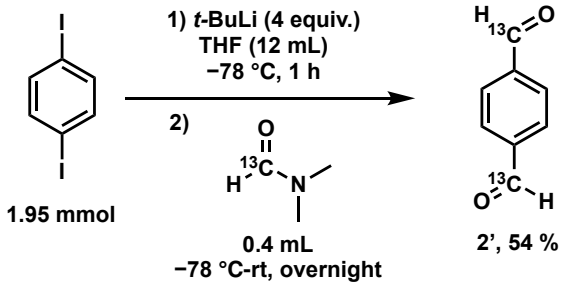
Chemicals: Anhydrous 1,4-dioxane, Mesitylene, terephthalaldehyde, glacial acetic acid were purchased from Sigma-Aldrich. ^{13}C-labeled *N,N*-dimethylformamide (carbonyl-^{13}C, purity 99%)

was purchased from Cambridge Isotope Laboratories. Chloroform-d_3 and dimethyl sulfoxide-d_6, were purchased from Cambridge Isotope. All the chemicals were used without further purification. *Analytical techniques:* High Resolution Mass spectra (HR-MS) measurements were performed by the QB3/Chemistry Mass Spectrometry Facility at UC Berkeley. Masses are reported in m/z units as the molecule ion $[M + H]^+$. Elemental microanalyses (EA) were performed by using a LECO CHNS-932 CHNS elemental analyzer. Single crystal X-ray diffraction data of the linker and the model compound was collected on a Bruker D8 Venture diffractometer with PHOTON-100 detector. FT-IR spectra were collected in-house using a Bruker ALPHA Platinum ATR-FT-IR Spectrometer equipped with a single reflection diamond ATR module. Thermogravimetric analysis (TGA) curves were recorded on a TA Q500 thermal analysis system under nitrogen flow. Solid state NMR spectra were collected using a 7.05 T magnet with a Tecmag Discovery spectrometer operating at 300.13 MHz for 1 H and 75.48 MHz for ^{13}C. Scanning electron microscopy (SEM) images were recorded on a FEI Quanta 3D FEG scanning electron microscope with an accelerating voltage of 10 kV and a working distance of 10.0 mm. Wide-angle X-ray scattering (WAXS) patterns were acquired on beamline 7.3.3 at the Advanced Light Source (ALS) with a Pilatus 2M detector. Powder X-ray diffraction (PXRD) data was collected on a Bruker D8 Advance diffractometer (Bragg-Brentano geometry) employing Ni filtered Cu Kα1 (λ = 1.54059 Å) radiation. Low-pressure N_2 adsorption measurements were carried out on a Micromeritics ASAP 2420 surface area analyzer. The N_2 isotherms were measured using a liquid nitrogen bath (77 K).
Ultrahigh-purity-grade N_2 and He (99.999% purity) were used throughout adsorption experiments.

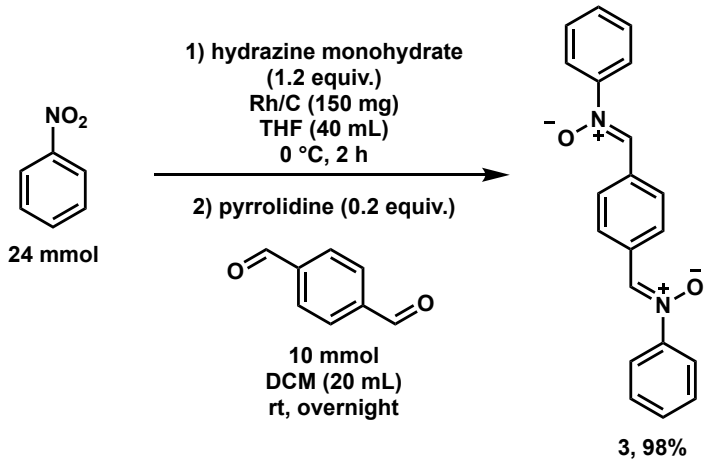
4.5.2 Synthetic Procedures



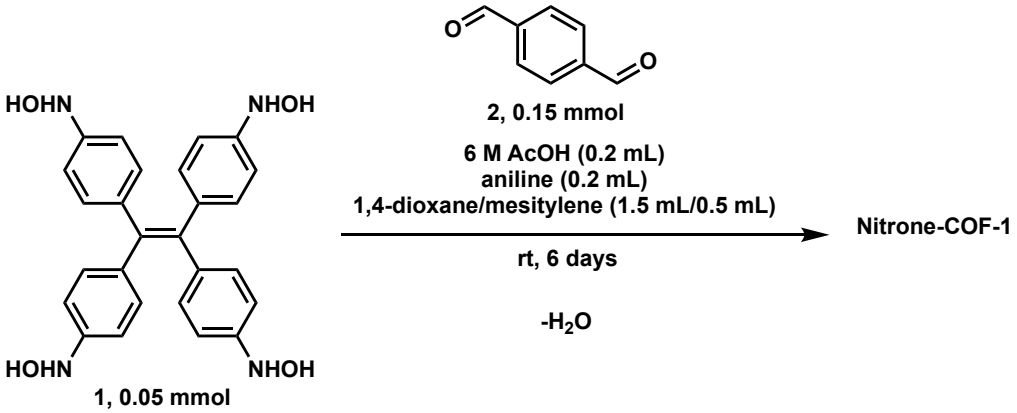
***N*, *N*', *N*', *N*'''-(ethene-1,1,2,2-tetrayltetrakis(benzene-4,1-diyl))tetrakis-(hydroxylamine) (1):** A 100 mL round bottom flask was placed under vacuum before backfilled with N_2; it was then charged with a stir bar, 1,1,2,2-tetrakis(4-nitrophenyl)ethene (512 mg, 1.0 mmol), Rh/C (25 mg), and THF (20 mL). The reaction vessel was cooled to 0 ˚C. To this vigorously stirring mixture was slowly added hydrazine monohydrate (1.2 equiv., 0.23 mL). Gas evolution was observed. The reaction mixture was stirred for 2 hours at 0 ˚C. The suspension was then filtered through a pad of Celite and rinsed with EtOAc. The filtrate was concentrated *in vacuo*. The residue was recrystallized with EtOAc/pentane solvents. Resulting brown solid was collected by filtration to afford compound **1** (356 mg, 78%). Note: before use, sparge all the solvents used in this procedure with N_2 for 5 min. ^{1}H NMR (500 MHz, DMSO-d_6) δ 8.17 (d, J = 2.2 Hz, 4H), 8.14 (br. s, 4H), 6.74 (ap. d, J = 8.6 Hz, 8H), 6.55 (ap. d, J = 8.4 Hz, 8H). ^{13}C NMR (126 MHz, DMSO-d_6) δ 149.86, 137.93, 135.66, 131.15, 112.18.



^{13}C-Labeled terephthalaldehyde (2'): A flame-dried 100 mL round bottom flask cooled 1,4-diiodobenzene (643 mg, 1.95 mmol), and dry THF (12 mL). The reaction vessel was cooled to −78 ˚C and a solution of *t*-BuLi (7.8 mmol, 4 equiv.) was added dropwise. The solution was stirred at −78 ˚C for 1 hour before formaldehyde-^{13}C (0.4 mL) was added dropwise. The reaction mixture was allowed to warm to room temperature and stirred overnight. The resulting solution was quenched by addition of sat. aqueous NH_4Cl solution. The organic solvents were evaporated *in vacuo* and the resulting oil was dissolved in diethyl ether. The organic layer was washed with water (twice) and saturated brine, dried over Na_2SO_4, and concentrated in *vacuo*. The crude product was purified by silica gel column chromatography (ethyl acetate/hexane = 1:10) to afford the title compound **2'** (145 mg, 54%).^{1}H NMR (600 MHz, $CDCl_3$-d_3) δ 10.31 (s, 1H), 10.02 (s, 1H), 8.08 (dd, J = 3.1, 2.3 Hz, 4H).



(1*Z*,1'*Z*)-1,1'-(1,4-phenylene)bis(*N*-phenylmethanimine oxide) (3): A 100 mL round bottom flask was placed under vacuum before backfilled with N_2; it was then charged with a stir bar, nitrobenzene (3.0 g, 24 mmol), Rh/C (160 mg), and THF (40 mL). The reaction vessel was cooled to 0 ˚C. To this vigorously stirring mixture was slowly added hydrazine monohydrate (1.2 equiv., 1.4 mL). Gas evolution was observed. The reaction mixture was stirred for 2 hours at 0 ˚C. The suspension was then filtered through a pad of Celite and rinsed with EtOAc. The filtrate was concentrated *in vacuo*. The residue was dissolved in anhydrous DCM (20 mL), followed by the addition of pyrrolidine (4.8 mmol, 340 mg) and terephthalaldehyde (10 mmol, 1.3 g). The reaction mixture was stirred in dark overnight at room temperature. Yellow precipitate was collected by filtration to afford compound **3** (3.1g, 98%).^{1}H NMR (600 MHz, DMSO-d_6) δ 8.59 (s, 2H), 8.57 (s, 4H), 7.97 – 7.93 (m, 4H), 7.61 – 7.54 (m, 6H). ^{13}C NMR (151 MHz, DMSO-d_6) δ 148.98, 133.54, 132.98, 130.53, 129.63, 129.09, 121.98.



Nitrone-COF-1: A 18 × 150 mm borosilicate glass tube (Type I, Class B, Chemglass) was loaded with terephthalaldehyde (**2**) (20.4 mg, 0.15 mmol, 3 equiv.) and linker **1** (23.0 mg, 0.05 mmol). After closing the tube with a septum inside a glovebox, 1,4-dioxane (1.5 mL) was added. The resulting suspension was sonicated for 5 min to allow the linkers to be completely dissolved before adding mesitylene (0.5 mL), aniline (200 mL, 2.2 mmol, 43.8 equiv.) and 6 M aq. AcOH (200 mL). The reaction mixture was sonicated for 10 min and left undisturbed for 6 days in the dark. The solid was isolated by filtration, washed with dry 1,4-dioxane (4 x 20 mL) and dry acetone (4 x 20 mL) within 1.5 days. Subsequent supercritical CO_2 drying followed by activation under vacuum at room temperature for 4 hours and then at 50 °C for 4 hours resulted in Nitrone-COF-1 as orange powder (20 mg, 61%).
Elem. Anal. of activated Nitrone-COF-1: Calcd. for $C_{126}H_{84}N_{12}O_{12}$: C, 77.29; H, 4.32; N, 8.58%. Found: C, 75.82; H, 4.61; N, 9.26%.

4.5.3 Gas Sorption Experiments

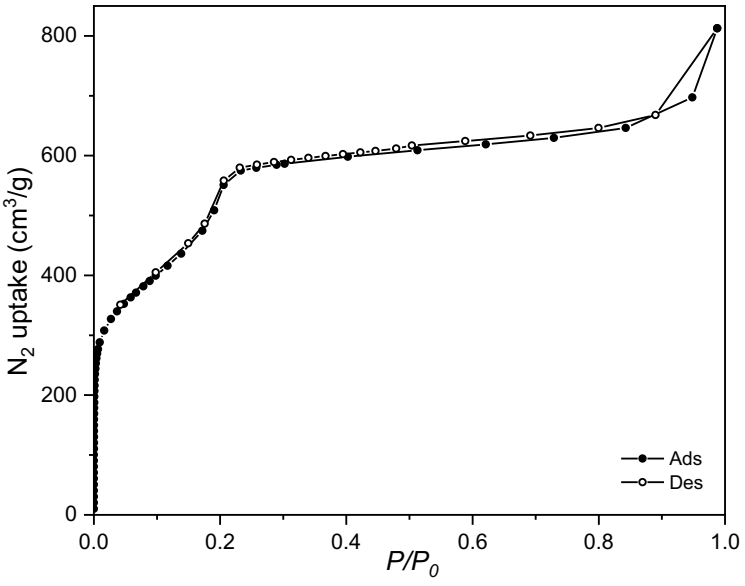


Figure S4.1 Nitrogen sorption of Nitrone-COF-1 at 77 K.

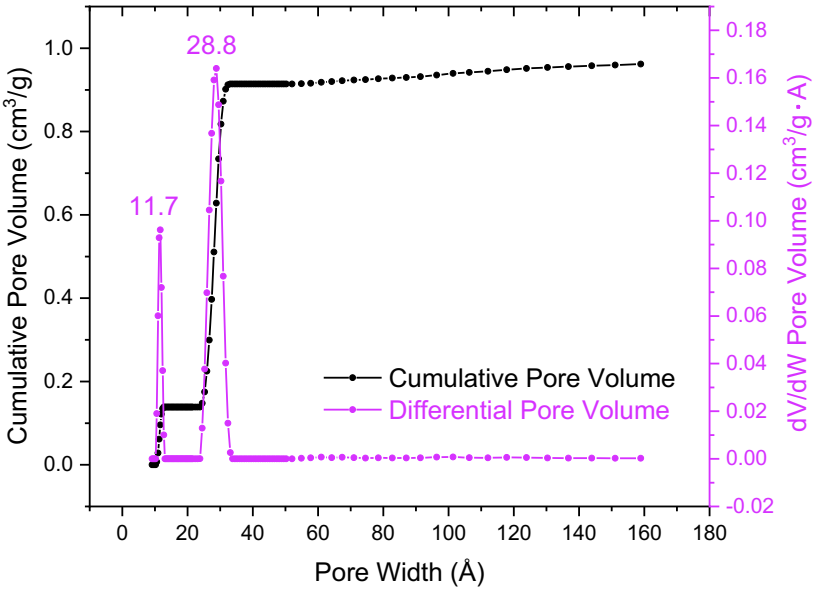


Figure S4.2 Pore size distribution of Nitrone-COF-1 derived from N_2 sorption isotherm measured at 77 K. Density functional theory for oxide surfaces with cylindrical pores was applied. Pore width = 11.7 Å and 28.8 Å.

4.5.4 Scanning Electron Microscopy Image

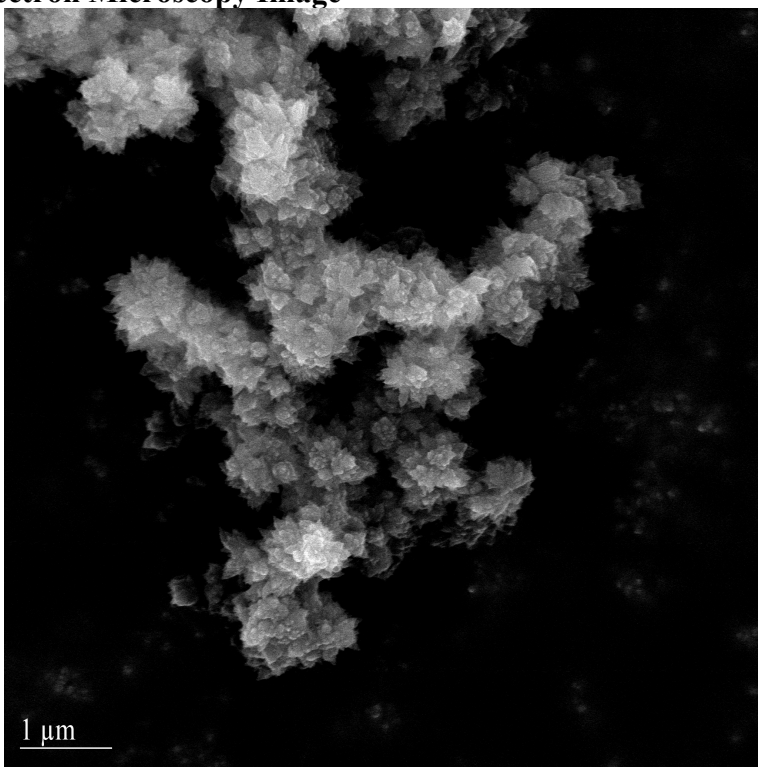


Figure 4.3 Scanning electron micrograph of Nitrone-COF-1 particles.

4.5.5 Irradiation Studies

Irradiation of model compound **3**: A saturated anhydrous DMSO solution of **3** was placed in a NMR tube with septum cap under N_2. The solution was irradiated with a 52 W Kessil PR160L LED lamp with a peak emission at 370 nm for 1 hour. Resulting solution was analyzed by NMR spectroscopy.

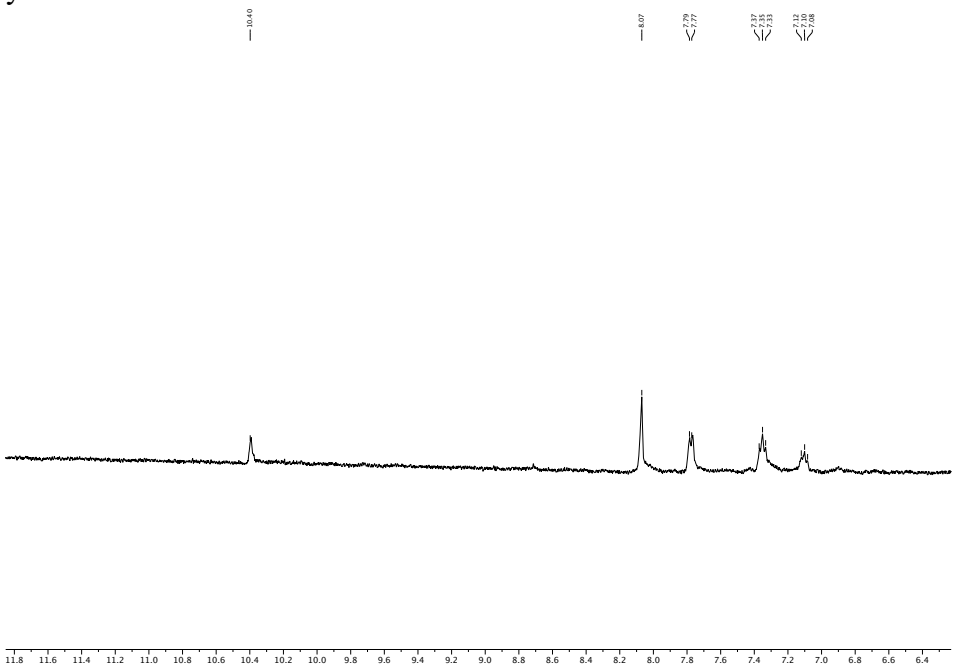


Figure S4.4 No-Deuterium ^{1}H NMR spectrum of post-irradiation sample of **3**

Irradiation of Nitrone-COF-1: Nitrone-COF-1 (5 mg) was placed in a 2-dram vial with septum cap under N_2. The solid was irradiated with a 52 W Kessil PR160L LED lamp with a peak emission at 370 nm for 50 hours. Resulting solid was placed under nitrogen in the dark for another 24 hours before being analyzed by ^{13}C multiCP-MAS NMR spectroscopy.

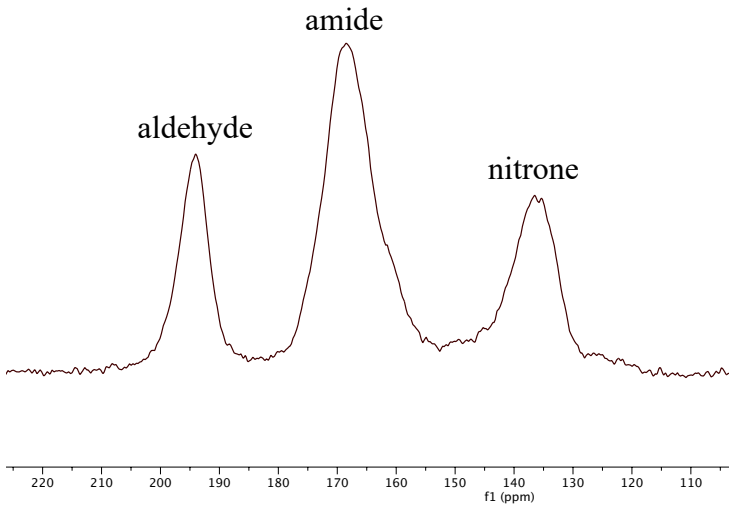


Figure S4.5 ^{13}C multiCP-MAS NMR spectrum of post-irradiation sample of Nitrone-COF-1

4.5.6 NMR Spectra

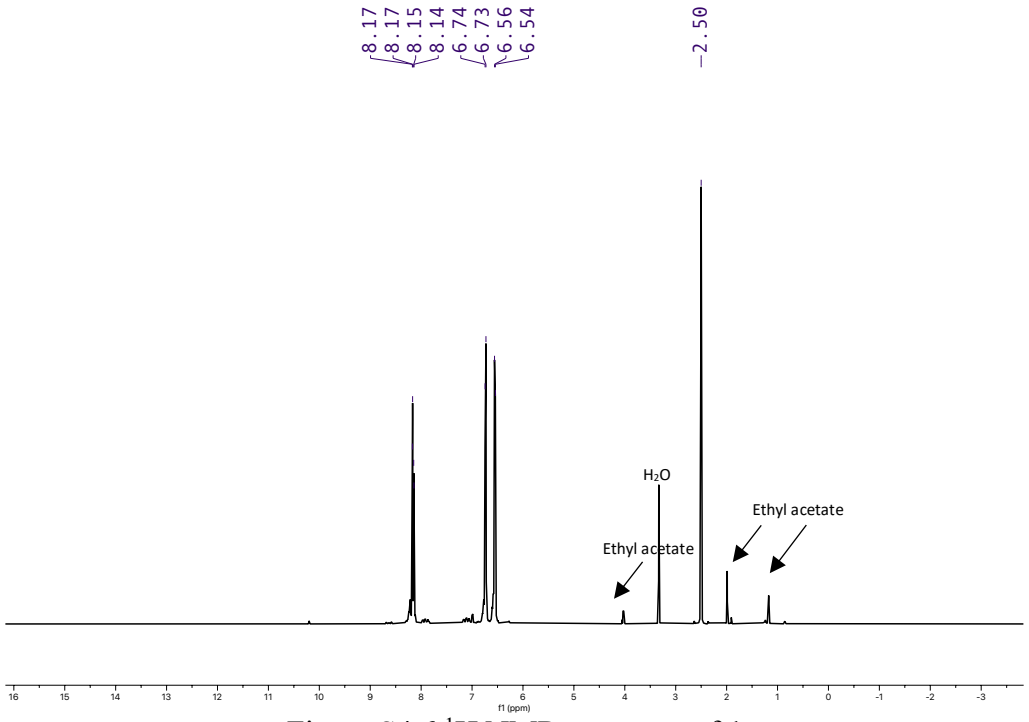


Figure S4.6 ^{1}H NMR spectrum of **1**

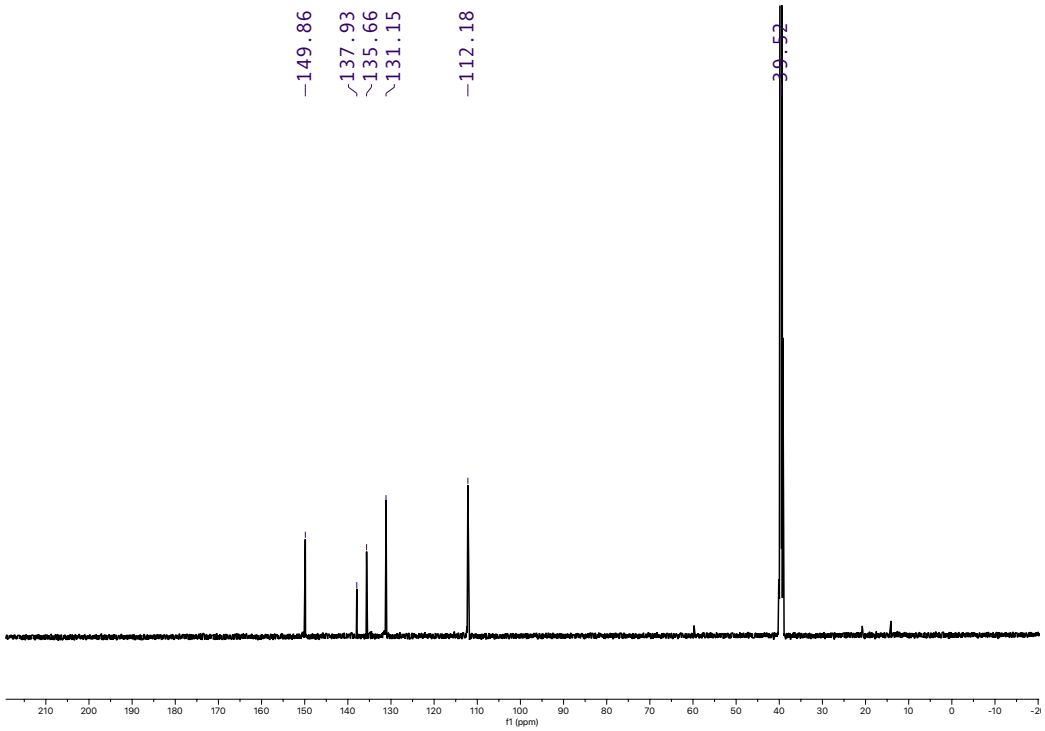


Figure S4.7 ^{13}C NMR spectrum of **1**

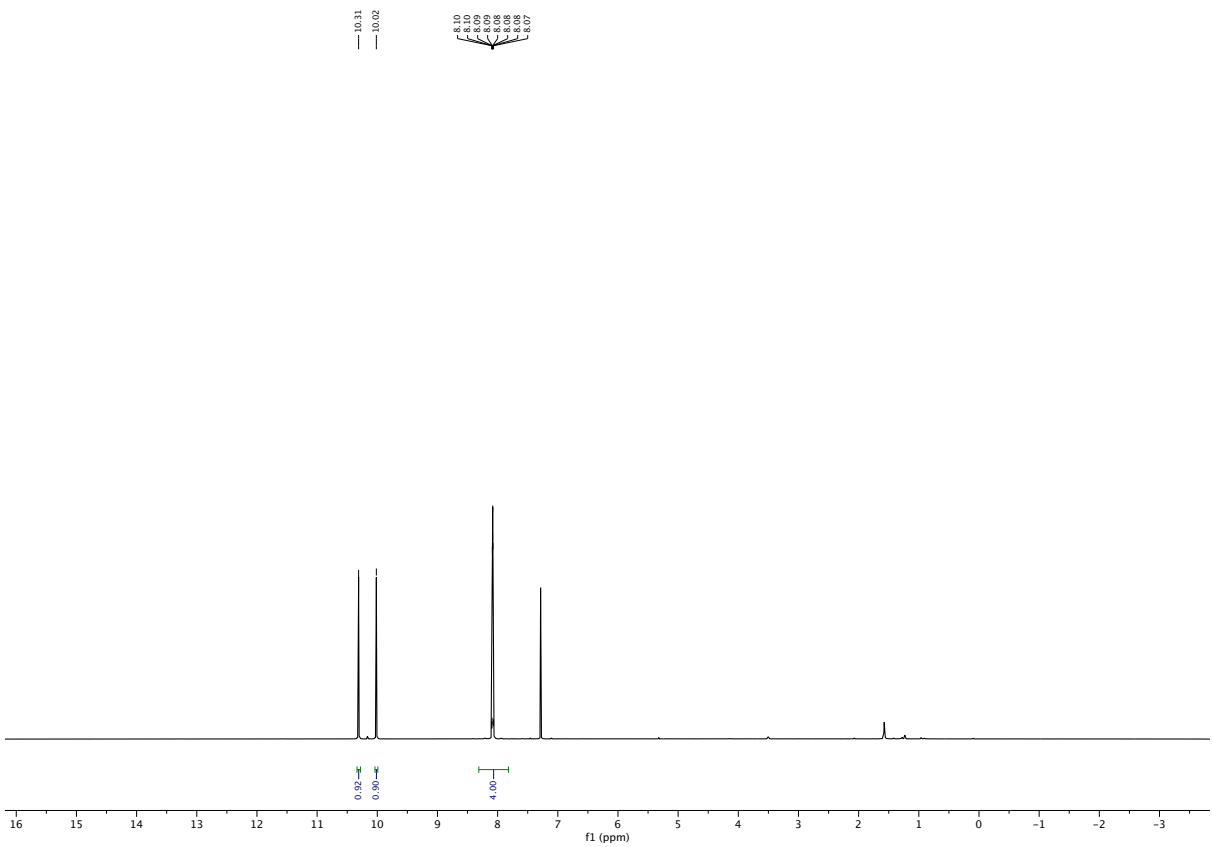


Figure S4.8 ^{1}H NMR spectrum of ^{13}C-Labeled terephthalaldehyd (**2'**)

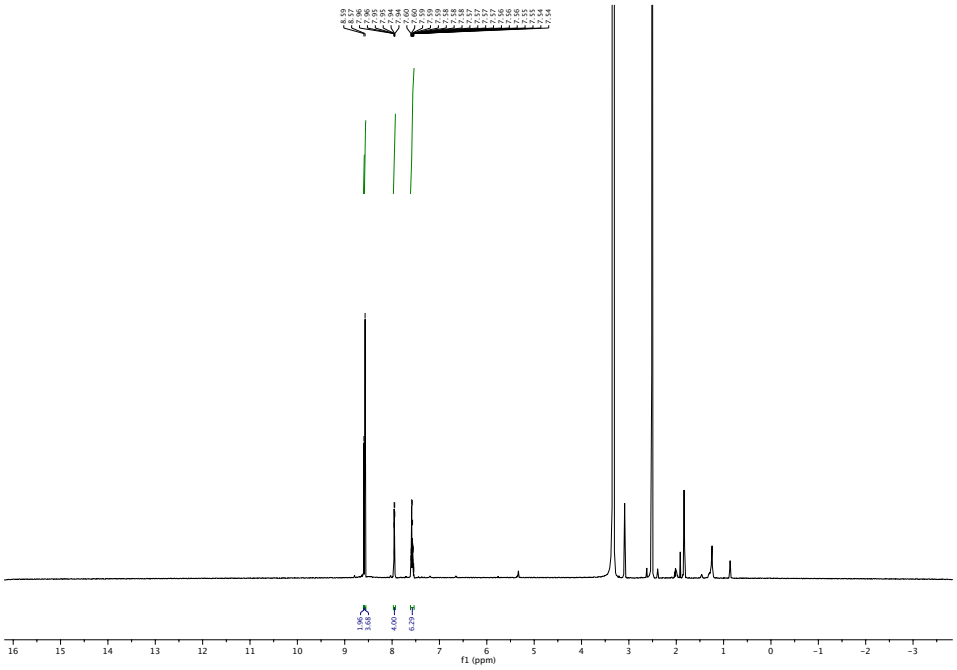


Figure S4.9 ^{1}H NMR spectrum of **3**

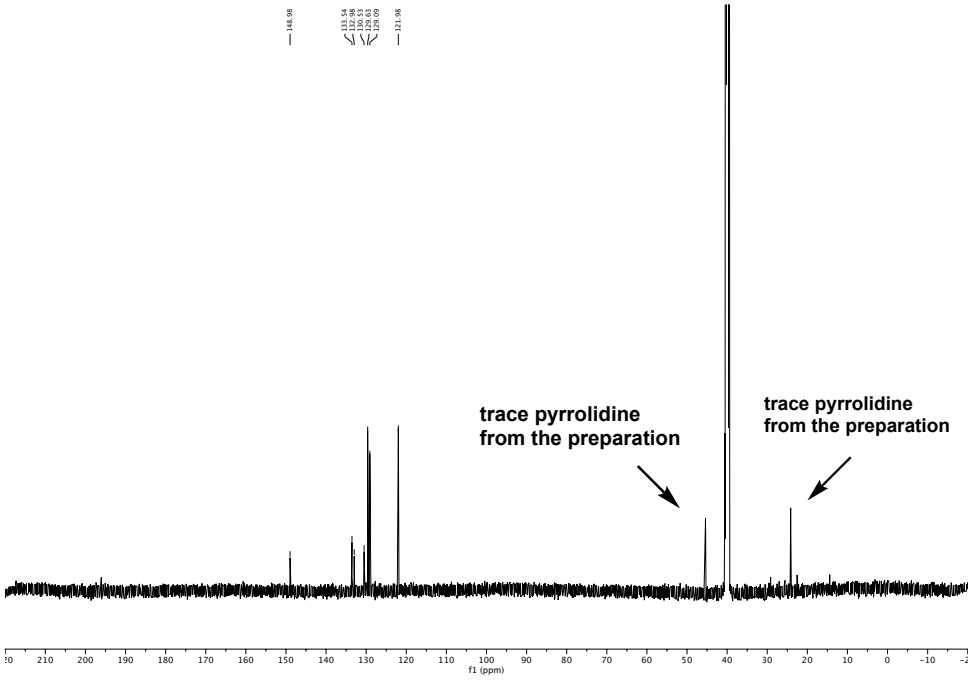


Figure S4.10 ^{13}C NMR spectrum of **3**